Experimental Measurements of Cerebral Haemodynamics and Oxygenation and Comparisons with a Computational Model: a Near-Infrared Spectroscopy Investigation

Ilias Tachtsidis, M.Sc.

Department of Medical Physics and Bioengineering
University College London

Supervisors:
Prof. David T. Delpy, FRS
Dr. Clare E. Elwell

Thesis submitted for the degree of Doctor of Philosophy (Ph.D.) at the University of London

May 2005

UMI Number: U602443

All rights reserved

INFORMATION TO ALL USERS
The quality of this reproduction is dependent upon the quality of the copy submitted.

In the unlikely event that the author did not send a complete manuscript
and there are missing pages, these will be noted. Also, if material had to be removed,
a note will indicate the deletion.

UMI U602443
Published by ProQuest LLC 2014. Copyright in the Dissertation held by the Author.
Microform Edition © ProQuest LLC.
All rights reserved. This work is protected against
unauthorized copying under Title 17, United States Code.

ProQuest LLC
789 East Eisenhower Parkway
P.O. Box 1346
Ann Arbor, MI 48106-1346

Abstract

This thesis describes studies of cerebral oxygenation, autoregulation and metabolism carried out on human volunteers and patients. These studies are intended to aid both the development and the validation of a new physiology based mathematical model of the cerebral circulation and metabolism. The thesis contains comparisons between the experimentally derived data and predictions from this model.

The experimental studies involve the measurement of systemic and cerebral haemodynamic parameters and their response to physiological challenges. In particular, near-infrared spectroscopy (NIRS) is used to monitor cerebral blood volume, oxygenation and flow. NIRS is a non-invasive technique, which uses the differing optical absorption of oxy- and deoxy- haemoglobin in the near infrared to monitor variations in oxygenation and blood volume deep within the tissue. A 2 channel NIRS instrument with spatially-resolved capabilities (NIRO 300, Hamamatsu Photonics KK), was used to monitor cerebral changes in response to physiological challenges such as hypercapnia, hypoxia and passive tilt in healthy volunteers. Furthermore we studied patients with primary autonomic failure with severe orthostatic hypotension undergoing a tilt test. The main reason for using data from these patients is that a comparatively minor physiological challenge (a 60° tilt) produces a major drop in arterial blood pressure and cerebral haemodynamics.

The computational model, against which the experimental data is compared, is being developed at UCL. The model is capable of accepting experimentally determined data as an input and predicting changes in other measured and non-measured parameters. The thesis describes the model and illustrates its abilities using both theoretical and experimental data, in particular examining the measured and predicted changes in cerebral tissue oxygenation.

Finally, practical aspects of clinical data monitoring are addressed and the capabilities and limitations of the cerebral modelling work are discussed. The findings and conclusions of these studies should be relevant to the wider mathematical, physiology and biomedical optics community.

Acknowledgements

Firstly I would like to thank my supervisors: Prof. David Delpy, for his inspirational guidance and excellent supervision throughout the course of my studies; and Dr Clare Elwell, for her support, encouragement and guidance throughout this Ph.D.

I would also particularly like to thank and acknowledge Dr Martin Smith, to whom I am extremely grateful for all his time and effort spent helping me in the clinical part of my work.

This thesis would not have been possible without the contribution made by Dr Murad Banaji, whose original work of the BRAINCIRC UCL cerebral model allowed me to perform the simulations described herein and who engaged me in discussions that resulted in many of the ideas introduced in this thesis.

I must express my gratitude to Dr Terence Leung for his guidance and support through out the course of my studies.

I would like to thank all my colleagues and friends at the Medical Physics Department in UCL for their enduring support and the invaluable transfer of knowledge; and all the clinicians from the National Hospital for Neurology and Neurosurgery for their important support for my clinical experiments.

Special thanks go to the MIAS-IRC multiscale modelling group; in particular the Oxford university Signal Processing and Artificial Neural Networks team lead by Prof. Lionel Tarassenko for their challenging discussions and support.

Finally, I want to thank my partner, my family and friends for their love during my Ph.D.

The funding for this project was provided by both the Engineering and Physical Sciences Research Council (EPSRC) and the Medical Research Council (MRC).

Publications Resulting from this Work

Journal Papers

*Banaji M., **Tachtsidis I.**, Delpy D., Baigent S. "A physiological model of cerebral blood flow control." Mathematical Biosciences, 194(2):125-173, (2005).

***Tachtsidis I.**, Elwell C.E., Leung T.S, Lee C.W., Smith M., Delpy D.T., "Investigation of cerebral haemodynamics by near infrared spectroscopy in young healthy volunteers reveals posture dependent spontaneous oscillations." Physiological Measurement, 25(2):437-445, (2004).

***Tachtsidis I.**, Elwell C.E., Lee C.W., Leung T.S, Smith M., Delpy D.T. "Spectral characteristics of spontaneous oscillations in cerebral haemodynamics are posture dependent." Advances in Experimental Medicine and Biology, 540:31-36, (2004).

Leung T.S, Elwell C.E., **Tachtsidis I.**, Henty J.R.,Delpy D.T. "Measurement of optical properties in the adult human head with spatially resolved spectroscopy and changes of postures." Advances in Experimental Medicine and Biology, 540:13-18, (2004).

***Tachtsidis I.**, Elwell C.E., Leung T.S., Bleasdale-Barr K., Hunt K., Toms N., Smith M., Mathias C.J., Delpy D.T. "Rate of change in cerebral oxygenation and blood pressure in response to passive changes in posture: a comparison between Pure Autonomic Failure patients and Controls." Advances in Experimental Medicine and Biology, In Press, (Submitted 2003).

***Tachtsidis I.**, Leung T.S., Oliver C., Henty J.R., Jones H., Smith M., Delpy D.T., Elwell C.E. "Quantification of adult cerebral blood volume using tissue oxygenation index." Advances in Experimental Medicine and Biology, In press, (Submitted 2004).

---

* Reproduced in Appendix C

Leung T.S., **Tachtsidis I.**, Oliver C., Henty J.R., Jones H., Smith M., Delpy D.T., Elwell C.E. "Investigation of apparent oxygen saturation from the pulsatile signals measured on adult heads using Near Infrared Spectroscopy." Advances in Experimental Medicine and Biology, In press, (Submitted 2004).

Conference Proceedings

Tachtsidis I., Jones H., Oliver C., Delpy D.T., Smith M., Elwell C.E., "Investigation of the changes in cerebral tissue oxygenation measured with near infrared spectroscopy in response to moderate hypercapnia." XXIInd International Symposium on Cerebral Blood Flow, Metabolism, and Function, Amsterdam, The Netherlands (2005).

Tisdall M., **Tachtsidis I.**, Bleasdale-Barr K., Mathias C.J., Delpy D.T., Elwell C.E., Smith M., "Investigation of the cerebral haemoglobin and cytochrome signals using near infrared spectroscopy during head up tilt in patients with orthostatic hypotension." XXIInd International Symposium on Cerebral Blood Flow, Metabolism, and Function, Amsterdam, The Netherlands (2005).

Tachtsidis I., Leung T.S., Oliver C., Jones H., Elwell C.E., Smith M., "Non-invasive measurement of absolute cerebral blood volume in adults using a tissue oxygen index." J Neurosurg Anesthesiol, 16: 372 (2004).

Tachtsidis I., Cooper C.E., McGown A.D., Makker H., Delpy D.T., Elwell C.E. "Changes in cerebral total haemoglobin volume and cytochrome oxidase redox state during deep apnoeas in patients with obstructive sleep apnoea." Biomedical Topical Meetings on CD-ROM (The Optical Society of America, Washington, DC), WF6 (2004).

Tachtsidis I., Banaji M. "A computational model of the cerebral circulation: model predictions with experimental data during a CO_2 challenge." Proceedings of IPEM Annual Scientific Meeting inYork (2004).

Banaji M., **Tachtsidis I.** "A computational model of the cerebral circulation: model construction and theoretical considerations." Proceedings of IPEM Annual Scientific Meeting inYork (2004).

Smith M., **Tachtsidis I.**, Elwell C.E., Leung T.S., Delpy D.T., "Posture Dependence of Spontaneous Oscillations in Cerebral Haemodynamics." Anesth. Analg. , 98: S140 (2004).

Banaji M., **Tachtsidis I.**, Delpy D., Baigent S. "A physiological model of the human brain circulation" Proceedings of IPEM meeting on the modelling of blood flow in cardiovascular disease in York (2003).

Bleasdale-Barr K., **Tachtsidis I.**, Hunt K., Toms N., Henty J.R., Elwell C.E., Delpy D.T., Smith M. and Mathias C.J. "Changes in Cerebral oxygen saturation on postural change in patients with autonomic failure and orthostatic hypotension and controls." Clin Auton Res, 12:409-410, (2002).

Hunt K., **Tachtsidis I.**, Bleasdale-Barr K., Thoms N., Henty J., Elwell C., Mathias C., Smith M. "Changes in Cerebral Tissue Oxygenation during Postural Hypotension in Patients with Autonomic Failure" Journal of Neurosurgical Anaesthesiology, 14(4):347, (2002).

Contents

List of Figures

List of Tables

Glossary

ABP	arterial blood pressure
ADP	adenosine diphosphate
AF	primary autonomic failure
ATP	adenosine triphosphate
AVM	arteriovenous malformations
BBB	blood brain barrier
Ca^{++}	calcium ions
CBF	cerebral blood flow
CBV	cerebral blood volume
$CMRO_2$	cerebral oxygen consumption
CNS	central nervous system
CO_2	carbon dioxide
CPP	cerebral perfusion pressure
CPP	cerebral perfusion pressure
CSF	cerebrospinal fluid
CSF	cerebrospinal fluid
CtOx	cytochrome oxidase
CW	continuous wave
CytOx	cytochrome oxidase
DBP	diastolic blood pressure
DP	differential pathlength
DPF	differential pathlength factor
ECG	electrocardiogram
EDCF	endothelium derived contractile factor
EDRF	endothelium derived relaxing factor
ETS	electron transport chain
FAD	flavin adenine dinucleotide
FFT	fast Fourier transform
GDP	guanosine diphospate
H^+	hydrogen ions
HbO_2	oxygenated haemoglobin
HbT	total haemoglobin
HCO_3^-	bicarbonate ions
HHb	deoxygenated haemoglobin or reduced haemoglobin
HR	heart rate
ICG	indocyanine green
ICP	intracranial pressure
K^+	potassium ions
MABP	mean arterial blood pressure
MBP	mean blood pressure
MCA	middle cerebral artery
MRI	magnetic resonance imaging
MSA	multiple system atrophy
NAD^+	nicotinamide adenine dinucleotide
NADH	nicotinamide adenine dinucleotide hydride
NIRS	near infrared spectroscopy
NO	nitric oxide
O_2	oxygen

HbO_2	oxygenated haemoglobin
$PaCO_2$	partial carbon dioxide pressure
PAF	pure autonomic failure
PCO_2	partial carbon dioxide pressure
PET	positron emission tomography
pH	a measure of the acidity or alkalinity of a solution ($-\log[H^+]$)
pO_2	partial oxygen pressure
PSD	power spectrum density
SaO_2	arterial oxygen saturation
SAP	systemic arterial pressure
SBP	systolic blood pressure
SPECT	single photon emission computed tomography
SRS	spatial resolved spectroscopy
TCA	tricarboxylic acid cycle (or Krebs cycle)
TCD	transcranial Doppler
tHb	total haemoglobin
THI	tissue haemoglobin index
TOI	tissue oxygenation index
UCL	University College London
V_{MCA}	blood flow velocity of middle cerebral artery
VSM	vascular smooth muscle

Chapter 1

Introduction

This chapter introduces the aims of this project, and outlines some of the key aspects of this thesis. In particular the reader is introduced to the medical background pertinent to this project; and the technique of near-infrared spectroscopy (NIRS) is introduced, in particular its application to physiological monitoring. In the subsequent section the computational modelling of physiological systems, mainly the cerebral circulation, is briefly discussed. The last section summarises the details of the subsequent chapters in this thesis.

To the background of this project, this Ph.D. project is part of a large Interdisciplinary Research Consortium (IRC), which comprises four universities, Kings College (KCL), Manchester University, Oxford University and University College London (UCL) working on the topic of "Medical Images and Signals to Clinical Information" (MIAS). In 2001 the original MIAS programme of work was refined and re-structured to three grand challenges (intelligent acquisition, structure and function and multiscale modelling). This Ph.D. thesis is part of the multiscale modelling grand challenge. The primary motivation of this grand challenge is the combination of the large amounts of clinical data (both images and signals) in a coherent, hierarchical way using a series of overlapping mathematical models in order to produce qualitative and quantitative clinical information. In 2001 a sub group was formed in UCL under the guidance of Professor David T. Delpy to tackle the multiscale modelling grand challenge as applied to the brain. This group includes mathematicians working on the mathematical formulation of a computational model of the cerebral circulation and engineers and physicists working in collaboration with clinicians on the collection of physiological signals using a variety of existing and novel techniques. This Ph.D., which began in October 2001, coincided with the start of work by the group at UCL on the development of a physiologically-based model of the cerebral physiology (including haemodynamics, autoregulation and metabolism).

1.1 Objectives and motivations

Measurement and monitoring of changes in haemodynamics and oxygenation in the brain, reliably and non-invasively is a major aim in patient diagnosis and care. The central nervous system (CNS) is a system that functions at a high metabolic rate most of the time. This system is critically dependent on a unique, highly regulated vascular supply for rapid, on demand, regional delivery of oxygen and structural substrates, the removal of toxic metabolic products, a tight control of its fluid, ionic, and temperature environment, and for the transport of significant amounts of neuroendocrine information [1-3]. Therefore monitoring and recording this tight balance of blood flow and metabolites is of great importance, especially during sickness.

The majority of cerebral clinical monitoring techniques are invasive or involve invasive procedures and cover these following main areas of measurement: (i) vessel calibre and flow; (ii) cerebral blood flow (CBF); (iii) cerebral blood volume (CBV); (iv) cerebral blood oxygenation; (v) and levels of cerebral metabolites. One of the emerging technologies in clinical brain monitoring is the technique of near-infrared spectroscopy (NIRS), which is a non-invasive method of monitoring cerebral haemodynamics and oxygenation [4-6]. The relatively low absorption of near-infrared (NIR) light in biological tissue allows the light to penetrate the skin and skull layers and hence to sample the brain tissue beneath. Recent advances in the NIRS technology allow for *absolute* measurements of tissue haemoglobin saturation or cerebral tissue oxygenation, providing clinicians with additional information. The need for understanding and managing the flow of this information and its physiological context has therefore become increasingly important.

The aims of this project were therefore to explore the information derived from NIRS by planning and carrying out clinical studies; to interpret and analyse NIRS and other physiological data using computational and signal processing techniques in order to derive additional knowledge and to extract hidden patterns from the large quantities of experimental data, hence enabling the testing of physiological and clinical hypotheses.

In the challenge of understanding clinical data, the development/synthesis of physiologically based models of cerebral physiology (including haemodynamics, autoregulation and metabolism) can provide us with additional tools [7]. By modelling the cerebral circulation one attempts to understand it and predict its response to various physiological challenges. This could then help with diagnosis by developing clinical intuition and suggesting courses of action for given general scenarios. Linking the model to experimentally measured signals that can be obtained continuously it can also allow the use of the model to identify "state changes" which may be clinically predictive. A key intention of this project was to contribute to the design of the computational model of the cerebrovascular circulation and metabolism and provide some validation by comparisons between simulated and experimental data of the response to physiological challenges.

1.2 Clinical introduction

The circulation of blood in the brain is a complex network of interconnecting vessels with a characteristic ability to maintain total and regional blood flows relatively constant, a property known as flow autoregulation. This homeostatic mechanism allows the blood supply to the brain to match metabolic demands in spite of fluctuations in a number of systemic factors such as blood pressure. Failure of autoregulation can lead to brain ischemia due to reduced blood flow or brain oedema due to excessive blood flow.

Cerebral autoregulation is a topic that has received considerable attention. Investigations, performed mainly in animals, have produced evidence that cerebral autoregulation can be controlled by myogenic, metabolic or neurogenic mechanisms possibly acting in combination via complex feedback pathways [8,9]. The myogenic mechanism relates to an intrinsic ability of arterioles to contract in response to stretching of the vascular wall due to rises in blood pressure. The metabolic hypothesis suggests that the vascular wall responds to both the chemical content of the blood and to disturbances in the environment of the brain tissue. Such disturbances can be caused specifically through vasoactive substances such as oxygen, carbon dioxide, hydrogen ions, nitrous oxide, potassium ions, adenosine and others. Finally the neurogenic

mechanism postulates additional control through mainly sympathetic innervation of cranial vessels.

Cerebral blood flow autoregulation has its limitations; it has both maximal and minimal responses and time delays. These limits become quite important when impaired due to pathologies or by other global, focal, chronic or acute conditions that affect the cerebral physiology. It is therefore important that we monitor this tight control of blood flow and metabolites, and be able to identify the boundaries and ranges of these control mechanisms as they are likely to be altered during disease.

1.3 Near-infrared spectroscopy introduction

In the near-infrared region of the spectrum (700–1000nm), light can travel deep into most tissues, and hence it is a suitable probe for in vivo measurements. Near-infrared oximetry is based on the oxygen dependence of the haemoglobin absorption spectrum (see Chapter 4.3); by comparing light absorption at different wavelengths enables the degree of oxygen saturation in the blood to be measured. NIRS is increasingly used as a non-invasive technique for monitoring cerebral oxygenation and haemodynamics. Simple continuous-wave (CW) NIRS systems utilising differential spectroscopy (i.e. measuring *changes* in attenuation) can measure quantitative *changes* in oxy- and deoxy- haemoglobin concentrations ($\Delta[HbO_2]$, $\Delta[HHb]$) but only from an arbitrary baseline. NIRS can also monitor oxidative processes at the intracellular level via the redox-dependence of the cytochrome c oxidase absorption spectrum. Cytochrome c oxidase (CytOx) is an intracellular respiratory enzyme which interacts directly with oxygen in the cells; hence changes in its absorption can indicate the availability of cellular oxygen.

Recent advances in the NIRS technology have enabled quantitative *absolute* measurements of tissue saturation using spatially resolved spectroscopy (SRS) systems [10]. *Absolute* cerebral tissue oxygenation is the average percentage of oxygenated blood in the brain, and this signal is related not only to the oxygenation status but also depends on the blood volume, flow changes and the oxygen utilisation.

The development of clinical NIRS in the last 15–20 years has seen an increased focus on the monitoring of cerebral function in patients with cerebral global and focal pathologies such as primary autonomic failure, stroke and head injury, patients undergoing surgery such as cardiac bypass and patients under treatment in intensive care units [4,11]. Other fields that NIRS has been extensively applied to include monitoring of the cerebral physiology in the neonate [12], muscle haemodynamics during exercise [6] and functional activation studies [13,14]. The non-invasive nature of the technique, its portability and relatively low cost make it an ideal choice for studying cerebral haemodynamics at the bedside.

1.4 Modelling introduction

The second half of the 20-th century has been marked by an enormous increase in the amount of information regarding the investigation of the brain during health and disease. This flood of data on cerebrovascular physiology and metabolism has provided clinicians with additional information when interpreting individual cerebrovascular phenomena, while in parallel it has challenged researchers in different areas to catalogue the information appropriately. This, together with the fact that cerebrovascular disorders and trauma are one of the major causes of mortality and morbidity in Western Countries today, has led to an interdisciplinary collaboration of physiology, biology, clinical medicine, biomedical engineering, physics and mathematics in a quest to develop computational models of the brain.

Mathematical modelling is widely accepted as an essential tool of analysis in the physical sciences, engineering and biology. Modelling biological systems is not novel, this field of research, often referred to as system biology or computational biology, is 40 years old [15]. Recent developments in the field of biology, especially after the deciphering of the human genome, have led to one of the greatest challenges to researchers and this is the physiome project. The "physiome" is the quantitative and integrated description of the functional behaviour of the physiological state of an individual or species. The physiome describes the physiological dynamics of the normal intact organism and is built upon information and structure (genome, proteome, and

morphome). The term comes from "physio-" (life) and "-ome" (as a whole). In its broadest terms, it should define the relationships from genome to organism and from functional behaviour to gene regulation. The physiome project, includes integrated models of components of organisms, such as particular organs or cell systems, biochemical, or endocrine systems [16,17] (definition taken from http://www.physiome.org/).

In terms of modelling the brain, real progress on attempting to model intracranial dynamics and the cerebral circulation dates back to the 1960's [18,19]. However it is only recently that the modelling of intracranial dynamics has evolved from simplified hydrodynamic or electrical analogue models to computationally complex networks of hundreds of variables and parameters spanning from cellular homeostasis to intracranial haemodynamic and the cerebral autoregulation phenomena. Furthermore the needs to combine models of the systemic physiology (such as baroreceptor regulatory mechanisms and gas exchange) with cerebrovascular models (such as cerebral blood flow regulation and cerebral hydrodynamics) have started to be addressed [20].

Computational models of the physiology and metabolism of the brain are now reaching a significant turning point, where their clinical usefulness can be addressed. Indeed now models are becoming more exact in mimicking the brain, and they are starting to become accepted by a large numbers of medical users [21].

1.5 Thesis overview

Having discussed the main aims of this project, in this section we will give an overview of the development of the thesis.

Chapter 2 introduces the reader to the anatomy of the brain and discusses the main processes involved in the mechanism of cerebral autoregulation. A comprehensive and thorough literature review is provided. Cerebral circulation and pathology are also discussed. Finally a brief description regarding cell metabolism is also given at the end of the chapter.

In Chapter 3 a literature review is provided regarding computational modelling. The aspects of physiological and time series modelling are introduced and explained together with short descriptions of the most cited models. In particular the extensive work by Ursino and colleagues is discussed and presented together with simulations using their 1998 and 2000 models [22,23]. In this chapter the work carried out the last three years in our lab and which has led to the UCL BRAINCIRC cerebral computational model is also discussed.

In Chapter 4 the basis of tissue optics are described and the important optical parameters and equations are explained. Following this, the technique of NIRS is presented in greater detail. The theory and practical aspects of NIRS measurement are described, with emphasis on the NIRO 300 near-infrared spectrometer (Hamamatsu Photonics KK) employed in this project. A detailed description and explanation of the measurements made by this system are given at the end of this chapter.

Chapters 5, 6 and 7 discuss the clinical experiments carried out the last three years together with simulations using the UCL BRAINCIRC cerebral computational model (version 1, 2004-2005) with the clinical experimental data used as an input to the model. Chapters 5 and 6 describe the effects of hypercapnia and hypoxia challenges respectively in young healthy volunteers; Chapter 7 discusses a passive tilt test in patients suffering from primary autonomic failure with severe orthostatic hypotension together with studies on healthy controls. Systematic analysis of the physiological data is presented together with a discussion of the significance of the results and possible explanations of the measurements, in particular the NIRS measurement of cerebral tissue oxygenation. Finally, the model is used to simulate each physiological challenge comparing the predictions to the experimental data with the purpose of testing the correctness of the model.

In Chapter 8 preliminary results are given from recent uncompleted studies both in healthy volunteers and patients identifying additional work yet to be done and highlighting the future directions for both the NIRS studies and the computational model development.

Chapter 9 presents an overall discussion of the results presented in this thesis and the future of both the NIRS and the modelling work is discussed.

1.6 Personal statement

The work presented in the thesis can be broken up into three major parts; these are (i) the description of the cerebral physiological model; (ii) the experimental design and collection of physiological data and (iii) finally, simulations using the model and its comparisons with experimental data. The work described included the collaboration of many individuals and so it is necessary to identify for the reader those components which were carried out by me as part of this Ph.D.

The work in this Ph.D. forms part of a larger IRC project to develop and validate a physiological based model of the cerebral blood flow and metabolism. The model construction was carried out in UCL by Dr Murad Banaji, my main involvement was in carrying out a major review of the existing literature on the cerebral physiology and modelling and assist in the development of some physiological modules.

The majority of the work I carried out was in the design, collection and analysis of the experimental data. This work involved the drafting of ethical committee applications, designing the experiments, setting up and calibrating the physiological monitoring systems, collecting the data (including writing data collection software) and finally carrying out its analysis. All of the experiments described in this thesis were performed in the National Hospital for Neurology and Neurosurgery in London and were carried out with the involvement of clinical colleagues from the department of Neuroanaesthesia and Neurocritical Care under the supervision and guidance of Dr M. Smith.

The final major element of this thesis comprises the processing and analysis of the experimental data and its comparison with predictions of the model. The cerebral physiological model developed in UCL is a computational model based on physiological concepts, which need to be tested with experimental data. In this thesis, the physiological data that I have collected has been used with the model to test its

response and accuracy. I have carried out the computational simulations and performed the analysis of the models outputs and comparisons with the measured data that are reported here.

Both the modelling and the experimental parts of this project are part of a continuous development, mutually providing and feeding back data to improve the model and to help explain the experimental observations. As parts of this work, other studies have been undertaken, which are not discussed in this thesis, but the publication arising from these are included in Appendix C.

References

1. H. Goldman, "Techniques for measuring cerebral blood flows," *The regulation of cerebral blood flow,* Phillis J.W., ed., (CRC Press, Florida, 1993), 3-32.

2. R.B. Panerai, "Assessment of cerebral pressure autoregulation in humans-a review of measurement methods," *Physiol. Meas.* **19**, 305-338 (1998).

3. U. Dirnagl, L. Edvinsson, and A. Villringer, "Measuring cerebral blood flow and metabolism," *Cerebral blood flow and metabolism,* Edvinsson L. and Krause D.N., eds., (Lippincott Williams & Wilkins, Philadelphia, 2002), 371-383.

4. H. Owen-Reece, M. Smith, C.E. Elwell, and J.C. Goldstone, "Near infrared spectroscopy," *Br. J. Anaesth.* **82**, 418-426 (1999).

5. A.K. Gupta and A. Summors, "Near infrared spectroscopy," *Notes in neuroanaesthesia and critical care,* Gupta A.K. and Summons A., eds., (Greenwich Medical Media Ltd, London, 2001), 229-232.

6. M. Ferrari, L. Mottola, and V. Quaresima, "Principles, techniques, and limitations of near infrared spectroscopy," *Can. J. Appl. Physiol.* **29**, 463-487 (2004).

7. M. Banaji, I. Tachtsidis, D.T. Delpy, and S. Baigent, "A physiological model of cerebral blood flow control," *Mathematical Bioscienses* **194**, 125-173 (2005).

8. L. Edvinsson, E.T. MacKenzie, and J. McCulloch, "Autoregulation: Arterial and intracranial pressure," *Cerebral blood flow and metabolism,* Edvinsson L., MacKenzie E.T., and McCulloch J., eds., (Raven Press, New York, 1993), 553-580.

9. L. Edvinsson, E.T. MacKenzie, and J. McCulloch, "Changes in arterial gas tensions," *Cerebral blood flow and metabolism,* Edvinsson L., MacKenzie E.T., and McCulloch J., eds., 1993), 524-552.

10. S. Suzuki, S. Takasaki, T. Ozaki, and Y. Kobayashi, "A tissue oxygenation monitor using NIR spatially resolved spectroscopy," *Proc. SPIE* **3597**, 582-592 (1999).

11. P.L. Madsen and N.H. Secher, "Near-infrared oximetry of the brain," *Prog. Neurobiol.* **58**, 541-560 (1999).

12. J.S. Wyatt, M. Cope, D.T. Delpy, C.E. Richardson, A.D. Edwards, S. Wray, and E.O. Reynolds, "Quantitation of cerebral blood volume in human infants by near-infrared spectroscopy," *J. Appl. Physiol.* **68**, 1086-1091 (1990).

13. H. Obrig and A. Villringer, "Beyond the visible--imaging the human brain with light," *J. Cereb. Blood Flow Metab.* **23**, 1-18 (2003).

14. M.L. Schroeter, M.M. Bucheler, K. Muller, K. Uludag, H. Obrig, G. Lohmann, M. Tittgemeyer, A. Villringer, and D.Y. von Cramon, "Towards a standard analysis for functional near-infrared imaging," *NeuroImage* **21**, 283-290 (2004).

15. P. J. Hunter, "Putting Humpty Dumpty back together again," *The Scientist* **17**, 20-21 (2003).

16. P.J. Hunter, P.M. Nielsen, and D. Bullivant, "The IUPS Physiome Project. International Union of Physiological Sciences," *Novartis Found Symp.* **247**, 207-217 (2002).

17. P.J. Hunter, P. Robbins, and D. Noble, "The IUPS human Physiome Project," *Pflugers Arch.* **445**, 1-9 (2002).

18. W.A. Himwich, F.M. Knapp, R.A. Wenglarz, J.D. Martin, and M.E. Clark, "The circle of Willis as simulated by an engineering model," *Arch. Neurol.* **13**, 164-172 (1965).

19. M.E. Clark, J.D. Martin, R.A. Wenglarz, W.A. Himwich, and F.M. Knapp, "Engineering analysis of the haemodynamics of the circle of Willi's," *Arch. Neurol.* **13**, 173-182 (1965).

20. K. Lu, J.W. Clark, F.H. Ghorbel, C.S. Robertson, D.L. Ware, J.B. Zwischenberger, and A. Bidani, "Cerebral Autoregulation and Gas Exchange Studied Using A Human Cardiopulmonary Model," *Am. J. Physiol.* **286(2)**, H584-H601 (2003).

21. M. Ursino, "Cerebrovascular modelling: a union of physiology, clinical medicine and biomedical engineering," *Medical Engineering & Physics* **25**, 617-620 (2003).

22. M. Ursino and C.A. Lodi, "Interaction among autoregulation, CO_2 reactivity, and intracranial pressure: a mathematical model," *Am. J. Physiol.* **274** , H1715-H1728 (1998).

23. M. Ursino, A. Ter Minassian, C.A. Lodi, and L. Beydon, "Cerebral hemodynamics during arterial and CO_2 pressure changes: in vivo prediction by a mathematical model," *Am. J. Physiol.* **279**, H2439-H2455 (2000).

Chapter 2

Anatomical and Physiological Background of the Cerebral Circulation

In this chapter an overview of the brain anatomy, physiology and biochemistry (from cell to tissue) is provided. The important concept of cerebral autoregulation is extensively discussed together with paradigms of blood flow and oxygenation maintenance. For more rigorous and detailed information the reader is advised to look in brain physiology text books [1-4]. Finally a short discussion on brain pathology and cell biochemistry is given at the end.

2.1 Anatomical and Physiological Basis

In conjunction with the spinal cord, the brain forms part of the body's central nervous system (CNS). The brain contains tens of billions of neurons organized into hundreds of neuronal pools; it has a complex three-dimensional structure and performs a bewildering array of functions.

The adult human brain contains about 98% of the body's neural tissue. A "typical" brain weights 1400gr and has a volume of 1200cc. The average adult man's brain weighs about 1600gr; that of a woman averages 1450gr; in terms of brain weight per body weight, however, males and females have equivalent brain sizes.

2.1.1 Introduction

The brain is surrounded and protected by a bony enclosure (the skull), membranes (the meninges), and a watery cushion (CSF). Figure 2.1 shows the gross anatomy of the brain and its four main regions: (1) cerebral hemispheres, (2) diencephalons, (3) brain stem and (4) cerebellum.

The cerebral hemispheres and cerebellum have grey matter nuclei[1] surrounded by white matter[2] and an outer cortex of grey matter. An outer layer approximately 5mm in thickness, known as the cerebral cortex, covers the cerebral hemispheres. The cortex consists of grey matter and is highly folded into ridges and dips, known as gyri and sulci, which greatly increase its surface area. The brain stem lacks a cortex.

[1] Gray matter is the area in the CNS that is dominated by neuronal cell bodies, neuroglia and unmyelinated axons.

[2] White matter is the region in the CNS that is dominated by myelinated axons.

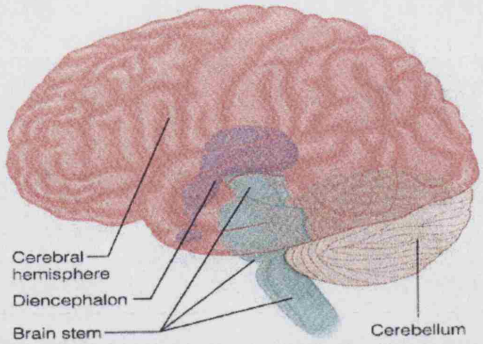

Figure 2.1: Regions of the brain (taken from [5]).

Tightly covering the convoluted surface of the cortex is the pia mater. External to this is the arachnoid mater, a loose covering that does not follow the contours of the cortex. In between the pia mater and the arachnoid mater is the subarachnoid space, which is filled with CSF and contains the blood vessels that serve the brain. Finally inward folds of the inner layer of the dura mater secure the brain to the skull. The two layers of the dura mater, the meningeal and the periosteal layer are fused together except where they surround large chambers known as the dural sinuses into which most of veins in the brain drain.

The cerebrum consists of two cerebral hemispheres, which form the most superior part of the brain (Figure 2.2). Each cerebral hemisphere consists of the cerebral cortex, the cerebral white matter, and the basal nuclei.

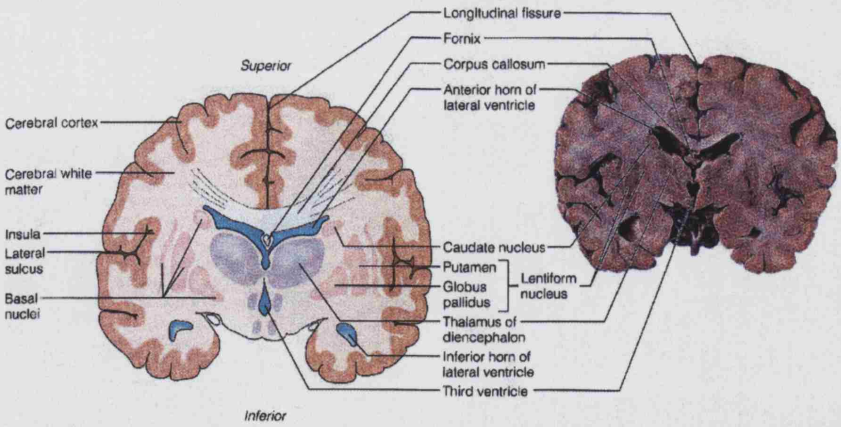

Figure 2.2: Major regions of the cerebral hemispheres. The human brain has been sectioned coronally to reveal the relative positions of the cerebral cortex, white matter, and basal nuclei within the cerebral hemispheres. Since the cerebral hemispheres enclose the structures of the diencephalon, that region of the cerebrum is also shown (taken from [5]).

The nerve axons in the sub-cortical white matter provide the route by which information is passed between different parts of the cerebral cortex and also to other parts of the CNS. Deep within the hemispheres are the basal nuclei, or basal ganglia, shown in Figure 2.2, clusters of nuclei that, in tandem with the motor cortex, are involved in the control of movement.

2.1.2 The ventricles of the brain

The brain includes four ventricles filled with cerebrospinal fluid (or CSF) as illustrated in Figure 2.3. The lateral ventricles are in the cerebral hemispheres; the third ventricle is in the diencephalon; the fourth ventricle is in the brain stem and connects with the central canal of the spinal cord.

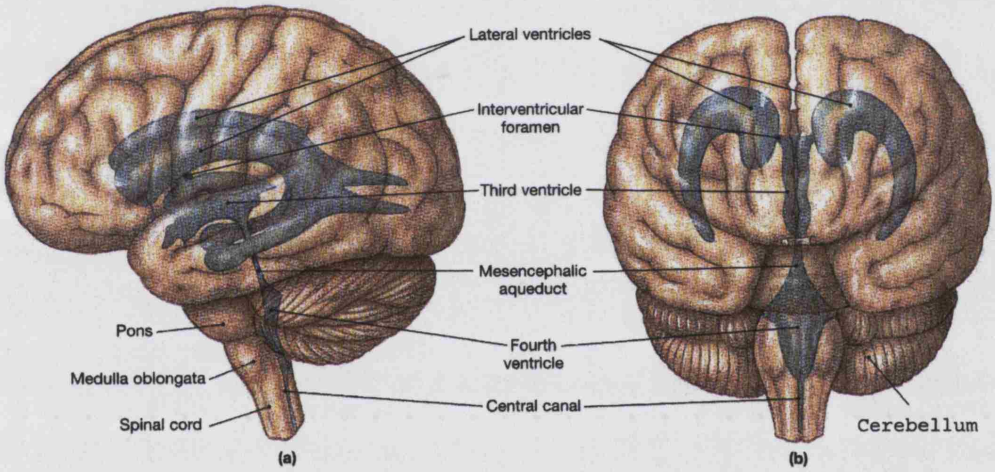

Figure 2.3: Ventricles of the brain (taken from [6]). The orientation and extent of the ventricles as they would appear if the brain were transparent. **(a)** A lateral view; **(b)** An anterior view.

2.1.3 The cerebrospinal fluid

The cerebrospinal fluid, found in and around the brain and spinal cord, forms a liquid cushion [5]. By floating the brain, the CSF effectively reduces brain weight by 97% and prevents the brain from crushing under its own weight. CSF also protects the brain and spinal cord from blows and other trauma. Additionally, although the brain has a rich blood supply, cerebrospinal fluid helps to nourish the brain.

CSF is a watery "broth" similar in composition to blood plasma, from which it arises (see Table 2.1). CSF composition is important in the control of cerebral blood flow.

Table 2.1: Comparison of the chemical composition of blood plasma and cerebrospinal fluid (taken from [7]).

Component	Blood Plasma	Cerebrospinal Fluid
Protein	60-80 gr/l	200-400 mgr/l
Urea	2.5-6.5 mmoles/l	2.0-7.0 mmoles/l
Glucose (fasting)	3.0-5.0 mmoles/l	2.5-4.5 mmoles/l
Sodium	136-148 mmoles/l	144-152 mmoles/l
Potassium	3.8-5.0 mmoesl/l	2.0-3.0 mmoles/l
Calcium	2.2-2.6 mmoles/l	1.1-1.3 mmoles/l
Chloride	95-105 mmoles/l	123-128 mmoles/l
Bicarbonate	24-32 mmoles/l	24-32 mmoles/l

The choroid plexus that hang from the roof of each ventricle (Figure 2.4) forms CSF. These plexus are frond-shaped clusters of broad, thin-walled capillaries enclosed by a layer of ependymal cells lining the ventricles. The capillaries of the choroids plexus are fairly permeable and tissue fluid filters continuously from the bloodstream. In adults the total CSF volume of about 150ml is replaced every 3 to 4 hours; hence 900-1200ml of CSF are formed daily [5]. The choroid plexus also help to cleanse the CSF by removing waste products and other unnecessary solutes.

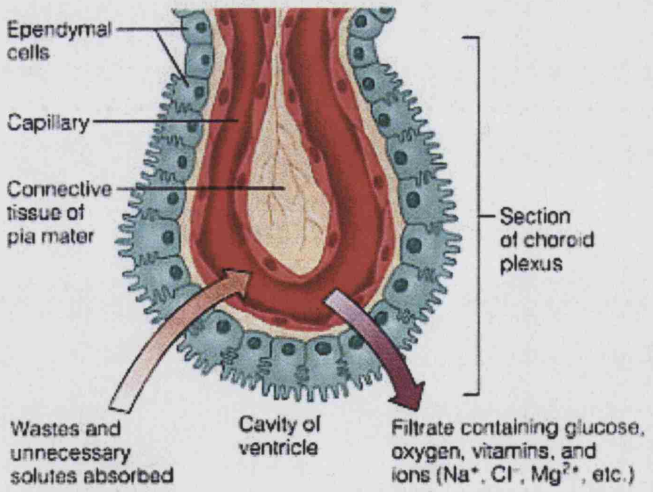

Figure 2.4: Choroid plexus forms CSF. Each choroid plexus consists of porous capillaries surrounded by a single layer of ependymal cells joined by tight junctions and bearing long microvilli with blunted ends. Although the filtrate moves easily from the capillaries, it must move through and be processed by the ependymal cells before it is allowed to enter the ventricles as cerebrospinal fluid (taken from [5]).

Once produced, CSF moves freely through the ventricles. Some CSF circulates from the ventricles into the central canal of the spinal cord, but most enters the subarachnoid space.

2.1.4 The cerebral circulation

Blood is transported through out the body via a continuous system of blood vessels. Arteries transport blood away from the heart; veins carry blood back to the heart and capillaries carry blood to tissue cells comprising the exchange sites.

All blood vessels except capillaries have three layers (Figure 2.5): tunica intima (or interna), tunica media, and tunica adventitia (or externa); capillary walls are composed of the tunica intima only [8].

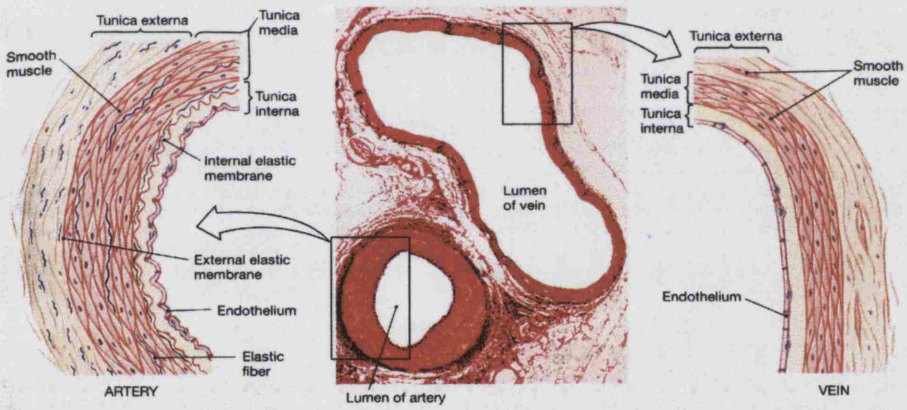

Figure 2.5: A comparison of a typical artery and a typical vein (taken from [9]).

The tunica intima contains the endothelium, the simple squamous epithelium that lines the lumen of all vessels. The tunica media is mostly circularly arranged smooth muscle cells and sheets of elastin. The activity of smooth muscle is regulated by vasomotor nerve fibres of the sympathetic division of the autonomic nervous system [8,9]. The tunica adventitia, the outermost layer of the blood vessel wall is composed largely of loosely woven collagen fibres that protect the blood vessel and anchor it to surrounding structures.

The blood-brain barrier (or BBB) is the specialized system of capillary endothelial cells that protects the brain from harmful substances in the blood stream, while supplying the

brain with the required nutrients for proper function. Unlike peripheral capillaries that allow relatively free exchange of substance across/between cells, the BBB strictly limits transport into the brain through both physical (tight junctions) and metabolic (enzymes) barriers. Thus the BBB is often the rate-limiting factor in determining permeation of therapeutic drugs into the brain. The BBB is a selective rather than an absolute barrier. Nutrients such as glucose, essential amino acids, and some electrolytes, move passively by facilitated diffusion through the endothelial cell membranes. Bloodborne metabolic wastes, such as urea and creatinine, as well as proteins, certain toxins and most drugs are prevented from entering brain tissue. Small non-essential amino acids and potassium ions are not only prevented from entering the brain, but also actively pumped from the brain across the capillary endothelium [5]. The barrier is ineffective against fats, fatty acids, oxygen and carbon dioxide, and other fat soluble molecules that diffuse easily through all plasma membranes. This explains why bloodborne alcohol, nicotine, and anesthetics can affect the brain.

The brain constitutes 2% of total body weight but receives 15% of cardiac output [10]. Oxygen and glucose utilization are also high compared with that of other organs (Table 2.2). The vascular anatomy is unusual in that multiple potential collateral channels exist to supply the high blood flow and metabolism. Since the brain is contained within the rigid skull, cerebral blood volume must be tightly controlled to prevent elevation of intracranial pressure (or ICP).

Table 2.2: Cerebral blood flow and metabolic rate in normal young adult man (taken from [10]).

	Per 100gr of brain tissue per min	**Average per total brain per min***
Cerebral blood flow	57ml	798ml (15% of cardiac output)
Cerebral oxygen consumption	3.5ml (156mmoles/l)	49ml (20% of basal body O_2)
Cerebral glucose utilization	5.5mgr (31mmoles/l)	77mgr

*Calculated on basis of assumed brain weight of 1.4Kg (2% of body weight).

2.1.4.1 The cerebral arterial system

Compared to other organs the brain is singular in that it is supplied by four major arteries that eventually coalesce to form an equalizing distributor: "the circle of

Willis" [11-13]. These primary vessels are two carotid and two vertebral arteries, which unite intracranially to form the basilar artery. The carotid arteries are quantitatively more important, each contributing approximately 40% to the total perfusion of the brain [13]. Therefore the carotid arteries contribute 335ml/min, whereas the vertebral-basilar flow is 75ml/min [10].

The circle of Willis is a pentagonal formation of anastomosing arteries located at the central base of the cranial cavity and supplied by the two internal carotid arteries and the basilar artery. It is formed in the front by the anterior cerebral arteries, branches of the internal carotid, which are connected together by the anterior communicating artery; and at the rear, by the two posterior cerebral arteries, branches of the basilar, which are connected on either side with the internal carotid by the posterior communicating artery (Figure 2.6).

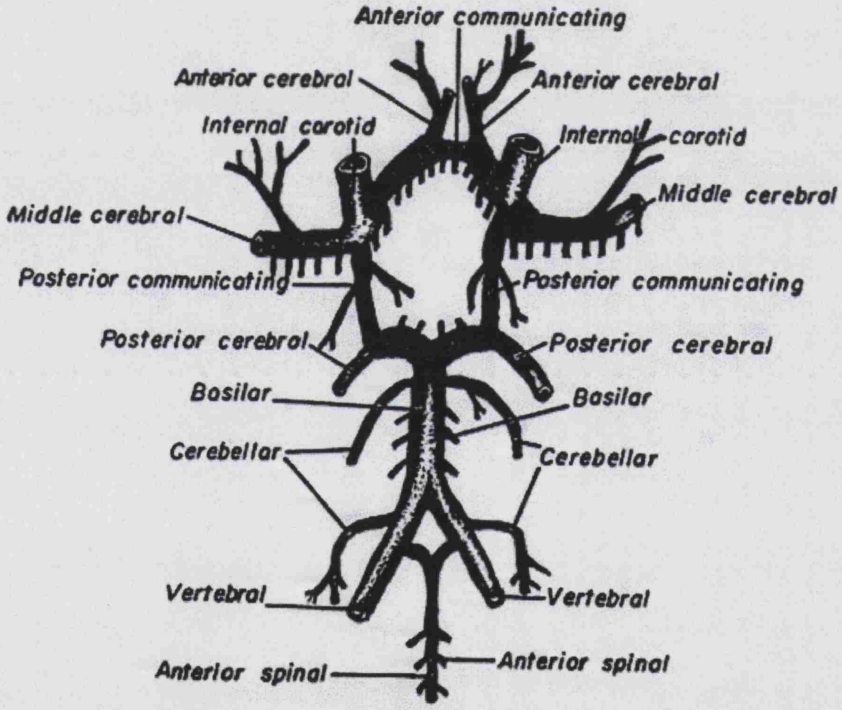

Figure 2.6: The circle of Willis in man (taken from [12]).

It should however be stressed that the arrangement just described is only the most frequent situation, there is considerable variation not only in man but also in experimental animals.

2.1.4.2 The cerebral venous system

The major fraction of the blood that drains the brain is collected in the transverse sinus, which together with the inferior petrosal sinus, forms the internal jugular vein (Figure 2.7). A small fraction of cerebral blood, mainly from the occipital sinus, is drained into the internal vertebral plexus.

The venous return from the brain is accomplished through vessels of three groups – superficial cerebral veins, deep cerebral veins, and cerebral venous sinuses.

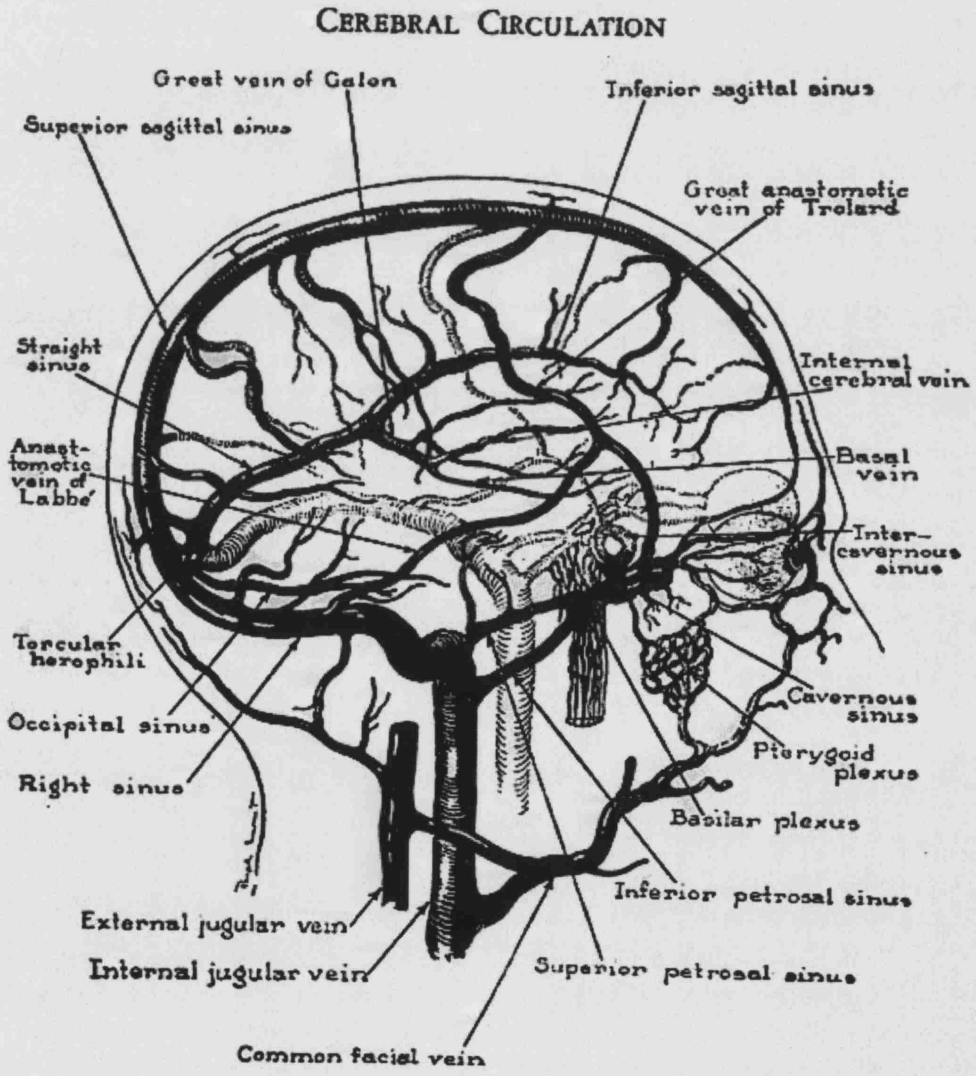

Figure 2.7: The cerebral venous system (taken from [12]).

2.2 Cerebral autoregulation

Autoregulation of blood flow has occasionally been defined in a broad sense as the capability of an organ to regulate its blood supply in accordance with its needs [14].

Although the brain is the most metabolically active organ in the body, it is the least able to store essential nutrients [5]. Cerebral blood flow is regulated by one of the most precise autoregulatory systems in the entire body and is tailored to local neuronal need.

As mentioned before total blood flow to the brain averages about 750ml/min (about $57ml.100g^{-1}.min^{-1}$) and is maintained at relatively constant levels. The necessity for constant cerebral blood flow becomes crystal clear when one remembers that the brain lies within the rigid cranium and neurons are totally "intolerant" of ischemia. The factors controlling cerebral blood flow are, therefore, of considerable importance.

A characteristic feature of the cerebral circulation is its ability to maintain total and regional blood flows relatively constant over a wide range of arterial blood pressures [15]. The independence of cerebral blood flow (CBF) from arterial blood pressure typically is called cerebral autoregulation. Another way to define cerebral autoregulation is as the intrinsic ability of the cerebral resistance vessels to alter their calibre and maintain a constant blood flow in the face of alterations in perfusion pressure (the difference between mean arterial pressure and intracranial pressure) [16,17]. The importance of autoregulation is that it allows blood flow to match metabolic needs in spite of fluctuations in arterial blood pressure by maintaining capillary perfusion pressure at levels to ensure adequate capillary exchange.

Cerebral autoregulation is a topic that has received considerable attention. While it is clear that cerebral autoregulation occurs, and that a number of factors are able to modulate vascular responses, the underlying mechanisms driving cerebrovascular adjustments to changes in arterial blood pressure are controversial. The purpose of the next sections is to discuss the characteristics and mechanisms of cerebral autoregulation.

2.2.1 Perfusion pressure and blood flow relationship

The perfusion pressure of the blood supplying the brain is the difference between the mean arterial blood pressure (MBP) and the intracranial pressure. MBP can be altered over a fairly wide range (about 50 and 150 mmHg) without affecting CBF (Figure 2.8). This is effected by constriction of the cerebral arterioles during increases in MBP and dilatation when the MBP is lowered. There are higher and lower limits beyond which the autoregulatory mechanism fails. At MBP above 150mmHg there is force dilation of the cerebral vessels, the flow rises and cerebral oedema eventually results giving a clinical condition known as hypertensive encephalopathy. At extreme hypotension, flow falls with pressure and signs of cerebral ischemia become evident.

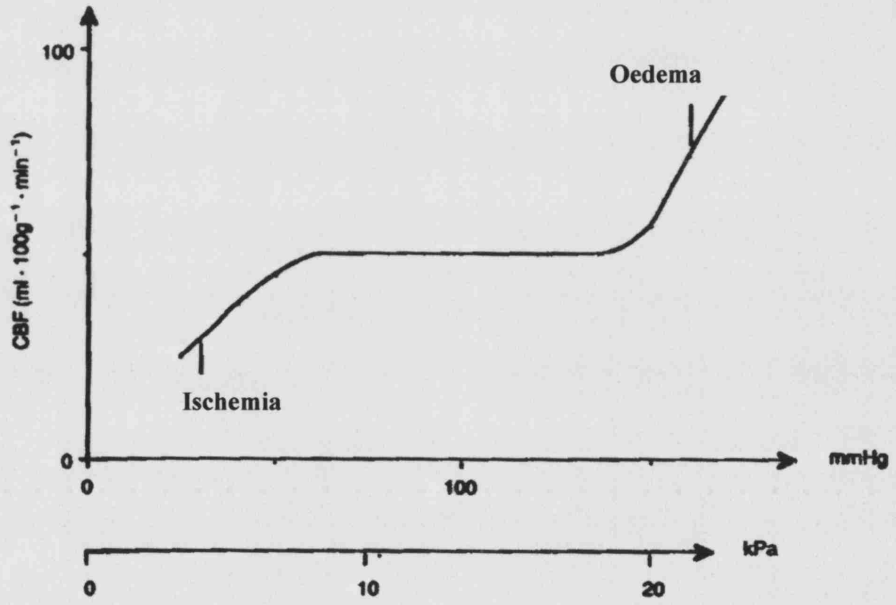

Figure 2.8: Diagram showing the response of the cerebral circulation to changes in arterial blood pressure with the upper and lower limits of autoregulation (taken from [16]).

2.2.2 Mechanisms of autoregulation

Considerable controversy exists concerning the mechanisms underlying autoregulatory responses in the cerebral circulation [15]. There are three main hypotheses, which would account for cerebral arteriolar constriction or vasodilation in response to hypertension or hypotension [16,18].

2.2.2.1 The metabolic hypothesis

The various metabolic hypotheses are primarily based on the supposition that a decrease in blood flow causes vascular relaxation by accumulation of vasodilator metabolites in the tissue or by decreased nutrient supply [14]. One possible metabolic scheme postulates that a reduction in blood pressure causes a transient reduction in flow, which allows a build up of metabolites, which in turn causes vasodilatation and a restoration of flow [16]. A broader explanation is that metabolic regulation of blood flow in any tissue may be defined as adjustments in blood flow, which are elicited by and in the same direction as changes in the metabolic activity of that tissue [19]. Hence, increased perfusion pressure will result in the increased washout of dilator metabolites while the opposite effects occur at reduced perfusion pressures.

Metabolic factors are currently thought to play an important role in cerebral autoregulation include extracellular fluid concentrations of CO_2, H^+, O_2, K^+, Ca^{++}, adenosine, adenine nucleotides and prostagladins [15,18,20]. The most powerful systemic stimulus is elevation of the arterial partial pressure of CO_2 ($PaCO_2$) (discussed later).

Summarising one could ask whether the metabolic hypothesis regarding the blood pressure changes primarily involves metabolic molecules released either during hypertension or hypotension inducing vasoconstriction or vasodilation respectively, or if autoregulation is mediated by a secondary release of molecules triggered by the primary metabolites. In a later chapter the role of the primary metabolites is identified and discussed.

2.2.2.2 The myogenic hypothesis

Autoregulation of cerebral vessels could result from an intrinsic property of vascular smooth muscle to contract in response to a rise in transmural pressure (known as the Bayliss effect [21]).

The rapidity of the autoregulatory response, which is initiated within a few seconds after a change in transmural pressure of the resistance vessels and largely completed

within 15 to 30 seconds, favours a myogenic response [17]. According to this hypothesis a quick change in intravascular pressure alters the state of the actin and myosin filaments in the smooth muscle cells.

Smooth muscle strips from certain arteries contract when stretched [22]. The mechanism, however, by which a force applied to vascular smooth muscle initiates an active response, are not well understood. Myogenic mechanisms would represent events intrinsic to the vessel wall. Numerous investigators have shown that cerebral arterioles in vitro develop tone [23,24]and that this tone can be augmented by increasing intraluminal pressure via a calcium dependent mechanism [23-25]. Thus, it is possible that stretching arterial muscle cells results in activation by alteration of membrane permeability to ions. Harder and colleagues [26] observed in middle cerebral arteries from cats that changes in intracellular membrane potential were positively correlated with alterations in transmural pressure. Ngai and Winn [27] observed by in vitro experiments on rat cerebral arteries that increasing pressure at zero flow in 20mmHg steps from 20 to 100mmHg resulted in myogenic regulation of cerebral arterial diameter. They observed that with a step increase in pressure from 20 to 40mmHg, the vessels constricted by 16% and in most cases required 1 to 2 minutes to attain steady state diameter. The next step increase in pressure from 40 to 60mmHg induced a smaller constrictor response (5%). Further increase in pressure did not enhance tone but instead led to a progressive increase in vessel diameter. Elevating pressure to or beyond 100mmHg in a few experiments resulted in failure to regain control diameter, probably because of irreversible damage caused by forced distension.

Associated with maintained tone or increased tone during increased intraluminal pressure is progressive smooth muscle depolarisation. Ever since the first description of the myogenic response by Bayliss [21], the site of mechanoreception in the vessel wall to pressure has been attributed to the vascular smooth muscle [22]. More recently, however, there is dispute as to whether the endothelium may act as the sensor in contractile responses to pressure [28]. It is possible that the endothelial cells may serve as a transducer in the autoregulatory response to pressure [24].

Furthermore, numerous investigations in isolated artery segments have shown that endothelial cells may cause relaxation of vascular smooth muscle by the release of an

endothelium derived relaxing factor (EDRF or nitric oxide). The presence of an endothelium-derived contractile factor (EDCF) has been presented as well. Harder and colleagues [29] have shown that endothelium removal abolishes maintenance of constriction of tone during increased intraluminal pressure and that the endothelium-derived factor is transferable to intact vessel segments. Rubanyi and colleagues [30] addressed the role of the endothelium in pressure-induced vasoconstriction in the cerebral vessels. A rapid increase in transmural pressure triggered active contraction that was prevented by the removal of endothelium. This response was considered to be mediated by depression of the synthesis and/or release of EDRF.

Finally there is evidence for the presence of a secondary shear stress mediated response due to changes in flow caused by changes in pressure. Increments in flow without changes in transmural pressure through isolated vessel sections both in situ and in vitro apply shear stress forces on the arterial endothelium, which induce vasodilation that can be abolished by the removal of endothelium [31,32]. These observations suggest that endothelial cells release a vasodilator mediator in response to shear stress caused by an increase in flow [17]. Ngai and Winn [27] found that flow induced dilator responses of segment of rat cerebral arterioles are mediated by an arginine metabolite, such as nitric oxide (or NO). The above conclusions can lead to the belief that there is an additional response caused by flow and that is present in the original vasodilation induced by increased arterial blood pressure and that this secondary response is mediated via the endothelium and involves NO.

In summary because of the physiological significance of the myogenic response, its mechanistic basis represents an important subject for research [28]. Currently there are several broad hypotheses concerning the sequence of events that couple changes in intravascular pressure or stretch with alterations in vascular smooth muscle activation. These hypotheses include: (i) altered membrane properties leading to activation of ion channels; (ii) modulation of biochemical cell signalling pathways within vascular smooth muscle; (iii) length-dependent changes in contractile protein function and (iv) endothelial-dependent modulation of vascular smooth muscle tone (for further reading the reader is referred to Meininger and Davis [28]).

2.2.2.3 The neurogenic hypothesis[3]

Cerebral blood vessels are supplied extensively by several different types of innervation, including sympathetic, parasympathetic and sensory fibres [18]. In addition, it has been suggested that cerebral pathways, existing exclusively within the brain itself, supply innervation to cerebral resistance vessels [15]. Thus the potential exists for nerves to play a role in cerebral autoregulation.

It has been argued that the vasoconstriction and vasodilatory responses to changes in blood pressure are under sympathetic or parasympathetic control. However autoregulation is still preserved after surgical division of aortic and carotid sinus nerves (a component of a possible reflex arc) and after division or chemical blockade of the cervical sympathetic and parasympathetic nerves which accompany the major cerebral arteries [16]. While it is clear that cerebral autoregulation occurs despite removal of various neural influences, it is clear that nerves can modulate various features such as speed of vascular responses and the range over which autoregulation occurs.

Neither surgical division nor electrical stimulation of the cervical sympathetic nerves influences cerebral blood flow under normal conditions. There is a modest constriction of the pial arterioles during sympathetic stimulation, but presumably this is accompanied by a fall in blood pressure in the more distal arterioles in the brain parenchyma, which undergo the usual autoregulatory vasodilation and resulting in a constant blood flow [33]. Sympathetic nerves clearly are able to modify the cerebrovascular response to changes in arterial blood pressure. Busija and colleagues [34] observed in anaesthetized cats that when arterial blood pressure is raised abruptly but is still within the autoregulatory range, there is a transient rise in CBF before autoregulatory adjustments are able to restore CBF back to control; they also found that under these conditions, electrical stimulation of sympathetic nerves is able to dramatically attenuate this cerebral hyperaemia. Their conclusions show that the cervical sympathetic response has a very important function, namely in protecting the

[3] The UCL Braincirc version 1.0 (2004-2005) model described in later chapters currently does not include the neurogenic feedback pathway. A recent publication [93] has measured in cats the CBV changes resulting from a neurogenic stimulation and observe a clear vascular response. They found that the arteries, arterioles and capillaries showed the largest responses whereas the venous response was the smallest.

cerebral capillaries from sudden surges in arterial blood pressure. An acute and severe rise in arterial blood pressure could result in overwhelming of autoregulatory vasoconstriction and hence a sudden rise in blood flow; this is prevented by constriction of the inflow tract and pial arteries and arterioles by the cervical sympathetic system [33]. Figure 2.9 shows the shift of the autoregulatory curve to the right during electrical stimulation of the cervical sympathetic nerves.

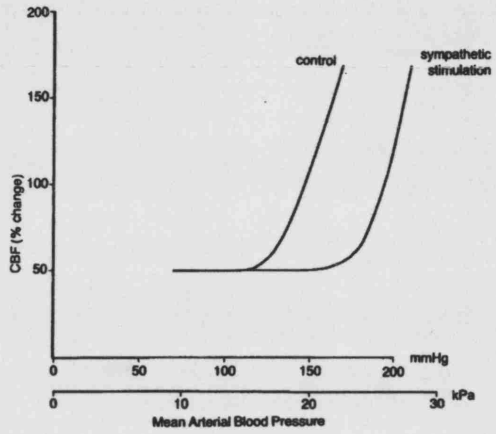

Figure 2.9: During cervical sympathetic stimulation the threshold for break through is raised considerably in this case from a mean arterial BP of 130mmHg to 160mmHg (taken from [16]).

The sympathetic nervous system predominantly exerts its vasomotor function in the larger cerebral resistance vessels, whereas autoregulation predominantly is a function of the smaller resistance vessels [35]. During sympathetic activation with constriction of the larger resistance vessels, the smaller resistance vessels further downstream will dilate as an autoregulatory response to keep blood flow constant as long as arterial pressure is within the autoregulatory range; the opposite takes place if the sympathetic tone is reduced [17]. It is only at the limits of the autoregulation that the vasomotor function of the larger resistance vessels may affect cerebral tissue perfusion because the smaller resistance vessels no longer have any autoregulatory capacity. Thus, in case of hypotension the larger resistance vessels have constricted and the smaller ones have dilated as an autoregulatory response, then less capacity is left for further autoregulatory dilation of the smaller vessels [36]. If systemic blood pressure now is lowered, the lower limit of autoregulation will be reached at a higher pressure than if the larger resistance vessels had not constricted [17].

Parasympathetic nerve supply also has no effect on CBF under normal conditions, although in certain circumstances cholinergic nerves have been shown to have a

cerebral vasodilatory effect [33,37]. Branston and colleagues [38] in a study performed on normotensive rats conclude that parasympathetic fibres do not contribute to the tonic level of regional cerebral blood flow or its autoregulatory control, but parasympathetic fibres conduct impulses tending to resolve postischaemic hyperaemia. Kano and colleagues [39] also observed that there is a protective role for autonomic parasympathetic fibres in the pathophysiology of focal cerebral ischemia. Koketsu et al [40] confirmed the results of Kano et al [39] by observing increases in the volume of infarction (by 30%, from 155-198mm^3), after sectioning the parasympathetic innervation to the circle of Willis in spontaneously hypertensive rats.

Finally, considerable interest has focused on the possibility that pathways that exist entirely within the brain innervate cerebral blood vessels, and that activation of these pathways can alter CBF independently of changes in metabolic rate and can alter characteristics of the blood-brain barrier [15]. Functional studies have provided evidence that central innervation may play an important role in control of CBF, however at present anatomical evidence establishing such a connection are not well documented (for further information the reader is referred to Busija [15]).

2.3 Blood gases and cerebral blood flow

The maintenance of an adequate blood supply to the brain implies a matching of the flow rate in microvessels to the metabolic requirements of the tissues they perfuse [15]. Maintenance of appropriate levels of oxygen and carbon dioxide in the blood is very important for normal cerebral metabolism. A significant amount of oxygen is utilized for oxidative phosphorylation on a continuing basis by brain tissue, and carbon dioxide, the principal end-product of aerobic metabolism, must be constantly removed. Oxygen and carbon dioxide readily diffuse across the microvessels wall and hence their tensions (partial pressures) in the blood in cerebral microvessels and in surrounding tissues tend to be in equilibrium under normal physiological conditions. The relationships between the oxygen and carbon dioxide contents of arterial blood and cerebral blood flow have been extensively investigated, and they will be briefly discussed here [1,3,4,18,41-45].

2.3.1 Carbon dioxide and the cerebral circulation

Since the middle of the 19th century, direct observation of the cortical vasculature has shown that an increase in CO_2 will provoke a generalized vasodilation of the pial circulation [46]. Observers also noted that the dilation occurred without a change in arterial pressure, which could account for it; indeed hypercapnia was invariably accompanied by a rise in intracranial pressure and following this reduction in perfusion pressure, the dilation became more significant [47].

The cerebral blood flow is very sensitive to changes in arterial carbon dioxide. An increase in $PaCO_2$ (hypercapnia) results in marked rises in CBF; a decrease in $PaCO_2$ (hypocapnia) produce a fall in CBF (Figure 2.10).

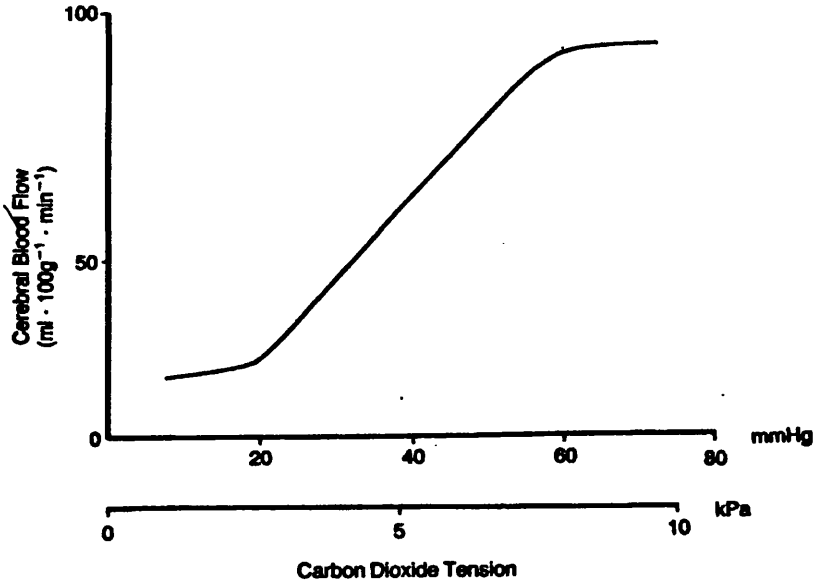

Figure 2.10: The response of the cerebral circulation to changes in arterial carbon dioxide tension (taken from [16]).

There are upper and lower limits to the response. The vasodilatory effect of an increase in $PaCO_2$ is in an increase in CBF of approximately $3ml.100gr^{-1}.min^{-1}$ for every 1mmHg (0.13Kpa) rise in $PaCO_2$ in the range 40-60mmHg (5.3-8.0KPa). Below 40mmHg (5.3KPa), flow falls progressively with reduction in $PaCO_2$ until 20mmHg (2.7KPa), there is no further reduction in flow below this value [16].

Several hypothesis have been introduced regarding how CO_2 alters cerebrovascular tone, the most favoured hypothesis is that $PaCO_2$ affects cerebrovascular tone via changes in the interstitial fluid pH [15,46]. Additional research on hyper and hypocapnia evoked increases or decreases in CBF excluding the pH mediated changes have also been focused on other additional metabolic factors, some of which are adenosine [48-50], nitric oxide [51,52] and prostanoids [18,53-55].

The highly diffusible CO_2 molecule can readily circumvent the blood-brain barrier mechanisms that reside in cerebral endothelial cells (Figure 2.11). New sophisticated methods for the measurement of pial arteriolar calibre have shown that the topical application of low-pH solution induces vasodilation, whereas the perivascular instillation of high-pH solution provokes vasoconstriction. These responses are observed with solutions of varying $PaCO_2$ but constant bicarbonate (HCO_3^-) concentrations as well as with those of constant $PaCO_2$ and varying HCO_3^- concentrations [56,57]. From these and similar experiments the concept has arisen that systemic CO_2 exerts its cerebrovascular effects by modulating extracellular pH in the immediate vicinity of the smooth muscle cells.

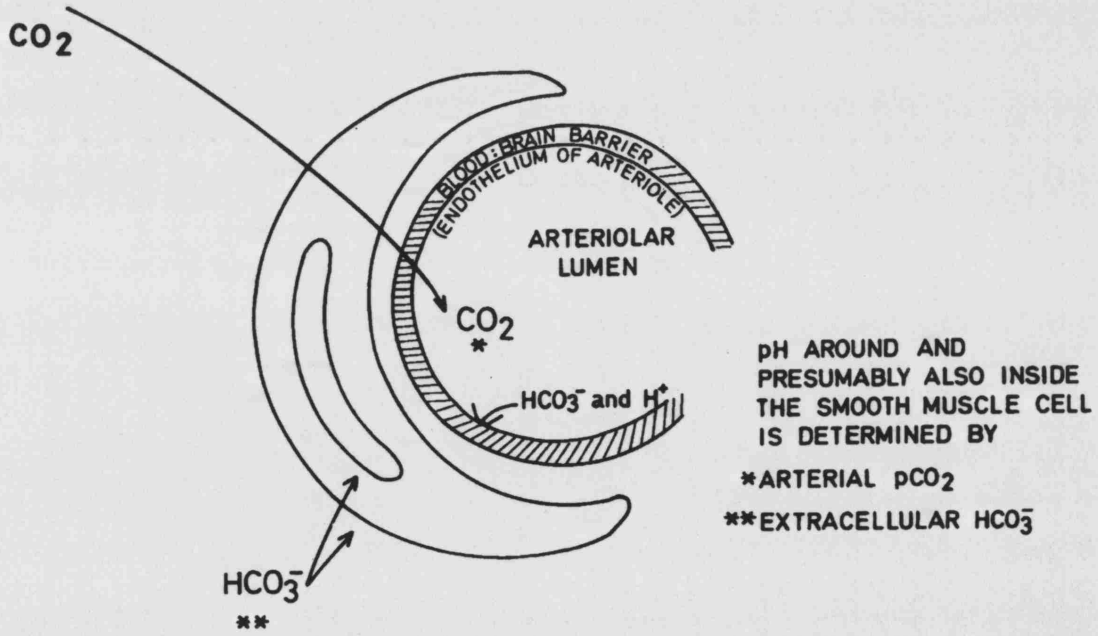

Figure 2.11: The overall model of cerebral arteriole reactivity called the "$PaCO_2$ electrode". Diagrammatic representation of how systemic $PaCO_2$ and pH changes may modulate the tone of the cerebral arterioles (taken from [58]).

2.3.2 Oxygen and the cerebral circulation

The normal brain consumes oxygen at an average rate of 3.5ml.100gr^{-1}.min^{-1} and has total oxygen uptake of about 50ml.100gr^{-1}.min^{-1} [41]. Thus nearly 20% of the oxygen taken up by the whole body at rest is utilized by the brain. Normal mental functions are uniquely dependent on an uninterrupted and ample oxygen supply. If cerebral oxygen delivery is arrested by stopping the cerebral circulation, consciousness is lost in few seconds.

A decrease in the arterial partial pressure of O_2 (PaO_2) during hypoxia reliably increase cerebral perfusion by decreasing cerebrovascular resistance as a result of arterial vasodilation. Conversely, an increase in PaO_2 (hyperoxia) result in a decrease in cerebral blood flow (Figure 2.12). Inhalation of low oxygen tension causes dilation of the pial arteries, whereas high oxygen tension causes a moderate vasoconstriction. Thus, the effect of O_2 is in the opposite direction to that of CO_2. Moderate variations of oxygen tensions below and above the normal level do not affect the cerebral blood flow or metabolism. Most of the work and studies carried out involving oxygen and cerebral circulation have been concentrated more on the effects of hypoxia [59], and it is these, which will be discussed in more detail.

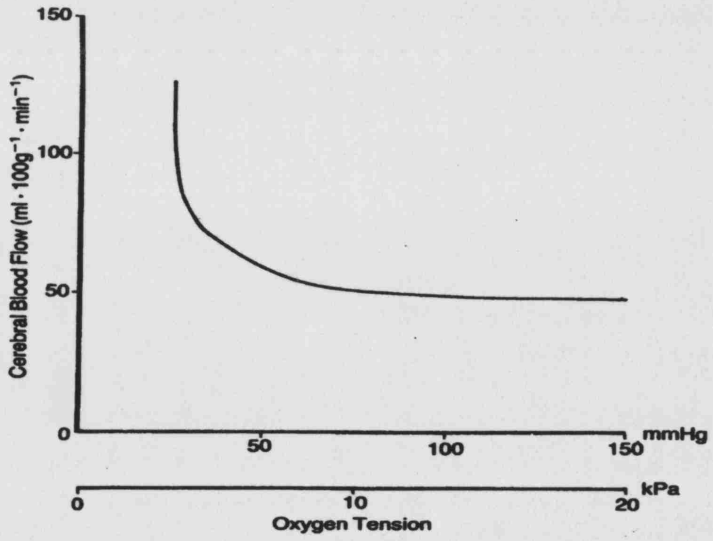

Figure 2.12: The response of cerebral circulation to changes in arterial oxygen tension (taken from [16]).

Decreases in PaO_2 below 40 to 50mmHg result in arterial dilation and increased CBF. Following the reduction in PaO_2, detectable increases in pial arterial diameter and CBF occur rapidly (within 30 to 60sec) and steady state responses are achieved within 5 to 10 minutes [60]. Hypoxia modulates cerebrovascular tone through competing contractile and relaxant influences, via both direct and indirect effects on the smooth muscle of cerebral arteries. These effects can be categorised into three groups: (i) this concerns the actions of hypoxia on the neural and glial tissues of the brain with secondary effects on cerebral vessels; (ii) this group concerns the direct effects of hypoxia on cerebrovascular endothelium, with secondary effects on the underlying smooth muscle; (iii) this group focuses on the direct effect of hypoxia on cerebrovascular smooth muscle [60]. In view of the strong and extensive evidence that neurovascular effects play, at most, a minor modulatory role in hypoxic cerebral vasodilatation [61,62], hypoxia-induced neurovascular effects will not be considered in detail.

The idea that hypoxia acts on the tissues of the brain to promote the release of vasodilator metabolites was first proposed more that 100 years ago by Roy and Sherrington [63]. Among the tissue effect hypotheses is the idea that hypoxia promotes the release of hydrogen ions, perhaps in the form of lactic acid, which then diffuses to the perivascular surface to promote vasodilation [43]. Similarly potassium ions were also proposed as a perivascular signal of tissue hypoxia [60,64]. Clearly changes in perivascular hydrogen and potassium ions contribute to hypoxic vasodilatation, but this contribution probably is dominant only under conditions of prolonged severe hypoxia [65].

An increased brain adenosine concentration has been demonstrated in arterial hypoxia, the elevated production of adenosine under these conditions may be the result of hypoxia of the neural cells which leads to increased production of adenosine and subsequent dilation of blood vessels supplying that region, thus increasing oxygen delivery [59,60]. The adenosine hypotheses cannot explain hypoxic cerebral vasodilatation completely. As shown in multiple studies, adenosine receptor antagonists can block only half, or less, of the cerebral response to hypoxia [66]. Hypoxia and ischemia may also promote the release of NO, a direct vasodilator, via the action of excitatory amino acid release on neuronal and endothelial calcium levels [67].

Endothelial effects of hypoxia are also considered to mediate hypoxia and have been study by numerous investigators [68,69]. The role of endothelium in hypoxic cerebral vasodilatation is heterogeneous and tissue specific - as are endothelial responses to most pharmacological agents - this is probably due the capability of endothelium to release a varying mix of several different vasodilators, including NO, hyperpolarizing factor and prostacyclin, depending on the arteries and the methods employed [59].

Direct cerebrovascular effects of hypoxia have been proposed as mediators on hypoxic cerebral vasodilation. Pittman and Duling [70] provided a series of data in support of the idea that hypoxia may simply precipitate the depletion of vascular smooth muscle ATP levels.

Finally Doll and colleagues [71] have proposed the general "channel arrest theory", which speculates that in neurons, overall membrane permeability decreases to conserve energy during periods of oxygen shortage. Therefore given also the central role of calcium as a determinant of contractile tone, it is logical to suspect that hypoxia may produce vasodilatation by interfering in some way with the cytosolic calcium concentration available to support contraction [59]. Nelson and colleagues [72] have proposed one mechanism whereby hypoxia might reduce calcium uptake and that is through membrane hyperpolarization, which can result in a decreased membrane calcium permeability and influx. However the most accepted idea involving hypoxic membrane hyperpolarization is centred on ATP-sensitive potassium (K_{ATP}) channels [73]. K_{ATP} channels increase their conductance to potassium when intracellular ATP concentration falls, and thus act to hyperpolarize the smooth muscle membrane [72]. More importantly the K_m for ATP channels is up to an order of magnitude higher than that for actomyosin ATPase or myosin light chain kinase, which predicts that if ATP levels fall at all, then these ATP-sensitive potassium channels will respond long before ATP levels become limiting for contraction [59].

2.4 Cerebral circulation and disease

The brain is a very active organ and its survival depends on the accurate control and continuous flow of nutrients and oxygenation coupled with the adequate removal of

by-products such us CO_2. Neuronal function is abolished when the blood flow drops below 50% of its normal value, and if this persists the result can lead to cell death and serious neurological disorders such as paralysis (Figure 2.13).

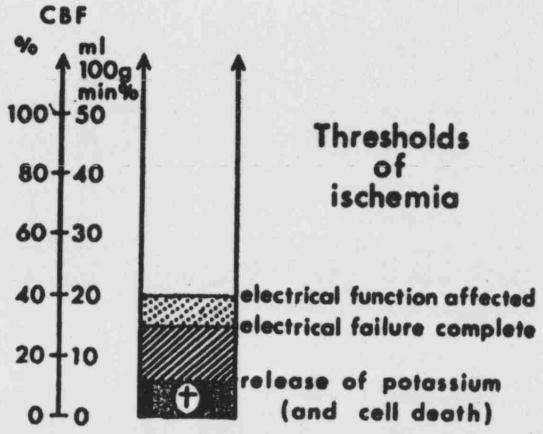

Figure 2.13: CBF with corresponding pathological phenomena in the cerebral tissue (taken from [74]).

The list of cerebral pathologies is generally divided into chronic and acute conditions, namely they range from tumours, aneurysms, hydrocephalus, haematomas, to stroke and traumatic brain injury. The list is far from exhaustive therefore here we only discuss very briefly what happens during acute brain injury and also provide a brief summary regarding differences between the healthy young and elderly in terms of their cerebral autoregulation.

2.4.1 Effects of traumatic brain injury

In cerebral trauma autoregulation is impaired. Severe head injury is accompanied by marked disturbances of blood pressure autoregulation and other autoregulatory mechanisms of CBF. In severe head injury the nature of damage is multifocal, with more and less diseased tissues neighbouring each other. Loss of autoregulation or false autoregulation is commonly observed.

A number of pathological conditions result in loss or diminution of cerebral autoregulation. These include cerebral ischemia/reperfusion, asphyxia/reventilation, subarcachnoid haemorrhage and trauma [75]. Depending upon the type and severity of

the insult, alterations in cerebrovascular autoregulatory ability may occur quickly or take time to develop and may or may not be reversible.

2.4.1.1 Ischemia

It has been suggested that cerebral ischemia may be one of the most important mechanisms in production of secondary brain damage after severe brain trauma [76]. Experimental studies in the effects of brain injury generally show that the most profound decrease in CBF occurs in the first few hours after injury [77]. Bouma and colleagues [78] reported that CBF was lower during the first 6 hours after injury and found CBF below the threshold for infarction ($CBF \leq 18ml.100gr^{-1}.min^{-1}$) in one third of the CBF values obtained within 6 hours suggesting that an acute period of ischemia does occur in a subset of severely head injury patients.

2.4.1.2 Subarachnoid haemorrhage

A subarachnoid haemorrhage is an abnormal and very dangerous condition in which blood collects beneath the arachnoid mater, the membrane that covers the brain. This area, called the subarachnoid space, normally contains cerebrospinal fluid. The accumulation of blood in the subarachnoid space can lead to stroke, seizures, and other complications. Additionally, subarachnoid haemorrhages may cause permanent brain damage and a number of harmful biochemical events in the brain. A subarachnoid haemorrhage and its related problems are frequently fatal. At the time of head trauma, forces are applied to the head that are transmitted intracranially to the brain as pressure, concussion, or shear.

Subarachnoid haemorrhage is classified into two general categories: traumatic and spontaneous. Traumatic refers to brain injury that might be sustained in an accident or a fall. Spontaneous subarachnoid haemorrhages occur with little or no warning and are frequently caused by ruptured aneurysms or blood vessel abnormalities in the brain.

Spontaneous subarachnoid haemorrhage is often due to an aneurysm (a bulge or sac-like projection from a blood vessel) which bursts. Arteriovenous malformations (AVMs), which are abnormal interfaces between arteries and veins, may also rupture and release

blood into the subarachnoid space. Both aneurysms and AVMs are associated with weak spots in the walls of blood vessels and account for approximately 60% of all spontaneous subarachnoid haemorrhages. The rest may be attributed to other causes, such as cancer or infection, or are of unknown origin.

The immediate danger due to subarachnoid haemorrhage, whether traumatic or spontaneous, is tissue damage caused by oxygen deprivation due to ischemia. Ischemia refers to oxygen deprivation caused by restricted or blocked blood flow. The areas of the brain that do not receive adequate blood and oxygen can suffer irreparable injury, leading to permanent brain damage or death. An individual who survives the initial haemorrhage is susceptible to a number of complications in the following hours, days, and weeks.

The most common complications are intracranial hypertension, vasospasm, and hydrocephalus. Intracranial hypertension, or high pressure within the brain, can lead to further bleeding from damaged blood vessels; a complication associated with a 70% fatality rate. Vasospasm, or blood vessel constriction, is a principal cause of secondary ischemia. The blood vessels in the brain constrict in reaction to chemicals released by blood breaking down within the subarachnoid space. As the blood vessels become narrower, blood flow in the brain becomes increasingly restricted. Approximately one third of spontaneous subarachnoid haemorrhages and 30-60% of traumatic bleeds are followed by vasospasm. Hydrocephalus, an accumulation of fluid in the chambers of the brain (ventricles) due to restricted circulation of cerebrospinal fluid, follows approximately 15% of subarachnoid haemorrhages. Because cerebrospinal fluid cannot drain properly, pressure accumulates on the brain, possibly prompting further ischemic complications.

2.4.2 Cerebral circulation and aging

Aging causes a variety of alterations in the cerebrovascular system, here we will summarise a few of those and we will discuss their importance (for more information the reader is referred to [79-81]).

The most important alterations during aging occur in the cerebral vasculature and include (i) vascular morphology and mechanics; (ii) resting levels of cerebral blood flow; (iii) innervation of cerebral blood vessels; (iv) vascular responses and endothelium dependent mechanisms (Figure 2.14).

Compared to the young adult in the elderly there is a decrease in CBF (the rate of decrease is 0.5% per year [82]) which is associated with a similar decrease in cerebral oxygen metabolism and an increase in oxygen extraction. There is an increased stiffness of the cerebral arterioles, which according to Hajdu and colleagues [83] is due to a decrease in the relative amount of distensible elements of the vessels wall.

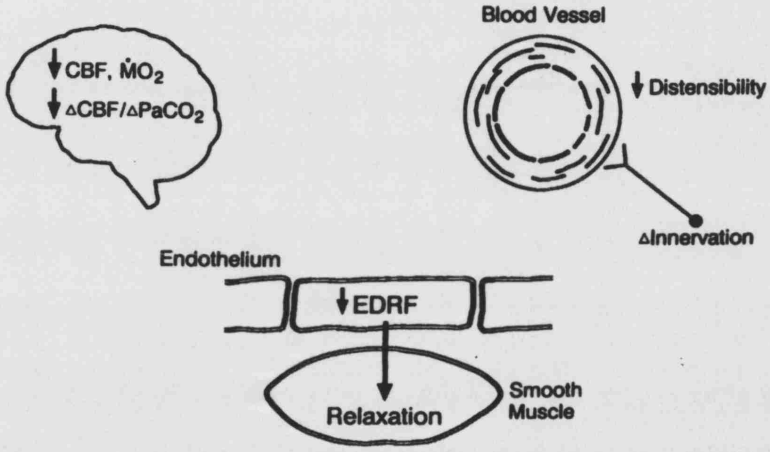

Figure 2.14: Summary of the changes that occur in cerebral circulation with aging (taken from [79]).

Also important is the impairment of the neural influence on cerebral circulation that occurs with aging. As discussed previously cerebral arteries are richly innervated by nerve fibres containing vasodilator and vasoconstrictor neurotransmitters. The activity of smooth muscle is regulated by vasomotor nerve fibres of the sympathetic division of the autonomic nervous system [8,9]. Normal human aging is associated with changes in the autonomic control of several bodily functions, since the autonomic nervous system functions to enable an organism to adapt rapidly to stress; these age related changes may impair an older person's adaptive capacity [80]. One such paradigm is the inability of the aged individual to adapt in a rapid change of posture [84-88].

Finally Mayhan and colleagues [89] investigated whether responses of cerebral arterioles were altered in aged Wistar rats. They concluded that dilator responses of

cerebral arterioles to agonists that may release EDRF are altered in aged compared with adult rats.

2.5 Cell metabolism

Cells use energy to extract more energy from foods and then this to drive their activities; even at rest the body uses energy on a grand scale. Cellular respiration, during which glucose is broken down within cells and some of its energy released, is captured to form ATP (adenosine triphosphate), the cells energy currency.

Glucose is the pivotal fuel molecule in the oxidative ATP producing pathways. The complete catabolism (Figure 2.15) of glucose ($C_6H_{12}O_6$) is summarised by the overall equation:

$$C_6H_{12}O_6 + 6O_2 \Rightarrow 6H_20 + 6CO_2 + 36ATP + \text{heat} \qquad \textbf{2-1}$$

Here we will describe a few key concepts regarding cell metabolism. We will briefly describe glycolysis, which occurs in the cytosol; and the Krebs cycle, which occur within the mitochondria. For more detail information the reader is referred to Marieb [90], Martini [91] and Karp [92].

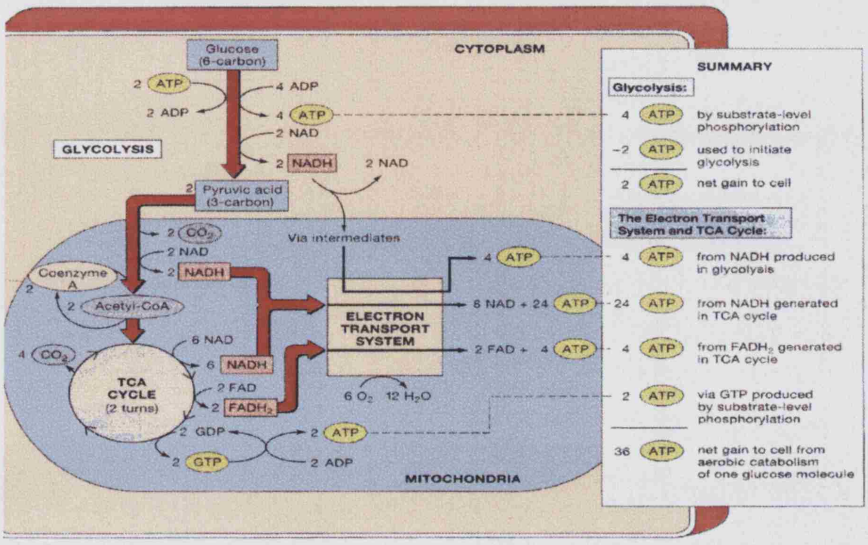

Figure 2.15: A summary of the aerobic yield of aerobic metabolism (taken from [91]).

2.5.1 Glycolysis

Glycolysis is a series of ten chemical steps by which glucose is converted into two pyruvic acid molecules (CH_3-CO-COOH), yielding a net gain of two ATP per glucose molecule and two molecules of reduced NAD^+ (nicotinamide adenine dinucleotide). Glycolysis occurs in the cytosol of cells, where in steps it is catalysed by specific soluble enzymes.

The fate of pyruvic acid, which still contains most of glucose's chemical energy, depends on the availability of oxygen at the time it is produced. If glycolysis is to continue and pyruvic acid is to enter the Krebs cycle, NAD^+ must be relieved of the accepted hydrogen so that it can continue to act as a hydrogen receptor.

When oxygen is readily available, this is no problem $NADH+H^+$ simply delivers the hydrogen atoms to the enzymes of the electron transport chain in the mitochondria which in turn delivers them to molecular oxygen forming water.

When oxygen is not present in sufficient amounts as might occur during strenuous exercise or hypoxia, the $NADH+H^+$ produced during glycolysis unloads its hydrogen back onto pyruvic acid, thus reducing it and forming lactic acid. When oxygen is again available, lactic acid is oxidised back to pyruvic acid and enters the aerobic pathway.

Mitochondria are not able to import the NADH formed in the cytosol by glycolysis. Instead the electrons from NADH are used to reduce a low-molecular weight metabolite that can either (i) enter the mitochondrion by the pathway called the malate-asparate shuttle and reduce NAD^+ to NADH or (ii) transfer its electrons to a FAD (flavin adenine dinucleotide) by a pathway called the glycerol phosphate shuttle to produce $FADH_2$.

2.5.2 Krebs cycle

The Krebs cycle (or tricarboxylic acid cycle, or citric acid cycle) occurs in the aqueous mitochondrial matrix and is fuelled largely by pyruvic acid produced during glycolysis. Before the start of the cycle, pyruvic acid enters the mitochondria and the

first order of business is to convert it to acetyl-CoA (a molecule comprised of two CH_3CO bound to coenzyme A).

The first step of the cycle is to convert acetyL-CoA to citric acid. Coenzyme A is released intact and thus can bind another CH_3CO (acetyl) group. A complete revolution of the Krebs cycle forms two molecules of CO_2, the only immediate energy benefit is the formation of a single GTP (guanosine triphosphate) from GDP (Guanosine diphospate) and Pi. Also six NADH and two $FADH_2$ molecules are produced.

The entire sequence can be summarised as:

$$CH_3CO - CoA + 3NAD + FAD + GDP + Pi + 2H_2O \Rightarrow$$
$$\Rightarrow CoA + 2CO_2 + 3NADH + FADH_2 + 2H^+ + GTP \qquad \textbf{2-2}$$

2.5.2.1 The electron transport system

The electron transport system (ETS) or respiratory chain is a sequence of proteins called cytochromes.

During glycolysis, which occurs in the cytoplasm, NAD is reduced to NADH; within mitochondria both NAD and FAD are reduced through reactions of the Krebs cycle to NADH and $FADH_2$ respectively. NADH and $FADH_2$ deliver hydrogen atoms to coenzymes embedded in the inner membrane of the mitochondrion. The electrons carry the energy and the protons that accompany them will be released before the electrons are transferred to the ETS.

The process is summarised in Figure 2.16. Coenzyme Q accepts hydrogen atoms and transfers electrons to cytochrome b. Electrons are passed along the electron transport chain losing energy in a series of small steps. The sequence is cytochrome b to c to a to a3. At the end of the ETS, an oxygen atom accepts the electrons creating an oxygen ion which binds with hydrogen ions forming water.

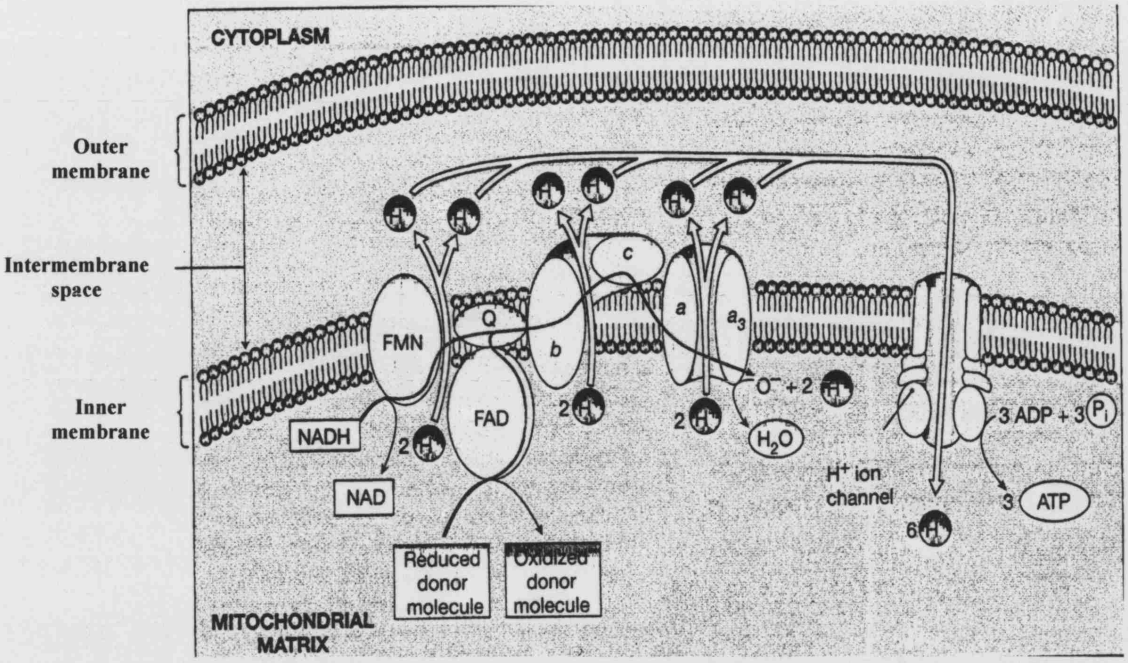

Figure 2.16: The location of coenzymes and the electron transport system (taken from [91]).

References

1. *The physiology of the cerebral circulation*, Purves M.J., ed., (Cambridge University Press, Cambridge, 1972).

2. *Cerebral Blood Flow and Metabolism*, Harper A.M. and Jennett S., eds., (Manchester University Press, Manchester and New York, 1990).

3. *The regulation of cerebral blood flow*, Phillis J.W., ed., (CRC Press, Florida, 1993).

4. *Cerebral blood flow and metabolism*, Edvinsson L. and Krause D.N., eds., (Lippincott Williams and Wilkins, Philadelphia, 2001).

5. E.N. Marieb, "The central nervous system," *Human anatomy and physiology,* Marieb E.N., ed., (Benjamin/Cummings Science Publishing, California, 1998), 404-455.

6. F.H. Martini, "The brain and the cranial nerves," *Fundamentals of anatomy and physiology,* F.H.Martini, ed., (Prentice Hall, New Jersey, 2001), 436-479.

7. D. Emslie-Smith, C.R. Paterson, T. Scratcherd, and N.W. Read, "The nervous system," *Textbook of physiology,* Emslie-Smith D., Paterson C.R., Scratcherd T., and Read N.W., eds., (Longman Singapore Publishers, Singapore, 1988), 374-381.

8. E.N. Marieb, "The cardiovascular system: blood vessels," *Human anatomy and physiology,* Marieb E.N., ed., (Benjamin/Cummings Science Publishing, California, 1998), 690-743.

9. F.H. Martini, "Blood vessels and circulation," *Fundamentals of anatomy and physiology,* F.H.Martini, ed., (Prentice Hall, New Jersey, 2001), 692-745.

10. R.H. Winn, R.G. Dacey, and M.R. Mayberg, "Cerebral circulation," *Textbook of physiology (Volume 2),* Patton H.D., Fuchs A.F., Hille B., Scher A.M., and Steiner R., eds., (W. B. Saunders Company, Philadelpia, 1989), 952-960.

11. T. Willis, *Cerebri anatome*, (Martin and Allestry, London, 1664).

12. C.F. Schmidt, "Anatomical conciderations," *The cerebral circulation in health and disease,* Schmidt C.F, ed., (Thomas, Springfield, 1950), 5-15.

13. L. Edvinsson, E.T. MacKenzie, and J. McCulloch, "General and comparative anatomy of the cerebral circulation," *Cerebral blood flow and metabolism,* Edvinsson L., MacKenzie E.T., and McCulloch J., eds., (Raven Press, New York, 1993), 3-39.

14. P.C. Johnson, "Review of previous studies and current theories of autoregulation," *Circulation Research Supplement* **I**, XIV and XV, 1.2-1.9 (1964).

15. D.W. Busija, "Cerebral autoregulation," *The regulation of cerebral blood flow,* Phillis J.W., ed., (CRC Press, Florida, 1993), 46-54.

16. A.M. Harper, "Physiological control of the cerebral circulation," *Cerebral blood flow and metabolism,* Harper A.M. and Jennett S., eds., (Manchester University Press, Manchester and New York, 1990), 4-25.

17. L. Edvinsson, E.T. MacKenzie, and J. McCulloch, "Autoregulation: Arterial and intracranial pressure," *Cerebral blood flow and metabolism,* Edvinsson L., MacKenzie E.T., and McCulloch J., eds., (Raven Press, New York, 1993), 553-580.

18. D.W. Busija and D. D. Heistad, "Factors involved in the physiological regulation of the cerebral circulation," *Rev. Physiol. Biochem. Pharmacol.* **101**, 161-211 (1984).

19. R.M. Berne, "Metabolic regulation of blood flow," *Circulation Research Supplement* **I**, XIV and XV, 1.261-1.267 (1964).

20. W. Kuschinsky and M. Wahl, "Local chemical and neurogenic regulation of cerebral vascular resistance," *Physiol. Rev.* **58**, 656-689 (1978).

21. W.M. Bayliss, "On the local reactions of the arterial wall to changes of internal pressure," *J. Physiol. (London)* **28**, 220-231 (1902).

22. B. Folkow, "Description of the myogenic hypothesis," *Circulation Research Supplement* **I**, XIV-XV, 1.279-1.291 (1964).

23. K. Nakayama, "Calcium-dependent contractile activation of cerebral artery produced by quick stretch," *Am. J. Physiol.* **242**, H760-H768 (1982).

24. G. Osol and W. Halpern, "Myogenic properties of cerebral blood vessels from normotensive and hypertensive rats," *Am. J. Physiol.* **249**, H914-H921 (1985).

25. D. R. Harder, "Pressure-induced myogenic activation of cat cerebral arteries is dependent on intact endothelium," *Circ. Res.* **60**, 102-107 (1987).

26. D. R. Harder, "Pressure-dependent membrane depolarization in cat middle cerebral artery," *Circ. Res.* **55**, 197-202 (1984).

27. A.C. Ngai and H.R. Winn, "Modulation of cerebral arteriolar diameter by intraluminal flow and pressure," *Circ. Res.* **77**, 832-840 (1995).

28. G. A. Meininger and M. J. Davis, "Cellular mechanisms involved in the vascular myogenic response," *Am. J. Physiol.* **263**, H647-H659 (1992).

29. D. R. Harder, C. Sanchez-Ferrer, K. Kauser, W. J. Stekiel, and G. M. Rubanyi, "Pressure releases a transferable endothelial contractile factor in cat cerebral arteries," *Circ. Res.* **65**, 193-198 (1989).

30. G. M. Rubanyi, "Endothelium-dependent pressure-induced contraction of isolated canine carotid arteries," *Am. J. Physiol.* **255**, H783-H788 (1988).

31. R. Busse, G. Trogisch, and E. Bassenge, "The role of endothelium in the control of vascular tone," *Basic Res. Cardiol.* **80**, 475-490 (1985).

32. V. Smiesko, J. Kozik, and S. Dolezel, "Role of endothelium in the control of arterial diameter by blood flow," *Blood Vessels* **22**, 247-251 (1985).

33. L. Edvinsson, "Innervation of the cerebral vasculature and its functional significance," *Cerebral blood flow and metabolism,* Harper A.M. and Jennett S., eds., (Manchester University Press, Manchester and New York, 1990), 27-47.

34. D.W. Busija, D.D. Heistad, and M.L. Marcus, "Effects of sympathetic nerves on cerebral vessels during acute, moderate increases in arterial pressure in dogs and cats," *Circ. Res.* **46**, 696-702 (1980).

35. L.M. Auer and N. Ishiyama, "Pial vascular behavior during bilateral and contralateral cervical sympathetic stimulation," *J. Cereb. Blood Flow Metab.* **6**, 298-304 (1986).

36. J. Hamar, A.G. Kovach, M. Reivich, I. Nyary, and F. Durity, "Effect of phenoxybenzamine on cerebral blood flow and metabolism in the baboon during hemorrhagic shock," *Stroke* **10**, 401-407 (1979).

37. L.G. D'Alecy and C.J. Rose, "Parasympathetic cholinergic control of cerebral blood flow in dogs," *Circ. Res.* **41**, 324-331 (1977).

38. N. M. Branston, A. Umemura, and A. Koshy, "Contribution of cerebrovascular parasympathetic and sensory innervation to the short-term control of blood flow in rat cerebral cortex," *J. Cereb. Blood Flow Metab.* **15**, 525-531 (1995).

39. M. Kano, M.A. Moskowitz, and M. Yokota, "Parasympathetic denervation of rat pial vessels significantly increases infarction volume following middle cerebral artery occlusion," *J. Cereb. Blood Flow Metab.* **11**, 628-637 (1991).

40. N. Koketsu, M.A. Moskowitz, H.A. Kontos, M. Yokota, and T. Shimizu, "Chronic parasympathetic sectioning decreases regional cerebral blood flow during hemorrhagic hypotension and increases infarct size after middle cerebral artery occlusion in spontaneously hypertensive rats," *J. Cereb. Blood Flow Metab.* **12**, 613-620 (1992).

41. N.A. Lassen, "Cerebral blood flow and oxygen consumption in man," Physiological Reviews **39**, 183-238 (1959).

42. N.A. Lassen, "Autoregulation of cerebral blood flow," *Circulation Research Supplement* **I**, XIV and XV, 1-201-1-204 (1964).

43. N.A. Lassen, "Brain extracellular pH: the main factor controlling cerebral blood flow," *Scand. J. Clin. Lab. Invest.* **22**, 247-251 (1968).

44. T.L. Yaksh and R.E. Anderson, "In vivo studies on intracellular pH, focal flow, and vessel diameter in the cat cerebral cortex: Effects of altered CO_2 and electrical stimulation," *J. Cereb. Blood Flow Metab.* **7**, 332-341 (1987).

45. M. Erecinska and I.A. Silver, "Tissue oxygen tension and brain sensitivity to hypoxia," *Respiration Physiology* **128**, 263-276 (2001).

46. L. Edvinsson, E.T. MacKenzie, and J. McCulloch, "Changes in arterial gas tensions," *Cerebral blood flow and metabolism,* Edvinsson L., MacKenzie E.T., and McCulloch J., eds., 1993), 524-552.

47. M.J. Purves, "Regulation of cerebral vessels by carbon dioxide," *The physiology of the cerebral circulation,* Purves M.J., ed., (Cambridge University Press, Cambridge, 1972), 173-199.

48. R. Rubio, R.M. Berne, E.L. Bockman, and R.R. Curnish, "Relationship between adenosine concentration and oxygen supply in rat brain," *Am. J. Physiol.* **228**, 1896-1902 (1975).

49. A. Sollevi, K. Ericson, L. Eriksson, C. Lindqvist, M. Lagerkranser, and S. Stone-Elander, "Effect of adenosine on human cerebral blood flow as determined by positron emission tomography," *J. Cereb. Blood Flow Metab.* **7**, 673-678 (1987).

50. S. Ibayashi, A.C. Ngai, J.R. Meno, and H.R. Winn, "The effects of dipyridamole and theophylline on rat pial vessels during hypocarbia," *J. Cereb. Blood Flow Metab.* **8**, 829-833 (1988).

51. Q. Wang, O.B. Paulson, and N.A. Lassen, "Effect of nitric oxide blockade by NG-nitro-L-arginine on cerebral blood flow response to changes in carbon dioxide tension," *J. Cereb. Blood Flow Metab.* **12**, 947-953 (1992).

52. C. Iadecola, D.A. Pelligrino, M.A. Moskowitz, and N.A. Lassen, "Nitric oxide synthase inhibition and cerebrovascular regulation," *J. Cereb. Blood Flow Metab.* **14**, 175-192 (1994).

53. J.D. Pickard and E.T. Mackenzie, "Inhibition of prostaglandin synthesis and the response of baboon cerebral circulation to carbon dioxide," *Nat. New Biol.* **245**, 187-188 (1973).

54. J.D. Pickard, "Role of prostagladins and arachidonic acid derivatives in the coupling of cerebral blood flow to cerebral metabolism," *J. Cereb. Blood Flow Metab.* **1**, 361-384 (1981).

55. A.D. Edwards, J.S. Wyatt, C. Richardson, A. Potter, M. Cope, D.T. Delpy, and E.O.R. Reynolds, "Effects of indomethacin on cerebral haemodynamics in very preterm infants," *The Lancet* **335**, 1491-1495 (1990).

56. E. Betz, H. G. Enzenrobb, and V. Vlahov, "Interaction of H+ and Ca++ in the regulation of local pial vascular resistance," *Pflugers Arch.* **343**, 79-88 (1973).

57. H.A. Kontos, E.P. Wei, A.J. Raper, W.I. Rosenblum, R.M. Navari, and J.L. Patterson, "Role of tissue hypoxia in local regulation of cerebral microcirculation," *Am. J. Physiol.* **234**(5), H582-H591 (1978).

58. M. Wahl, P. Deetjen, K. Thurau, D.H. Ingvar, and N.A. Lassen, "Micropuncture evaluation of the importance of perivascular pH for the arteriolar diameter on the brain surface," *Pflugers Arch.* **316**, 152-163 (1970).

59. W.J. Pearce, "Mechanisms of hypoxic cerebral vasodilation," *Pharmc. Ther.* **65**, 75-91 (1995).

60. J.W. Phillis, "Cerebral vascular responses to hypoxia, hyper- and hypo- capnia and hypotension," *The regulation of cerebral blood flow,* Phillis J.W., ed., (CRC Press, Florida, 1993), 249-258.

61. M. Miyabe, M.D. Jones Jr., R.C. Koehler, and R.J. Traystman, "Chemodenervation does not alter cerebrovascular response to hypoxic hypoxia," *Am. J. Physiol.* **257**, H1413-H1418 (1989).

62. E.P. Wei and H.A. Kontos, "Cerebrovascular flow regulation by adenosine," *The regulation of cerebral blood flow,* Phillis J.W., ed., (CRC Press, Florida, 1993), 282-293.

63. C.W. Roy and C.S. Sherrington, "On the regulation of the blood-supply of the brain," *J. Physiol. (London)* **11**, 85-108 (1890).

64. J. Astrup, D. Heuser, N. A. Lassen, Nilsson B., Norberg K., and B. K. Siesjo, "Evidence against H+ and K+ as main factors for the control of cerebral blood flow: a microelectrode study," *CIBA Fndn. Symp.* **56**, 313-337 (1978).

65. T. Shinozuka, E.M. Nemoto, and P.M. Winter, "Mechanisms of cerebrovascular O_2 sensitivity from hyperoxia to moderate hypoxia in the rat," *J. Cereb. Blood Flow Metab.* **9**, 187-195 (1989).

66. E. Pinard, S. Puiroud, and J. Seylaz, "Role of adenosine in cerebral hypoxic hyperemia in the unanesthetized rabbit," *Brain research* **481**, 124-130 (1989).

67. J.S. Beckman, "The double-edged role of nitric oxide in brain function and superoxide-mediated injury," *Journal of Developmental Physiology* **15**, 53-59 (1991).

68. R. Busse, U. Pohl, C. Kellner, and U. Klemm, "Endothelial Cells are involved in the vasodilatory responce to hypoxia," *Pflugers Arch.* **397**, 78-80 (1983).

69. F.M. Faraci and D.D. Heistad, "Regulation of the cerebral circulation: Role of endothelium and potassium channels," *Physiological Reviews* **78**, 53-97 (1998).

70. R. N. Pittman and B. R. Duling, "Oxygen sensitivity of vascular smooth muscle. I. In vitro studies," *Microvasc. Res.* **6**, 202-211 (1973).

71. C. J. Doll, P. W. Hochachka, and P. B. Reiner, "Effects of anoxia and metabolic arrest on turtle and rat cortical neurons," *Am. J. Physiol.* **260**, R747-R755 (1991).

72. M. T. Nelson, J. B. Patlak, J. F. Worley, and N. B. Standen, "Calcium channels, potassium channels, and voltage dependence of arterial smooth muscle tone," *Am. J. Physiol.* **259**, C3-18 (1990).

73. N. B. Standen, J. M. Quayle, N. W. Davies, J. E. Brayden, Y. Huang, and M. T. Nelson, "Hyperpolarizing vasodilators activate ATP-sensitive K+ channels in arterial smooth muscle," *Science* **245**, 177-180 (1989).

74. J.H. Wood, *Cerebral blood flow: Physiologic and clinical aspects*, Wood J.H., ed., (McGraw-Hill, 1987).

75. G. J. Bouma, J. P. Muizelaar, S. C. Choi, P. G. Newlon, and H. F. Young, "Cerebral circulation and metabolism after severe traumatic brain injury: the elusive role of ischemia," *J. Neurosurg.* **75**, 685-693 (1991).

76. J. D. Miller, "Head injury and brain ischaemia--implications for therapy," *Br. J. Anaesth.* **57**, 120-130 (1985).

77. E. G. Pfenninger, A. Reith, D. Breitig, A. Grunert, and F. W. Ahnefeld, "Early changes of intracranial pressure, perfusion pressure, and blood flow after acute head injury. Part 1: An experimental study of the underlying pathophysiology," *J. Neurosurg.* **70**, 774-779 (1989).

78. G. J. Bouma, J. P. Muizelaar, S. C. Choi, P. G. Newlon, and H. F. Young, "Cerebral circulation and metabolism after severe traumatic brain injury: the elusive role of ischemia," *J. Neurosurg.* **75**, 685-693 (1991).

79. F.M. Faraci, "Cerebral circulation during aging," *The regulation of cerebral blood flow,* Phillis J.W., ed., (CRC Press, Florida, 1993), 342-349.

80. L.A. Lipsitz, "Ageing and the autonomic nervous system," *Autonomic failure: A textbook of clinical disorders of the autonomic nervous system,* Mathias C.J. and Bannister R., eds., (Oxford University Press, Oxford, 1999), 534-544.

81. R. Grzanna, "Aging and dementia," *Cerebral blood flow and metabolism,* Edvinsson L. and Krause D.N., eds., (Lippincot Williams & Wilkins, Philadelphia, 2001), 480-495.

82. K.L. Leenders, D. Perani, A.A. Lammertsma, J.D. Heather, P. Buckingham, M.J. Healy, J.M. Gibbs, R.J. Wise, J. Hatazawa, and S. Herold, "Cerebral blood flow, blood volume and oxygen utilization. Normal values and effect of age," *Brain* **113**(Pt 1), 27-47 (1990).

83. M.A. Hajdu, D.D. Heistad, J.E. Siems, and G.L. Baumbach, "Effects of aging on mechanics and composition of cerebral arterioles in rats," *Circ. Res.* **66**, 1747-1754 (1990).

84. E. Vargas and M. Lye, "Physiological responses to postural change in young and old healthy individuals," *Exp. Gerontol.* **17**, 445-451 (1982).

85. S. Braune, A. Auer, J. Schulte-Monting, S. Schwerbrock, and C.H. Lucking, "Cardiovascular parameters: sensitivity to detect autonomic dysfunction and influence of age and sex in normal subjects," *Clin. Auton. Res.* **6**, 3-15 (1996).

86. D.J. Mehagnoul-Schipper, L.C.M. Vloet, W.N.J.M. Colier, W.H.L. Hoefnagels, and R.W.M.M. Jansen, "Cerebral Oxygenation Declines in Healthy Elderly Subjects in Response to Assuming the Upright Position," *Stroke* **31**, 1615-1620 (2000).

87. T. Kawaguchi, O. Uyama, M. Konishi, T. Nishiyama, and T. Iida, "Orthostatic hypotension in elderly persons during passive standing: a comparison with young persons," *J. Gerontol. A. Biol. Sci. Med. Sci.* **56**, M273-M280 (2001).

88. D.J. Mehagnoul-Schipper, W.N. Colier, and R.W. Jansen, "Reproducibility of orthostatic changes in cerebral oxygenation in healthy subjects aged 70 years or older," *Clin. Physiol.* **21**, 77-84 (2001).

89. W.G. Mayhan, F.M. Faraci, G.L. Baumbach, and D.D. Heistad, "Effects of aging on responses of cerebral arterioles," *Am. J. Physiol.* **258**, H1138-H1143 (1990).

90. E.N. Marieb, "Nutrition, metabolism, and body temperature regulation," *Human anatomy and physiology,* Marieb E.N., ed., (The Benjamin/Cummings Publishing Company, California, 1998), 908-957.

91. F.H. Martini, "Metabolism and energetics," *Fundamentals of anatomy and physiology,* Martini F.H., ed., (Prentice-Hall Inc, New Jersey, 2001), 900-938.

92. G. Karp, "Bioenergetics, enzymes and metabolism," *Cell and molecular biology: Concepts and experiments,* Karp G., ed., (John Wiley & Sons Inc, New York, 2002), 83-121.

93. I. Vanzetta, R. Hildesheim, and A. Grinvald, "Compartment-Resolved Imaging of Activity-Dependent Dynamics of Cortical Blood Volume and Oximetry," *J. Neurosci.* **25**, 2233-2244 (2005).

Chapter 3

Computational Modelling of the Brain

In this chapter the background to the mathematical techniques for modelling physiological systems are discussed. The concept of 'physiological' and 'black box' (or 'time series') models are introduced and a literature review of the most sited models is provided together with examples of simulations. An overview of the most relevant models published in the last 20 years is provided in Appendix A.

An extensive discussion regarding the physiological modelling work in UCL [1] is given together with simulations of the UCL BRAINCIRC cerebral computational model under steady state conditions. The reader is also advised to look on the web (http://www.medphys.ucl.ac.uk/braincirc/) where the UCL BRAINCIRC cerebral model (version 1.0, 2004-2005) itself and the detailed documentation is available.

3.1 Introduction

Models can be broadly placed into two distinct categories, which will be referred to as 'black box' models and 'physiologically based models'. Physiologically based models attempt to describe systems in the human brain acting in the cerebral autoregulation by means of differential and algebraic equations, which are derived from the underlying physiological processes. Black box models take a data driven approach and attempt to identify the dynamic relationships of the model purely from experimentally obtained data.

The data-driven nature of 'black box' models means that the form of the dynamic relationship between input and output is not assumed in advance. This has a clear advantage since the system that is being modelled does not need to be fully understood. However, it produces a model that is difficult to interpret clinically. Conversely, physiological models impose a defined structure on the system. Physiological models impose prior assumptions about the structure, function and interaction of the cerebral physiology and autoregulation, and they have the advantage that the variables and signals simulated have clinical significance and can be interpreted.

3.2 Physiological models

We start with a discussion of the most cited physiological models involving the cerebral circulation and mostly the notion of cerebral autoregulation [2-6].

In physiological modelling a model is proposed based on assumptions about the underlying physiology. A set of linear or non-linear equations are thus provided with a set of unknown constants. The constants are found by fitting experimental data to the model. Existing models of cerebral autoregulation include the extensive work by Ursino and colleagues [3-5]. A brief description of these and results from simulations are provided below for the (1998) [4] and (2000) [5] Ursino models.

The core component of the model is a solution describing the basic flow behaviour of the cerebral vasculature. In many of the physiological models of cerebral autoregulation, blood flow is taken to be the output variable and is described by considering lumped elements whose transfer characteristics are represented as first order non-linear differential equations. As a first approach, a hydrodynamic model of the blood flow passing through a series of vessels and compartments is provided. This is a simplistic approach to what is a complex problem. Limitations of this type of initial approach include lack of considerations of the cerebral homeostasis (e.g. cell metabolic processes) and most importantly the notion that a single organ can work in isolation from the rest of the body and the systemic circulation.

Most of the physiological mathematical models in the literature are biophysical models of the relevant vasculature. There are also specific metabolic and biochemical models in the literature, which are mostly for single cells or homeostatic mechanisms in the body such as acid regulation. Few models exist that combine both biochemical and biophysical feedback mechanisms; one such model relevant for the cerebral physiology is that of Golding and Golding (2002) [7].

3.2.1 The Olufsen et al (2002) model [6]

The basis of the work by Olufsen and colleagues [6] was to use a lumped parameter model of the cerebral blood flow to analyse changes in key parameters (systemic and peripheral cerebrovascular resistances) during posture change from sitting to standing.

Their model was based on investigation of the cerebrovascular and cardiovascular responses to hypotension; they used a "Windkessel" model with two resistors and a capacitor (as shown in Figure 3.1) to reproduce beat-to-beat changes in middle cerebral artery blood flow velocity (V_{mca}) measured by transcranial Doppler in response to mean blood pressure (MBP) changes measured in the finger continuously and non-invasive by the Finapres®.

The Finapres® instrument is based on the arterial volume clamp method of Peñáz [8], which relies on the dynamic (pulsatile) unloading of the finger arterial wall using an

inflatable finger cuff with a built-in photoplethysmograph. A fast pneumatic servo system and a dynamic servo set point adjuster assure arterial unloading at zero transmural pressure and consequent full transmission of the arterial blood pressure to cuff air pressure. From the finger pressure waveform, blood pressure is calculated in a beat-to-beat mode.

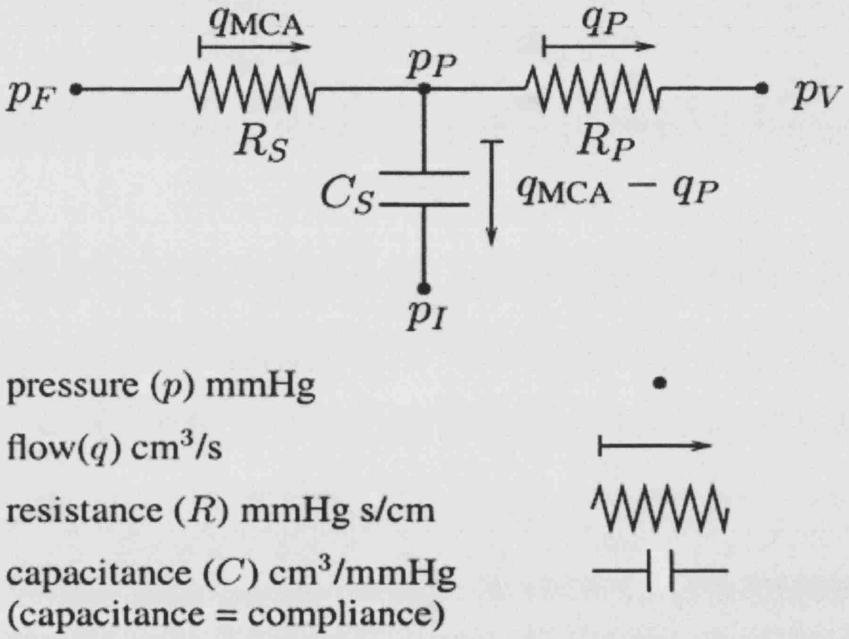

Figure 3.1: The figure shows an electrical analogue of the Olufsen et al [6] model. The circuit represents the middle cerebral artery (MCA) and its peripheral cerebrovascular bed (subscript p). The capacitor C_S and resistor R_S are lumped parameters including the MCA and systemic arteries leading to the MCA. They assume that the pressure at the finger p_F is approximately the same as the pressure into the MCA and used that as an input to the model. Finally, p_V is the pressure of the venous bed and p_I is the intracranial pressure.

The authors estimate the values of the parameters of the model on a beat-to-beat basis, effectively showing that in healthy subjects, changes in the lumped parameter values of the model occur as MBP changes in order to maintain blood flow. This provides experimental validation of the active feedback control of cerebral autoregulation; however it does not provide a full active model of the feedback processes. Finally the lumped parameters used in this model simplify the cerebral vasculature to such an extent that clinical information is hard to obtain and interpret.

3.2.2 The Czosnyka et al (1997) model [2]

Czosnyka and colleagues [2] have also modelled cerebral autoregulation as a possible useful technique for reliable and repeatable bedside monitoring of the variations in the autoregulatory reserve as a guide for therapy.

The autoregulation mechanism was modelled through a variable cerebral vascular resistance whose value depended on the cerebral perfusion pressure (CPP), i.e the pressure drop across the whole cerebral vascular bed, was prescribed for both an active and impaired autoregulatory state.

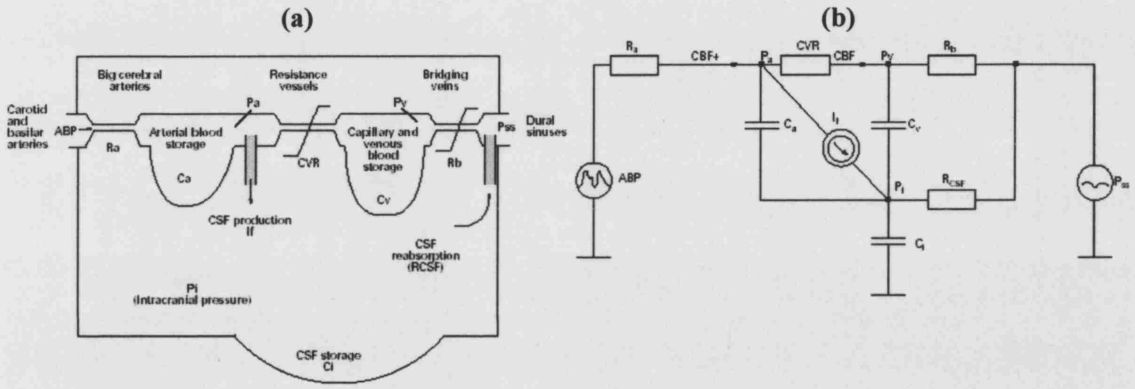

Figure 3.2: (a) Hydrodynamic equivalent of the Czosnyka et al [2] model, comprising pathways of CBF and the CSF circulation. A rigid skull is represented by the outer box, with a compensatory reserve Ci associated with the compliant dural sac within the lumbar channel. **(b)** Electrical structure equivalent to the hydrodynamic model. All components are described in Czosnyka et al [2].

Their model is described by three first order differential equations, there are eight model parameters, and all are non-linear. In terms of physiology, the model contains two major flow pathways. The CBF pathway, which starts with the arterial blood inflow to the brain through the resistance of large intracranial arteries; and the CSF pathway that encompasses CSF formation storage and reabsorption.

They used the model to simulate patterns of blood flow during either short or longlasting decreases in cerebral perfusion pressure. These simulations can be considered as clinically equivalent to a short compression of the common carotid artery, systemic hypotension, or intracranial hypotension.

The results obtained by Czosnyka et al [2] suggested that an active autoregulation mechanism may increase flow pulsatility in the large arteries as cerebral perfusion pressure (CPP) is decreased towards the low limit of autoregulation and in addition may cause an increase in intracranial pressure, which remained constant if autoregulation was impaired.

3.2.3 The Ursino (1998) and (2000) models [4,5]

Here we will discuss two of the most important models published by Ursino and colleagues, the Ursino and Lodi (1998) [4] model (which will also be referred to as the Ursino (1998) model) and the Ursino et al (2000) model (which will also be referred to as the Ursino (2000) model). Emphasis will be given on the Ursino (1998) model [4] as this forms the backbone of the UCL BRAINCIRC cerebral computational model [1], which is introduced in Section 3.4.

Ursino and Lodi [4] use a description of the haemodynamics and biomechanical behaviour in a compartmental model with compartments representing different sections of the cerebral circulation and intracranial space. Four intracranial compartments were considered in this model together with the extracranial venous drainage pathway. The first compartment is the proximal cerebral arteries, which includes the large pial arteries, second is the distal cerebral arteries, which includes the medium and small diameter pial arteries. The other two segments involve the cerebral venous circulation with the third compartment being the cerebral veins and the fourth and final compartment including the terminal portion of the intracranial venous bed, which includes the bridge veins and lateral lacunae. In addition the authors have included the CSF compartment and assumed that the processes of both CSF production at the cerebral capillaries and CSF outflow at the dural sinuses are passive and unidirectional.

The basis of the model can be regarded as electrical or fluid dynamic. An electrical analogue of the Ursino (1998) [4] model is shown in the next page (Figure 3.3).

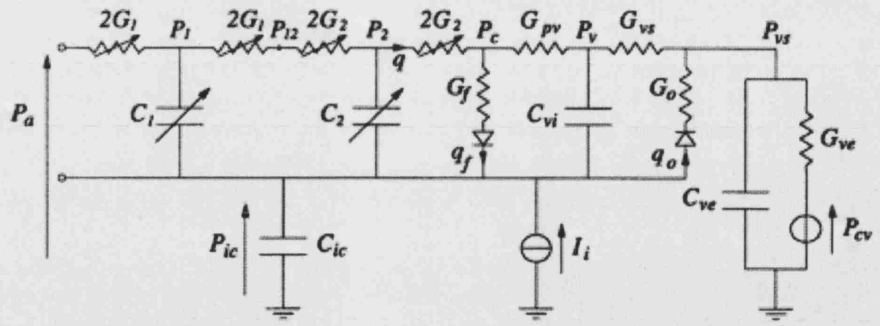

Figure 3.3: Electric analogue of intracranial dynamics. G_1 and C_1, hydraulic conductance and compliance, respectively, of proximal cerebral arteries; G_2 and C_2, hydraulic conductance and compliance, respectively, of distal cerebral arteries; P_a, systemic arterial pressure (SAP); P_1 and P_2, intravascular pressure of large pial arteries and medium and small arteries, respectively; q, cerebral blood flow (CBF); P_c and P_v, capillary and cerebral venous pressure, respectively; P_{vs} and P_{cv}, sinus venous and central venous pressure, respectively; P_{ic}, intracranial pressure (ICP); C_{ic}, intracranial compliance; G_{pv} and C_{vi}, hydraulic conductance and compliance of large cerebral veins; G_{vs}, hydraulic conductance of terminal intracranial veins (bridge veins and lateral lacunae or lakes); G_{ve} and C_{ve}, hydraulic conductance and compliance, respectively, of extracranial venous pathways; G_f and G_o, conductance's to cerebrospinal fluid (CSF) formation and CSF outflow; q_f and q_o, rates of CSF formation and CSF outflow; and I_i, artificial CSF injection rate (taken from [4]).

The importance of this work and the significant improvements it represents over previous work [9,10] are the involvement of CO_2 reactivity of the cerebral vessels, its nonlinear interaction with ICP and with cerebral autoregulation and the description of the intracranial Doppler velocity signal, hence the link to measurement of middle cerebral artery flow velocity.

This attention to detail necessitates the use of over 50 model parameters (56 to be exact). The authors have assumed that autoregulation acts on large pial arteries and small arterioles by means of two distinct feedback mechanisms: (i) the mechanism on large arteries depending on changes in CPP, therefore reflecting a myogenic or neurogenic mechanism; and (ii) the mechanism on small arteries which is triggered by alterations in blood flow, according to metabolic or endothelial dependent response.

Also CO_2 is assumed to affect smooth muscle tension, in both large and small pial arteries through a similar mechanism. Emphasis should be given to the fact that the model response depends on the logarithm of CO_2 change rather than on the arterial partial pressure of CO_2 ($PaCO_2$) itself, as the hypothesis of CO_2 vasoreactivity implies that pH changes in the perivascular space are the main mechanism.

Cerebral vasculature autoregulation and CO_2 reactivity of cerebral vessels are physiologically linked, therefore when considering the overall autoregulation mechanism one should consider both. This supposition of the two mechanisms was accommodated by Ursino and Lodi [4] by including two kinds of non-linear interaction between autoregulation and CO_2 reactivity. First they assumed that the strength of the CO_2 mechanism is not independent of CBF but rather is attenuated during severe brain ischemia. Second, autoregulation and CO_2 reactivity are not simply summed, but rather interact through a sigmoidal relationship, which accounts for the existence of lower and upper limits of cerebrovascular reactivity.

The above assumptions regarding the links of cerebrovascular autoregulation and CO_2 reactivity gave rise to three time constants. Two for the cerebrovascular regulation and one for the CO_2 reactivity. These are first, the pressure dependent mechanism acting on large pial arteries, which exhibits rapid dynamic changes with a time constant of 10sec; second, the flow dependent response of pial arterioles which is slightly slower with a time constant of 20sec; and third, the time constant of the CO_2 reactivity for both large and small pial arteries which is of the order of 20sec.

Figure 3.4 below shows the changes in CBF under steady state conditions at different values of mean blood pressure. Autoregulation is able to maintain a fairly constant CBF in the range of 50-150mmHg when CO_2 is kept constant in the normal range.

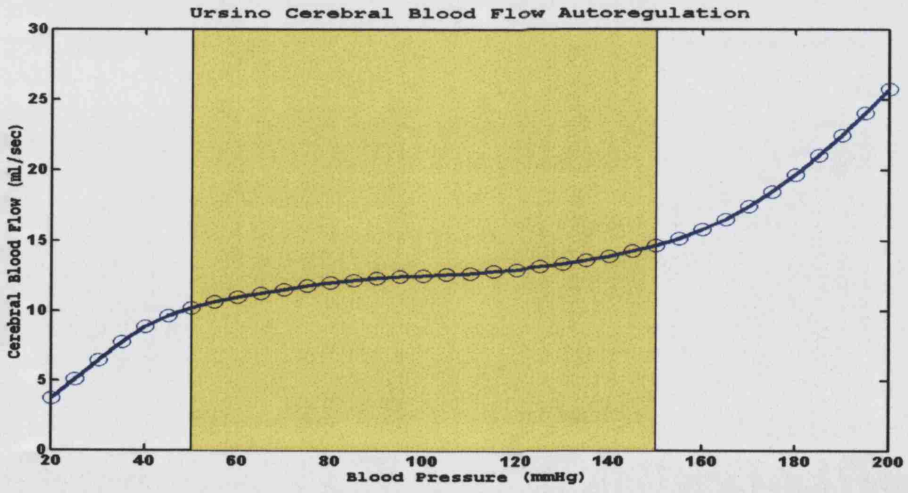

Figure 3.4: Cerebral autoregulation simulation using the Ursino (1998) [4] model.

As this is an extensive model of the cerebral autoregulation mechanism, a subsequently paper by Lodi and colleagues [11] described simulations for validation, which included analysis of predictions for (i) cerebral autoregulation (ii) CO_2 reactivity, (iii) the interactions between these two mechanisms and (iv) the effect of acute changes in CO_2 on intracranial pressure (ICP); and simulations over a wide range of pathological conditions, which included the application of the model to data obtained from patients with severe head injury.

More recently Ursino and colleagues [5] have simplified their previous model [4] by representing each compartment of the circulation with a "Windkessel" model, comprising a resistance and capacitance. The previous model was considered computationally too heavy to be routinely used in a clinical setting. Therefore the aim of this most recent paper was to describe and validate a simplified model that could incorporate the main mechanisms involved in intracranial dynamics and permit their quantitative individual assessment with a drastic reduction in mathematical complexity. This simplified model reduced the number of parameters to 24 (18 fixed).

3.2.3.1 Simulation results with the Ursino (1998) and (2000) models [4,5]

In this section, the results of simulations generated with artificial data, mostly step changes in parameters are reported to investigate how the two different versions of the Ursino models [4,5] behave. Ursino and colleagues have also done their own simulations, which the reader can find in the original papers [4,5].

The first sets of simulation centre on the capability of cerebral autoregulation to maintain CBF despite changes in blood pressure (Figure 3.5). These simulations could give us a good indication of the model performance during dynamic changes with observations of the absolute changes in CBF and an indication of the temporal resolution of the autoregulation mechanisms, mainly those that are pressure and/or flow dependent.

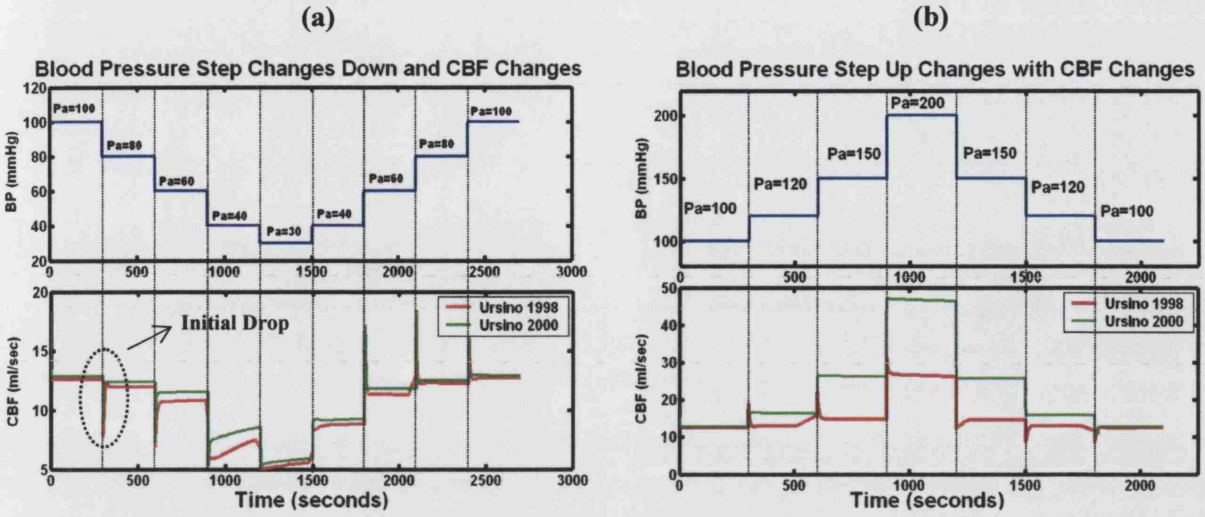

Figure 3.5: Simulations of step changes in blood pressure for both models during normocapnia **(a)** Step down changes in blood pressure; **(b)** Step up changes in blood pressure. (Pa: arterial pressure)

Comparison of the results for the step down changes in blood pressure demonstrate a reasonable similarity between the models. With the sudden drop in pressure, there is a large initial transient drop in CBF, which is passive and governed by pressure dependent mechanisms. Following that there is an active response of the cerebral vessels to the drop in flow via the flow mechanism action to try and maintain a constant CBF. One can see that the initial drop in CBF becomes smaller as the lower limits of autoregulation are reached and is almost abolished at the last step where blood pressure is outside the autoregulation limits.

There is also a distinct difference between the models during the 60mmHg to 40mmHg blood pressure step down change with the Ursino (2000) [5] model appearing to exhibit greater autoregulatory capability. These effects are governed mostly by the compliance and the resistance of the different arterial compartments as it is discussed later.

Finally looking at the CBF maintenance, it is very clear that during the last step where cerebral autoregulation has been breached, the CBF is about half the normal value.

Almost identical results are shown during the step up changes in blood pressure but this time in the opposite direction. However now there is a very distinct difference between

the Ursino (1998) [4] and the Ursino (2000) [5] models. As one can see, the latter does not exhibit evidence of autoregulation. The Ursino (2000) [5] model parameters as they stand, give a very low steady state ABP (of around 70 mmHg), since the steady state resistance is only $5.14 mmHg.ml^{-1}.s^{-1}$. The ABP traces are thus a long way from the 'normal' value, so we do not see any autoregulation except at lower ABP values. One can solve this problem by altering the original parameter values of the Ursino (2000) [5] model, and running the model with a higher value of basal cerebral blood flow (q_n) to give a higher baseline value of ABP. If this is done then one gets more realistic autoregulation when ABP is increased. Finally, at the highest blood pressure step, CBF is about double the normal value for the Ursino (1998) [4] and about three times larger for the Ursino (2000) [5], both indicating a failure of cerebral autoregulation.

Figure 3.6 provides more information on the inner workings of the Ursino (1998) [4] model during the changes in blood pressure. As blood pressure falls from the normal range of autoregulation the dominant effects happen in the cerebral arteries, with different importance for each pial segment for the same blood pressure values. During moderate changes in blood pressure, the changes in vessel radius are more pronounced in the large pial arteries than the arterioles. As arterial pressure falls further reaching the lower autoregulation limit, dilation of the small pial arteries becomes progressively greater causing an increase in cerebral blood volume, whereas the response of the large vessels is quickly exhausted. As blood pressure approaches its lowest or highest values, the vessel radii demonstrate a completely passive behaviour with pressure. Beyond the lower limit of autoregulation, CBF starts to decrease despite the evident vasodilation of the small pial arteries. One can see in Figure 3.5 for the step change from 40 to 30mmHg and from 150 to 200mmHg, the CBF change is either halved or doubled respectively indicating the inability of the cerebral circulation to autoregulate.

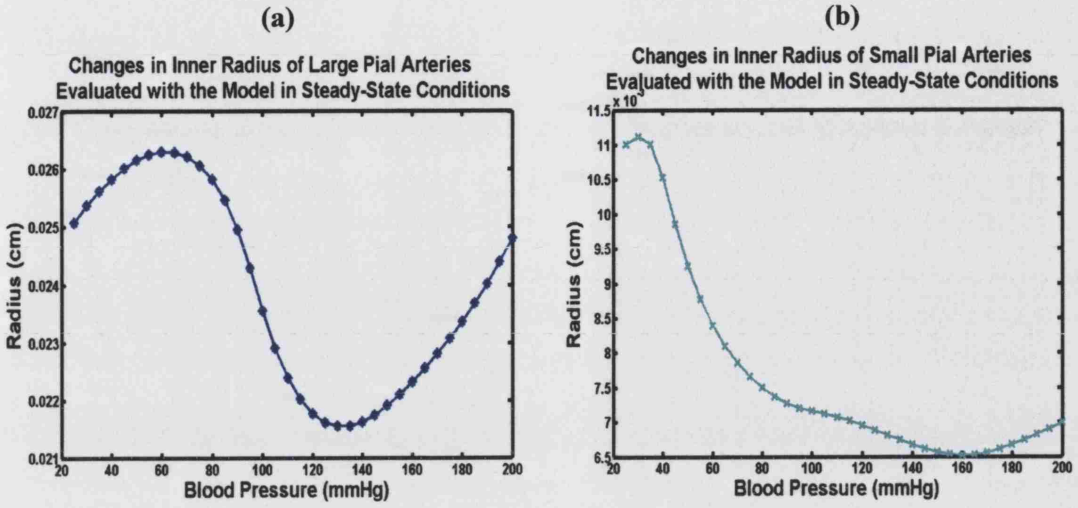

Figure 3.6: Changes in the **(a)** inner radius of large; **(b)** and small pial arteries; evaluated with the Ursino (1998) [4] model in steady-state conditions at different levels of blood pressure.

On the other hand, Figure 3.7 shows the steady state values for the pial arteriolar resistance, compliance and volume predicted by the Ursino (2000) [5] model during changes in ABP. One can clearly see that after a 20% increase in ABP, arterial volume remains constant with compliance and resistance changing only by a small amount. This could explain once more the inability of the Ursino (2000) [5] model to maintain constant CBF at higher levels of blood pressure; it looks as though the autoregulation curve has been shifted to the left.

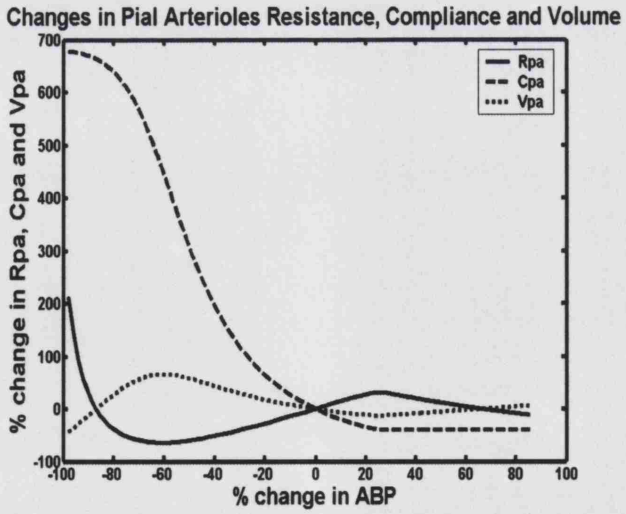

Figure 3.7: Percent changes in the pial arteriolar resistance, compliance and volume evaluated with the Ursino (2000) [5] model in steady-state conditions at different levels of blood pressure (R_{pa}: resistance, C_{pa}: compliance and V_{pa}: volume of the pial arteries).

Simulations were also performed to test the Ursino (1998) [4], and Ursino (2000) [5] models in response to changes in $PaCO_2$ (Figure 3.8). As discussed in Chapter 2, CO_2 is a potent affector of the cerebral blood flow, which alters it via a pH modulated pathway. Such an action is claimed to have been modelled by the authors.

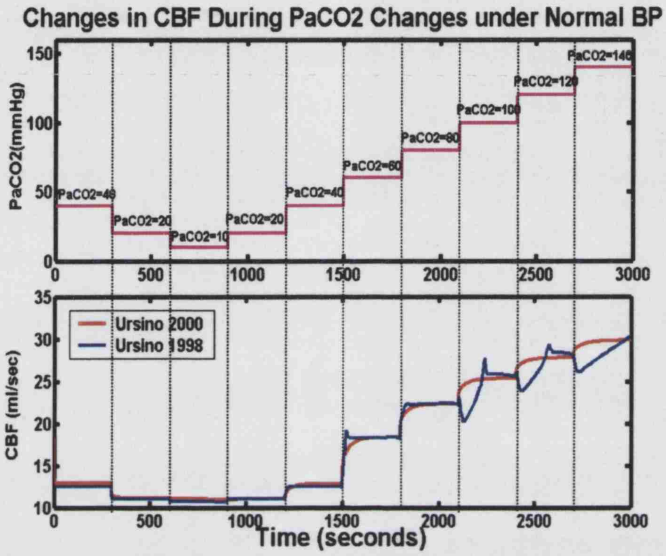

Figure 3.8: Simulation results from the Ursino (1998) [4] and Ursino (2000) [5] models during step changes $PaCO_2$ at a normal level of BP (100mmHg).

CBF decreases or increases quite rapidly (slope 2.5% $ml.100g^{-1}.min^{-1}$ CBF/mmHg $PaCO_2$) between the $PaCO_2$ ranges of 40 to 150mmHg. Below 40mmHg the slope of change is more gradual and it looks as if it reaches a plateau. The same observations can be seen in Figure 3.8 as hypocapnia causes a reduction in CBF but not below 10ml/sec even though $PaCO_2$ is at 10mmHg. As $PaCO_2$ increases, CBF increases dramatically and when $PaCO_2$ is at 80mmHg, CBF is doubled. One can also see very clear distinct differences between the two versions of the model. The Ursino (1998) [4] model shows overshoot transient spikes during the last three steps; this is probably due to the fact that it is trying to autoregulate unsuccessfully as the larger arteries have a limited capability to alter their radius (Figure 3.9). However in the Ursino (2000) [5] model this overshoot is not present as one of the simplifications of that model is the removal of that segment, which is treated as having a constant blood flow.

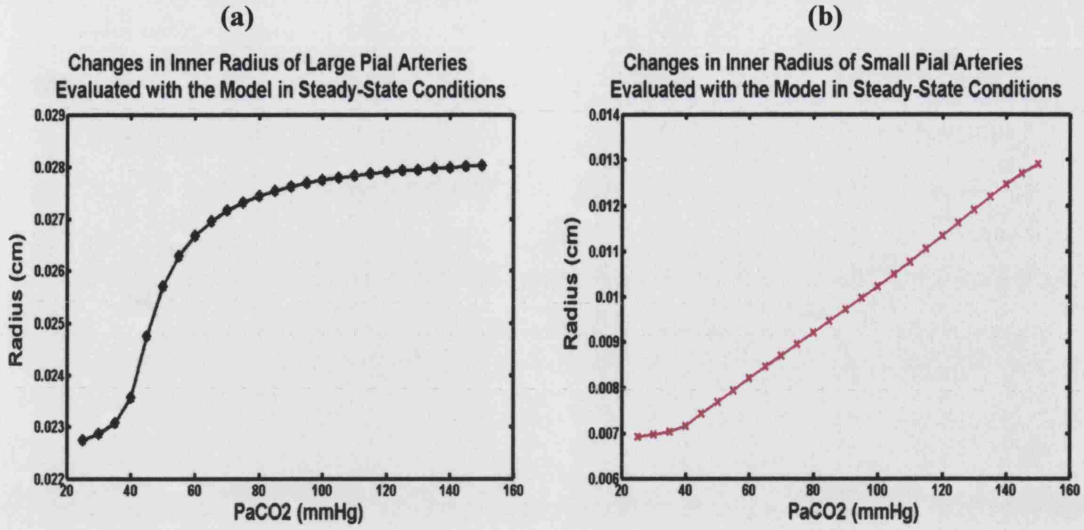

Figure 3.9: Changes in **(a)** inner radius of large; **(b)** and small pial arteries; evaluated with the Ursino 1998 [4] model in steady state conditions at different levels of $PaCO_2$. Through out simulations BP was kept constant at normal basal levels.

Finally simulations were also performed to test the Ursino (1998) [4], and Ursino (2000) [5] models under step changes in BP at different levels of $PaCO_2$ (Figure 3.10). This would show us how autoregulation copes with complementary and contradictory effects in the two models.

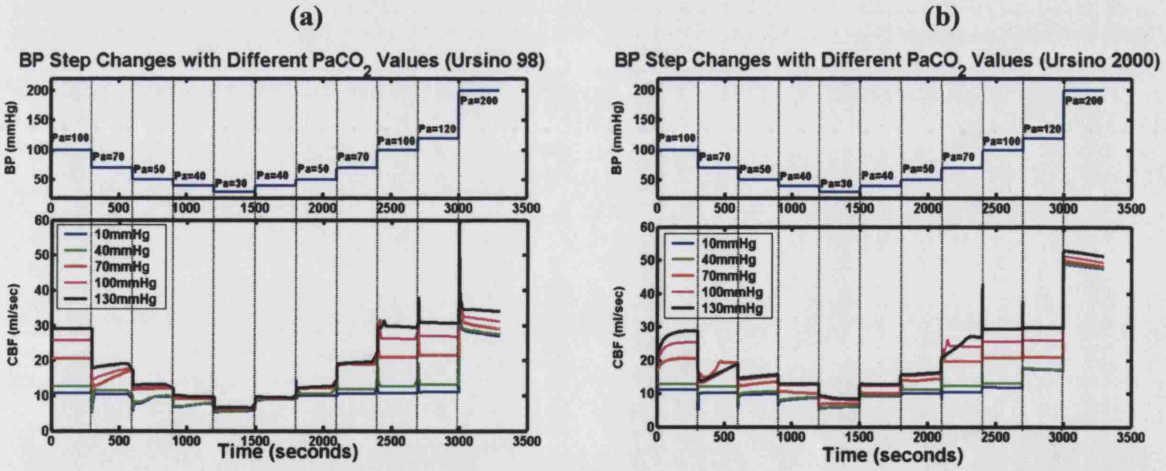

Figure 3.10: Dynamic simulations of the **(a)** Ursino (1998) [4]; **(b)** and Ursino (2000) [5]; models during step changes in blood pressure at various levels of $PaCO_2$.

By observation from Figure 3.10 one can see that even when $PaCO_2$ is in the hypercapnic region, which precipitates an increase in CBF, the drop in blood pressure abolished that effect. As blood pressure decreases, starting from a normal level, the CO_2

reactivity becomes initially greater, suggesting a facilitatory overlapping of the two mechanisms. However when arterial pressure approaches the autoregulation lower limit, the CO_2 responsiveness also progressively disappears indicating an overlapping attenuation mechanism of pressure autoregulation and hypercapnia.

It is well known that hypercapnia shifts the autoregulation plateau to higher CBF levels and hypocapnia reduces it to lower CBF. It has been claimed that the failure of cerebral vessels to constrict with hypocapnia during hypertension, indicates that the maintenance of adequate tissue oxygen supply prevails over the maintenance of adequate CO_2 and acid-base levels. This is something that a simple vascular biophysical model could not show directly. CO_2 reactivity increases with reduction in the blood pressure; later when vasodilation in the small pial vessels becomes appreciable, the CO_2 reactivity rapidly decreases.

Obviously an increase in $PaCO_2$ causes an increase in CBF at a given arterial pressure value. At the same time, the lower autoregulation limit shifts towards higher pressure; in fact cerebral vessels are nearly maximally dilated because of hypercapnia and are therefore unable to dilate further in response to arterial hypotension. These findings have been confirmed by several authors who studied the effects of induced hypotension at various $PaCO_2$ levels and these results have been discussed in Chapter 2. It can also be seen that arterial hypotension progressively reduces CO_2 reactivity. The greatest effect of hypotension is visible during hypercapnia, when the arterial bed is already dilated to its maximum. On the other hand, experimental data (see Chapter 2) suggests that the vasoconstrictory effect of hypocapnia is also reduced during severe hypotension. Both versions of the model can reproduce this behaviour, attributing it to a reduction in the CO_2 reactivity during cerebral ischemia.

The difference again between the Ursino (1998) [4] and Ursino (2000) [5] models is seen during the last two blood pressures step up changes in Figure 3.10. Again the inability of the Ursino (2000) [5] model to show autoregulation is clearly seen. This is for the reasons discussed previously.

We have seen how both the Ursino models behave both under steady state and dynamic changes. Some physiological characteristics are generally in agreement in both. These

are the non-linear shape of the autoregulation curve, vasoconstriction at high ABP and vasodilation at low ABP. However there are quantitative differences between the two arising from the simplification of the Ursino (2000) [5] model. Also very clear is the overshoot in the step responses, and the autoregulation capability which tends to differ at high blood pressures between the two models.

3.3 Black box models

We have discussed the physiologically based models and we now look at another type and method of modelling called 'black box' modelling or 'time series' models. These are models constructed to reproduce a specific experimental result and that can have a predictive power without linking this to the physiological background.

Some general points of such models are that most of the times they use a transfer function relating the input to the output, which in our case is physiological data from monitoring equipment. Thus the transfer function is found from the experimental data. The transfer function is assumed to be of a given order, and can be linear or non-linear. One of the major limitations of this approach is the inability to interpret results in terms of the underlying physiology or pathology.

We now discuss some models of this type presented in the literature and briefly describe models from, Tiecks et al, (1995) [12], Chon et al, (1998) [13], Panerai et al (2000) [14], and Zhao and Marmarelis et al, (2000) [15]. In particular the models developed by Panerai and colleagues (1999) [16] and Kirkham et al (2001) [17] are discussed in more detail.

Starting with Tiecks et al [12], this is one of the most cited mathematical models of cerebral autoregulation. The authors wanted to evaluate cerebral autoregulation both under dynamical and static changes. The model comprises a set of discrete difference equations governed by three parameters, namely (i) a gain factor, (ii) a damping factor and (iii) a time constant. In this study they compared results from step responses with predicted responses in order to define an autoregulatory index.

We continue with the work of Panerai et al [14] where they used a linear transfer function derived from the power spectrum they obtained by averaging transcranial Doppler velocity over each heart beat. They only consider the overall frequency response and found that blood flow precedes blood pressure but by decreasing amounts at higher frequencies.

We would like here to point out that both the Tiecks et al [12] and Panerai et al [14] are linear models. The assumption that dynamic autoregulation can be approximated by linear systems is questionable. As we discussed in Chapter 2 and earlier in this chapter, there are several nonlinearities present in the cerebral autoregulation such as the change in cerebrovascular resistance which is influenced by the arteriolar diameter, which may be influenced by both neurogenic and metabolic mechanisms. There have been nonlinear black box models such as those of Zhao and Marmarelis [15] and Chon et al [13], which are discussed here, but for further details the reader should look at the original paper of Panerai and colleagues [16] for comparisons between linear and nonlinear models.

The approach from Zhao and Marmarelis [15] and the Chon et al [13] is based on Volterra kernels. Volterra kernel analysis includes the entire linear and nonlinear system behaviour. To be completed, this requires the use of an infinitely large number of infinitely long kernels, and it would be difficult later to relate these to physiological parameters.

To summarise, it is clear that one probably has to look at nonlinear mathematical models of cerebral autoregulation as it is a highly nonlinear process. Similarly, one can question the reason for using techniques such as black box modelling, which can only give a limited insight into the underlying physiological behaviour. However, these methods can provide information regarding specific challenges and responses; they have a simpler mathematical formulation (and less complexity), and do not require accurate knowledge of biochemical reaction sequences and their rate constants.

3.3.1 The Panerai et al (1999) model [16]

Panerai et al [16] attempt to produce data-driven models of the system of cerebral autoregulation using a variety of techniques including both linear and non-linear methods. MBP is taken to be the input to the system and the middle cerebral artery velocity (V_{mca}) measured using transcranial Doppler (TCD) is taken to be the output. Models generated using this approach allow reasonable prediction of the output of the cerebral autoregulation system once trained on a set of data. However these models, which are in the form of multidimensional kernels that can be convolved with input data, are difficult to interpret clinically.

The mathematical methods adopted by Panerai et al [16] are generally system identification techniques, which allow modelling of the input-output relationship between any two parameters in the cerebral autoregulation system. Given the difficulties described above, which are inherent in validating physiological models, these system identification techniques promise to provide independent validation of any dynamical relationship between the input and the output of the cerebral autoregulation system.

3.3.2 The Kirkham et al (2001) model [17]

Work by Kirkham and colleagues [17] discusses a dynamic mathematical model where cerebral autoregulation is represented as a flow feedback mechanism. They define the autoregulation process through a flow dependent feedback, which responds to changes in flow from its baseline value.

Their work is based on a linear transfer function with only two parameters namely λ the rate of restoration and a time delay τ both of which are constants. The flow rate is found from the velocity profile in the MCA measured by TCD and the time delay allowing for the delay between stimulus and response as an inherent part of the feedback mechanism.

They have validated the model against experimental data taken from physiological tests involving rapid thigh cuff release and lower body negative pressure challenges. Data from the thigh cuff test was obtained from the original study of Aaslid et al [18]. Their second set of data was collected from a study involving a lower body negative pressure

box, where lower body negative pressure is varied sinusoidally to produce oscillatory variations in ABP with amplitude of 5-10% of the mean and period of 12sec.

The derived model gives a velocity profile in the MCA for a generally imposed pressure gradient and could be applied to any experimental method that utilizes changes in ABP as a stimulus for assessing dynamic autoregulation. Their conclusions were that with the proposed cerebral autoregulation model it is possible to determine values of λ and τ that reproduce the experimental data. In a further separate comparison between results, they found that the model and the experimental data yielded similar values for the parameters λ and τ required to reproduce the data. This suggests that the parameters may be independent of the form of the pressure stimulus but are related to the physiology of the cerebral autoregulation mechanism. In particular, the underlying physiology could be further explored by investigating the relationships between the model parameters λ, τ and physiological parameters such as carbon dioxide concentration and metabolite levels.

Limitations of their approach include the fact that they consider a constant radius of the MCA artery and also ignored the subject to subject variability. Furthermore they consider venous pressure as constant in the presence of changes in ABP. Finally when modelling impaired autoregulation with only partial restoration, they have not included the limits of the autoregulation mechanism.

3.4 The BRAINCIRC UCL model (version 1.0 2004-2005)

A brief description of the extended modelling work carried out by Dr Murad Banaji and colleagues [1] in the department is given below. The intention is to provide a general summary of the UCL BRAINCIRC cerebral model (version 1.0, 2004-2005), which in this thesis will be referred to as the UCL model. For a much more detailed description, regarding both the mathematics and the biochemistry, the reader is referred to the original paper by Banaji and colleagues [1], which is reproduced in Appendix C. At this stage the model is a functioning computational software available on the web (http://www.medphys.ucl.ac.uk/braincirc/). Although it is likely to undergo significant

refinement over time, it is able to produce meaningful results as we shall illustrate throughout this thesis.

3.4.1 Introduction

The UCL model consists of a set of ordinary differential equations and algebraic equations. This is a continuous in time, but discrete in space model. The Ursino and Lodi (1998) [4] model has been extended by combining it with a model of biochemical processes occurring within both blood and brain tissue on different time and space scales (see Figure 3.11).

Initially the model consists of a set of chemical reactions, a set of existing differential equations (from Ursino and Lodi, 1998 [4]) and a set of algebraic relations (partly from Ursino and Lodi, 1998 [4]), which describe conservation of various phenomena or dynamics. Such a combined model allows prediction of both, physical variables such as blood velocity in the MCA but most important the concentrations of key metabolites such as ATP and hydrogen ions, making it possible to model the chemical feedback mechanisms which govern autoregulation in addition to the existing physical mechanisms. Furthermore, it opens up the possibility of modelling the signals produced both by non-invasive methods such as near-infrared spectroscopy, as well as invasive systems such as microdialysis, which measure the concentrations of chemicals within the blood or the brain tissue.

The UCL model can be constructed without assigning numerical values to the parameters it includes, but it cannot of course be integrated until this task has been done. Assigning numerical values to these parameters is highly non-trivial. The reason for this is the large numbers of parameters which (to our knowledge) most have not been measured in humans together with their likely individual variability. As one eventual aim of the modelling work is to use it to predict parameters at the patient's bedside, attention is now being focussed on methods of estimating key model parameters for a given individual.

Promising results have been obtained so far, with the extended model qualitatively reproducing biophysical and biochemical events known to occur in the brain. The

biochemistry has been simplified to make the numerical integration of the model more rapid as there are fewer parameters to estimate, while attempting to preserve features considered as being physiologically essential. Later, a brief description will be given of some of the biochemical feedback mechanisms together with some simulated results from the model in the steady state.

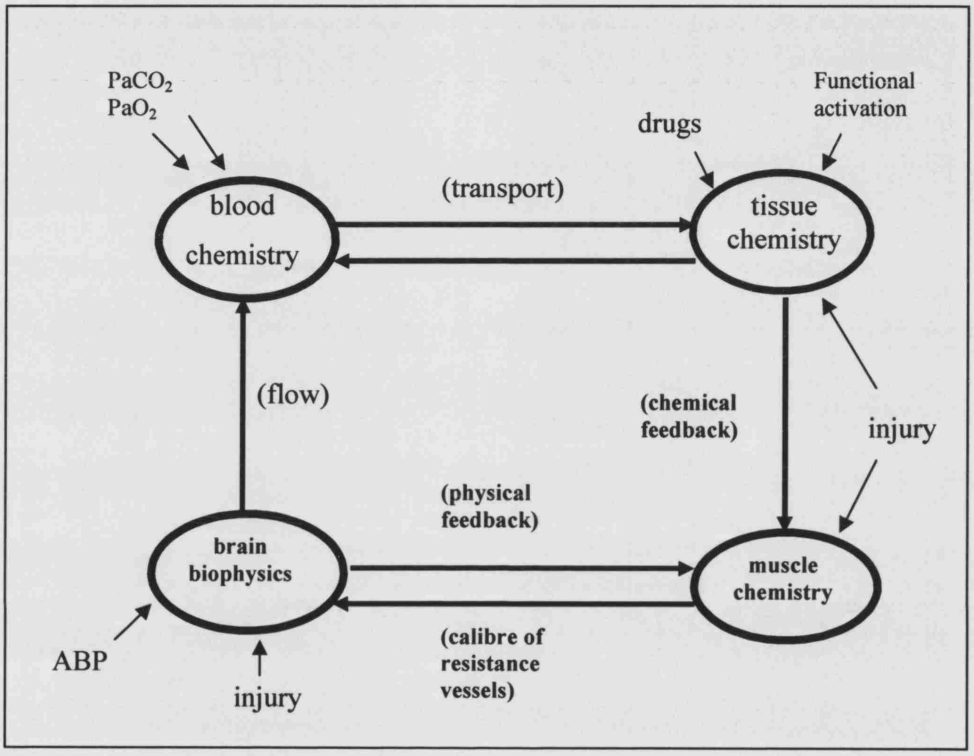

Figure 3.11: A simplified schematic diagram of the important compartments in an integrated biophysical and biochemical model of the human brain. Representation of the group of processes and the connection between them are shown by ovals and bold arrows respectively. The sites where external stimuli feed into the model are also shown.

3.4.2 Spatial structure

To begin the description of the UCL model we first look at the spatial structure. Namely there are three sites in the model and these are the (i) cerebral vasculature, (ii) the tissue, and (iii) the vascular smooth muscle. Each of these is further subdivided allowing exchange of information and substances between the sites. Figure 3.12 shows a diagrammatical representation of the model's spatial structure and summarises some of the most important processes which are included in the model.

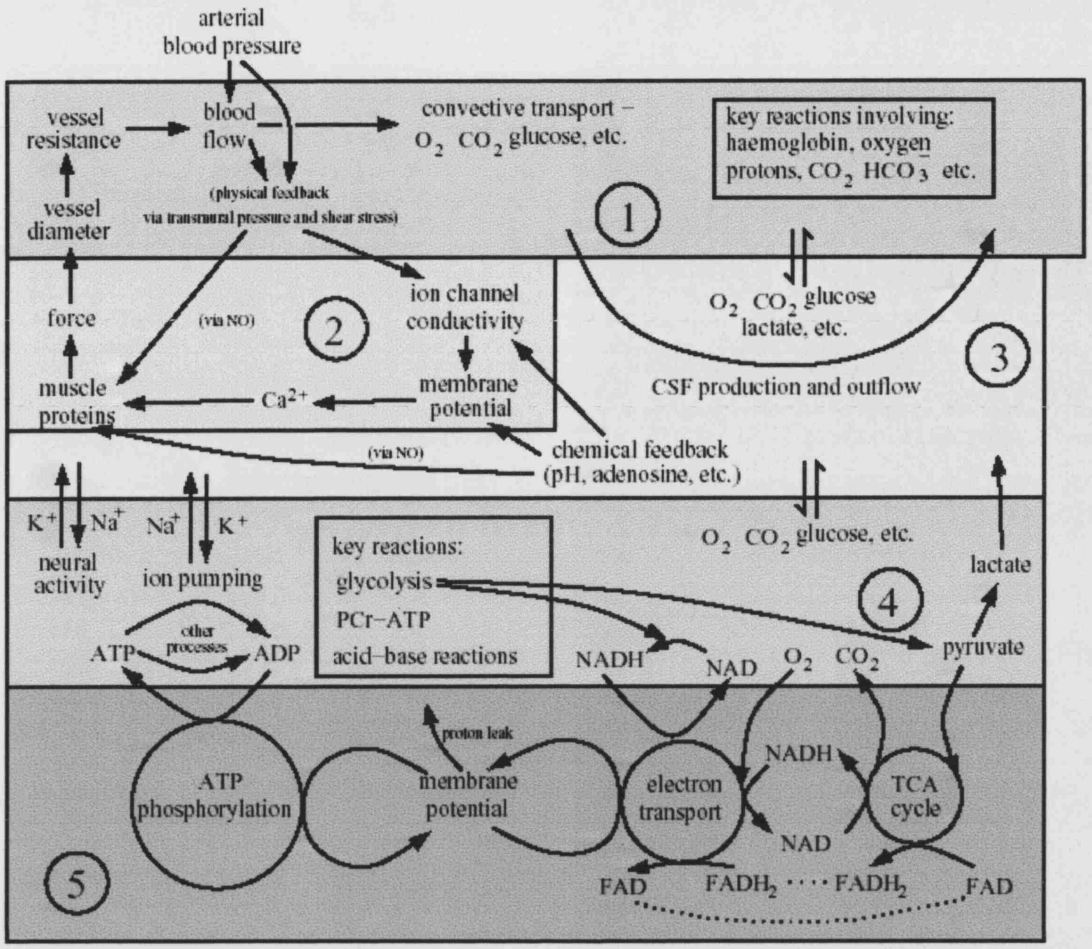

Figure 3.12: A summary of the main processes occurring across the five main sites in the model. The sites are (1) The vascular system, (2) Vascular smooth muscle (VSM) surrounding the arterial compartments, (3) The extracellular space, (4) The intracellular space-cell cytoplasm, (5) The mitochondria matrix. Figure taken from [1].

The first site is the cerebral vasculature; this consists of (i) the large pial arteries, (ii) the pial arterioles, (iii) the cerebral capillaries and (iv) the veins. The biophysics of the cerebral vasculature has been taken from the Ursino and Lodi (1998) [4] model. One of the important features of this site and especially the division of the arterial compartment is that these are the vessels that can actively change their radius to alter blood flow, which in effect controls the active cerebral autoregulation.

The second site in the model is the cerebral tissue, which is again divided into a number of compartments and sub-regions. These are (i) an extracellular compartment (ec), (ii) an intracellular but extramitochondrial compartment (cytosol or cyt) and (iii) an intra-mitochondrial space. These compartments comprise the majority of the brain volume, which in the model is about 80% of the total cerebral volume.

The final site is the endothelium or vascular smooth muscle (VSM), which is one of the major contributors to the exchange of chemicals and ions which affect cerebral arterial diameter and hence muscular tone. Again this site comprises two compartments and these are (i) the intra-cellular space of the smooth muscle cells of the large arteries, and (ii) that of the smaller arteries and arterioles. Although the endothelium is not explicitly represented, NO produced in the endothelium is modelled.

Figure 3.13 outlines and summarises all the sites and the compartments of the model.

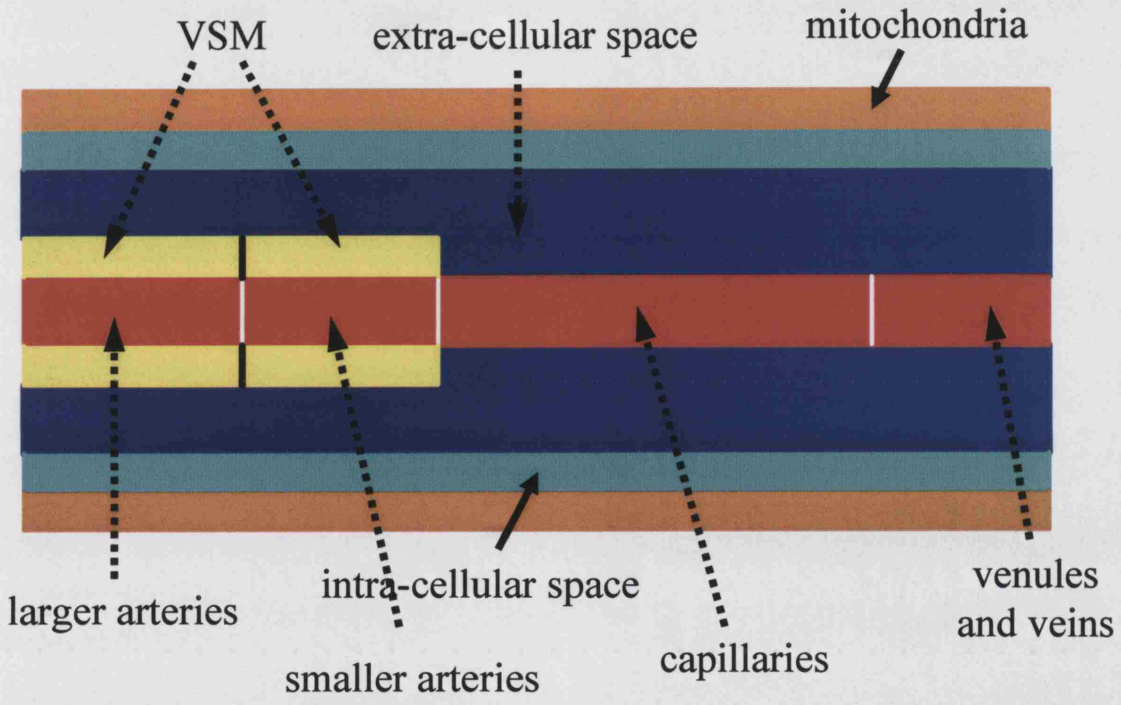

Figure 3.13: Schematic of the physical layout of the different compartments, indicating which compartments can communicate directly with which others (represented by them having adjacent boundaries in this representation).

As this model is highly compartmentalised with a lot of sites interacting and in dynamic equilibrium with each other, communication and chemical equilibrium is a very important aspect of this work and is extremely complicated.

3.4.3 Communication between sites

The means by which these sites and compartments communicate are:

(i) blood flow between successive segments of the vascular network carrying associated chemicals,

(ii) chemical exchange taking place between the tissue extracellular and capillary compartments,

(iii) fluid dynamic exchange occurring between the capillary compartment and the tissue extracellular compartment (production of CSF),

(iv) fluid dynamic exchange between the tissue extracellular space and the venous compartment (outflow of CSF); chemicals in the CSF are carried out this way too,

(v) chemical exchange between the tissue extracellular and the cytoplasmic compartments,

(vi) chemical exchange, which takes place between the cytoplasmic and the tissue intra-mitochondrial compartments,

(vii) chemical communication between the tissue extracellular compartment and the muscle compartments,

(viii) physical communication between the muscle compartments and the arterial and the arteriolar compartments via alteration in vessel calibre,

(ix) physical communication, which takes place from the arterial and arteriolar compartments to their respective muscular compartments (via the endothelium, or through directly pressure-mediated events).

3.4.4 Model variables and parameters

As one can appreciate this model is large in size and in complexity with a very large number of parameters and variables involved, (currently around 200). These

variables and parameters include chemical concentrations, resistances, compliance, pressures, membrane potentials, permeabilities, vascular wall thickness etc.

Continuing with the description of the UCL model we would like to remind the reader and emphasize that the backbone of this model is based on the work from Ursino and Lodi [4] model. However as discussed in previous chapters this is a biophysical model; in modelling cerebral circulation one should and must include the key components of basic metabolic biochemistry. As discussed in Chapter 2 one key aspect of cerebral autoregulation theory is based on the hypothesis that metabolic substances or metabolic bioproducts are largely responsible for vasodilatation. Furthermore, most of the pathologies involving the brain are linked to tissue biochemistry and metabolism either as the main cause of the particular disease, or as chemical imbalances caused by the pathological insult or as means for therapeutic interventions by the clinicians. Including such a metabolic submodel is a complex mathematical process which is not discussed here; some key points of these chemical reactions are based on mass action reactions, Michaelis-Menten reactions, zeroth order dynamics, active transport, and convective transport. For more information the reader would be advised to look at Keener and Sneyd [19] and Banaji et al [1].

To help in understanding the metabolic reactions present in the UCL model, we can crudely split them according to the sites of action or/and the site where the reaction is taking place. In the UCL model three such major sites are recognised and these are the (i) brain tissue, (ii) the blood biochemistry and (iii) the smooth muscle cells. A brief summary of these is provided below with some of the major biochemical reactions occurring at the above sites described.

3.4.5 The brain tissue compartment

First we look at the brain tissue compartment where a caricature of the metabolic pathway from glucose to CO_2 and ATP has been modelled. Although the biochemistry of the brain tissue is physiologically complex, it is however generally governed by simple rules and dynamic processes that drive the system into equilibrium. These aspects of the biochemistry must include the intracellular space (both intra- and extra-mitochondrial) as this is where the essential metabolic biochemistry takes place. The

extracellular space is given limited biochemical dynamics and the blood has some that are unique to it.

The most important aspect of the biochemical balance in the brain is the supply of the brain's energy requirements, which dictates the need for ATP. One of the primary needs for ATP is to provide energy for the gates to pump potassium coming out from the cells during neural activity back to the cells. In the model the brain needs a sufficient supply of ATP, to support all the metabolic processes. This of course requires an adequate supply of glucose and the associated glycolysis pathways.

Glucose in the model is supplied from the blood to the extracellular space from where it diffuses in to the cell. We are not entirely interested in modelling glycolysis in all its detail; however a simplified caricature of this process has been modelled.

This brings us to the TCA cycle which takes place in the intramitochondrial space. Oxygen and CO_2 diffuse in three steps between the blood and extracellular space, the extracellular space and intracellular space and the intracellular space and intramitochondrial space. Other chemicals such as the NADH, pyruvate and inorganic phosphate have particular transport processes. The TCA cycle in the model is caricatured as a three stage process. The first stage is taken to be the combination of pyruvate with oxaloacetate to give rise to CO_2 and alpha-ketoglutamate; the second stage is the conversion of the alpha-ketoglutamate to succinate and CO_2; and the third stage is the conversion of succinate back to oxaloacetate along with the reduction of one molecule of NAD and one of FAD.

Looking at all the above in terms of energy production, according to the model glycolysis and the TCA cycle produce NADH, $FADH_2$ and a small amount of ATP. At this point oxygen enters the process. In the UCL model the electron transport and oxidative phosphorylation has again been caricatured and for more details of this the reader should look at Banaji et al [1]. In terms of our abstract description, energy production follows the standard reactions of glycolysis, the TCA cycle and oxidative phosphorylation. According to the model, one molecule of glucose requires six molecules of O_2 for its complete oxidation, and this produces six molecules of CO_2. Furthermore, the oxidation of one molecule of NADH produces 2.5 molecules of ATP

and the oxidation of one molecule of $FADH_2$ produces 1.5 molecules of ATP. Thus, the complete oxidation of one molecule of glucose gives us 32 molecules of ATP. However, the conversion of one molecule of pyruvate to lactate, with the accompanying oxidation of one molecule of NADH, gives rise to a possible net loss of 15 molecules of ATP.

In parallel with this simple model of energy production, there are several subsidiary reactions. One of these is the pH dependent conversion of pyruvate to lactate accompanied by the reduction of one molecule of NADH. This process is important when considering metabolic imbalances due to insults affecting the brain circulation. The production of lactic acid can alter pH which is known to have a feedback effect on vascular smooth muscle.

This brings us to the question of the pH concentration changes in the four key biochemical compartments of the model; these are the capillary, the extracellular space, the intracellular space and the mitochondrial matrix. Maintenance of pH is of great importance to cerebral autoregulation and in the model is treated as a complex process with several feedback mechanisms. Firstly CO_2 moves quite freely between compartments, but as there is a net production in the mitochondria and a net outflow via the blood, there is a CO_2 gradient from mitochondria to cytoplasm to extracellular space to blood. Secondly there is a relatively rapid transport of bicarbonate ions between blood and the extracellular space (but less rapid transport between extracellular and intracellular spaces). Thirdly, the actual pumping of protons out of the mitochondria during oxidation of NADH and $FADH_2$ tends to raise the pH inside the mitochondria. Finally we have an additional important agent in the blood - haemoglobin - which acts as a buffer in two ways by combining with both carbon dioxide and with protons. These factors mean that we do not expect pH in all three compartments to be equal. In general the typical values of pH in the model are 8 for mitochondria, 7.35 for capillary blood, 7.25 for extracellular space and 7.0 for intracellular (but extramitochondrial) space.

Clearly, increases in the concentration of lactic acid or CO_2 will tend to decrease the pH and increases in the concentration of Lac^- or HCO_3^- will have the opposite effect. At physiological pH, almost all the lactate will be dissociated. This means that the production of extra lactate puts serious strains on the buffer systems of the cell. In the

cytoplasm, the pH level is determined essentially by the levels of lactate and CO_2/bicarbonate (and perhaps to some extent pyruvate). The production and dissociation of carbonic acid in the model is treated as a single, reversible process in which CO_2 is converted to bicarbonate (HCO_3^-) and hydrogen ions (H^+).

3.4.6 The blood biochemistry

Continuing with the modelling of the metabolism and biochemistry, we move to the next compartment of the UCL model where biochemical reactions are taking place, namely the blood. The key reaction in the blood is oxygen delivery and the combination of oxygen and haemoglobin. Haemoglobin is an important molecule that in the model is used for carrying oxygen, carbon dioxide and the previously mentioned buffering effects. Other reactions in the blood include the production and dissociation of carbonic acid and of lactic acid.

3.4.7 The vascular smooth muscle

Finally we come to the biochemistry of smooth muscle action, which acts as the bridging point between a model of blood and brain biochemistry, and any physical model of the basic fluid flow processes occurring in the vasculature.

Calcium is a crucial determinant of vascular smooth muscle tone, and in particular its concentration in the muscle cytoplasm. Consequently, membrane potential is a key variable in the model as it is alterations in membrane potential which are the primary stimulus causing calcium to flow into and out of the cell. The most important influences on the membrane potential are the resting potential of potassium ions which is taken to depend solely on the extracellular concentration of potassium and the total potassium channel conductance which affects membrane potential in the opposite way, causing the cell to hyperpolarise when conductance increases therefore causing vasodilation.

As the reader can clearly understand, the potassium channels in the model are very important to the whole cerebral autoregulation process. Currently there are three types of channel, one sensitive to potassium concentration, one to pH and one to transmural pressure; these all affect the overall potassium channel conductivity.

A change in the extracellular potassium in the model has two contradictory effects. Firstly, it is altering potassium resting potential and secondly, it is changing potassium conductance. The way the model responds to a small increase in extracellular potassium is that it mainly affects the conductance and hence causes vasodilation. However, for larger increases in extracellular potassium, the vasoconstriction effect of the consequent change in the potential dominates.

We have now discussed how different stimuli in the model can alter potassium channel conductance and hence membrane potential and thus calcium concentration in the vascular smooth muscle cells. We now turn to the actual muscle action and how this is regulated in the model. In VSM and in the model, regulation is currently treated as being entirely via alterations in the phosphorylation and dephosphorylation rate of the myosin (phosphorylated crossbridge heads) LC20 chains (the chemical actin is never modelled).

Thus the two key regulators of muscle tone in the model are calcium and endothelium-derived relaxing factor (EDRF) which we take to be nitric oxide (NO), which act in complementary ways by increasing the phosphorylation/dephosphorylation rate of myosin.

From the above discussion, it is clear that currently there are two ways that a stimulus can cause contraction or dilation in the model. First, by increasing or decreasing the quantity of cytoplasmic calcium and therefore altering membrane potentials; and secondly, by changes in the rate of dephosphorylation at a given concentration of calcium.

3.4.8 Model simulations

Finally some results of simulations with the model at steady state are presented. The model is able to reproduce qualitatively the autoregulation of cerebral blood flow in response to blood pressure changes, arterial CO_2 and O_2 concentration changes. The reader should look for comparisons with physiological data from Chapter 2.

Before we discuss the results of the steady state model simulation we digress briefly to mention another physiological quantity that the model reproduces and that we can measure experimentally; this is the cerebral tissue oxygenation index (TOI) obtained from NIRS. In chapter 4 we discuss in detail the principles and the physiological meaning of this measurement; here we present the analytical solution that the model uses to predict this physiological quantity.

TOI is essentially the average oxygen saturation of the haemoglobin in the blood in the brain. In the model there are three compartments with different volumes (Vol) where haemoglobin resides: (i) an arterial compartment, (ii) a capillary compartment and (iii) a venous compartment. TOI is the average ratio of the oxygenated haemoglobin (HbO_2) divided by the total haemoglobin (HbT) from each compartment respectively (Equation 3-1).

$$TOI = \frac{HbO_{2(a)} \cdot Vol_{(a)} + HbO_{2(c)} \cdot Vol_{(c)} + HbO_{2(v)} \cdot Vol_{(v)}}{HbT_{(a)} \cdot Vol_{(a)} + HbT_{(c)} \cdot Vol_{(c)} + HbT_{(v)} \cdot Vol_{(v)}} \times 100\% \qquad \textbf{3-1}$$

where subscripts (a), (c) and (v) refer to the arterial, capillary and venous compartments respectively.

3.4.8.1 Blood pressure autoregulation

Simulations were done by fixing arterial blood pressure at a particular value and allowing the model to settle; then blood pressure was gradually increased/decreased in steps of 1mmHg, allowing the model to settle each time. Parameter values are the model default values. Figures 3.14(a) shows a typical steady-state autoregulation curve as predicted by the model while Figure 3.14(b) shows tracings of cerebral arterial diameter and cerebral blood flow versus arterial pressure taken from a physiology textbook [20]. Visual comparison shows a reasonable agreement. Figure 3.15 shows steady-state autoregulation curves with changes in blood pressure as simulated by the model for the changes in cerebral blood volume and cerebral TOI.

(a)

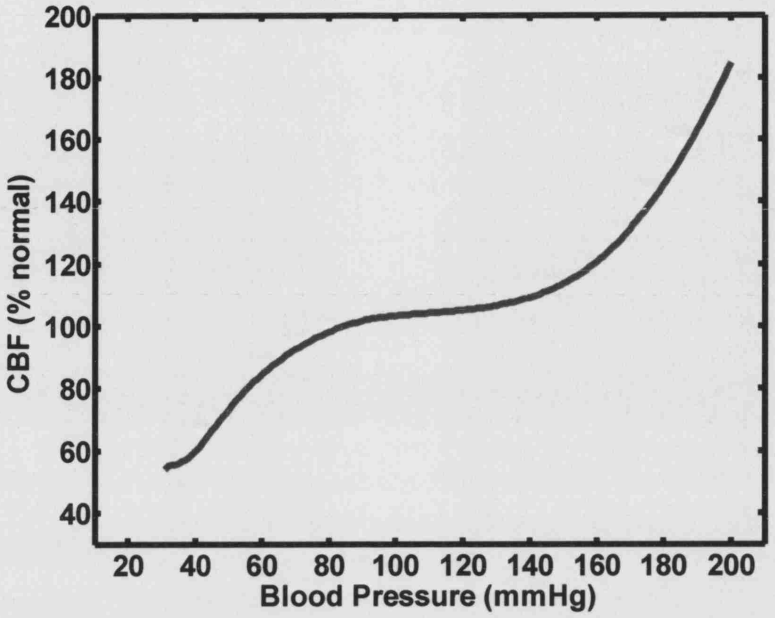

(b)

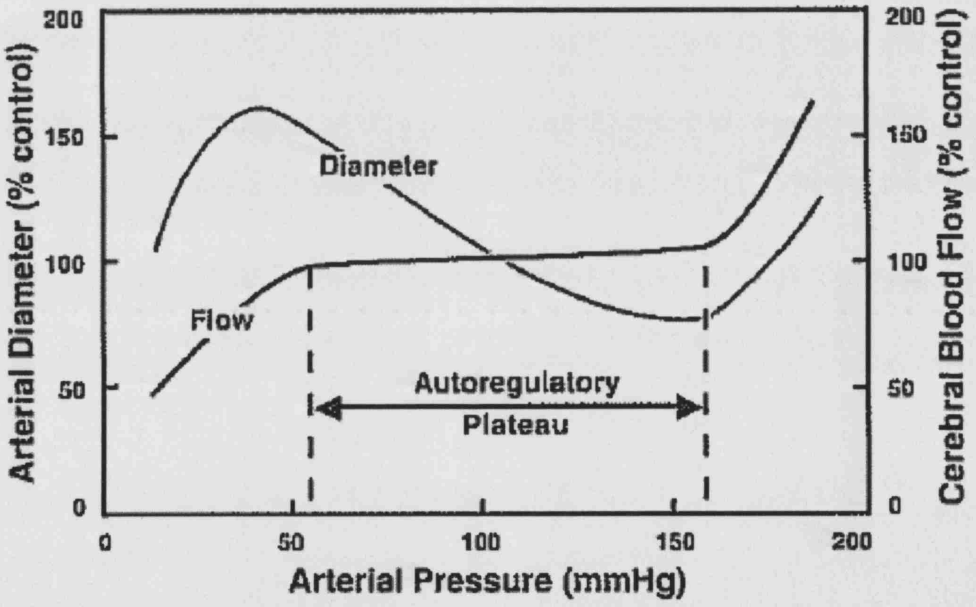

Figure 3.14: (a) A typical steady-state autoregulation curve as predicted by the model. **(b)** Physiology textbook tracings of cerebral arterial diameter and cerebral blood flow versus arterial pressure (taken from [20]).

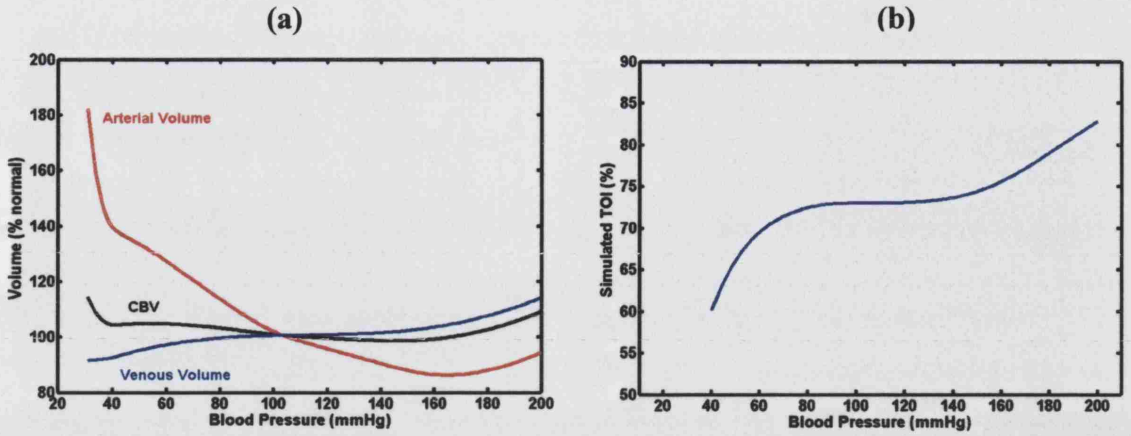

Figure 3.15: Typical steady-state simulations that show **(a)** Arterial, venous and total volume reactions with changes in blood pressure as predicted by the model; **(b)** Simulated cerebral TOI as predicted by the model during step changes in blood pressure.

3.4.8.2 $PaCO_2$ autoregulation

Simulations were done by fixing arterial blood pressure at a particular value (100mmHg), and then gradually increment/decrement $PaCO_2$ from 40mmHg in steps of 1mmHg, allowing the model to settle each time. Parameter values are the model default values. Figure 3.16 shows steady-state autoregulation curves as simulated by the model.

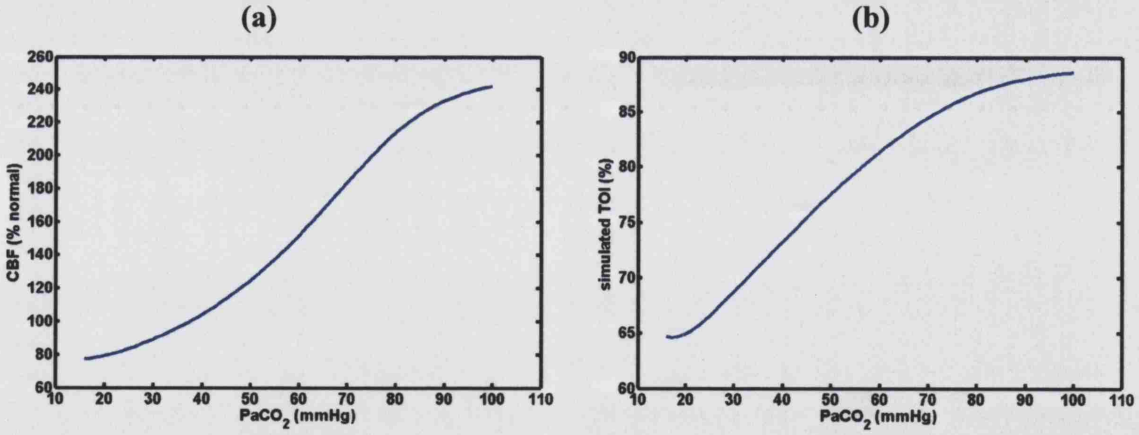

Figure 3.16: Typical steady-state simulations that show **(a)** CBF percentage changes with changes in $PaCO_2$ as predicted by the model; **(b)** Simulated cerebral TOI as predicted by the model during step changes in $PaCO_2$.

Visual comparison between Figure 3.16(a) and Figure 2.10 from Section 2.3.1 show a reasonable agreement.

3.4.8.3 PaO_2 autoregulation

Simulations were done by fixing arterial blood pressure at a particular value (100mmHg), and then gradually increment/decrement PaO_2 from 95mmHg in steps of 1mmHg, allowing the model to settle each time. Parameter values are the model default values. Figure 3.17 shows steady-state autoregulation curves as simulated by the model.

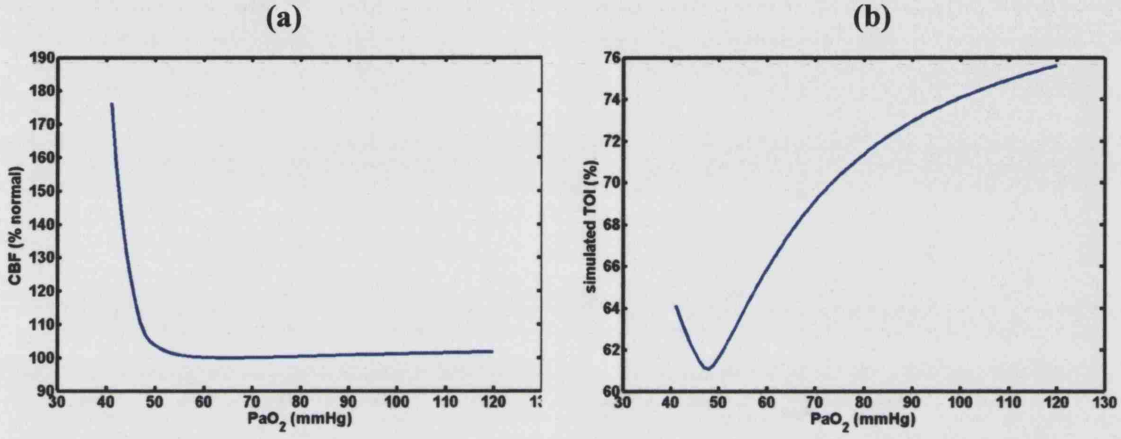

Figure 3.17: Typical steady-state simulations that show **(a)** CBF percentage changes with changes in PaO_2 as predicted by the model; **(b)** Simulated cerebral TOI as predicted by the model during step changes in PaO_2.

Visual comparison between Figure 3.17(a) and Figure 2.12 from Section 2.3.2 show a reasonable agreement.

3.4.9 Concluding remarks

The UCL model represents the first attempt to integrate work on the biophysics of the vascular system, the metabolic biochemistry of the brain, and the properties of vascular smooth muscle on a complete computational system.

Although the work is incomplete and the model is under constant evolution, what we have here represents a first step towards an in silico model of the human brain circulation. We have shown using steady state simulations that despite the UCL model complexity, it produces meaningful outputs, and is able to reproduce qualitatively results from the literature (e.g. autoregulation curves). As we will discuss in later chapter it is feasible to feed in to the model real patient data, and get predictions of a number of physiological quantities associated with the patient.

References

1. M. Banaji, I. Tachtsidis, D.T. Delpy, and S. Baigent, "A physiological model of cerebral blood flow control," *Mathematical Bioscienses* **194**, 125-173 (2005).

2. M. Czosnyka, S. Piechnik, H.K. Richards, P. Kirkpatric, and P. Smielewski, "Contribution of mathematical modelling to the interpretation of bedside tests of cerebrovascular autoregulation," *Journal of Neurology, Neurosurgery, and Psychiatry* **63**, 721-731 (1997).

3. M. Ursino, and C.A. Lodi, "A simple mathematical model of the interaction between intracranial pressure and cerebral hemodynamics," *J. Appl. Physiol.* **82(4)**, 1256-1269 (1997).

4. M. Ursino, and C.A. Lodi, "Interaction among autoregulation, CO_2 reactivity, and intracranial pressure: a mathematical model," *Am. J. Physiol.* **43**, H1715-H1728 (1998).

5. M. Ursino, A. Ter Minassian, C.A. Lodi, and L. Beydon, "Cerebral hemodynamics during arterial and CO2 pressure changes: in vivo prediction by a mathematical model," *Am. J. Physiol.* **279**, H2439-H2455 (2000).

6. M.S. Olufsen, A. Nadim, and L.A. Lipsitz, "Dynamics of cerebral blood flow regulation explained using a lumped parameter model," *Am. J. Physiol.* **282**, R611-R622 (2002).

7. E.M. Golding, and R.M. Golding, "Mathematical modelling of responses of cerebral blood vessels to changing intraluminal pressure," *Physiological Measuremenst* **22**, 727-743 (2001).

8. J. Peñáz, "Photoelectric measurement of blood pressure, volume and flow in the finger," *Int. Conf. Med. Biol. Eng. 104[Digest 10th]* (1973).

9. M. Ursino, "A mathematical study of human intracranial hydrodynamics part 1 - The cerebrospinal fluid pulse pressure," *Annals of Biomedical Engineering* **16**, 379-401 (1988).

10. M. Ursino and P. Di Giammarco, "A mathematical model of the relationship between cerebral blood volume and intracranial pressure changes: The generation of plateau waves," *Annals of Biomedical Engineering* **19**, 15-42 (1991).

11. C.A. Lodi, A. Ter Minassian, L. Beydon, and M. Ursino, "Modeling cerebral autoregulation and CO_2 reactivity in patients with severe head injury," *Am. J. Physiol.* **43**, H1729-H1741 (1998).

12. F.P. Tiecks, A.M. Lam, R. Aaslid, and D.W. Newell, "Comparison of Static and Dynamic Cerebral Autoregulation Measurements," *Stroke* **26**, 1014 (1995).

13. K.H. Chon, Y-Ming Chen, N.H. Holstein-Rathlou, and V.Z. Marmarelis, "Nonlinear system analysis of renal autoregulation in normotensive and hypertensive rats," *IEEE Transactions on Biomedical Engineering* **45**, 342-353 (1998).

14. R.B. Panerai, D.M. Simpson, S.T. Deverson, P. Mahony, P. Hayes, and D.H. Evans, "Multivariate dynamic analysis of cerebral blood flow regulation in humans," *IEEE Transactions on Biomedical Engineering* **47**, 419-423 (2000).

15. X. Zhao, and V. Marmarelis, "On the relation between continuous and discrete nonlinear parametric models," *Automatica* **33**, 81-84 (1997).

16. R.B. Panerai, S.L. Dawson, and J.F. Potter, "Linear and nonlinear analysis of human dynamic cerebral autoregulation," *Am. J. Physiol.* **277**, H1089-H1099 (1999).

17. S.K. Kirkham, R.E. Craine, and A.A. Birch, "A new mathematical model of dynamic cerebral autoregulation based on a flow dependent feedback meachanism," *Physiological Measurements* **22**, 461-473 (2001).

18. R. Aaslid, K.F. Lindegaard, W. Sorteberg, and H. Nornes, "Cerebral autoregulation dynamics in humans," *Stroke* **20**, 45-52 (1989).

19. J. Keener and J. Sneyd, *Mathematical physiology*, Marsden J.E., Sirovich L., and Wiggins S., eds., (Springer-Verlag, New York, 1998).

20. J. Chillon and G.L. Baumbach, "Autoregulation:Arterial and Intracranial Pressure," *Cerbral blood flow and metabolism,* Edvinsson L. and Krause D.N., eds., (Lippincott Williams & Wilkins, Philadelphia, 2001), 395-412.

Chapter 4

The Technique of Near-Infrared Spectroscopy: Theory and Practical Aspects

Near-infrared spectroscopy (NIRS) is a non-invasive method of estimating regional cerebral oxygenation, and is based on the relatively transparency of biological tissue in the near-infrared (NIR) region (700-1000nm). In order to discuss the technique of NIR tissue spectroscopy in more detail, it is important to establish an understanding of the manner in which light propagates through biological tissue. This chapter also discusses the practical aspects of NIRS measurements in biological tissue. Since the NIRS studies described in this thesis are based on continuous wave measurements, the focus will be on this type of instrumentation. Finally a thorough description of the NIR spectrometer used for the studies described in this thesis is given.

4.1 Introduction

Optical spectroscopy is a long-established technique for the observation of oxygenation and haemodynamic effects in tissue, although the specific popularity of near-infrared spectroscopy largely followed the 1977 publication of Jöbsis [1], where he first described the *in vivo* application of NIRS to monitor changes in the oxygenation of the brain in the intact cat head. In this paper he showed that changes in the spectrum measured across the head could be related to changes in chromophore concentration.

Briefly, NIR light penetrates skin, subcutaneous fat/skull, and underlying muscle/brain, and is absorbed and scattered within the tissue. The relatively high attenuation of NIR light in tissue is mainly due to light scattering and certain chromophores of variable (dependent on oxygenation and flow) and fixed concentrations.

Tissue NIRS can be implemented by a variety of measurement techniques, all of which attempt to relate the spectroscopic measurements to the physiological parameter of interest via the optical properties of tissue [2]. Continuous wave techniques are based on measurements of the light transmittance or reflectance from the tissue.

4.2 Measurement of light absorption

Quantitative measurements in spectroscopy are based upon observation by Bouguer in 1729, which is often called the Lambert-Bouguer law. It states that successive layers of material of thickness δd absorb the same fraction dI/I of the light I incident upon them.

$$\frac{dI}{I} = -\mu_a \cdot \delta d \qquad \textbf{4-1}$$

where μ_a is often called the absorption coefficient expressed in cm^{-1} and defines the probability over a minute path that a photon will be absorbed.

Hence the transmitted intensity I after incident light intensity I_o travels length d through an absorber is given by:

$$I = I_0 e^{-\mu_a \cdot d} \qquad 4\text{-}2$$

This equation is also expressed in base 10 logarithms as:

$$I = I_0 10^{-k \cdot d} \qquad 4\text{-}3$$

The constant k is now known as the extinction coefficient and is expressed in cm^{-1}.

A hundred years later, Beer in 1852 [3], derived an absorbance relationship dependent upon the number of absorbing molecules in a solution. It states that for an absorbing substance dissolved in a non-absorbing medium, the light attenuation is proportional to the concentration of the solution.

If we consider a simple case of a solution in a laboratory cuvette, which comprises a non-absorbing medium in which an absorbing compound of concentration c is dissolved. Since the solution does not scatter light, the light travels through the medium in a straight line, covering a distance d. The intensity of the transmitted light *(I)* is less than the intensity of the incident light *(I_o)* because some of the light has been absorbed by the compound in the solution. This loss of light intensity is referred to as attenuation *(A)* and is measured in units of optical density (OD) and can be described by combining the Lambert-Bouguer and Beer laws which form what is commonly known as the Beer-Lambert law.

$$A = \mathrm{Log}\left(\frac{I_0}{I}\right) = \varepsilon \cdot c \cdot d \qquad 4\text{-}4$$

where ε is the specific extinction coefficient of the chromophore ($molar^{-1}.cm^{-1}$), c is the concentration of the chromophore (μmolar), and d the distance (cm) between light entry and light exit point. The product εc is known as the extinction coefficient of the absorbing medium *(k)*.

Using natural logs the Beer-Lambert law is defined as:

$$I = I_0 e^{-\alpha \cdot c \cdot d} \qquad \textbf{4-5}$$

where α measured in (molar^{-1}cm^{-1}) represents the level of absorption per mole of compound per centimeter of optical path, defined as:

$$\alpha = \frac{\mu_a}{c} \qquad \textbf{4-6}$$

The Beer-Lambert law thus describes the attenuation of light travelling through a uniform medium containing an absorbing substance (Figure 4.1). It predicts that monochromatic incident light of intensity I_o enters the medium; a part of the light is transmitted through the medium while another part is absorbed and the intensity of light travelling through the medium decreases exponentially with distance.

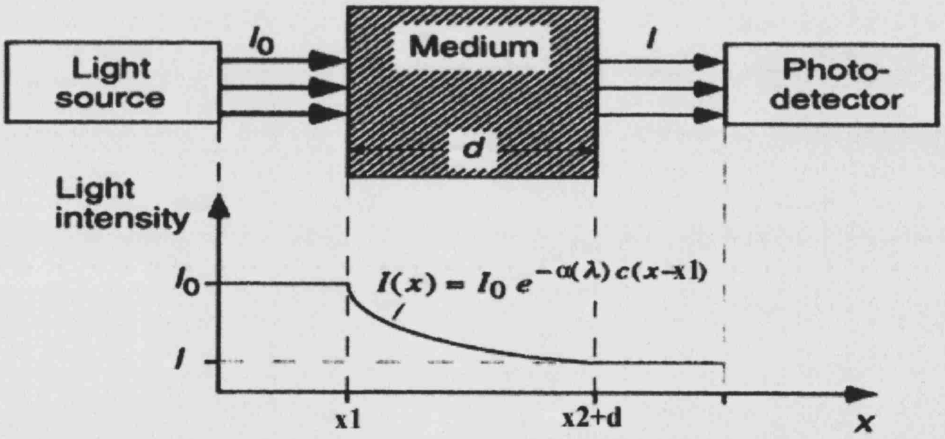

Figure 4.1: Beer's law: Incident light of intensity I_o travels distance $x1$ from a light source to the medium without being absorbed in the air. The light intensity decreases exponentially with distance in the absorbing medium. The intensity of the transmitted light I is determined by Beer-Lambert's law. It stays constant after exiting the medium with optical path length d and can be measured by a photodetector (modified from [4]).

The Beer-Lambert law is valid even if more than one substance absorbs light in the medium. Each absorber contributes its part to the total absorbance. The mathematical representation of this system of absorbers is a superposition of the individual absorbing processes.

The Beer-Lambert law is based on the property that the sum of the transmitted and absorbed light equals the incident light. It does not account for physical processes, which include reflection of the light at the surface of the medium and most importantly the scattering of the light whose affects are described in Section 4.4.

4.3 Absorbing compounds in tissue

There are many compounds in tissue that absorb light radiation and they are known as tissue chromophores. Water accounts for 60 to 80% of total body mass; the content varies between tissue types and is very much age related. Because of its high concentration in most biological tissue, water is considered to be one of the most important chromophores in tissue spectroscopic measurements (the extinction spectrum of water is shown in Figure 4.2).

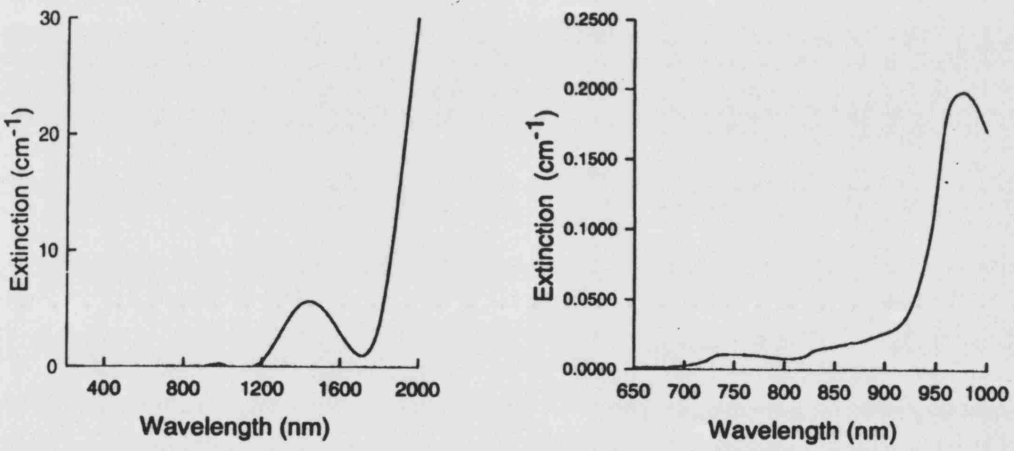

Figure 4.2: The extinction spectra for pure water over the range 200-2000nm and 650-1000nm, demonstrating the window of transparency (taken from [5]).

The extinction spectrum of lipids is very similar to that of water. Lipids in the body exist in the form of triglycerides (neutral fats) and are found in subcutaneous tissues around internal organs. Phospholipids another group of lipids are the main component of cell membranes and are thus found in every organ in the body. As shown in Table 4.1 the lipid content of the brain varies with age [6]. The importance of lipid as an absorber in NIRS depends upon the tissue in question, since the water content is much greater than the lipid content in the brain, absorption due to lipid may be insignificant. One

further important point to note is that the concentrations of water and lipids do not normally change rapidly and so would not influence measurement of changes in attenuation.

Table 4.1: Percentage mass of water, lipid and protein in the human brain.

Age	Water(%)	Lipid(%)	Protein(%)
Foetus (14 weeks)	93.2	1.5	3.8
New-born	89.6	2.6	6.2
Infant (18 months)	83.9	6.1	8.2
Child (3-18 years)	75.5	11.6	10.7
Adult	75.5	11.6	10.7

The region of low absorption (in both water and haemoglobin), between 650-1000nm, acts as a window of transparency allowing NIR spectroscopic measurements through several centimetres of tissue to be made. Within the water window of transparency the most dominant absorption of NIR light is by haemoglobin in its various forms.

Haemoglobin is carried by the erythrocytes or red blood cells, which are small biconcave cells. All vertebrate haemoglobins have been found to have similar structures; they comprise a tetramer of globin molecules, each molecule containing a haem group in a hydrophobic pocket. The haem group consists of a Fe^{+2} ion encased in a porphyrin ligand. Each haem group can bind one oxygen molecule, which means that each haemoglobin molecule may carry a maximum of four molecules of oxygen [7].

Oxygen transport is the major function of erythrocytes, which constitute approximately 40-45% of whole blood [8]. In the lungs oxygen binds to iron atoms in haemoglobin molecules producing oxy-haemoglobin ([HbO_2]). In body tissues oxygen dissociates from the iron producing deoxy-haemoglobin ([HHb]). These two states of haemoglobin happen to have different absorption spectra (Figure 4.3), which we can use for our spectroscopic measurements. Arterial blood is 98% oxygen saturated (red colour), venous blood is about 70% oxygen saturated (purple colour or most commonly referred to as blue colour). The typical value of haemoglobin concentration in the adult brain tissue has been calculated to be 84μmolar (assuming a venous haemoglobin concentration 15mg/dl) [9,10].

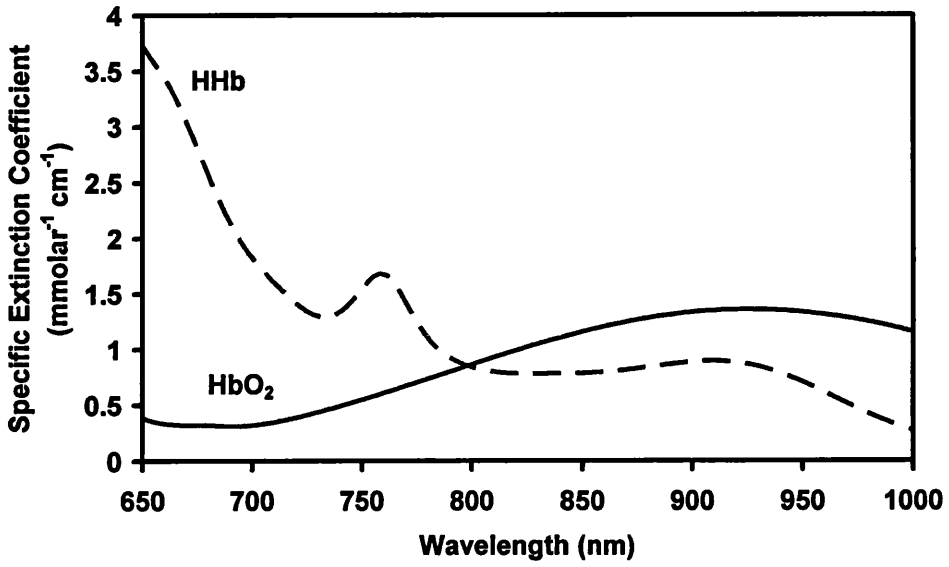

Figure 4.3: Specific absorption spectra of HHb and HbO_2 in the NIR (taken from [6]).

Besides the haemoglobins an additional tissue chromophore is cytochrome oxidase ([CytOx]). Cytochrome oxidase is the terminal protein in the electron transport chain within the inner mitochondrial membrane. Most components of the electron transport chain are proteins bound to metal atoms; these proteins, which form part of the structure of the inner mitochondrial membrane, are quite varied, but most are brightly coloured iron-containing pigments called cytochromes [11]. The electron transport chain is the pathway along which electrons are passed for the purpose of oxidative phosphorylation. This process involves the conversion of adenosine diphosphate (ADP) into adenosine triphosphate (ATP), the molecule that stores chemical energy used for all cellular activity. The cumulative effect of the electron transport chain is the indirect oxidation of nicotinamide adenine dinucleotide hydride (NADH) by molecular oxygen. The first component of the chain accepts electrons from NADH and passes them on to subsequent components, each of which is at higher potentials than the previous ones. The final transfer occurs between the cytochrome oxidase complex and oxygen, whereby oxygen is reduced to water (this process is summarised in Figure 4.4).

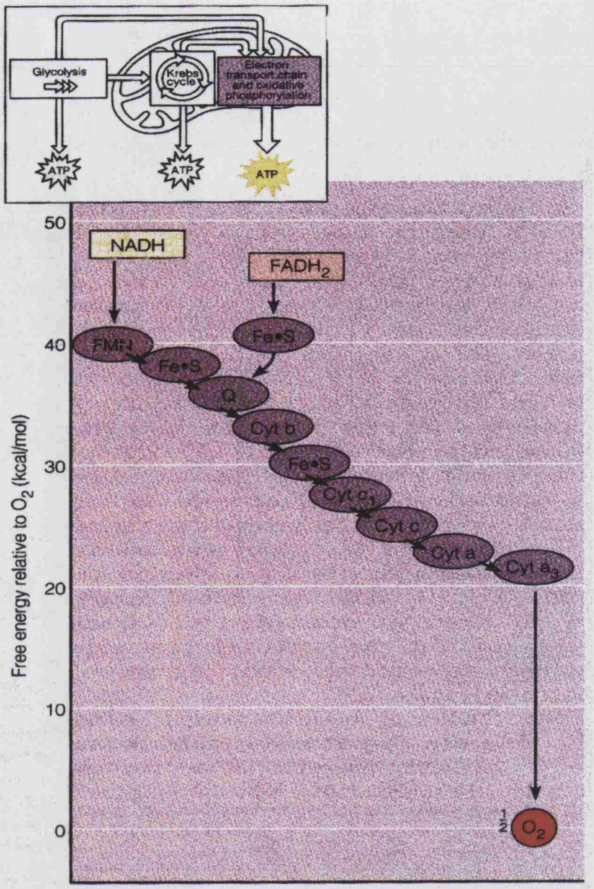

Figure 4.4: Electronic energy gradient in the electron transport chain. Each member of the chain oscillates between a reduced state and an oxidised state. A component of the chain becomes reduced when it accepts electrons from its 'uphill' neighbour (which has lower affinity for the electrons). Each member of the chain reverts to its oxidised form as it passes electrons to its 'downhill' neighbour (which has greater affinity for the electrons). At the 'bottom' of the chain is oxygen, which is very electronegative (taken from [11]).

The cytochrome oxidase complex consists of two binuclear units, each containing a haem and a copper centre. The units involved in the reduction of oxygen contain a haem *a3* and *CuB* group, whilst the other contains a haem *a* and a *CuA* group. Each of the metal groups undergoes oxidation and reduction during the transfer of electrons; the haem groups contain iron, which reversibly oxidises from Fe^{+2} to Fe^{+3}. The NIR absorption spectrum of cytochrome oxidase (see Figure 4.5) depends on the redox state of the *CuA* group, which in turn depends on the availability of oxygen in the cells.

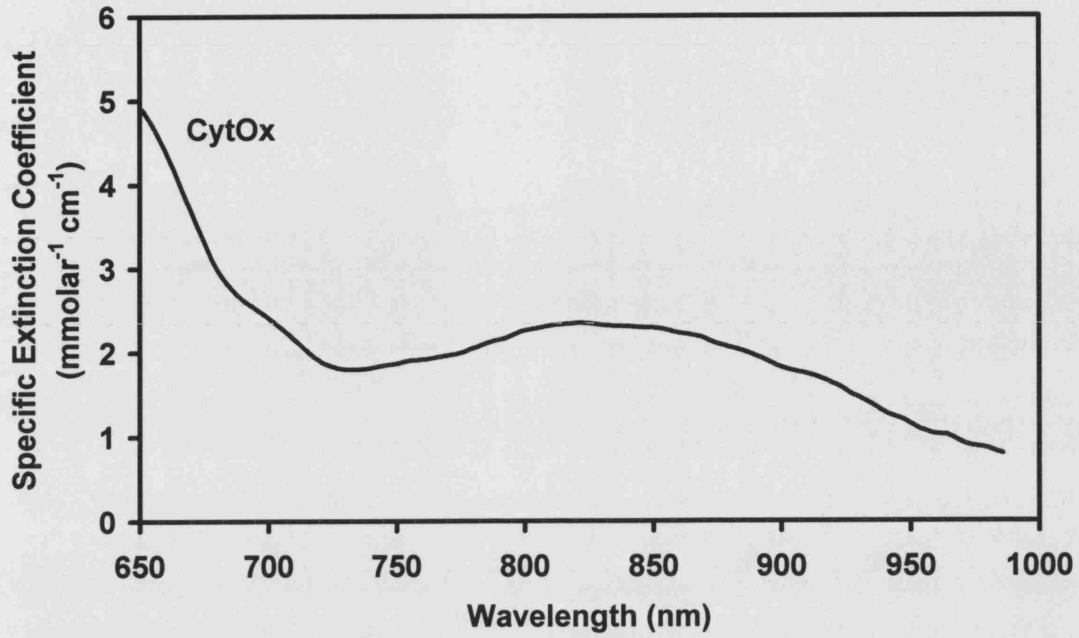

Figure 4.5: The difference absorption spectrum between the oxidised and reduced forms of cytochrome oxidase (taken from [6]).

Other chromophores in tissue are melanin and myoglobin. Melanin is the pigment found in the epidermal layer of human skin. It has a high absorption in the ultraviolet region, which protects the skin from damaging UV radiation from the sun. It also absorbs to a lesser extent in the NIR region, making a significant contribution to overall light attenuation but its concentration does not change over normal measurement periods. Myoglobin, found within the cells of the skeletal muscle, is a red pigment that binds to oxygen, similar to haemoglobin in red blood cells. In fact it has a similar absorption spectrum to haemoglobin however myoglobin is much less sensitive to variations in blood oxygenation as long as this is >30-50% saturation.

4.4 Effects of light scattering on measurements

Light scattering in tissue is the product of tissue heterogeneity. The scattering arises due to relative refractive index mismatch at the boundaries of different media. Evidence suggests that cell and sub cellular membranes are the most important source of scattering in brain tissue since they account for a large proportion of the solid content of the tissue. Conversely erythrocytes account for approximately 2% of the solid content of

tissue and as such the contribution to attenuation by scattering due to red blood cells is low [5].

Scattering can give rise to attenuation of a light beam by deflecting photons from their path. The scattering coefficient (μ_s) for a medium containing a single type of scattering component is a measure of the likelihood that a photon will be scattered in the given medium. If we assume no absorption occurs and attenuation of light is only due to scattering then by analogy with absorption we have:

$$I = I_0 e^{-\mu_s \cdot d} \qquad 4\text{-}7$$

A true description of light transport in tissue needs to take into account anisotropic scattering, which is a very complex problem. The degree to which the scatterer is not equal over all the angles is commonly characterised by the mean cosine of the scattering angle. This mean cosine of the scattering angle is known as the anisotropy factor *g* and provides a measure of the mean direction of scatter. Most tissues have high *g* (typical values of 0.7-0.97), which mean that light scatters forward.

When multiple scattering occurs, light rapidly loses directionality. It is then often useful for mathematical convenience to assume isotropic scatter (i.e. equal to all directions) where the scattering coefficient has been reduced by a factor (1-g). This modified scattering coefficient is called the transport scattering coefficient defined as:

$$\mu_{st} = \mu_s \cdot (1 - g) \qquad 4\text{-}8$$

4.5 Light attenuation in tissue

It is clear that when light travels through tissue it is attenuated due to the combined effects of both scatter and absorption, and hence the effects of both of these parameters must be taken into account when considering spectroscopic measurements. In tissue illuminated with NIR approximately 80% of the total attenuation is due to scattering and the remaining 20% is due to absorption.

Hence attenuation in tissue can be approximated by the modified Beer-Lambert law (MBL) [12], which accounts for the effects of both absorption and multiple scattering. This is expressed as:

$$A = \mathrm{Log}\left(\frac{I_o}{I}\right) = \varepsilon \cdot c \cdot d \cdot B + G \qquad \textbf{4-9}$$

where G represents the oxygen independent light losses due to scattering in the tissue (assumed to be constant) and B is the dimensionless differential pathlength factor (DPF), a multiplier to account for the increased optical pathlength due to scattering.

There must be a number β, such that any measured attenuation change δA observed across the scattering medium is related to the change in the extinction coefficient of that medium. β has been named the "differential pathlength" (DP, or effective optical pathlength) and has units of length (cm).

As shown in Figure 4.6 and discussed previously, in tissue due to scattering photons travel a mean distance which is far greater than the geometrical pathlength d [12]. Hence the true optical distance is defined as:

$$\beta = B \cdot d \qquad \textbf{4-10}$$

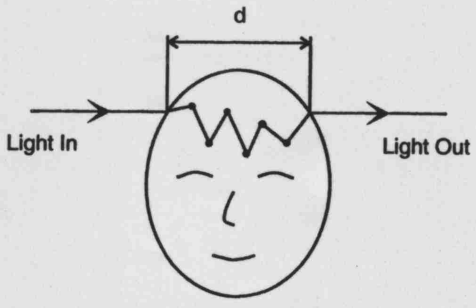

Figure 4.6: Schematic showing the scattering effect of tissue causing the total optical pathlength to be much greater than the geometrical distance (taken from [5]).

4.6 Differential spectroscopy

The solution of the MBL cannot provide a measure of the absolute concentration of the chromophore in the medium and that is because of the unknown factor *G*, which is dependent upon the measurement geometry and the scattering coefficient of the tissue interrogated. However, if *G* does not change during the measurement period, it is possible to determine the *changes* in the chromophore concentration from the *changes* in attenuation. Hence:

$$\Delta A = \Delta c \cdot \varepsilon \cdot d \cdot B \qquad \textbf{4-11}$$

It is clear from equation 4-11 that quantification of the *changes* in concentration depends on the measurement of the geometrical distance *d* and the differential pathlength factor *B*.

The DPF of light in a highly scattering media such as tissue is not only strongly dependent upon the scattering coefficient μ_s but is also a weaker function of the absorption coefficient μ_a. The relationship between μ_a and DPF can be demonstrated using theoretical data generated using a diffusion equation model of attenuation as a function of μ_a in a scattering and non scattering medium. This is illustrated in Figure 4.7, which shows attenuation of light as a function of μ_a for a medium of thickness *d* for four different scattering coefficient conditions [2]. The figure shows that in general, the differential path of light will increase with increasing scattering coefficient and decrease with increasing absorption coefficient. In order to make quantified measurements of the *changes* in concentration, it is assumed that DPF is approximately constant for a given tissue, since the measured *changes* in attenuation are small compared to the large constant background attenuation in tissue [2,5] (absorption dependent variation in optical pathlength in physiological measurements in the NIR is smaller than 15% with a typical value of 5%).

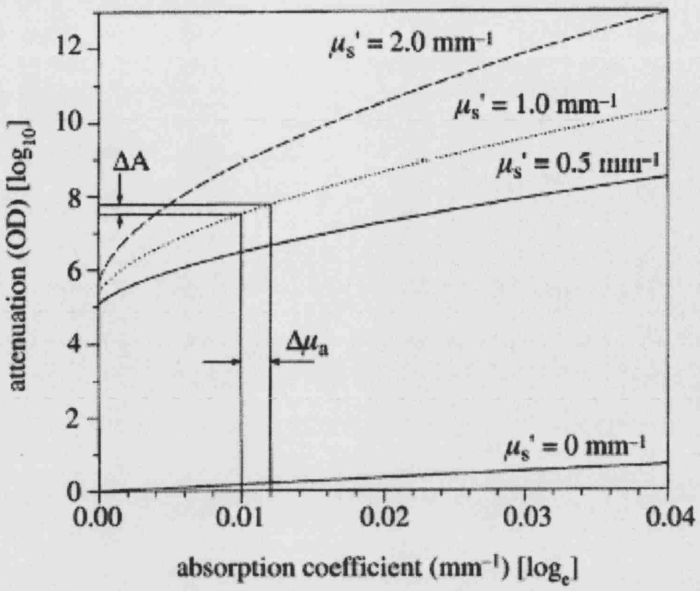

Figure 4.7: Predicted plot of attenuation as a function of absorption coefficient for four different values of scattering coefficient (taken from [2]).

Several methods have been used to estimate the DPF such as measurement of the time of flight of photons or optical phase delay [5]. A study has also been made using these techniques to investigate the change of cranial DPF with age. An intensity modulated spectrometer was used to measure phase delay and hence DPF in total 283 subjects whose age ranged from 1 day to 50 years [13]. The results suggest a slowly varying age dependence of DPF following the relation:

$$DPF_{780} = 5.13 + 0.07A_Y^{0.81} \qquad \textbf{4-12}$$

where DPF_{780} is the DPF at 780nm and A_y is the age of the subject in years.

Assuming that *G* remains constant during a measurement and that *d* and *B* are known, the modified Beer-Lambert law can be used to derive *absolute changes* in chromophore concentration in a highly scattering medium in non arbitrary units. This methodology has been incorporated in most of the near-infrared commercial systems made by Hamamatsu Photonics KK, such as the NIRO-1000, -500, -300, -200 and -100.

4.7 Diffusion approximation of light transport in a highly scattering medium

Propagation of photons in a multiple scattering medium such as tissue can be described by the diffusion approximation to the transport equation [14]. For a semi-infinite half-space geometry, the solution of the photon diffusion equation for an impulse (δ-function) input is expressed as:

$$R(\rho,t) = (4\pi Dv)^{\frac{-3}{2}} \cdot \frac{1}{\mu_{st}} \cdot t^{\frac{-5}{2}} \cdot \exp(-\mu_a \cdot v \cdot t) \cdot \exp\left(-\frac{\rho^2 + \mu_{st}^{-2}}{4Dvt}\right) \qquad \textbf{4-13}$$

where R is the intensity of the reflected light at a distance ρ, t is the time from the impulse input, μ_a and μ_{st} are the absorption and transport scattering coefficients respectively, D is the diffusion coefficient ($D=1/3(\mu_a+\mu_{st})$ and v is the velocity of light in the medium.

In the case of continuous wave (cw) light, the intensity $I(\rho)$ is expressed as the integral of $R(\rho,t)$ over the time, and the light attenuation $A(\rho)$ is defined as the negative logarithm of $I(\rho)$. Thus $A(\rho)$ is expressed by:

$$A(\rho) = -\log_{10} \int_0^\infty R(\rho,t)dt \qquad \textbf{4-14}$$

In order for the NIRO 300 to measure concentration changes, it uses the modified Beer-Lambert law, which as a mathematical identity in terms of A can be derived:

$$\Delta A = \beta \cdot \Delta\mu_a \qquad \textbf{4-15}$$

where

$$\beta = \frac{\partial A}{\partial \mu_a} \qquad \textbf{4-16}$$

By application of the MBL and by measuring the light attenuation changes ΔA at several wavelengths and by knowing the differential pathlength β, then the changes in absorption coefficients $\Delta\mu_a$ can be calculated. So later we can derive the concentration changes Δc by using the relation:

$$\Delta c = \left(\frac{1}{\beta}\right)\varepsilon^{-1} \cdot \Delta A \qquad \textbf{4-17}$$

where ε represents the molar extinction coefficients of the measured components.

As mentioned previously the NIRO uses four wavelengths to measure three components (i.e. $\Delta c=\Delta[HbO_2]+\Delta[HHb]+\Delta[CytOx]$) by employing the least square error method for the calculation. Thus the equation is expressed in a matrix form as:

$$\begin{bmatrix} \Delta HbO_2 \\ \Delta HHb \\ \Delta CytOx \end{bmatrix} = \frac{1}{\beta}\left[\varepsilon_{i,j}\right]^{-1}\begin{bmatrix} \Delta A(\lambda 1) \\ \Delta A(\lambda 2) \\ \Delta A(\lambda 3) \\ \Delta A(\lambda 4) \end{bmatrix} \qquad \textbf{4-18}$$

where i= HbO_2, HHb and CytOx and j=λ_1, λ_2, λ_3, λ_4.

The differential pathlength β coincides analytically with the product of light velocity v and its mean time of flight T as shown:

$$\beta = \frac{\partial A}{\partial \mu a} = v \cdot T \qquad \textbf{4-19}$$

where

$$T = \frac{\int_0^\infty t \cdot R(\rho, t)dt}{\int_0^\infty R(\rho, t)dt} \qquad \textbf{4-20}$$

Therefore by measuring $R(\rho,t)$ with a very high speed light detector such as a streak camera, T can be calculated as the temporal mean of the measured $R(\rho,t)$, then the differential pathlength is derived from equation (4.19) also when β cannot be determined one can measure the relative concentration changes expressed by $\beta\Delta C$ (μmolar.cm).

4.8 Near Infrared Spectrometer (NIRO 300)

A limitation of mostly previous NIRS measurements on the head had been lack of depth resolution, which did not allow for a separation of blood signals in the skin and skull from these in the brain. This limitations can partly be overcome by the newer NIRS techniques of time resolved, frequency domain or spatially resolved spectroscopy [15,16].

In all of the studies reported in this thesis, a continuous wave near-infrared spectrometer (NIRS), with a sampling rate of 6Hz (NIRO 300, Hamamatsu Photonics KK) was used. This system in addition to monitoring changes in $\Delta[HbO_2]$ and $\Delta[HHb]$ by utilizing the modified Beer-Lambert law [12] can also measure absolute cerebral tissue oxygen saturation as a percentage using spatially resolved spectroscopy (SRS) [17,18]. This new measure has been term the Tissue Oxygenation Index (TOI), and is the ratio of oxygenated to total tissue haemoglobin concentrations.

In this instrument light is emitted through an optical fibre built into the probe and detected as a function of distance using a three segment PIN photodiode chip. Sequentially pulsed laser diodes are used as the light source, emitting at four wavelengths, these are 775nm, 813nm, 853nm and 910nm.

4.8.1 Spatially resolved spectroscopy

The principle of the SRS technique can be derived from the diffusion approximation Equation 4-14. By differentiating $A(\rho)$ with respect to ρ (see Appendix B) we obtain:

$$\frac{\partial A}{\partial \rho} = \frac{1}{\ln 10} \cdot \left(\sqrt{3 \cdot \mu_a \cdot \mu_{st}} + \frac{2}{\rho} \right) \qquad \textbf{4-21}$$

In SRS, by measuring $\partial A / \partial \rho$ at several wavelengths (λ), we can calculate $\mu_{a(\lambda)} \cdot \mu_{st(\lambda)}$ using Equation 4-21. To a first order approximation, $\mu_{st(\lambda)}$ can be regarded as a constant k with respect to λ in the near infrared region. Therefore, we can get relative absorption coefficients $k\mu_{a(\lambda)}$, thus the relative concentration $kHbO_2$ and kHHb are derived. Then the ratio of HbO_2 to total haemoglobin ($HbT=HbO_2+HHb$) is calculated. In practice, $\mu_{st(\lambda)}$ decreases slightly with respect to λ [16] and this can be expressed in the form $\mu_{st(\lambda)}=k(1-h\lambda)$. Here h is the normalised slope of μ_{st} with λ, which is fairly constant among tissue types and subjects [15,17], so the introduction of h into the calculation will increases the accuracy of the derived TOI. Thus $k\mu_{a(\lambda)}$ are calculated by the following formulas:

$$k \cdot \mu_{a(\lambda)} = \frac{1}{3(1 - h \cdot \lambda)} \cdot \left(\ln 10 \cdot \frac{\partial A(\lambda)}{\partial \rho} - \frac{2}{\rho} \right)^2 \qquad \textbf{4-22}$$

In the instrument, four wavelengths and an h of $6.3 \times 10^{-4} (mm^{-1}/nm)$ [17] are used to determine $kHbO_2$ and kHHb, and a least square method is used in the calculation as shown:

$$\begin{bmatrix} kHbO_2 \\ kHHb \end{bmatrix} = [\varepsilon_{i,j}]^{-1} \cdot \begin{bmatrix} k \cdot \mu_a(\lambda 1) \\ k \cdot \mu_a(\lambda 2) \\ k \cdot \mu_a(\lambda 3) \\ k \cdot \mu_a(\lambda 4) \end{bmatrix} \qquad \textbf{4-23}$$

However data on the linear change of A with ρ is a prerequisite for SRS, so three sensors continuously monitor the signal. As previously mentioned, in the NIRO 300 a

three-segmented PIN photodiode is used in the detector (Figure 4.8) and the TOI (i.e $\partial A / \partial \rho$) is measured by using the signals from all three photodiodes whilst the concentration changes such as $\Delta[HbO_2]$ (i.e ΔA) are measured using the signal from the middle photodiode.

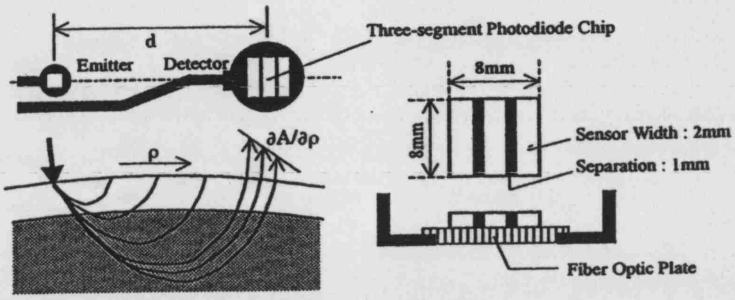

Figure 4.8: NIRO 300 probe schematic (taken from [17]).

The NIRO 300 can also calculate a tissue haemoglobin index (termed THI) by adding the concentration changes, $kHbO_2$ and kHHb as measured by the three photodiodes. This is a relative new quantity representing a scaled tissue blood volume which currently is under evaluation.

4.8.2 Cerebral Tissue Oxygenation Index

The methods and physical principles used to derive the TOI from the NIRS signal have previously been explained. A thorough investigation of what the TOI signal is and how it changes with various stimuli such as arterial blood pressure would involve investigating the following.

Cranial NIRS interrogates a multi-compartmental system of arteries, arterioles, capillaries, venules and veins; each of these compartments has different saturations and volumes. In order to investigate the origins of the cerebral TOI signal one has to simplify the above multi-compartmental system and it is usual to consider just two compartments, one arterial and one venous, with a typical arterial:venous volume ratio of one to three (25% arterial volume, 75% venous volume) [19]. There is little data on the changes in the arterial:venous volume ratio in humans; however a recent paper from Ito and colleagues [20] investigated the changes in cerebral arterial and venous volume during hypercapnia and hypocapnia concluded that changes in CBV are caused by changes in arterial blood volume without changes in venous and capillary blood

volume. Considering an arterial saturation of 97-99% and venous saturation of 65-75% [21] and assuming that $[HbO_2]_{art}$ is the oxyhaemoglobin concentration of the arterial compartment (in mmolar) and *Va* the arterial blood volume per unit mass of tissue (in L/g), and $[HbO_2]ven$ is the oxyhaemoglobin concentration of the venous compartment (in mmolar) and *Vv* the venous blood volume per unit mass of tissue (in L/g); one can derive the equations below:

$$[HbO_2] = V_a \cdot [HbO_2]_{art} + V_v \cdot [HbO_2]_{ven} \qquad \textbf{4-24}$$

where $[HbO_2]$ is the total oxygenated haemoglobin per unit mass of tissue (in mmoles/g) and:

$$[HbT] = (Hb \cdot 10^2) \cdot MW_{Hb}(V_a + V_v) \qquad \textbf{4-25}$$

where *[HbT]* is the total haemoglobin per unit mass of tissue (in mmoles/g), *Hb* is the concentration of haemoglobin in blood (in g/dL), which is assumed constant in all compartments and MW_{Hb} is the molecular weight of haemoglobin (mmoles/g). We know that:

$$TOI = \frac{[HbO_2]}{[HbT]} \times 100\% \qquad \textbf{4-26}$$

Therefore substituting equations 4-24 and 4-25 in equation 4-26 we have:

$$TOI = \frac{\frac{V_a}{V_v}[HbO_2]_{art} + [HbO_2]_{ven}}{(Hb \cdot 10^2) \cdot MW_{Hb}(1 + \frac{V_a}{V_v})} \times 100\% \qquad \textbf{4-27}$$

Equation 4-27 demonstrates the complex nature of the TOI signal as measured by the NIRO 300. Clearly one can see that the TOI is dependent on the arterial venous volume ratio and their relative oxygenations but with a greater sensitivity to the venous oxygenation signal (given the V_a/V_v volume ratio).

Bearing in mind that the tissue oxygenation is a mixed arterial:venous oxygen saturation signal [22], and by considering the definitions of arterial oxygen saturation ($SaO_2=[HbO_2]_{art}/[HbT]_{art}$) and venous oxygen saturation ($SvO_2=[HbO_2]_{ven}/[HbT]_{ven}$), Equation 4-27 can be rewritten as:

$$TOI = SaO_2 \cdot \frac{V_a}{V_a + V_v} + SvO_2 \cdot \frac{V_v}{V_a + V_v} \qquad \textbf{4-28}$$

One now can replace SvO_2 in equation 4-28 by considering the definition of the Fick equation [23-25] shown below:

$$SvO_2 = SaO_2 - \frac{CMRO_2}{k \cdot CBF \cdot [Hb \cdot 10^{-2}]} \qquad \textbf{4-29}$$

where $CMRO_2$ is the oxygen consumption (in ml of Oxygen/min), k is the oxygen combining power of Hb (~1.306 ml of Oxygen/g of Hb) and CBF is cerebral blood flow (in ml/min) and Hb is the haemoglobin (in g of Hb/dL of blood). Therefore:

$$TOI = SaO_2 - \left(\frac{V_v}{V_a + V_v}\right) \cdot \left(\frac{CMRO_2}{k \cdot CBF \cdot [Hb \cdot 10^{-2}]}\right) \times 100\% \qquad \textbf{4-30}$$

Equation 4-30 demonstrates the direct relationship of the NIRO 300 TOI signal with the arterial/venous volume ratio, oxygen consumption and the indirect relationship with CBF.

From the above it is clear that the factors that could cause a change in TOI (except from an alteration in SaO_2) are:

1. Arterial vasodilation, which might be caused by a minor decrease in arterial blood pressure (ABP) or a rise in arterial partial pressure of carbon dioxide

($PaCO_2$), results in an increased ratio of arterial to venous volumes. This effect could produce an increase in TOI.

2. Arterial vasoconstriction, due to a small increase in ABP or decrease in $PaCO_2$ could cause a decreased ratio of the arterial to venous volumes. This effect could produce a decrease in TOI.
3. Venous passive dilation due to a small increase in venous BP could result in a decreased ratio of the arterial to venous volumes. This effect could produce a decrease in TOI.
4. Venous passive contraction due to a minor decrease in venous BP resulting in an increased ratio of arterial to venous volumes. This effect could produce an increase in TOI.
5. Change in the oxygen extraction due to changes in demand or in CBF. A decrease in oxygen extraction or increased CBF could produce an increase in TOI.

The situation is however more complicated if one considers extreme changes at the limits of autoregulation. For example a drop or an increase in ABP beyond the autoregulation capacity of the brain would definitely cause a decrease or an increase respectively in CBF, this change coupled with the alteration of the arterial venous volume ratios produces an unpredictable net result.

Let us consider a situation where a slow decrease in the ABP is being induced in a volunteer. Such a decrease would produce a slow but steady increase in TOI via the increase arterial:venous volume ratio. As the ABP drops even lower and the brain autoregulation limit is breached, CBF would then start to decrease. Assuming oxygen extraction stays constant the brain venous blood becomes less oxygen saturated. The net effect of this would most probably recorded by the TOI signal as a reduction in its absolute value. Therefore a comparatively large percentage change in TOI might represent a comparatively small change in tissue oxygenation, even though the net change is qualitatively correct.

Finally one of the concerns in NIRS and consequently TOI is the potential signal contamination from extracranial tissues. Al-Rawi and colleagues [18] have recently published a study investigating the NIRO 300 extracranial contamination by studying

sixty patients undergoing carotid endarteroctomy. Their approach has been to sequentially clamp the external carotid artery and internal carotid artery allowing the opportunity to separate the intracranial and extracranial signal contributions and to identify changes in the cutaneous circulation affecting the NIRS measurements (see Figure 4.9). The data showed that the TOI signal is relatively insensitive to extracranial contamination. Their observations demonstrated that the sensitivity and specificity of TOI to intracranial changes were 87.5% and 100%, respectively.

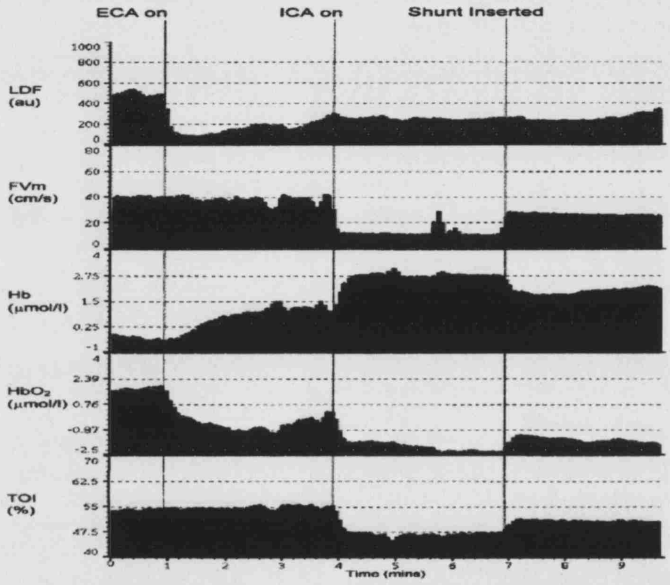

Figure 4.9: Data obtained from a patient during selective carotid endarterectomy (ECA and ICA external and internal carotid artery respectively; LDF, laser Doppler flow; FVm, flow velocity of middle cerebral artery measured by TCD; Hb, [HHb]). The vertical lines demonstrate time of application of vascular clamps (taken from [18]).

4.8.3 Haemoglobin Concentration Measurements

Before discussing the absolute changes in oxy- and deoxy- haemoglobin that the NIRO 300 records, one should bear in mind the effect of the extracranial contamination on this signal. Al-Rawi and colleagues[18] have shown that unlike the TOI signal the $\Delta[HbO_2]$ and $\Delta[HHb]$ values using the MBL cannot reliably be taken to represent only the intracranial compartment and they have greater percentage of extracranial contamination (Figure 4.9). As has been discussed previously, the skin vasculature does not have such tight autoregulation capabilities as the brain, therefore making it difficult to draw consistent conclusions especially when considering physiological stimuli such as blood pressure changes and passive tilt which have major systemic effects.

Let us first consider which factors could produce a true cerebral change (see equation 4-24). An increase in the arterial partial pressure of oxygen (PaO_2) could produce an increase in $\Delta[HbO_2]$ and that is obvious. However the effect of other factors must be more carefully considered. These are:

1. Arterial vasodilation, which might be caused by a minor decrease in arterial BP or rise in $PaCO_2$ could produce an increase in $\Delta[HbO_2]$.
2. Arterial vasoconstriction, due to a small increase in arterial BP or decrease in $PaCO_2$ could produce a decrease in $\Delta[HbO_2]$.
3. Venous passive dilation due to a small increase in venous pressure could result in an increase in $\Delta[HbO_2]$.
4. Venous passive contraction due to a minor decrease in venous pressure could produce a decrease in $\Delta[HbO_2]$.
5. Change in the oxygen extraction due to changes in need or CBF. For example a decrease in oxygen extraction resulting from decrease need, or increased CBF could produce an increase in $\Delta[HbO_2]$.

By looking at the third and fourth hypotheses one can immediately understands the difference between TOI and $\Delta[HbO_2]$, which appear to do opposite things for the same physiological stimulation. One must also be careful when interpreting changes in the $\Delta[HbO_2]$ signal as this is a mixed arterial ($\Delta[HbO_2]_{art}$) and venous ($\Delta[HbO_2]_{ven}$) signal. Because there is three times as much cerebral venous volume as cerebral arterial volume, a unit change in venous saturation would have a comparatively larger effect in the total tissue $\Delta[HbO_2]$ signal than a unit change in arterial saturation.

If we now consider a volunteer in whom the ABP drops below the lower limit of the autoregulation; this will lead to active vasodilation, however the net effect will be a decrease in CBF as the autoregulatory limits have been breached. According to the hypothesis above, this again could result in two competing effects, first the increase in $\Delta[HbO_2]$ because of the vasodilation but a larger decrease in $\Delta[HbO_2]$ due to increased oxygen extraction. The net effect is likely to be a net decrease in the $\Delta[HbO_2]$ signal.

Let us now consider the [HHb] signal:

$$[HHb] = V_a \cdot H_{art} + V_v \cdot H_{ven} \qquad \textbf{4-31}$$

where H_{art} and H_{ven} are the de-oxygenation of the arterial and venous compartments respectively. However using Equations 4-24 and 4-25 from before one can derive another representation of [HHb], which relates it to the [HbO_2] and [HbT].

$$\begin{aligned}[HHb] &= [HbT] - [HbO_2] = \\ &= Hb \cdot MW_{Hb} \cdot (Va + Vv) - Va \cdot [HbO_2]_{art} - Vv \cdot [HbO_2]_{ven}\end{aligned} \qquad \textbf{4-32}$$

Equation 4-32 shows again the complicated way in which volume and oxygenation contribute to the changes in Δ[HHb]. Now let us again consider the factors that could cause an increase in Δ[HHb] beside an obvious reduction in PaO_2 by analysing equation 4-32. These are:

1. Arterial vasodilation, which might be caused by a minor decrease in arterial BP or rise in $PaCO_2$, this effect could produce a decrease in Δ[HHb].
2. Arterial vasoconstriction, due to a small increase in arterial BP or decrease in $PaCO_2$ could produce an increase in Δ[HHb].
3. Venous passive dilation due to a small increase in venous BP could result in an increase in Δ[HHb].
4. Venous passive contraction due to a minor decrease in venous BP could produce a decrease in Δ[HHb].
5. Change in the oxygen extraction due to changes in need or CBF. For example a decrease in oxygen extraction or increased CBF could produce a decrease in Δ[HHb].

Interestingly, hypothesis three and four suggest that a passive venous expansion or contraction accompanied by an increase or decrease in total blood volume without a change in arterial volume would be manifested as an increase or decrease respectively for both Δ[HbO_2] and Δ[HHb] but not for TOI, which would demonstrate the opposite effect.

For example if ABP increases inside the autoregulation limits, this could produce an increase in cerebral total blood volume via venous expansion. This would show $\Delta[HbO_2]$ and $\Delta[HHb]$ rising but TOI decreasing. If ABP increases even further and the autoregulation limits are now breached arterial vasodilation will occur and CBF would increase, which might produce a decrease in $\Delta[HHb]$, but an increased in $\Delta[HbO_2]$ and TOI.

References

1. F.F. Jobsis, "Noninvasive, infrared monitoring of cerebral and myocardial oxygen sufficiency and circulatory parameters," *Science* **198**, 1264-1267 (1977).

2. D.T. Delpy and M. Cope, "Quantification in tissue near-infrared spectroscopy," *Philosophical Transactions of the Royal Society of London Series B-Biological Sciences* **352**, 649-659 (1997).

3. A. Beer, "Bestimmung der Absorption des rothen Lichts in farbigen Flüssigkeiten," *Ann. Phys. Chem.* **163**, 78 (1852).

4. J.G. Webster, *Design of pulse oximeters*, Webster J.G, ed., (IOP publishing Ltd, 1997).

5. C.E. Elwell, *A practical users guide to near infrared spectroscopy*, Elwell C.E., ed., (Hamamatsu Photonics, London, 1995).

6. M. Cope, "The development of a near infrared spectroscopy system and its application for non invasive monitoring of cerebral blood and tissue oxygenation in the newborn infant," *Ph.D Thesis*, University College London, (1991).

7. C.M. Dobson, J.A. Gerrard, and A.J. Pratt, "From structure to metabolic function: the globins," *Foundations of chemical biology,* Dobson C.M., Gerrard J.A., and Pratt A.J., eds., (Oxford University Press, Oxford, 2001), 29-38.

8. E.N. Marieb, "Blood," *Human anatomy and physiology,* Marieb E.N., ed., (Benjamin/Cummings Science Publishing, California, 1998), 626-655.

9. J.S. Wyatt, M. Cope, D.T. Delpy, C.E. Richardson, A.D. Edwards, S. Wray, and E.O. Reynolds, "Quantitation of cerebral blood volume in human infants by near-infrared spectroscopy," *J. Appl. Physiol.* **68**, 1086-1091 (1990).

10. P. Hopton, T.S. Walsh, and A. Lee, "Measurement of cerebral blood volume using near-infrared spectroscopy and indocyanine green elimination," *J. Appl. Physiol.* **87**, 1981-1987 (1999).

11. E.N. Marieb, "Nutrition, metabolism, and body temperature regulation," *Human anatomy and physiology,* Marieb E.N., ed., (The Benjamin/Cummings Publishing Company, California, 1998), 908-957.

12. D.T. Delpy, M. Cope, Z.P. van der Zee, S. Arridge, S. Wray, and J. Wyatt, "Estimation of optical pathlength through tissue from direct time of flight measurement," *Phys. Med. Biol.* **33**, 1433-1442 (1988).

13. C.C. Duncan, J.H. Meek, M. Clemence, C.E. Elwell, L. Tyszczuk, M. Cope, and D.T. Delpy, "Optical pathlength measurements on adult head, calf and forearm and the head of the newborn infant using phase resolved optical spectroscopy," *Phys. Med. Biol.* **40**, 295-304 (1995).

14. S.R. Arridge, M. Cope, and D.T. Delpy, "The theoretical basis for the determination of optical pathlengths in tissue: temporal and frequency analysis," *Phys. Med. Biol.* 37, 1531-1560 (1992).

15. S.J. Matcher, K. Nahid, M. Cope, and D.T. Delpy, "Absolute SO_2 measurements in layred media.," *OSA TOPS on Advantages in Optical Imaging and Photon Migration* **3**, 83-91 (1996).

16. S.J. Matcher, P. Kirkpatrick, K. Nahid, M. Cope, and D.T. Delpy, "Absolute quantification methods in tissue near infrared spectroscopy.," *Proc. SPIE* **2389**, 486-495 (1995).

17. S. Suzuki, S. Takasaki, T. Ozaki, and Y. Kobayashi, "A tissue oxygenation monitor using NIR spatially resolved spectroscopy," *Proc. SPIE* **3597**, 582-592 (1999).

18. P.G. Al Rawi, P. Smielewski, and P.J. Kirkpatrick, "Evaluation of a near-infrared spectrometer (NIRO 300) for the detection of intracranial oxygenation changes in the adult head," *Stroke* **32**, 2492-2500 (2001).

19. H. An, and W. Lin, "Cerebral venous and arterial blood volumes can be estimated separately in humans using magnetic resonance imaging," *Magn. Reson. Med.* **48**, 583-588 (2002).

20. H. Ito, M. Ibaraki, I. Kanno, H. Fukuda, and S. Miura, "Changes in the arterial fraction of human cerebral blood volume during hypercapnia and hypocapnia measured by positron emission tomography," *J. Cereb. Blood Flow Metab.* Advance Online Publication, February 16, (2005).

21. A.K. Gupta, "Jugular venous oximetry," *Notes in neuroanaesthesia and critical care,* A. K. Gupta and A. Summors, eds., Greenwich medical media LTD, 2001), 225-228.

22. M. Kaminogo, A. Ichikura, S. Shibata, T. Toba, and M. Yonekura, "Effect of acetazolamide on regional cerebral oxygen saturation and regional cerebral blood flow," *Stroke* **26**, 2358-2360 (1995).

23. M.J. Purves, "The cerebral circulation experimental approaches," *The physiology of the cerebral circulation,* Purves M.J., ed., (Cambridge University Press, Cambridge, 1972), 101-155.

24. M.K. Sykes, M.D. Vickers, C.J. Hull, P.J. Winterburn, and B.J. Shepstone, "Measurement of blood flow," *Principles of measurement and monitoring in anaesthesia and intensive care,* Sykes M.K., Vickers M.D., Hull C.J., Winterburn P.J., and Shepstone B.J., eds., (Blackwell Scientific Publications, 1991), 207-222.

25. G.A. Dienel, "Energy generation in the central nervous system," *Cerebral blood flow and metabolism,* Edvinsson L. and Krause D.N., eds., (Lippincott Williams & Wilkins, Philadelphia, 2001), 140-161.

Chapter 5

Model Predictions with Experimental Data during a CO_2 Challenge

Having described in previous chapters the concepts of cerebral autoregulation, the cerebral computational modelling and the principles of near-infrared spectroscopy (NIRS), the next three chapters describe a set of experimental studies together with simulations using the BRAINCIRC UCL model (version 1, 2004-2005) for the purpose of putting the previous discussed theory in a practical context. The results from each experimental study together with the results from the modelling are thoroughly discussed in an attempt to provide a physiological explanation for the observed changes in the signals.

In this chapter a study completed a year ago involving a moderate hypercapnia challenge in young healthy volunteers is discussed. Results from the NIRS measurements and the relationships between systemic changes and the cerebral tissue oxygenation measurement are presented. Using the experimental data, simulations were carried out using the UCL model. In the final section the relationship between the simulated cerebral tissue oxygenation and the experimental measured cerebral tissue oxygenation is investigated and discussed.

5.1 Introduction

The changes in cerebral haemodynamics due to changes in arterial partial pressure of carbon dioxide ($PaCO_2$) are well known: an increase in $PaCO_2$ (hypercapnia) results in vasodilation producing marked rises in cerebral blood flow (CBF) whereas a decrease in $PaCO_2$ (hypocapnia) results in vasoconstriction producing a fall in CBF [1-3]. Blood flow autoregulation and the $PaCO_2$ have predominant influence on the regulation of global cerebral perfusion. Cerebral vessels constrict and dilate during an increase and decrease of perfusion pressure. Myogenic (intrinsic response of vascular muscle to changes in stretch) and metabolic (release of mediators) mechanisms have been proposed as important regulatory control systems [4]. The potent effect of CO_2 is local action on cerebral arterioles and appears to be mediated by extracellular H^+ ions [5]. CO_2 readily diffuses from the blood to the brain causing alterations in the extracellular pH in the immediate vicinity of the smooth muscle cells. There are upper and lower limits to the $PaCO_2$ response. The vasodilatory effect of an increase in $PaCO_2$ is in an increase in CBF of approximately 3ml of blood for every 1mmHg (0.13kPa) rise in $PaCO_2$ in the range 40-60mmHg (5.3-8.0kPa). Below 40mmHg (5.3kPa), flow falls progressively with reduction in $PaCO_2$ until 20mmHg (2.7kPa), there is no further reduction in flow below this value [2].

Near Infrared Spectroscopy (NIRS) can be used to monitor cerebral haemodynamics and oxygenation, to changes in $PaCO_2$ [6-17]. It provides a real time assessment of fluctuations in cerebral changes in oxy-haemoglobin concentration $\Delta[HbO_2]$ and deoxy-haemoglobin concentration $\Delta[HHb]$ and allows for measurements of absolute tissue oxygenation index (TOI) using the technique of spatially resolved spectroscopy (SRS). The principle of the technique has been described in detail in Chapter 4.

The aims of this study were to investigate the NIRS response to changes in $PaCO_2$ and use the experimental data to investigate the predictive ability of the cerebral computational model. In particular the cerebral TOI and the change in total tissue haemoglobin ($\Delta[HbT]= \Delta[HbO_2]+ \Delta[HHb]$) reactivity in response to inhalation of 5% CO_2 are investigated. Regarding the modelling work, simulations were run with the

physiological data and qualitative and quantitative comparisons between the model output and the experimental data were performed.

5.2 Subjects and experimental methods

12 healthy volunteers of mean ±SD age 32 ±4years were investigated (the local ethics committee approved the protocol for the study, and all subjects gave informed consent for participation). The volunteers were recruited from the academic and hospital staff.

5.2.1 Monitoring configuration

In a quiet environment, volunteers were asked to breath through a face mask while NIRS optodes (NIRO 300, Hamamatsu Photonics KK) where attached to their heads. The NIRS optodes were placed on the frontal region away from the midline sinuses. The emitter was placed 4cm away from the detector. The probe was secured with adhesive tape, and a pressure bandage was applied beneath a lightproof cloth.

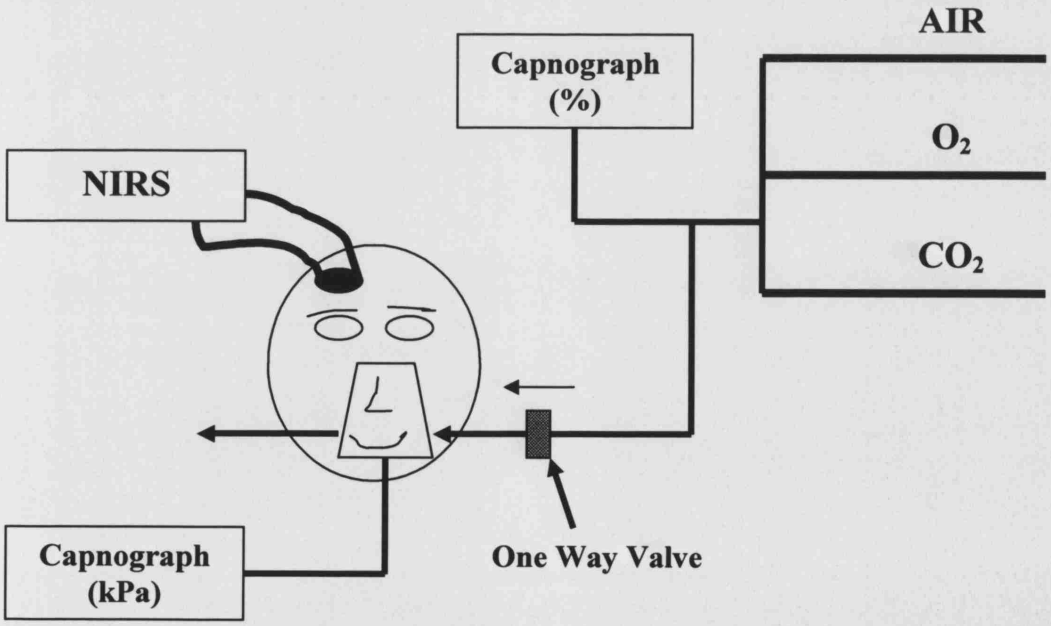

Figure 5.1: Schematic diagram of the experimental set up.

The subjects breathed through a facemask with a separated valve for inspiratory gas mixture. 5% hypercapnia was induced by mixing 0.2L of O_2, 0.35-0.4L of CO_2 and 8L of air. The percentage of CO_2 in the inspired gas was monitored continuously via a capnograph (SNOOPY, Merlin) connected at the ventilator end. The mask was connected to a second capnograph (SNOOPY, Merlin), which recorded continuously end tidal CO_2 (EtCO2), inspired CO_2 (InspCO2) and the inspired percentage fraction of oxygen (FiO_2). A modified beat-to-beat pulse oximeter (Novametrix 500) was placed on the ear lobe to record arterial saturation (SaO_2).

Finally mean blood pressure (MBP) was monitored continuously (Portapres®) and non-invasive with the use of an automated pressure cuff placed on the finger. The Portapres® system is a later version of the Finapres® blood pressure monitor system (described in Chapter 3, Section 3.2.1); with the capability of automatically correcting for changes in finger pressure induced by changes in the hydrostatic level between the heart and the instrumented finger.

5.2.2 Data collection

Signals of $EtCO_2$ and $InspCO_2$ were collected by an RS232 interface with a sampling rate of 0.97Hz, MBP was collected by an RS232 interface in a beat to beat mode, which later was resampled to 1Hz and SaO_2 was collected by an analog input at 6Hz. NIRS raw optical signals were collected by an RS232 interface at 6 Hz and later offline converted to micromoles per litre (μmoles/l) using a differential path length factor of 6.2 [18].

5.2.3 Protocol

Each study involved three physiological phases. These included an initial rest period (normocapnia), a 5% inspired CO_2 stimulus (moderate hypercapnia) and a final rest period (normocapnia). A typical example of examination recordings is presented in Figure 5.2.

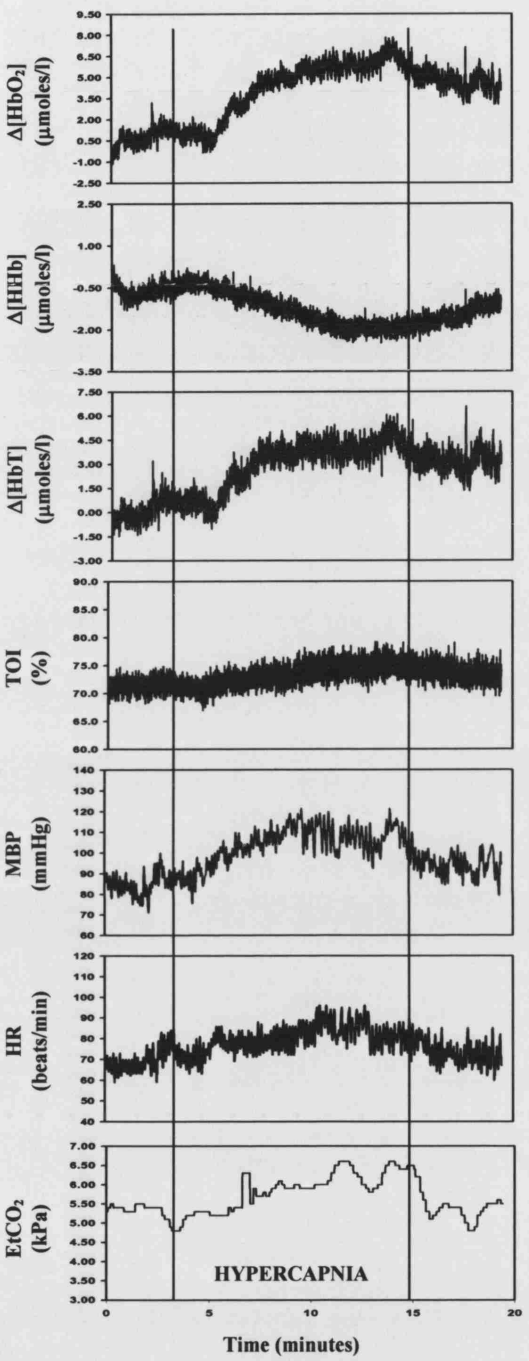

Figure 5.2: Graph shows example of time trends during the hypercapnic challenge. The event markers show the start and end of the hypercapnia.

5.3 Simulation methodology

Simulations were done using the UCL BRAINCIRC cerebral model (version 1.0, 2004-2005). The individual measured time traces of $EtCO_2$ (which were assumed to be equal to $PaCO_2$), MBP and SaO_2 were used as input parameters to the model after being smoothed by a 1 second non-overlapping moving averaging. The purpose of the

averaging was due to undesirable physiological oscillations in the signals and to reduce the quantity of data to be simulated. Other parameters in the model were set to their default values.

Simulated output variables CBF, CBV, pH, venous saturation (SvO_2) and simulated TOI (sTOI) together with the time were collected and imported into MatLab for further analysis.

5.4 Analysis

For each subject data was averaged for one minute, using the trapezoidal function *(trapz)* of MatLab, at the end of the rest period to obtain a baseline value, at the end of the hypercapnia where the $EtCO_2$ was at its highest and at the end of the return to rest. Data was tested for normality using the Shapiro-Wilk's test and are expressed as means with standard deviations during normocapnia and hypercapnia.

Correlation analysis was also performed to determine the relationship between systemic and cerebral variables and between experimental results and model predictions. Association was considered excellent for r values greater that 0.75, substantial or moderate in the range 0.50-0.75, fair in the range 0.25-0.50 and no association in the range 0.00-0.25 [19].

In order to test for agreement between model and experimental TOI measurements, the arithmetical difference between paired measurements was plotted against their average [20] to examine the difference between paired experimental and simulated measurements. If differences were normally distributed, 95% of them would lie within a range of ±2 S.D.s of the mean of arithmetical difference. This range will be reported as the limits of agreement.

Finally multi-regression analysis was also performed in order to determine association in more than two variables, with the Fisher methodology testing for significance of the results [21].

5.5 Experimental results

Table 5.1 shows the group mean values (with SD) during rest and hypercapnia. A statistically significant increase during hypercapnia was observed in $EtCO_2$ (paired t-test, $p<0.001$) and cerebral TOI (paired t-test, $p<0.001$).

Table 5.1: Mean values (with SD) for $EtCO_2$, MBP, heart rate (HR), and cerebral tissue oxygenation index (TOI), during normocapnia and hypercapnia

	$EtCO_2$ (mmHg) Mean(SD)	MBP (mmHg) Mean(SD)	HR (beats/min) Mean(SD)	TOI (%) Mean(SD)
Normocapnia	36.5 (4.6)	87 (14)	75 (13)	73 (7)
Hypercapnia	43.9 (4.3)	91 (14)	77 (11)	76 (7)

The results of the individual relationship between TOI and $EtCO_2$ are shown in Figure 5.3. A consistent increase is shown in the absolute paired values of $EtCO_2$ and TOI between the normocapnia and hypercapnia phases.

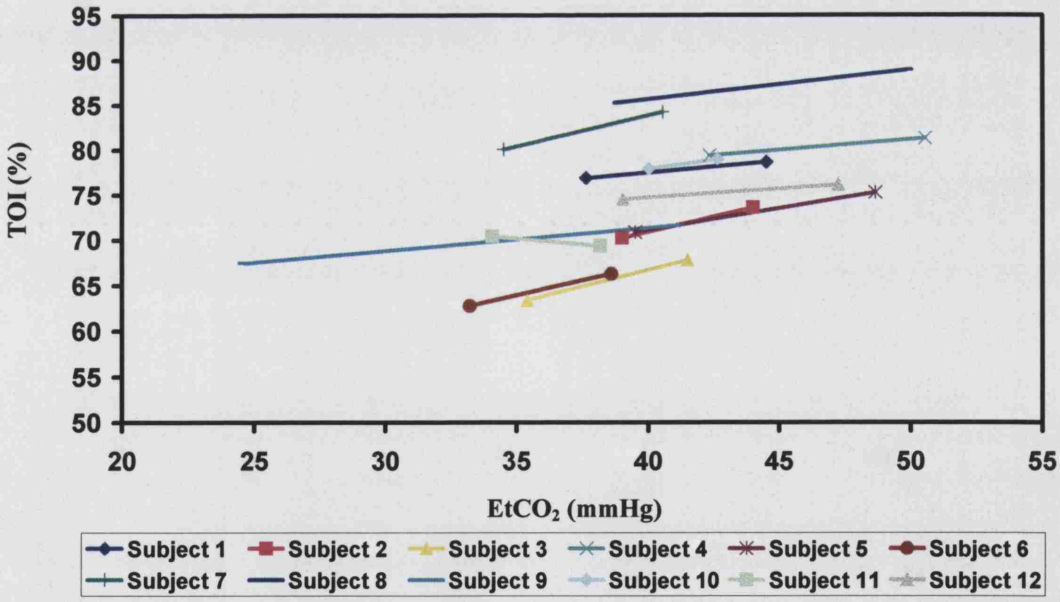

Figure 5.3: Individual responses of paired absolute values of $EtCO_2$ and TOI from normocapnia to hypercapnia.

Hypercapnia was induced by an increase of the inspired CO_2 to 5% this produced a mean increase in $EtCO_2$ of 7.4mmHg which ranged between individuals from 2.6 to 16.3mmHg. Other systemic variables such as MBP and HR did change during

hypercapnia; however the data did not show a consistent and statistically significant increase or decrease from the baseline.

Cerebral TOI increased for most of the volunteers, the mean change was 3 % and that ranged between -1 to 4%, cerebral Δ[HbT] also increased, the mean change was 2.4μmoles/l with a range of -1.12 to 4.17μmoles/l. Figure 5.4 shows the individual responses during hypercapnia for Δ[$EtCO_2$], Δ[MBP], Δ[TOI] and Δ[HbT] from normocapnia to hypercapnia.

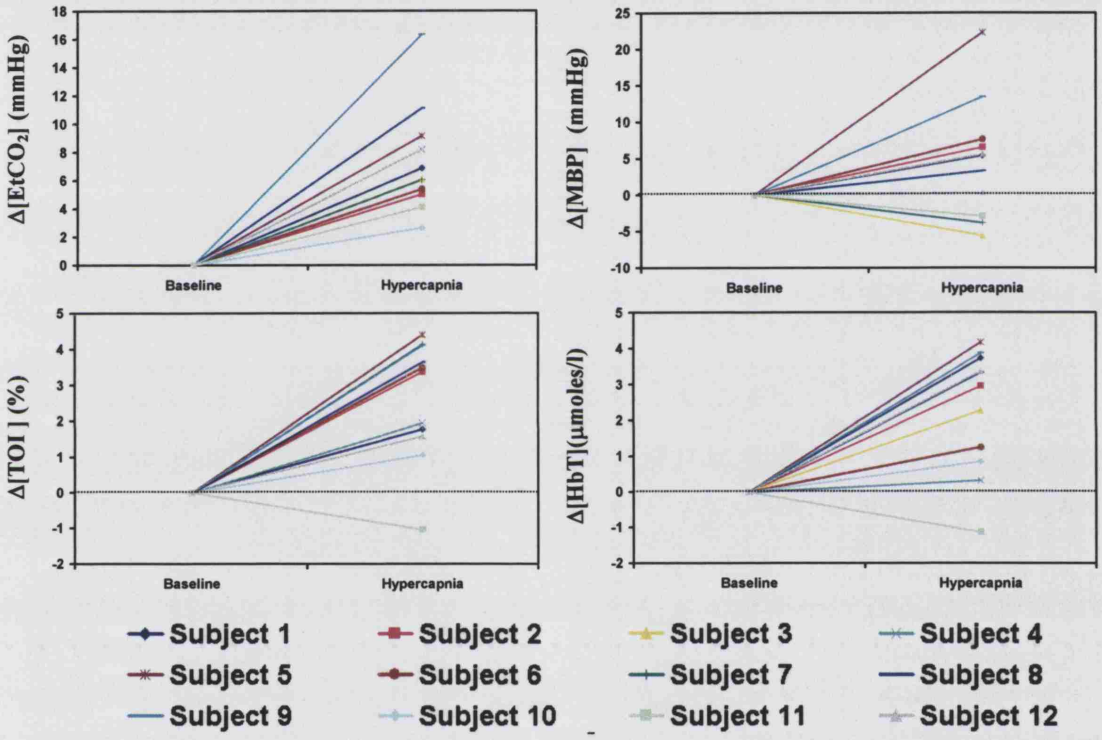

Figure 5.4: Individual changes for Δ[$EtCO_2$], Δ[MBP], Δ[TOI] and Δ[HbT] from normocapnia to hypercapnia.

Association analysis between the absolute raw cerebral TOI and $EtCO_2$ show a fair significant correlation (r=0.5, p=0.05) during rest, which become substantial (r=0.63, p=0.01) during hypercapnia.

Figure 5.5 shows the raw data of $EtCO_2$ and concomitant TOI values from all subjects during rest and during hypercapnia. Linear regression analysis was performed for both the rest and the hypercapnia data, resulting in the equations TOI=0.75*$EtCO_2$+45.8 and TOI=1*$EtCO_2$+32.3 (TOI: %; $EtCO_2$: mmHg) respectively.

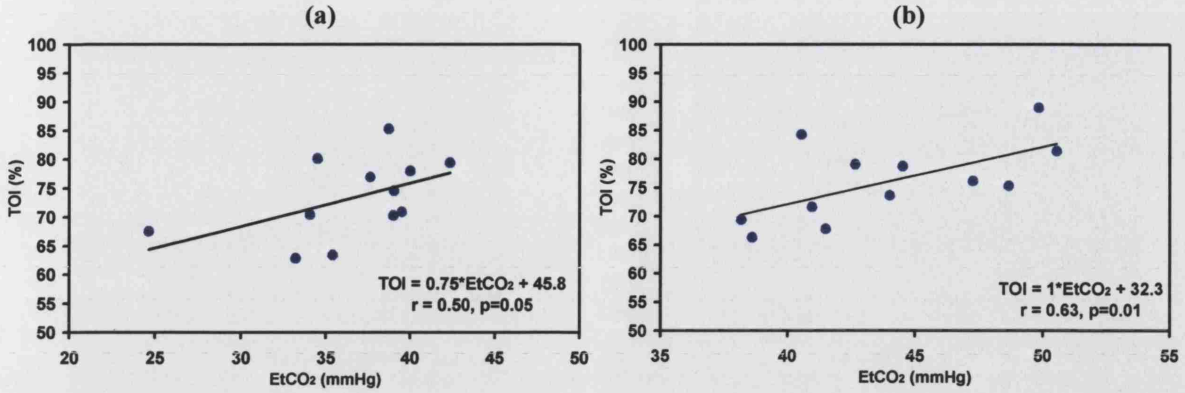

Figure 5.5: TOI/$EtCO_2$ reactivity absolute raw data of all subjects for **(a)** normocapnia and **(b)** hypercapnia.

No association was found between MBP versus TOI and MBP versus $EtCO_2$. However, multi-regression analysis between the hypercapnic raw values of $EtCO_2$, MBP and TOI revealed a linear relationship with $r^2=0.55$ and $p<0.05$ (Fisher test, F-observed value of 5.45 which is substantially greater than the F-critical value of 4.26 when $p<0.05$) and a result equation of $TOI=0.98*EtCO_2-0.19*MBP+50.78$ (TOI: %; $EtCO_2$: mmHg; MBP: mmHg).

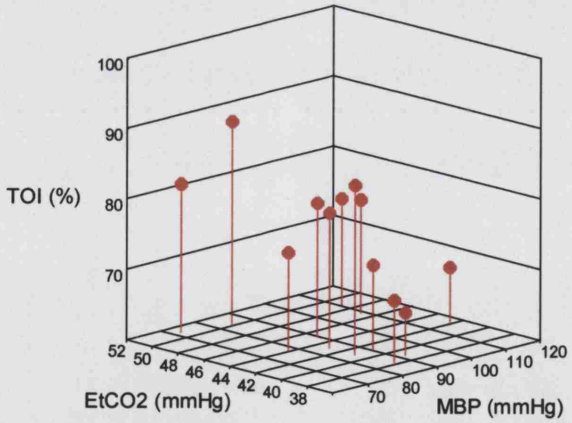

Figure 5.6: 3D scatter plot of hypercapnic raw values of TOI, $EtCO_2$ and MBP.

The arithmetical differences between paired measurements (hypercapnia minus normocapnia) of Δ[TOI] and Δ[HbT] was plotted against Δ[$EtCO_2$], for each subject. Correlation analysis and regression analysis was performed. These results are shown in Figure 5.7.

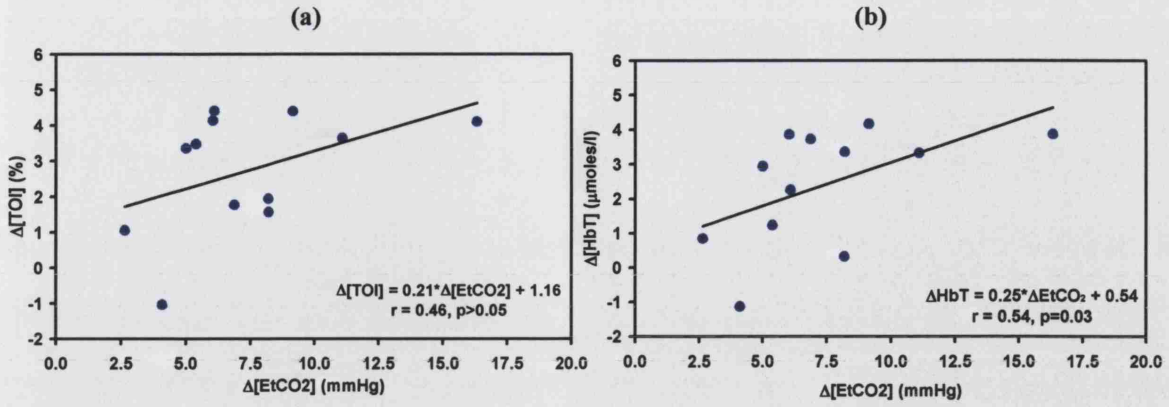

Figure 5.7: Correlation analysis of the changes in **(a)** $\Delta[EtCO_2]$ and Δ[TOI], **(b)** $\Delta[EtCO_2]$ and Δ[HbT] from normocapnia to hypercapnia.

No statistically significant association was found for the changes between $\Delta[EtCO_2]$ and Δ[TOI]; a good correlation with statistical significance was found between the changes in $\Delta[EtCO_2]$ and Δ[HbT] ($r=0.54$, $p=0.03$) with linear regression analysis resulting in the equation $\Delta[HbT]=0.25*\Delta[EtCO_2]+0.54$ ([HbT]: μmoles/l; $EtCO_2$: mmHg).

5.6 Simulation results

The results of the individual relationship between the simulated tissue oxygenation index (sTOI) and $EtCO_2$ are shown in Figure 5.8. A consistent increase is shown in the absolute paired values of $EtCO_2$ and sTOI between the normocapnia and hypercapnia phases.

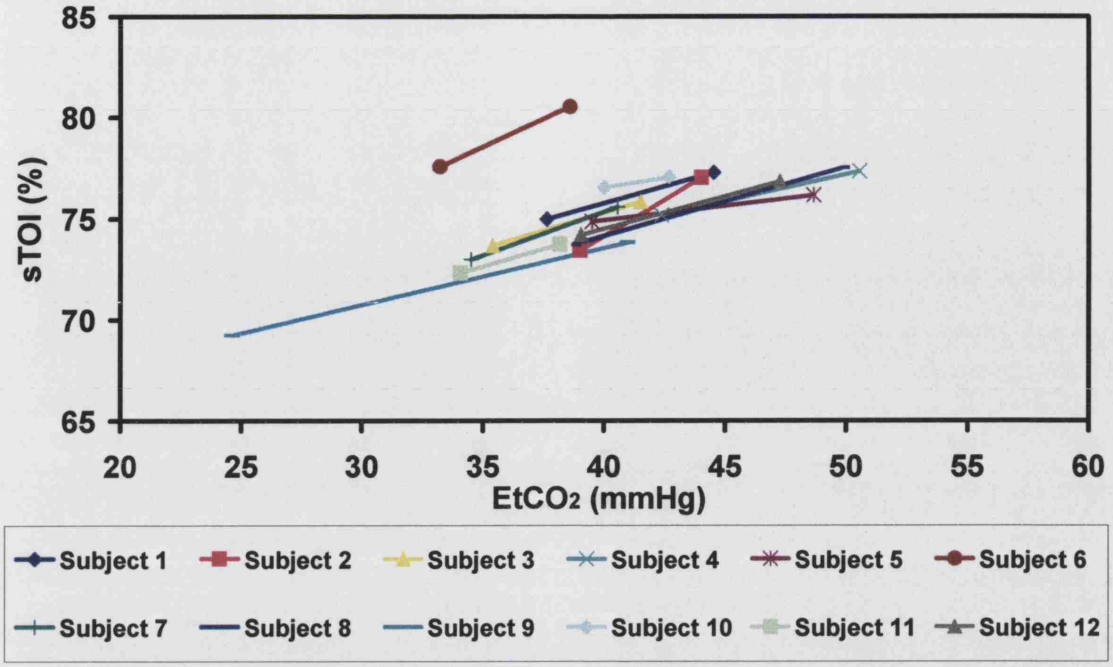

Figure 5.8: Individual responses of paired absolute values of $EtCO_2$ and sTOI from normocapnia to hypercapnia.

Table 5.2 shows the group mean values (with SD) during rest and hypercapnia. A statistically significant increase during hypercapnia was observed in CBF, CBV, sTOI and SvO_2 (paired t-test, $p<0.001$) and a significant decrease in pH (paired t-test, $p<0.001$).

Table 5.2: Mean values (with SD) for CBF, CBV, cerebral simulated tissue oxygenation index (sTOI), cerebral venous oxygenation (SvO_2), and pH during normocapnia and hypercapnia.

	CBF ($ml.100g^{-1}.min^{-1}$) Mean(SD)	CBV (ml/100g) Mean(SD)	sTOI (%) Mean(SD)	SvO_2 (%) Mean(SD)	pH () Mean(SD)
Normocapnia	56 (4)	3.22 (0.08)	74 (2)	64 (3)	7.08 (0.02)
Hypercapnia	60 (3)	3.28 (0.09)	77 (2)	67 (2)	7.04 (0.02)

Cerebral sTOI increased for all the volunteers, the mean change was 3% with a range between 0.5 to 4.6%, cerebral SvO_2 also increased, the mean change was 3% with a range of 1 to 7%, the pH demonstrate a significant decrease, the mean change being -0.04 and the range was between -0.09 to -0.01. CBF also increased for all the volunteers, the mean change was $5ml.100g^{-1}.min^{-1}$ with a range between 0.1 to 8.8 $ml.100g^{-1}.min^{-1}$. Figure 5.9 show the individual responses during hypercapnia for Δ[CBF], Δ[sTOI], $\Delta[SvO_2]$ and Δ[pH] from normocapnia to hypercapnia.

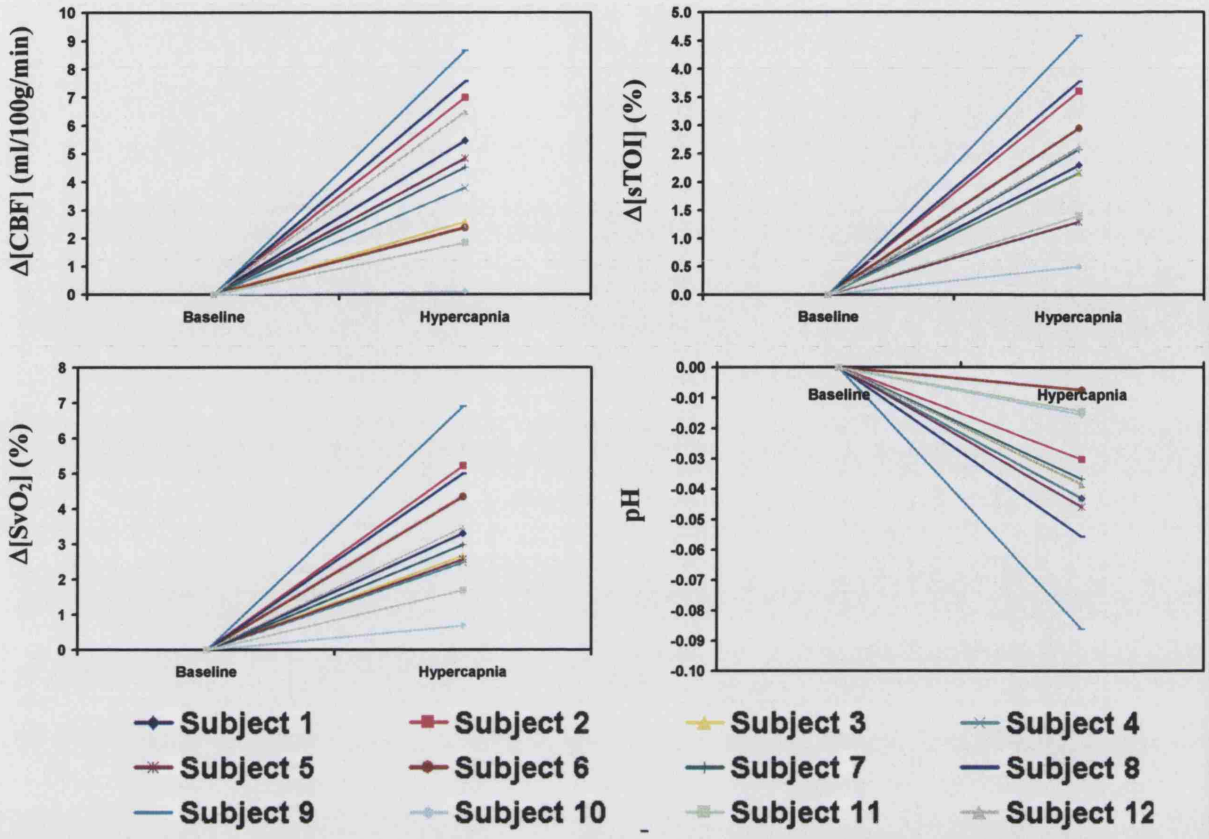

Figure 5.9: Individual changes for Δ[CBF], Δ[sTOI], Δ[SvO_2] and Δ[pH] from normocapnia to hypercapnia.

Association analysis between the absolute raw cerebral sTOI and $EtCO_2$ show a substantially significant correlation (r=0.64, p=0.01) during rest. Figure 5.10(a) shows the raw data of $EtCO_2$ with concomitant sTOI values for all subjects during rest. Linear regression analysis was performed resulting in the equation $sTOI=0.29*EtCO_2+63.43$ (sTOI: %; $EtCO_2$: mmHg).

Correlation analysis of the arithmetical differences between paired measurements (hypercapnia minus normocapnia) of Δ[sTOI] and Δ[$EtCO_2$] show a substantially significant correlation (r=0.68, p=0.01). These results are shown in Figure 5.10(b), with linear regression analysis resulting in the equation $\Delta[sTOI]=0.215*\Delta[EtCO_2]+0.9$ (sTOI: %; $EtCO_2$: mmHg).

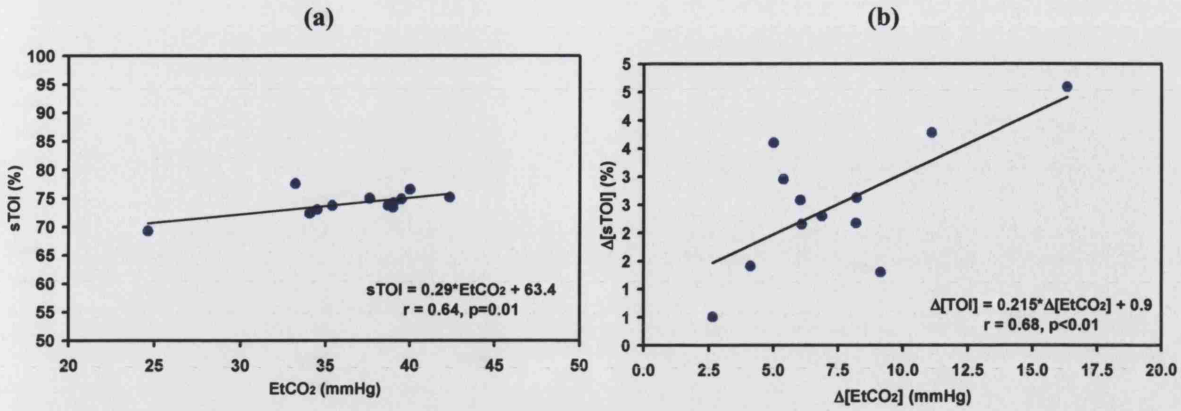

Figure 5.10: (a) Individual absolute sTOI/$EtCO_2$ reactivity during normocapnia; **(b)** association analysis between changes in Δ[sTOI] and Δ[$EtCO_2$] from normocapnia to hypercapnia for all subjects.

Multi-regression analysis of the arithmetical differences between paired measurements (hypercapnia minus normocapnia) of Δ[$EtCO_2$], Δ[MBP] and Δ[sTOI] revealed a linear relationship with r^2=0.40 with $p<0.05$ (Fisher test, F-observed value of 4.31 which is greater than the F-critical value of 4.26 when $p<0.05$) and a result equation of Δ[sTOI]=0.24* Δ[$EtCO_2$]-0.02* Δ[MBP] +0.8 (TOI: %; $EtCO_2$: mmHg; MBP: mmHg).

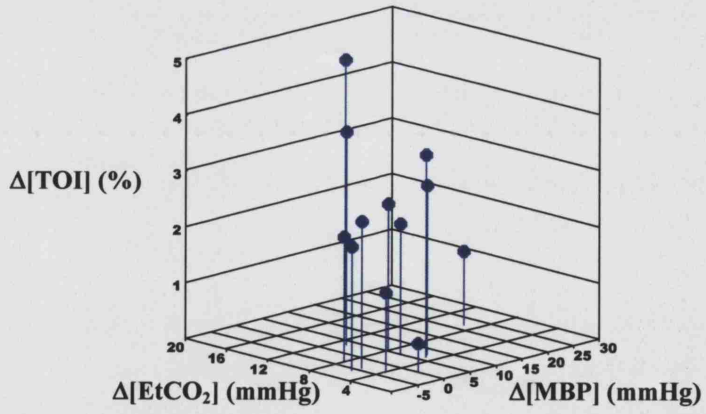

Figure 5.11: 3D scatter plot of the arithmetical differences between paired measurements (hypercapnia minus normocapnia) of Δ[$EtCO_2$], Δ[MBP] and Δ[sTOI].

5.7 Comparison between experimental and simulated data

Direct comparison between the simulated and measured TOI produced a general qualitative agreement regarding the changes between normocapnia and hypercapnia; in some cases there was a quantitative agreement in the absolute raw values (see Figure 5.12) but this was not true for most of the subjects (see Figure 5.13).

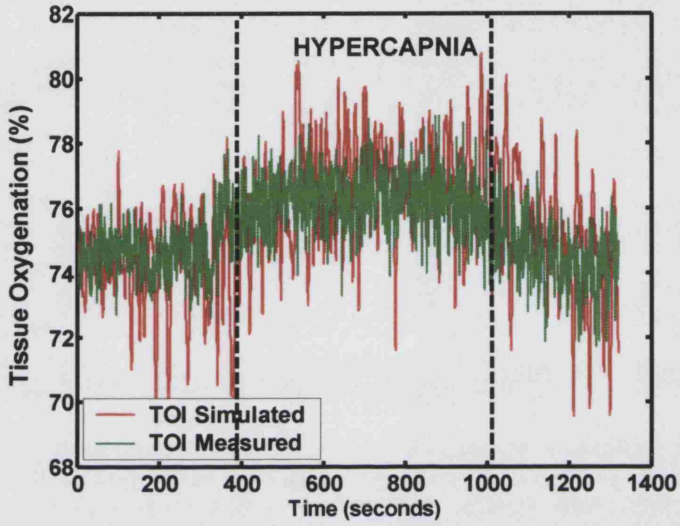

Figure 5.12: Simulated and measured TOI comparison for one subject.

In order to look for agreement and to investigate any possible relationship between the simulated and the measured cerebral TOI, a plot has been done of the difference between the signals against their mean. Under these circumstances one can summarise the lack of agreement by calculating the bias estimated by the mean difference and the standard deviation of the differences. Provided differences within mean difference ± 2SD would not be clinically important we could assume that the two different signals, the simulated and experimental TOI can be used interchangeably. The agreement between the measured and simulated TOI regarding the absolute raw values (see also Figure 5.13 for a scatter plot of simulated and measured TOI for all the phases) and the changes between normocapnia and hypercapnia are presented in Figure 5.14.

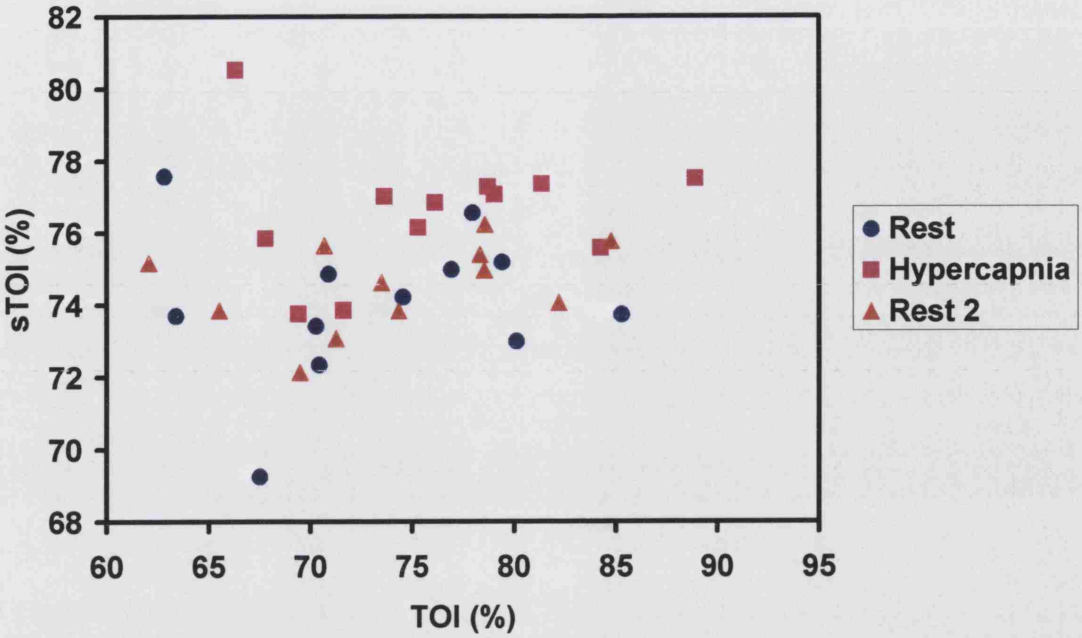

Figure 5.13: Scatter plot of simulated and measured TOI for the three phases.

From Figure 5.14 it can be seen that there is no agreement between the absolute raw values of simulated and experimental TOI, the mean difference ± 2SD in this case was minus -0.58±13.2% which is too high for physiological variables; however when looking at the changes this was 0.08±2.8%, with most of the values residing in the range of ±1% demonstrating a better agreement.

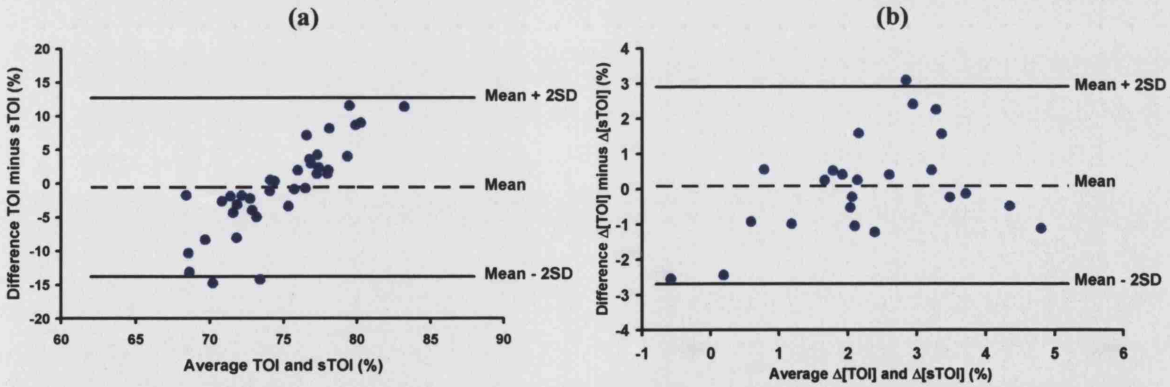

Figure 5.14: Agreement comparison between sTOI/TOI from normocapnia to hypercapnia and return to normocapnia using the: (a) absolute raw data of all subjects (b) the changes of all subjects.

5.8 Discussion

Results of cerebrovascular reactivity to acute induced hypercapnia have been presented. Specifically the effect of inhalation of 5% CO_2 on the cerebral haemodynamics using NIRS was examined. A consistent increase in Δ[HbT] and TOI with hypercapnia were found, confirming results of others [8,12-16,22]. The cerebral TOI increases significantly during the hypercapnic challenge as it has been observed by Yoshitani and colleagues [15] also a fair and significant correlation between the absolute TOI and $EtCO_2$ which became substantial during the hypercapnia (probably suggesting an $EtCO_2$ flow mediated association) was observed. A mean increase in cerebral Δ[TOI] of 3% which was not associated with the mean increase in $EtCO_2$ of 7.4mmHg from normocapnia to hypercapnia was found. No statistically significant association was observed between the changes in Δ[TOI] and Δ[$EtCO_2$]. A mean increase in Δ[HbT] of 2.4μmoles/l during hypercapnia was found together with a good correlation between the changes in Δ[HbT] and Δ[$EtCO_2$] as has been demonstrated by others [8,12]. No statistically significant or consistent changes were observed in the MBP systemic signal (paired t-test, $p>0.05$).

As mentioned previously the experimental results presented here agree with a recent study from Yoshitani and colleagues [15] who used a 5% hypercapnic challenge in 19 volunteers which increased $EtCO_2$ by 12mmHg and produce no significant changes in MBP and HR but resulted in an increase in TOI of 5%. The response of the cerebrovascular changes to CO_2 has also been studied by others looking at the response of Δ[HHb] and Δ[HbO_2] and the changes related to cerebral perfusion as determined by transcranial Doppler [8]. Smielewski and colleagues [8] have carried out a study in 50 healthy volunteers, where they determined the 'CO_2 reactivity' during 5 % hypercapnia. They demonstrated that Δ[HbO_2] and Δ[HbT] were related positively to $EtCO_2$ (2.1mmoles.l^{-1}.kPa^{-1} and 1.44mmoles.l^{-1}.kPa^{-1} respectively) and the Δ[HHb] was related negatively (-0.63mmoles.l^{-1}.kPa^{-1}). Rostrup et al [16] have carried out a simultaneous positron emission tomography (PET) and NIRS study during hypercapnia, where they produced an average change in $PaCO_2$ of 9.5mmHg that caused a significant increase in the Δ[HbT] of 3.6μmoles/l, this was in agreement with the PET measured CBF and CBV which show an increase of 14 ml.100g^{-1}.min^{-1} and of 1.5ml/100g respectively.

The interpretation of the NIRS data in this thesis has been based on certain physiological assumptions. Mainly, that metabolic rate does not change during inhalation of CO_2, and therefore changes in concentrations of $\Delta[HbO_2]$ and $\Delta[HHb]$ are purely due to a haemodynamic effects (changing diameter of the resistive vessels) providing that the cerebral perfusion pressure stays constant. Should metabolic rate change at all during inhalation of CO_2, the amount of consumed oxygen would change, and therefore the concentrations of $\Delta[HbO_2]$ and $\Delta[HHb]$ would change as well, rendering the reactivity assessment unreliable. Siesjo [23] reported that there is no change in metabolic rate observed except very high level of $PaCO_2$ (>11kPa).

The results presented in this thesis showed a wide inter-individual variability of systemic responses to the acute change in the inspired CO_2. The measured raw cerebral TOI association with the raw $EtCO_2$ value and MBP tends to suggest that the absolute TOI value is dependent on the equilibrium state of these two variables. As both $EtCO_2$ and MBP alter CBF one can assume a relationship between CBF and TOI, this has been quantified in neonatal studies [24] but in this study we do not have direct evidence as we were not measuring CBF.

Equation 5-1 below (see Chapter 4 for further explanation) suggests a relationship between changes in flow and changes in TOI. The data of this study did not show a direct association between the changes of $\Delta[EtCO_2]$, $\Delta[MBP]$ and $\Delta[TOI]$ in any combination. To our knowledge no others investigators have tried to find associations between these three variables. What our data implies is that the changes in $\Delta[TOI]$ are not simply driven from the changes in $\Delta[EtCO_2]$ and $\Delta[MBP]$ (SaO_2 was unchanged during the hypercapnia) for this to be true and Equation 5-1 to be correct there must be a non-linear relationship between CBF and the venous volume fraction. Clearly the relationship between TOI, CBF and the venous volume fraction requires further investigation particularly in studies where CBF is measured directly.

$$TOI = SaO_2 - \left(\frac{Vv}{Va + Vv}\right) \cdot \left(\frac{CMRO_2}{k \cdot CBF \cdot [Hb \cdot 10^{-3}]}\right) \qquad \textbf{5-1}$$

Results from the cerebral computational model with the experimental data suggest a qualitative agreement between the changes in simulated and the measured TOI (see Figure 5.14(b)). In particular the mean change in sTOI was 3% which was associated with a mean change of CBF of $5ml.100g^{-1}.min^{-1}$. Multiregression analysis of the Δ[sTOI], $\Delta[EtCO_2]$ and Δ[MBP] show a relationship and resulted the following equation (Equation 5-2).

$$\Delta[sTOI] = 0.24 * \Delta[EtCO_2] - 0.02 * \Delta[MBP] + 0.8 \qquad \textbf{5-2}$$

This was expected as the model recognises $EtCO_2$ and MBP as the main systemic effectors on the changes in TOI (one other is SaO_2 which is discussed in the next Chapter). The model was able to reproduce the changes in a similar way to the experimental data as it can be seen in Figure 8.12(b). However the absolute raw values of sTOI were far from the raw experimental TOI values. Possible reasons for this include the inter-subject variability of resting levels of CBF and arterial:venous volume ratios. All simulations with the model also used the default healthy adult parameters and no attempt at this stage has been made to provide customisation to each volunteer other than the use of their input data. The model was however successful in describing the changes seen in the measured Δ[TOI] with the changes in $\Delta[EtCO_2]$.

References

1. S.S. Kety and C.F. Schmidt, "The effects of altered arterial tensions of carbon dioxide and oxygen on cerebral blood flow and cerebral oxygen consumption of normal young men," *J. Clin. Invest.* **27**, 484-492 (1948).

2. A.M. Harper, "Physiological control of the cerebral circulation," *Cerebral blood flow and metabolism,* Harper A.M. and Jennett S., eds., (Manchester University Press, Manchester and New York, 1990), 4-25.

3. L. Edvinsson, E.T. MacKenzie, and J. McCulloch, "Changes in arterial gas tensions.," *Cerebral blood flow and metabolism,* L. Edvinsson, E. T. MacKenzie, and J. McCulloch, eds., 1993), 524-552.

4. L. Edvinsson, E.T. MacKenzie, and J. McCulloch, "Autoregulation: Arterial and intracranial pressure.," *Cerebral blood flow and metabolism,* Edvinsson L., MacKenzie E.T., and McCulloch J., eds., (Raven Press, New York, 1993), 553-580.

5. M. Wahl, P. Deetjen, K. Thurau, D.H. Ngvar, and N.A. Lassen, "Micropuncture evaluation of the importance of perivascular pH for the arteriolar diameter on the brain surface," *Pflugers Arch.* **316**, 152-163 (1970).

6. C.E. Elwell, M. Cope, D. Kirkby, H. Owen-Reece, C.E. Cooper, E.O. Reynolds, and D.T. Delpy, "An automated system for the measurement of the response of cerebral blood volume and cerebral blood flow to changes in arterial carbon dioxide tension using near infrared spectroscopy," *Adv. Exp. Med. Biol.* **361**, 143-155 (1994).

7. A. Tateishi, T. Maekawa, Y. Soejima, D. Sadamitsu, M. Yamamoto, M. Matsushita, and K. Nakashima, "Qualitative comparison of carbon dioxide-induced change in cerebral near-infrared spectroscopy versus jugular venous oxygen saturation in adults with acute brain disease," *Crit. Care Med.* **23**, 1734-1738 (1995).

8. P. Smielewski, P. Kirkpatrick, P. Minhas, J.D. Pickard, and M. Czosnyka, "Can Cerebrovascular Reactivity Be Measured With Near-Infrared Spectroscopy?," *Stroke* **26**, 2285-2292 (1995).

9. V. Pollard, D.S. Prough, A.E. DeMelo, D.J. Deyo, T. Uchida, and R. Widman, "The influence of carbon dioxide and body position on near-infrared spectroscopic assessment of cerebral hemoglobin oxygen saturation," *Anesth. Analg.* **82**, 278-287 (1996).

10. A.K. Gupta, D.K. Menon, M. Czosnyka, P. Smielewski, P.J. Kirkpatrick, and J.G. Jones, "Non-invasive measurement of cerebral blood volume in volunteers," *Br. J. Anaesth.* **78**, 39-43 (1997).

11. L.C. Henson, C. Calalang, J.A. Temp, and D.S. Ward, "Accuracy of a cerebral oximeter in healthy volunteers under conditions of isocapnic hypoxia," *Anesthesiology* **88**, 58-65 (1998).

12. R. Totaro, G. Barattelli, V. Quaresima, A. Carolei, and M. Ferrari, "Evaluation of potential factors affecting the measurement of cerebrovascular reactivity by near-infrared spectroscopy," *Clin. Sci. (London)* **95**, 497-504 (1998).

13. M.J.T. Van de Ven, W.N.J.M. Colier, B.T. Kersten, B. Oeseburg, and H. Folgering, "Cerebral blood volume responses to acute PaCO2 changes in humans, assessed with near infrared spectroscopy," *Adv. Exp. Med. Biol.* **471**, 199-207 (1999).

14. M.J.T. Van de Ven, W.N.J.M. Colier, M.C. van der Sluijs, B. Oeseburg, and H. Folgering, "Ventilatory response in metabolic acidosis and cerebral blood volume in humans," *Respiration Physiology* **124**, 105-115 (2001).

15. K. Yoshitani, M. Kawaguchi, K. Tatsumi, K. Kitaguchi, and H. Furuya, "A Comparison of the INVOS 4100 and the NIRO 300 Near-Infrared Spectrophotometers," *Anesth. Analg.* **94**, 586-590 (2002).

16. E. Rostrup, I. Law, F. Pott, K. Ide, and G.M. Knudsen, "Cerebral hemodynamics measured with simultaneous PET and near-infrared spectroscopy in humans," *Brain Research* **954**, 183-193 (2002).

17. J.C. Kolb, P.N. Ainslie, K. Ide, and M.J. Poulin, "Protocol to measure acute cerebrovascular and ventilatory responses to isocapnic hypoxia in humans," *Respiratory Physiology & Neurobiology* **141**, 191-199 (2004).

18. A. Dunkan, J.H. Meek, M. Clemence, C.E. Elwell, L. Tyszczuk, M. Cope, and D.T. Delpy, "Optical pathlength measurements on adult head, calf and forearm and the head of the newborn infant using phase resolved optoical spectroscopy.," *Phys. Med. Biol.* **40**, 295-304 (1995).

19. T. Colton, *Statistics in medicine*, Little Brown & Co, ed., 1974).

20. J.M. Bland and D.G. Altman, "Statistical methods for assessing agreement between two methods of clinical measurement," *Lancet* **1**, 307-310 (1986).

21. B. Dawson-Saunders and R.G. Trapp, "Association & Prediction," *Basic & Clinical Biostatistics,* B. Dawson-Saunders and R. G. Trapp, eds., (Appleton & Lange, Norwalk, Connecticut, 1994), 162-187.

22. P. Madsen, F. Lyck, M. Pedersen, H.L. Olesen, H. Nielsen, and N.H. Secher, "Brain and muscle oxygen saturation during head-up-tilt-induced central hypovolaemia in humans," *Clin. Physiol.* **15**, 523-533 (1995).

23. B.K. Siesjo, *Brain Energy Metabolism*, B.K. Siesjo, ed., (John Wiley & Sons, New York, 1978).

24. C.E. Elwell, J.R. Henty, T.S. Leung, T. Austin, J.H. Meek, D.T. Delpy, and J.S. Wyatt, "Regional measurement of $CMRO_2$ in neonates undergoing intensive care using near infrared spectroscopy," *Adv. Exp. Med. Biol.* **In press**, (2005).

Chapter 6

Model Predictions with Experimental Data during a Hypoxic Challenge

Having described the response of NIRS during a hypercapnia challenge and presented results using the model, in this chapter we discuss another indirect affector of cerebral blood flow, namely oxygen (O_2).

In this chapter a hypoxia study in young healthy volunteers is described and discussed. The relationship between changes in arterial oxygenation and near-infrared spectroscopy measurements is investigated together with analysis of associations between the cerebral and systemic changes during the hypoxic episode. Using the experimental data, simulations were carried out using the BRAINCIRC UCL cerebral model (version 1, 2004-2005). In the final section the relationship between the simulated cerebral tissue oxygenation and the experimentally measured cerebral tissue oxygenation is investigated.

6.1 Introduction

Decreases in the arterial partial pressure of oxygen (PaO_2) during hypoxia reliably increase cerebral perfusion by decreasing cerebrovascular resistance as a result of arterial vasodilation. Conversely, increases in PaO_2 (hyperoxia) result in moderate vasoconstriction and decreases in CBF. Thus, the effect of O_2 is in the opposite direction to that of CO_2. Decreases in PaO_2 below 40 to 50mmHg result in arterial dilation and increased CBF [1], detectable increases in pial arterial diameter and CBF occurring rapidly (within 30 to 60sec) and steady state responses are achieved within 5 to 10min. Cerebral metabolic integrity is critically dependent on arterial oxygen delivery for production of ATP by mitochondrial respiration; even brief disruptions in oxygen supply can result in metabolic failure and cell death.

Ventilatory events that threaten brain oxygenation are generally accommodated by changes in cerebral vascular resistance and consequential alteration in CBF in an attempt to restore oxygen delivery. Ellingsen and colleagues [2] demonstrated using non-invasive transcranial Doppler ultrasound (TCD) that a reduction in alveolar PaO_2 from about 13 to 8.7kPa with maintained constant alveolar $PaCO_2$ caused CBF to increase gradually over 10 min (half-time about 4min) to about 125% of control values. Gupta and colleagues [3] provided more evidence again using TCD that during hypoxia with SaO_2 below 90%, the cerebral perfusion increases.

Further studies with near-infrared spectroscopy (NIRS) (the principle of the technique has been described in detail in Chapter 4) in healthy volunteers and patients have provided more evidence of cerebral vasodilation during hypoxic episodes [4-8].

The aims of this study are to investigate the NIRS response of cerebral TOI to changes in SaO_2 and to use the experimental data to investigate the predictive ability of the cerebral computational model. In particular the cerebral TOI response and its association with the drop in SaO_2 are examined. Regarding the modelling work, simulations were run with the measured physiological data as an input and qualitative and quantitative comparisons between the model output and the experimental data were performed.

6.2 Subjects and experimental methods

12 healthy volunteers of mean ±SD age 32 ±4years were investigated (the local ethics committee approved the protocol for the study, and all subjects gave informed consent for participation). The volunteers were recruited from the academic and hospital staff.

6.2.1 Monitoring configuration

In a quiet environment, volunteers were asked to breath through a face mask while NIRS optodes (NIRO 300, Hamamatsu Photonics KK) were attached to their heads. The NIRS optodes were placed on the frontal region away from the midline sinuses. The emitter was placed 4 cm away from the detector. The probe was secured with adhesive tape, and a pressure bandage was applied beneath a lightproof cloth.

The subjects breathed through a facemask with a valve to separate the inspiratory and expiratory gas mixtures. Hypoxia was induced by mixing 7 litre of air with approximately 5 litre of nitrogen (N_2), which produced a drop in the inspired percentage fraction of oxygen (FiO_2) from 21% (normal atmospheric) down to 12-15%. The mask was connected to a capnograph (SNOOPY, Merlin), which recorded continuously end tidal CO_2 (EtCO2), inspired CO_2 (InspCO2) and the inspired percentage fraction of oxygen (FiO_2). A modified beat-to-beat pulse oximeter (Novametrix 500) was placed on the ear to record arterial saturation (SaO_2). Finally a Portapres® system (TNO Institute of Applied Physics, Biomedical Instrumentation) was used to continuously and non-invasively measure blood pressure from the finger (for description of Portapres® see Chapter 5, Section 5.2.1).

6.2.2 Data Collection

Signals of $EtCO_2$, $InspCO_2$ and FiO_2 were collected by an RS232 interface with a sampling rate of 0.97Hz, MBP was collected by an RS232 interface in a beat to beat mode, which later was resample to 1Hz and SaO_2 was collected by an analog input at 6Hz. NIRS raw optical signals were collected by an RS232 interface at 6Hz and later

offline converted to micromoles per litre (μmoles/l) using the differential pathlength factor of 6.2 [9].

6.2.3 Protocol

All measurements were made with the volunteers sitting comfortably in an armchair. The subject initially breathed normal air for 3-5min. The FiO_2 in the circuit was then gradually reduced to 10-15% by mixing air and nitrogen, until a baseline SaO_2 of 90% was achieved. At that point the subject was given 100% O_2 for five consecutive breaths. This was repeated a total of three times for each subject (see Figure 6.1). The data analysed here is from the first hypoxic drop, as this was the slowest and in most cases the most extensive hypoxic swing (see Figure 6.2).

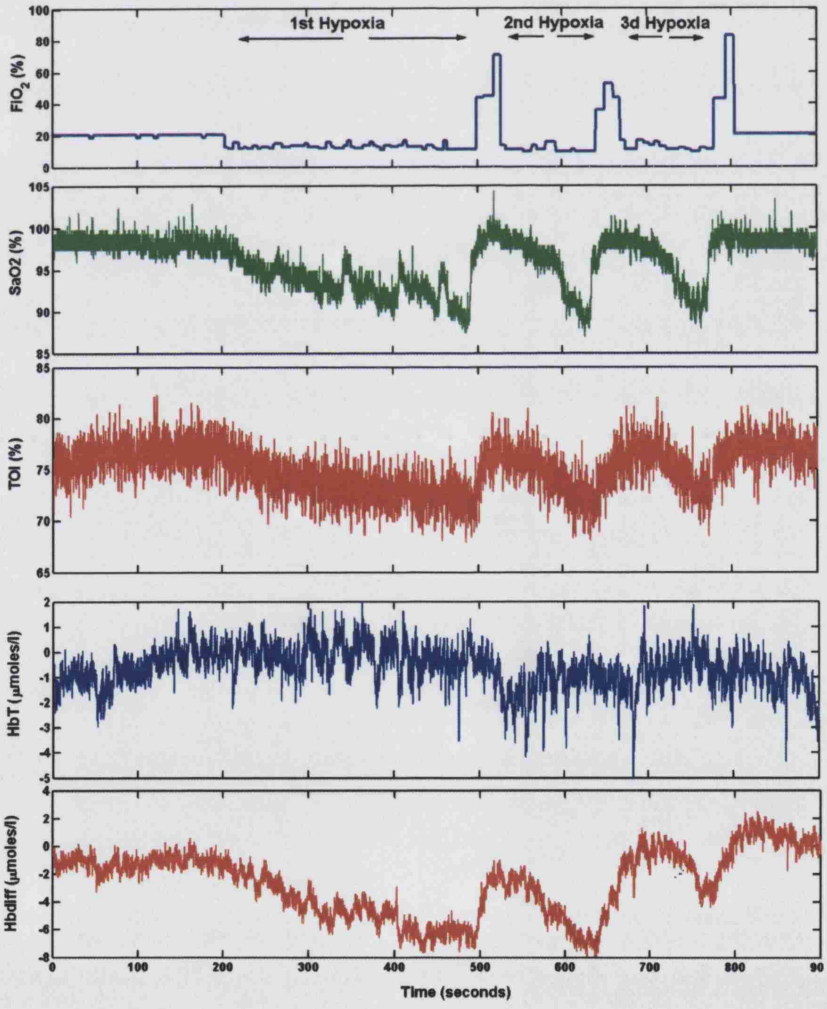

Figure 6.1: Representative data of the whole hypoxia study collected form one volunteer.

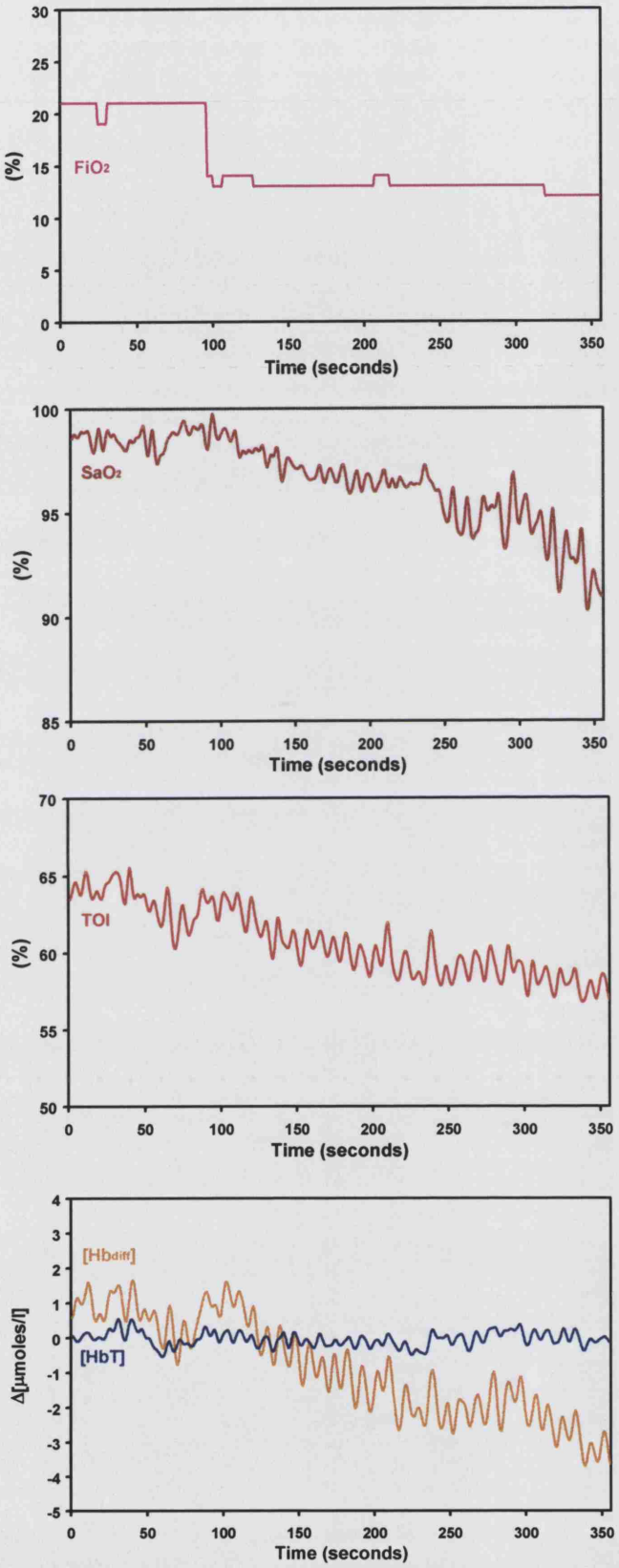

Figure 6.2: Representative data of the first hypoxic swing collected from one volunteer. For illustrative purposes data has been filtered to remove heart rate oscillations.

6.3 Simulation methodology

Simulations were done using the BRAINCIRC UCL cerebral model (version 1, 2004-2005). The individually measured time traces of $EtCO_2$ (which were assumed to be equal to $PaCO_2$), MBP and SaO_2 were used as input parameters to the model after being smoothed by one second non-overlapping moving averaging. The purpose of the averaging was to remove undesirable physiological oscillations in the signals and to reduce the quantity of data to be simulated. Other parameters in the model were set to their default values.

Simulated output variables CBF, CBV, pH, venous saturation (SvO_2), mitochondrial oxygen concentration and simulated TOI (sTOI) together with the time were collected and imported in MatLab for further analysis.

6.4 Analysis

For each signal four phases were recognised, these were baseline, start of hypoxia, middle of hypoxia and end of hypoxia (see Figure 6.3). The first and the last phase were manually identified in the SaO_2 and TOI signals, a program was written in MatLab to automatically identify the remaining phases and then calculated 10 second averages for each phase using the trapezoidal function (*trapz*) of MatLab. Data was tested for normality using the Shapiro-Wilk's test and are expressed as means with standard deviations during each phase.

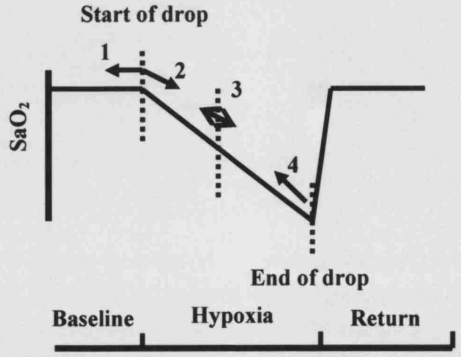

Figure 6.3: Schematic representation of the data analysis. 1: baseline, 2: start of hypoxia, 3: middle of hypoxia, 4: end of hypoxia.

Correlation analysis was also performed to determine the relationship between systemic and cerebral variables and between experimental results and model predictions. Association was considered excellent for r values greater that 0.75, substantial or moderate in the range 0.50-0.75, fair in the range 0.25-0.50 and no association in the range 0.00-0.25 [10].

In order to test for agreement between the model and experimental TOI measurements, the arithmetical difference between paired measurements was plotted against their average [11] to examine the difference between paired experimental and simulated measurements. If differences were normally distributed, 95% of them would lie within a range of ±2 S.D.s of the mean of arithmetical difference. This range will be reported as the limits of agreement.

Finally multi-regression analysis was also performed in order to determine association of more than two variables, with the Fisher methodology testing for significance of the results [12].

6.5 Experimental results

Table 6.1 shows the group mean values (with SD) during the four phases. There was a statistical significant decrease between baseline and end of hypoxia for SaO_2, cerebral TOI (paired t-test, $p<0.001$), $EtCO_2$ and MBP (paired t-test, $p<0.01$). Figure 6.4 shows the individual mean responses of SaO_2 versus TOI for all phases.

Table 6.1: Mean values (with SD) for $EtCO_2$, MBP, heart rate (HR), and cerebral tissue oxygenation index (TOI), during the four phases.

	SaO_2 (%) Mean(SD)	TOI (%) Mean(SD)	$EtCO_2$ (mmHg) Mean(SD)	MBP (mmHg) Mean(SD)
Baseline	98 (1)	74 (7)	38 (3)	95 (15)
Start of Hypoxia	97 (1)	73 (7)	38 (3)	92 (16)
Middle of Hypoxia	94 (2)	71 (6)	37 (3)	91 (14)
End of Hypoxia	91 (1)	68 (6)	36 (4)	87 (15)

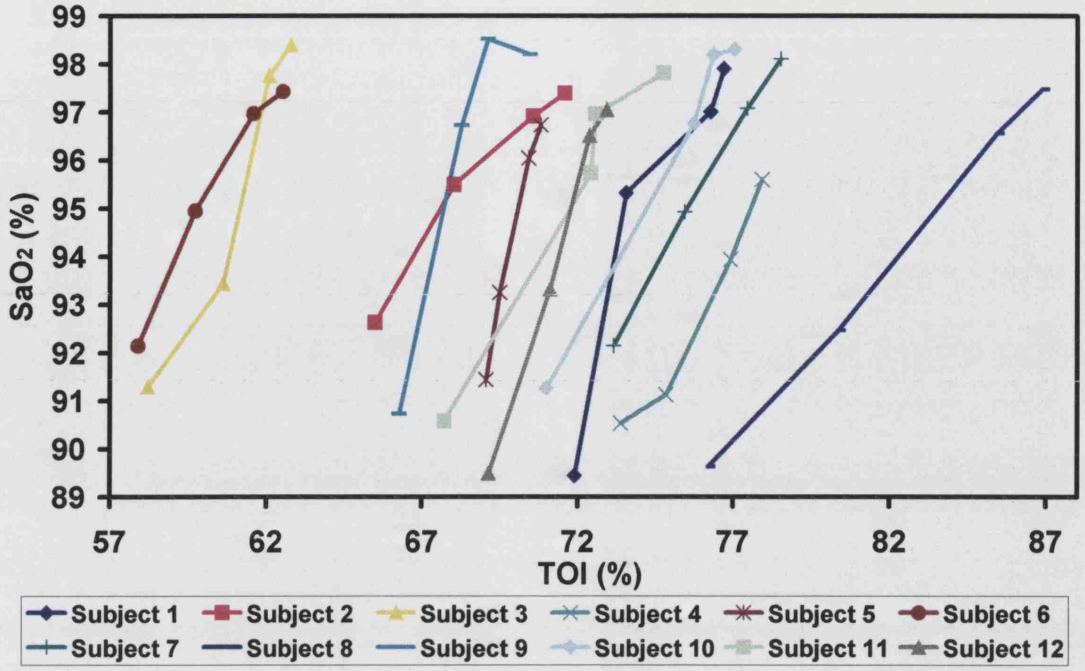

Figure 6.4: Individual responses of SaO_2 versus TOI from baseline to the end of the hypoxia.

There was a large inter-subject variability in the absolute values for the cerebral TOI signal but not as much for the SaO_2 signal. These results are shown in Figure 6.5.

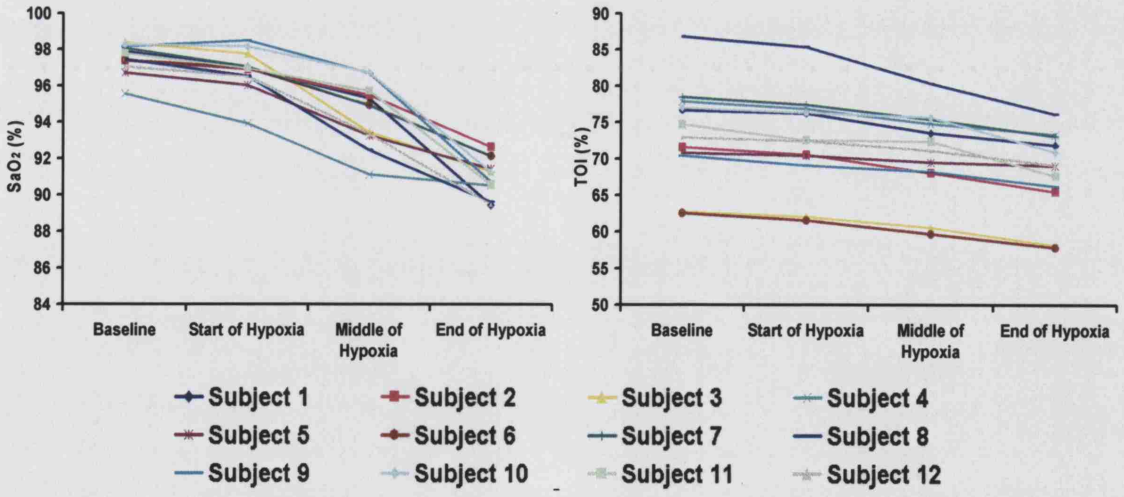

Figure 6.5: Individual absolute values of SaO_2 and TOI for each phase.

Hypoxia was induced by lowering the FiO_2 to 10-15%. That also caused a mean decrease in $\Delta[EtCO_2]$ of 2.3mmHg, which ranged between individuals from 0.7 to

6mmHg drop, with only subjects 4 and 12 exhibiting an increase of 0.3 and 1mmHg respectively. MBP also decreased with a mean fall of 8.1mmHg which ranged between individuals from 0.3 to 18.1mmHg. Figure 6.6 and Table 6.2 summarise these results.

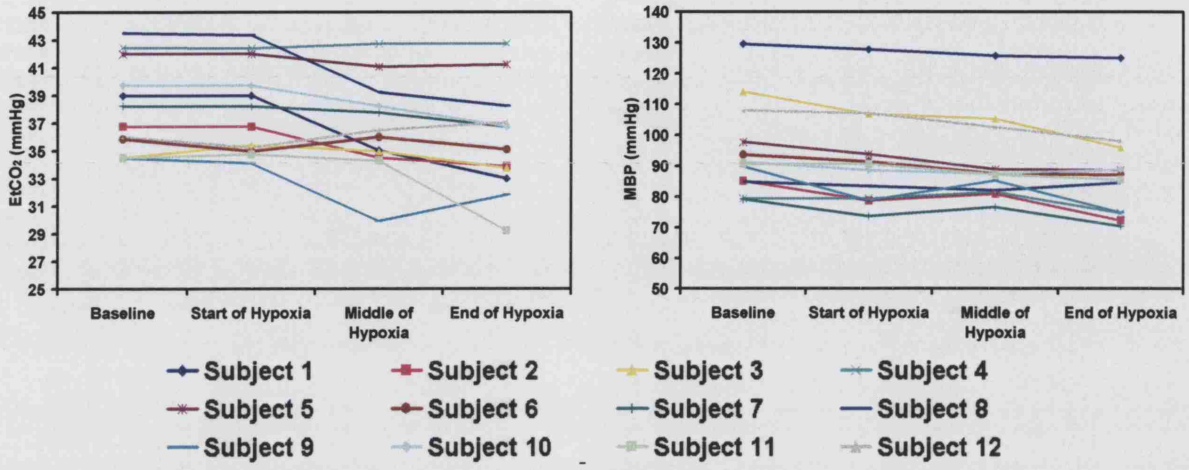

Figure 6.6: Individual absolute values of $EtCO_2$ and MBP for each phase.

Table 6.2: Changes from baseline, mean values (with SD) for $\Delta[SaO_2]$, $\Delta[TOI]$, $\Delta[EtCO_2]$, and $\Delta[MBP]$.

	$\Delta[SaO_2]$ (%) Mean(SD)	$\Delta[TOI]$ (%) Mean(SD)	$\Delta[EtCO_2]$ (mmHg) Mean(SD)	$\Delta[MBP]$ (mmHg) Mean(SD)
Start of Hypoxia	-0.7 (0.49)	-1 (0.51)	-0.1 (0.45)	-3.6 (3.34)
Middle of Hypoxia	-3.1 (1.27)	-2.8 (1.38)	-1.4 (1.91)	-4.3 (2.93)
End of Hypoxia	-6.6 (1.25)	-5.3 (2.16)	-2.3 (2.29)	-8.1 (5.24)

Cerebral $\Delta[TOI]$ decreased with a mean change of -5.3% (range -1.7 to -10.7%) cerebral haemoglobin difference ($\Delta[Hb_{diff}] = \Delta[HbO_2] - \Delta[HHb]$) also decreased, the mean change was -4.4μmoles/l (range -1.4 to -6.9μmoles/l). Cerebral total haemoglobin ($\Delta[HbT] = \Delta[HbO_2] + \Delta[HHb]$) did not demonstrate any significant changes.

Figure 6.7 show the individual responses for $\Delta[HbT]$ and $\Delta[Hb_{diff}]$ from baseline to the end of hypoxia and Table 6.3 summarises the haemoglobin concentration changes.

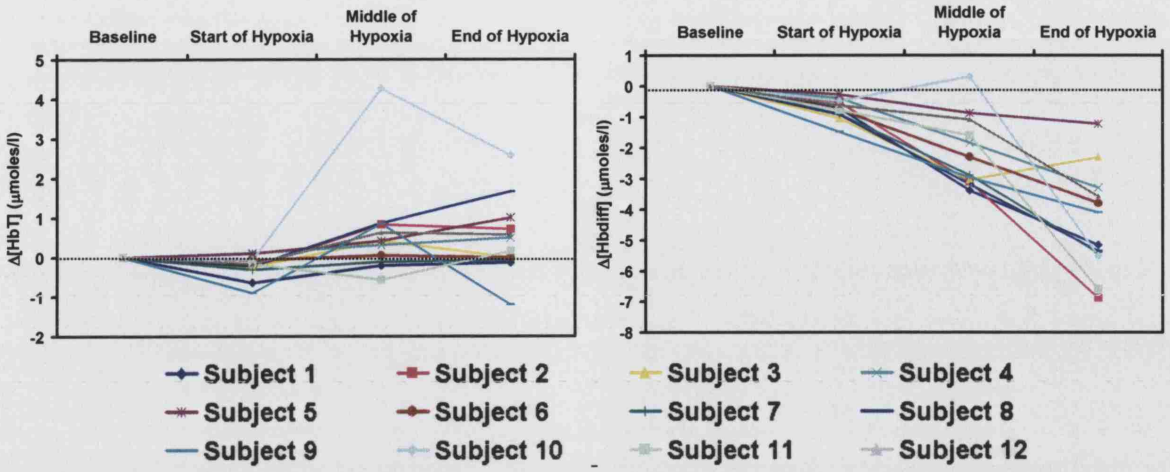

Figure 6.7: Individual arithmetical differences from baseline for $\Delta[Hb_{diff}]$ and $\Delta[HbT]$ for all phases.

Table 6.3: Changes from baseline, mean values (with SD) for $\Delta[HbO_2]$, $\Delta[HHb]$, $\Delta[Hb_{diff}]$, $\Delta[HbT]$.

	$\Delta[HbO_2]$ (μmoles/l) Mean(SD)	$\Delta[HHb]$ (μmoles/l) Mean(SD)	$\Delta[Hb_{diff}]$ (μmoles/l) Mean(SD)	$\Delta[HbT]$ (μmoles/l) Mean(SD)
Start of Hypoxia	-0.49 (0.29)	0.26 (0.1)	-0.75 (0.33)	-0.23 (0.29)
Middle of Hypoxia	-0.76 (1.06)	1.41 (0.54)	-2.17 (1.16)	0.65 (1.23)
End of Hypoxia	-1.98 (0.92)	2.46 (1.03)	-4.43 (1.69)	0.48 (0.96)

Correlation analysis between paired values of absolute SaO_2 and TOI and changes of $\Delta[SaO_2]$ and $\Delta[TOI]$ for each phase did not produce any significant results. The trends of the data for each phase are shown in Figure 6.8. The scatter plot of Figure 6.8(b) show a trend relationship between the changes in $\Delta[TOI]$ and the absolute values of SaO_2.

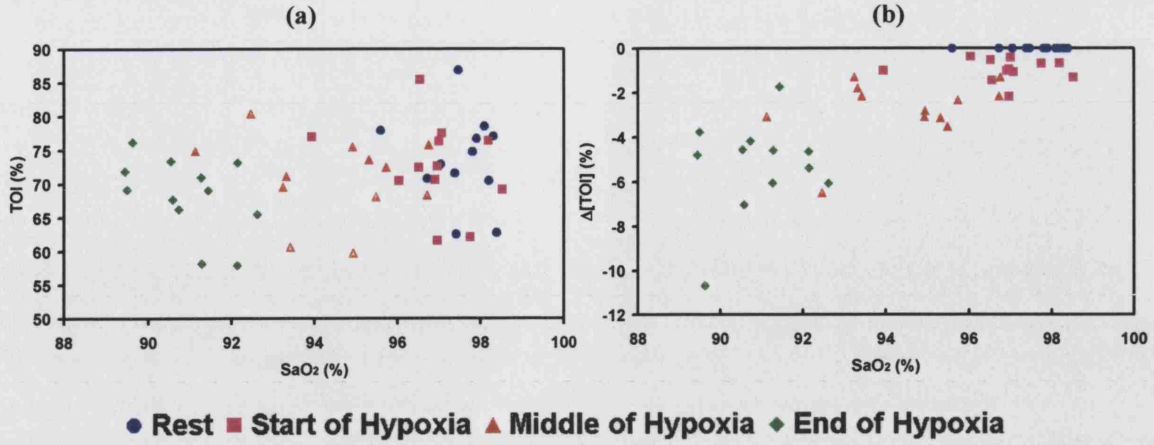

Figure 6.8: Individual data for each phase **(a)** absolute TOI measurements versus the SaO_2 measurements **(b)** arithmetical differences from baseline for Δ[TOI] versus absolute SaO_2 values.

Substantial association was found between the raw values of cerebral TOI and $EtCO_2$ during baseline ($r=0.68$, $p=0.01$) and the start of the hypoxia ($r=0.7$, $p<0.01$). These results together with the regression equation are shown in Figure 6.9.

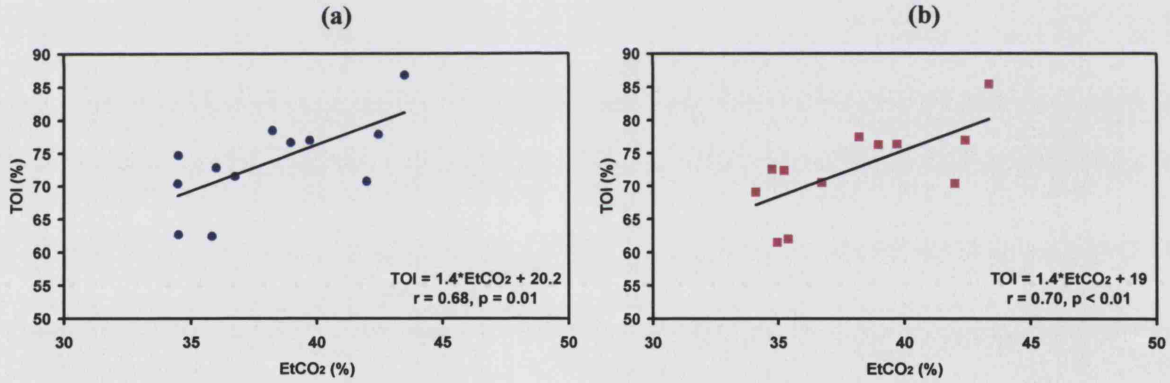

Figure 6.9: Individual raw data of TOI versus $EtCO_2$ for **(a)** baseline measurements **(b)** start of hypoxia measurements.

Substantial association was found between the changes in cerebral Δ[TOI] and Δ[$EtCO_2$] between baseline and the end of the hypoxia ($r=0.63$, $p<0.025$). This result together with the regression equation is shown in Figure 6.10.

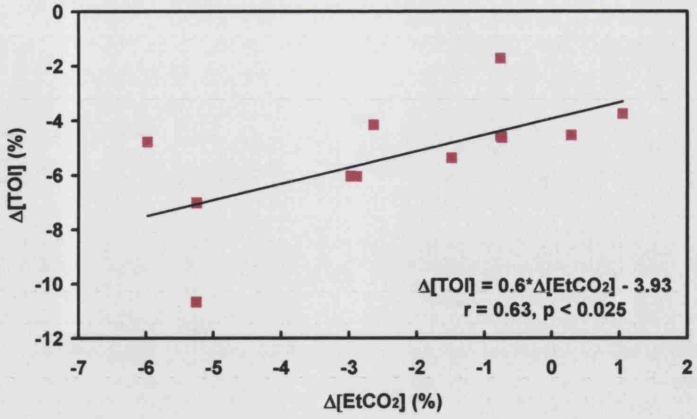

Figure 6.10: Individual changes of Δ[TOI] versus Δ[$EtCO_2$] at the end of hypoxia.

6.6 Simulation results

The results of the individual relationship between the simulated tissue oxygenation index (sTOI) and SaO_2 are shown in Figure 6.11. A consistent decrease is shown in the absolute paired values of SaO_2 and sTOI as the hypoxia progresses.

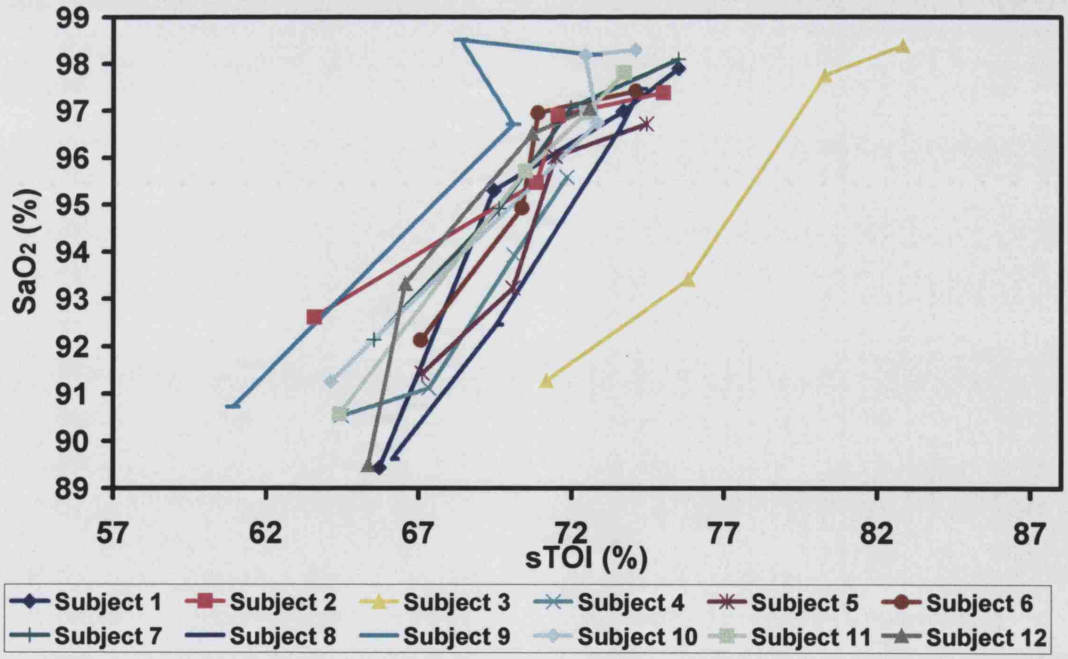

Figure 6.11: Individual absolute values of [TOI] versus [SaO_2] for each phase.

Table 6.4 shows the group mean values (with SD) for each of the four phases. There was a significant decrease from baseline values. The mitochondrial oxygenation (mO_2) demonstrated a mean drop of 50% from the baseline value at the end of hypoxia.

Table 6.4: Mean values (with SD) for CBF, sTOI, SvO2 and mitochondrial oxygenation (mO_2) during the four phases.

	CBF ($ml.100g^{-1}.min^{-1}$) Mean(SD)	sTOI (%) Mean(SD)	SvO_2 (%) Mean(SD)	mO_2 (μmoles/ml) Mean(SD)
Baseline	61 (9)	75 (3)	65 (4)	0.022 (0.003)
Start of Hypoxia	54 (8)	72 (3)	62 (4)	0.019 (0.003)
Middle of Hypoxia	57 (8)	70 (2)	60 (3)	0.015 (0.002)
End of Hypoxia	52 (8)	65 (2)	55 (3)	0.011 (0.001)

Figure 6.12 shows the individual absolute values for CBF, sTOI, SvO_2 and mO_2 for each of the four phases.

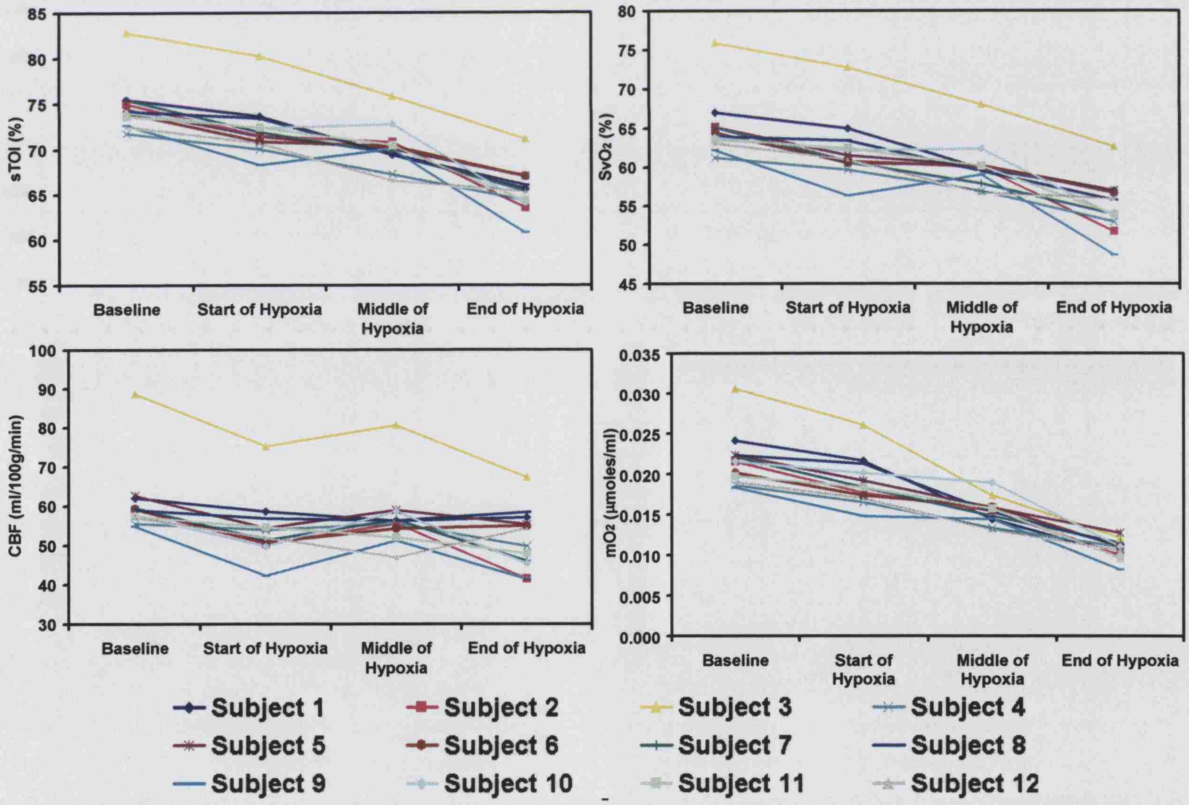

Figure 6.12: The individual absolute values for CBF, sTOI, SvO2 and mO_2 for each of the four phases.

Correlation analysis between paired values of absolute SaO_2 and sTOI and changes of $\Delta[SaO_2]$ and Δ[sTOI] for each phase did not produce any significant results. The trends of the data for each phase are shown in Figure 6.13. The scatter plot of Figure 6.13(a) shows a linear trend between the absolute SaO_2 and sTOI values (this was not seen in the experimental data Figure 6.8(a)). Figure 6.13(b) show a trend relationship between the changes in Δ[TOI] and the absolute values of SaO_2.

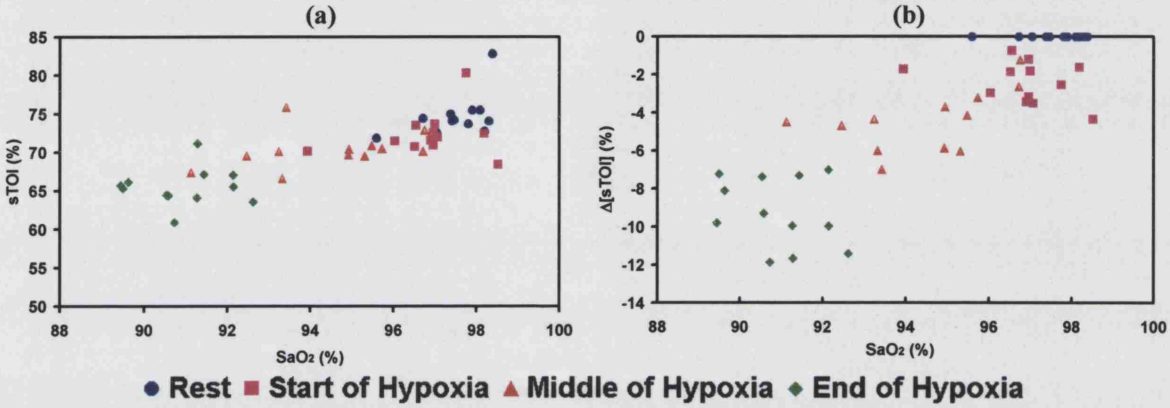

Figure 6.13: Individual data for each phase **(a)** absolute sTOI measurements versus the SaO_2 measurements **(b)** arithmetical differences from baseline for Δ[sTOI] versus absolute SaO_2 values.

Multi-regression analysis of the arithmetical differences between paired measurements (end of hypoxia minus baseline) of $\Delta[SaO_2]$, $\Delta[EtCO_2]$, Δ[MBP] and Δ[sTOI] revealed a linear relationship with $r^2=0.73$ and $p<0.025$ (Fisher test, F-observed value of 7.25 which is greater than the F-critical value of 5.42 when $p<0.025$) and a result equation of $\Delta[sTOI] = -0.04*\Delta[SaO_2] + 0.57*\Delta[EtCO_2] + 0.3*\Delta[MBP] -5.72$ (TOI: %; SaO_2: %; $EtCO_2$: mmHg; MBP: mmHg).

6.7 Comparison between experimental and simulated data

The scatter plots in Figure 6.14 summarise the relationship between sTOI and TOI; and between Δ[sTOI] and Δ[TOI]. It is obvious that there is a large discrepancy between the simulated and the experimental TOI values.

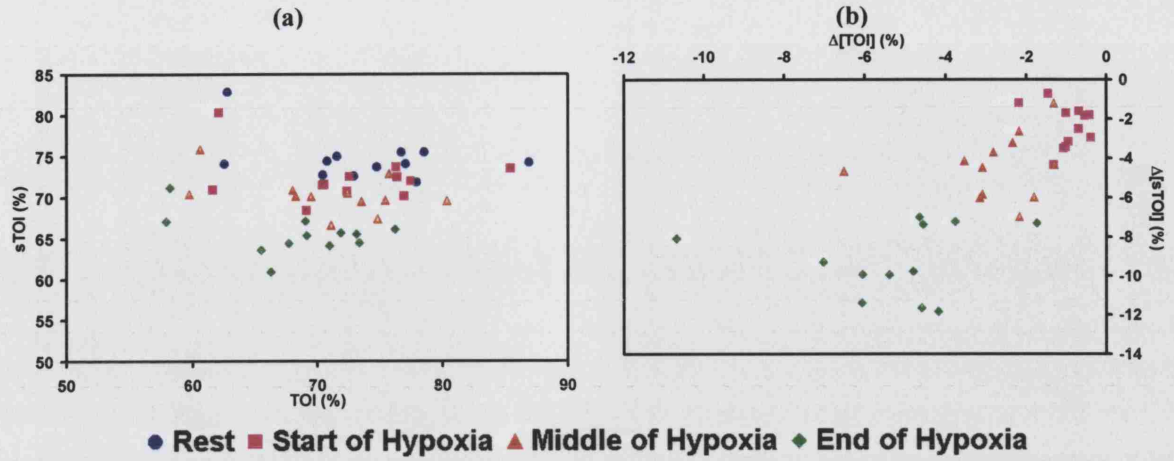

Figure 6.14: Association comparison between sTOI/TOI **(a)** absolute raw data of all subjects **(b)** the changes of all subjects.

In order to look for agreement and to investigate any possible relationship between the simulated and the measured cerebral TOI a plot has been done of the difference between the signals against their mean. Under these circumstances we can summarise the lack of agreement by calculating the bias estimated by the mean difference and the standard deviation of the differences. Provided differences within mean difference ±2SD would not be clinically important we could assume that the two different signals, the simulated and experimental TOI can be used interchangeably. In Figure 6.15 we investigate the agreement between the measured and simulated TOI regarding the absolute raw values and the changes from baseline.

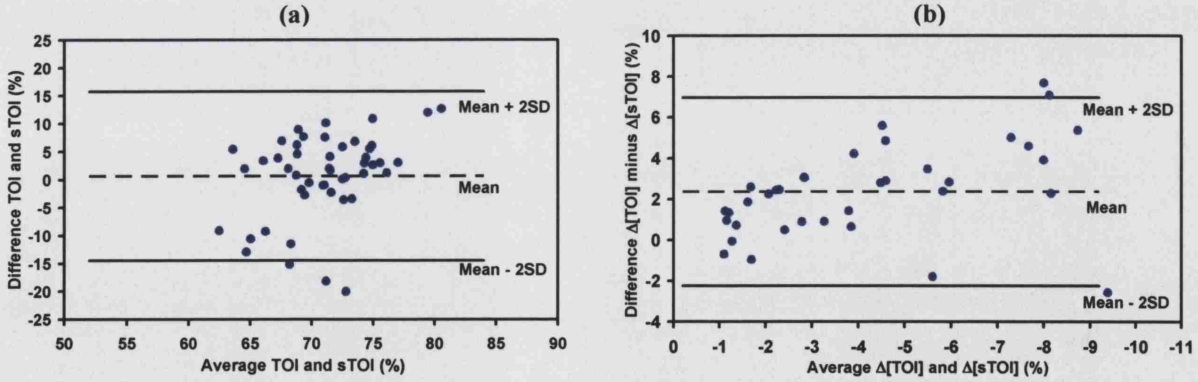

Figure 6.15: Agreement comparison between sTOI/TOI (a) absolute raw data of all subjects (b) the changes of all subjects.

From the Figure 6.15 it can be seen that there is no agreement between the absolute raw values of simulated and experimental TOI, the mean difference ±2SD in this case was

0.63±15.1% which is too high for physiological variables. When looking at the changes there was a considerable offset in the mean differences of 2.36±4.6% (ideally this should be closest to zero). These results suggest that the model was overestimating the true experimental values.

6.8 Discussion

We investigated the cerebral TOI response as measured by NIRS to a drop in arterial oxygen saturation down to 90%. The mean drop in $\Delta[SaO_2]$ at the end of hypoxia was 6.6%, as a result of which cerebral Δ[TOI] also decreased with a mean drop of 5.3%. During the hypoxic swing $\Delta[EtCO_2]$ and Δ[MBP] also dropped with a mean change between the end of hypoxia and baseline of 2.3mmHg and 8.1mmHg respectively. Other cerebral NIRS signals also changed, $\Delta[Hb_{diff}]$ drop by 4.43μmoles/l and Δ[HbT] rose by 0.48μmoles/l.

The cerebrovascular response to PaO_2 has been studied in terms of the response of Δ[HbT], $\Delta[HbO_2]$ and Δ[HHb] during hypoxic hypoxaemia in eight subjects by Hampson and colleagues [4]. Hypoxic swings of SaO_2 dropping down to 70% were produced during normocapnia and hypocapnia. They found that normocapnic hypoxia was characterized by a progressive reduction in PaO_2 (from 12 to 5kPa) and a stable arterial pH. Hypocapnic hypoxia resulted in a decreasing PaO_2 (to 4kPa) and $PaCO_2$ (to 3kPa), and an increase in the arterial pH of 0.1. In line with the expected hypoxic cerebrovascular vasodilation, Δ[HbT] increased; but in both hypoxic conditions $\Delta[HbO_2]$ decreased and the Δ[HbT] response to hypoxia was attenuated by hypocapnia (the increase in Δ[HbT] was only half of that obtained in normocapnic subjects). Some other interesting investigations of hypoxia with NIRS looked at severe drops in arterial saturation, below the threshold of 90%, as seen in patients suffering from sleep apnoea [13,14].

McCormick and colleagues [6] studied seven healthy volunteers breathing hypoxic air until the SaO_2 decreased below 55%. The $EtCO_2$ was maintained unchanged, and during

hypoxia the cerebral tissue saturation decreased from 64 to 38%. This finding has been reproduced by other groups [8,15].

In the present study the relationship between the average absolute values of SaO_2 and TOI for all the volunteers did not show any significant associations. In addition correlation analysis between paired values of changes in Δ[SaO2] and Δ[TOI] for each phase for all the volunteers did not also produce any significant results. Instead associations were found between the average absolute values of TOI and $EtCO_2$. However, individual plots of TOI versus SaO_2 show a direct relationship, with some subjects demonstrating a highly linear relationship (see Figure 6.16).

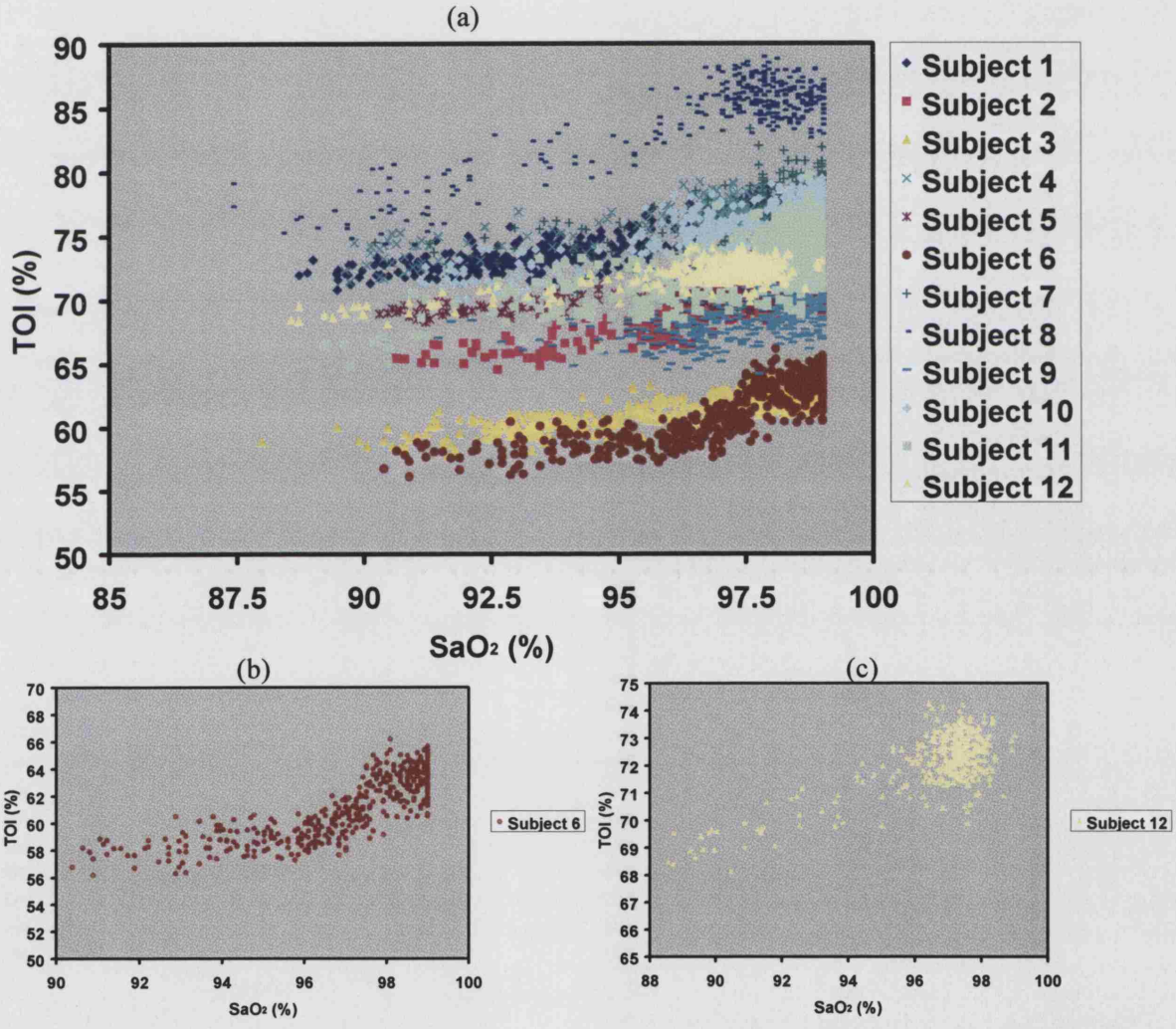

Figure 6.16: (a) Overall plots of TOI versus SaO_2 from baseline to the end of the hypoxia. **(b)** Subject 6 TOI versus SaO_2, demonstrate a threshold in SaO_2 (around 97%) where TOI starts to drop. **(c)** Subject 12 TOI versus SaO_2 demonstrate a highly linear relationship.

Near-infrared spectroscopy measures the oxygenation state in the underlying tissue and reflects a mixture of intravascular oxygenated/deoxygenated arterial and venous haemoglobin. Because the venous proportion predominantly determines the NIRS measurement of cerebral oxygenation, TOI represents a balance between oxygen delivery and oxygen consumption rather than a reflection of tissue oxygenation itself. Studies investigating the relationship between jugular venous oxygenation (SvO_2) and regional cerebral tissue saturation measured by NIRS provided controversial results [7,16-20]. Daubeney and colleagues [16] looking at children with cyanotic and non-cyanotic congenital heart defects during heart catheterisation found a good correlation between SvO_2 and cerebral tissue saturation. Weiss and colleagues [20] in a study of 155 neonates and infants aged from 0 to 365 days found a significant and substantial correlation between cerebral TOI and SvO_2 ($r=0.49$, $p<0.0001$). Less agreement between SvO_2 and cerebral tissue saturation was found in patients with head injury [7,17,18] which could possibly be explained by their pathology. Shaaban and colleagues [21] carried out a study during cardiac surgery with cardiopulmonary bypass and found no correlation between cerebral TOI and SvO_2. Quaresima et al [22] compared direct measurements of forehead TOI with the calculated SvO_2 (obtained by the methodology described by [23]) during venous occlusion in 16 adult volunteers and found a significant relationship. Other studies tried to investigate the association of TOI and SaO_2 and also TOI and venous SvO_2 and tissue PaO_2 [24,25]. Watzman and colleagues used a frequency domain NIRS instrument to obtain a cerebral tissue saturation measurement and compared this with SvO_2 and SaO_2 measurements obtained by jugular venous oximeter and arterial blood sample oximetry respectively in 20 anesthetised children during cardiac catheterisation under conditions of 100% inspired oxygen and hypocapnia. He found a good correlation between cerebral tissue saturation and SaO_2 ($r=0.47$), but a substantial correlation with SvO_2 ($r=0.71$). Nagdyman and colleagues [25] in a similar study to Watzman et al [24] demonstrated a significant correlation between TOI and SvO_2 ($r=0.52$) but only a slight correlation between TOI and SaO_2 ($r=0.26$) and PaO_2 ($r=0.26$).

The results discussed above tend to imply a strong relationship of cerebral tissue saturation and SvO_2 but not with SaO_2, these results agree to some extent with our data as we did not find any strong association between TOI and SaO_2. This is not particularly unexpected as in our study $EtCO_2$ changed together with SaO_2, therefore making the

TOI response somewhat unpredictable. If one examines the analytical derivation of TOI (Equation 6-1) one can assume that dropping the oxygenation does not necessary mean a linear change in cerebral TOI.

$$TOI = SaO_2 - \left(\frac{Vv}{Va + Vv}\right) \cdot \left(\frac{CMRO_2}{k \cdot CBF \cdot [Hb \cdot 10^{-3}]}\right) \qquad \textbf{6-1}$$

Results of the cerebral computational model using the experimental data as an input did not show any agreement between the changes in simulated and the measured TOI, regarding both the absolute values and the changes. The results suggest that the model overestimates the change in the cerebral tissue oxygenation by following rather closely the changes in SaO_2. Multi-regression analysis of the arithmetical differences between paired measurements (end of hypoxia minus baseline) of $\Delta[SaO_2]$, $\Delta[EtCO_2]$, Δ[MBP] and Δ[sTOI] revealed a linear relationship (r^2=0.73 with $p<0.025$) and resulted in Equation 6-2.

$$\Delta[sTOI] = -0.04*\Delta[SaO_2] + 0.57*\Delta[EtCO_2] + 0.3*\Delta[MBP] - 5.72 \qquad \textbf{6-2}$$

This is expected as the model recognises $EtCO_2$, MBP and SaO_2 as the main systemic effectors on the changes in TOI. The model overestimates the changes in cerebral tissue oxygenation as compared with the experimental data especially as SaO_2 dropped towards 90%. This can be seen in Figure 6.14(b). As also seen in Chapter 5, the absolute raw values of sTOI differed from the raw experimental TOI. Possible reasons for this are the inter-subject variability regarding resting levels of CBF and arterial:venous volume rations. All simulations with the model used the default healthy adult parameters and no attempt was made at this stage to provide customisation to each volunteer other than to use their input data.

References

1. J.W. Phillis, "Cerebral vascular responses to hypoxia, hyper- and hypo- capnia and hypotension.," *The regulation of cerebral blood flow,* Phillis J.W., ed., (CRC Press, Florida, 1993), 249-258.

2. I. Ellingsen, A. Hauge, G. Nicolaysen, M. Thoresen, and L. Walloe, "Changes in human cerebral blood flow due to step changes in PaO_2 and $PaCO_2$," *Acta Physiol. Scand.* **129**, 157-163 (1987).

3. A.K. Gupta, D.K. Menon, M. Czosnyka, P. Smielewski, and J.G. Jones, "Thresholds for hypoxic cerebral vasodilation in volunteers," *Anesth. Analg.* **85**, 817-820 (1997).

4. N.B. Hampson, E.M. Camporesi, B.W. Stolp, R.E. Moon, J.E. Shook, J.A. Griebel, and C.A. Piantadosi, "Cerebral oxygen availability by NIR spectroscopy during transient hypoxia in humans," *J. Appl. Physiol.* **69**, 907-913 (1990).

5. P.W. McCormick, M. Stewart, M.G. Goetting, M. Dujovny, G. Lewis, and J.I. Ausman, "Noninvasive cerebral optical spectroscopy for monitoring cerebral oxygen delivery and hemodynamics," *Crit. Care Med.* **19**, 89-97 (1991).

6. P.W. McCormick, M. Stewart, M.G. Goetting, and G. Balakrishnan, "Regional cerebrovascular oxygen saturation measured by optical spectroscopy in humans," *Stroke* **22**, 596-602 (1991).

7. P.J. Kirkpatrick, P. Smielewski, M. Czosnyka, D.K. Menon, and J.D. Pickard, "Near-infrared spectroscopy use in patients with head injury," *J. Neurosurg.* **83**, 963-970 (1995).

8. L.C. Henson, C. Calalang, J.A. Temp, and D.S. Ward, "Accuracy of a cerebral oximeter in healthy volunteers under conditions of isocapnic hypoxia," *Anesthesiology* **88**, 58-65 (1998).

9. A. Duncan, J.H. Meek, M. Clemence, C.E. Elwell, L. Tyszczuk, M. Cope, and D.T. Delpy, "Optical pathlength measurements on adult head, calf and forearm and the head of the newborn infant using phase resolved optical spectroscopy," *Phys. Med. Biol.* **40**, 295-304 (1995).

10. T. Colton, *Statistics in medicine*, Little Brown & Co, ed., 1974).

11. J.M. Bland and D.G. Altman, "Statistical methods for assessing agreement between two methods of clinical measurement," *Lancet* **1**, 307-310 (1986).

12. B. Dawson-Saunders and R.G. Trapp, "Association & Prediction," *Basic & Clinical Biostatistics,* B. Dawson-Saunders and R. G. Trapp, eds., (Appleton & Lange, Norwalk, Connecticut, 1994), 162-187.

13. A. Valipour, A.D. McGown, H. Makker, C.O'Sullivan, and S.G. Spiro, "Some factors affecting cerebral tissue saturation during obstructive sleep apnoea," *Eur. Respir. J.* **20**, 444-450 (2002).

14. I. Tachtsidis, C.E. Cooper, A.D. McGown, H. Makker, D.T. Delpy, and C.E Elwell, "Changes in cerebral total haemoglobin volume and cytochrome oxidase redox state during deep apnoeas in patients with obstructive sleep apnoea," *Biomedical Topical Meetings on CD-ROM (The Optical Society of America, Washington, DC)* WF6 (2004).

15. V. Pollard, D.S. Prough, A.E. DeMelo, D.J. Deyo, T. Uchida, and H.F. Stoddart, "Validation in volunteers of a near-infrared spectroscope for monitoring brain oxygenation in vivo," *Anesth. Analg.* **82**, 269-277 (1996).

16. P.E.F. Daubeney, S.N. Pilkington, E. Janke, G.A. Charlton, D.C. Smith, and S.A. Webber, "Cerebral Oxygenation Measured by Near-Infrared Spectroscopy: Comparison With Jugular Bulb Oximetry," *The Annals of Thoracic Surgery* **61**, 930-934 (1996).

17. S.B. Lewis, J.A. Myburgh, E.L. Thornton, and P.L. Reilly, "Cerebral oxygenation monitoring by near-infrared spectroscopy is not clinically useful in patients with severe closed-head injury: a comparison with jugular venous bulb oximetry," *Crit. Care Med.* **24**, 1334-1338 (1996).

18. A. Ter Minassian, N. Poirier, M. Pierrot, P. Menei, J.C. Granry, M. Ursino, and L. Beydon, "Correlation between cerebral oxygen saturation measured by near-infrared spectroscopy and jugular oxygen saturation in patients with severe closed head injury," *Anesthesiology* **91**, 985-990 (1999).

19. M.B. Kim, D. S. Ward, C. R. Cartwright, J. Kolano, S. Chlebowski, and L. C. Henson, "Estimation of jugular venous O_2 saturation from cerebral oximetry or arterial O_2 saturation during isocapnic hypoxia," *J. Clin. Monit. Comput.* **16**, 191-199 (2000).

20. M. Weiss, A. Dullenkopf, A. Kolarova, G. Schulz, B. Frey, and O. Baenziger, "Near-infrared spectroscopic cerebral oxygenation reading in neonates and infants is associated with central venous oxygen saturation," *Paediatr. Anaesth.* **15**, 102-109 (2005).

21. M. Shaaban Ali, M. Harmer, R. S. Vaughan, J. A. Dunne, and I. P. Latto, "Spatially resolved spectroscopy (NIRO-300) does not agree with jugular bulb oxygen saturation in patients undergoing warm bypass surgery," *Can. J. Anesth.* **48**, 497-501 (2001).

22. V. Quaresima, S. Sacco, R. Totaro, and M. Ferrari, "Noninvasive measurement of cerebral hemoglobin oxygen saturation using two near infrared spectroscopy approaches," *Journal of Biomedical Optics* **5**, 201-205 (2000).

23. C.E. Elwell, S.J. Matcher, L. Tyszczuk, J. H. Meek, and D. T. Delpy, "Measurement of cerebral venous saturation in adults using near infrared spectroscopy," *Adv. Exp. Med. Biol.* **411**, 453-460 (1997).

24. H.M. Watzman, C.D. Kurth, L.M. Montenegro, J. Rome, J.M. Steven, and S.C. Nicolson, "Arterial and venous contributions to near-infrared cerebral oximetry," *Anesthesiology* **93**, 947-953 (2000).

25. N. Nagdyman, T. Fleck, S. Barth, H. Abdul-Khaliq, B. Stiller, P. Ewert, M. Huebler, H. Kuppe, and P.E. Lange, "Relation of cerebral tissue oxygenation index to central venous oxygen saturation in children," *Intensive Care Med.* **30**, 468-471 (2004).

Chapter 7

Changes in Cerebral Oxygenation and Haemodynamics following a Postural Change in Patients with Autonomic Failure and Postural Hypotension and Control Subjects

In the previous two chapters experiments to examine the effects of changes in CO_2 and O_2 on the cerebral haemodynamics and oxygenation were discussed. In this chapter, blood pressure autoregulation is examined by investigating a group of primary autonomic failure patients and healthy age match controls during a passive tilt protocol.

In collaboration with both the Autonomic Clinic and the department of Neuroanaesthesia and Intensive Care of the National Hospital of Neurology and Neurosurgery in London, a group of primary autonomic failure patients (AF) with orthostatic hypotension have been investigated during a tilt table provocation test. Changes in cerebral oxygenation and blood volume that occur following a postural change in patients together with healthy controls were studied.

In this chapter details of the protocols are given and the resulting data is described and its significance is explained. Also the results of simulations using the data from the patients are presented.

7.1 Introduction

The responses of heart rate and blood pressure to changing from the supine to standing position, or to tilting on a tilt table, is the simplest non-invasive test of autonomic function [1,2]. Good cerebral autoregulation is critically important in rising to the upright position since this poses a significant challenge to cerebral perfusion.

The passive upright tilt challenge is widely employed as a diagnostic test in patients with syncope [3,4]. Passive head-up tilt is an orthostatic challenge used as a means to introduce mild central hypovoloaemic shock, leading to both systemic and cerebral changes such as blood pressure and cerebral blood volume respectively [5].

In healthy volunteers, standing causes an increase in peripheral resistance produced by the increase in muscle tone and sympathetic activity, which in turn produces an increase in the arterial blood pressure [6,7].

In human physiology, a posture change from supine to standing results in venous pooling in the lower limbs and pelvic area (equivalent to the loss of 500ml of blood from the systemic circulation) and an increased filtration from capillaries into interstitial space [8]. This reduces venous return to the heart, which lowers the cardiac stroke volume, and further reduces the central arterial pressure. In turn, these effects cause a transient dip in effective circulating blood volume and potentially a small reduction in cerebral and peripheral oxygen delivery. This effect is not prolonged in a healthy individual since the decrease in arterial pressure triggers an immediate response from the baroreceptor-mediated sympathetic mechanisms. Healthy individuals adjust their cardiovascular system to this gravitational displacement of blood by increasing systemic vascular resistance through autonomic reflex activity [9]. Figure 7.1 shows a brief description of the physiological interventions happening during imbalances in blood pressure.

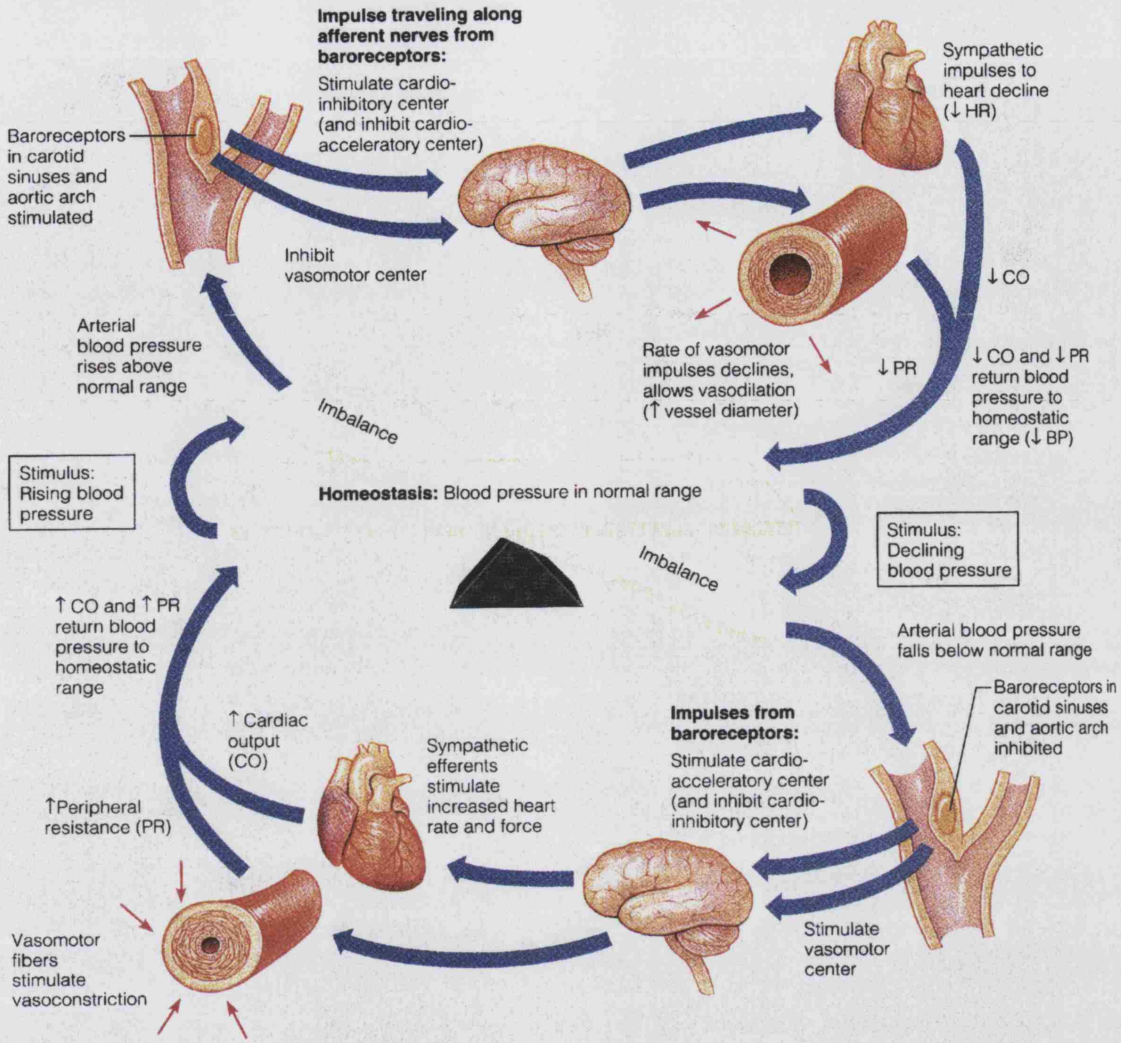

Figure 7.1: Baroreceptor reflexes that help to maintain blood pressure homeostasis (taken from [10]).

In the aged individual, baroreceptor sensitivity is reduced. Progressive age related impairment in function has been well demonstrated by reduction in the cardio-inhibitory response to hypertensive stimuli and by blunted cardio-acceleratory response to hypotensive stressors. Age associated elevations in blood pressure have been considered as the cause and/or consequence of baroreflex impairment [11,12]. Despite the lack of heart rate acceleration on standing, only a small percent of normotensive elderly persons have orthostatic hypotension. Most are probably protected from orthostatic hypotension by alpha-mediated vasoconstriction which is largely preserved with aging [12].

In patients with primary chronic autonomic failure, the cardiovascular responses to head-up postural change are severely compromised, mainly because of sympathetic denervation. In pure autonomic failure (PAF) without additional neurological features

this may be the result of peripheral damage, while in multiple system atrophy (MSA) with additional neurological features the lesions are predominantly central [13]. Orthostatic hypotension defined as a fall of more than 20mmHg in systolic blood pressure on standing [2] is the most incapitating symptom of autonomic failure patients and typically presents as light headedness and presyncope that occurs in response to postural changes [14,15]. In patients with autonomic failure, the blood pressure consistently falls; the degree of blood pressure fall depends on the severity of the autonomic dysfunction. The primary dysfunction of autonomic failure prevents reflex activation of sympathetic outflow to compensate for changes in blood pressure. Thus when patients with autonomic failure assume the upright posture blood pressure decreases because they are unable to counteract the effects of blood pooling in the lower extremities induced by gravity.

The aim of this study was to investigate changes in cerebral oxygenation and haemodynamics by application of near-infrared spectroscopy during a passive tilt protocol in patients with AF who exhibit severe orthostatic hypotension.

NIRS provides a real time assessment of fluctuations in cerebral changes in oxy-haemoglobin concentration $\Delta[HbO_2]$ and deoxy-haemoglobin concentration $\Delta[HHb]$ and allows for measurements of absolute tissue oxygenation index (TOI) using the technique of spatially resolved spectroscopy (SRS). The principle of the technique has been described in detail in Chapter 4.

7.2 Subjects and experimental methods

18 patients with primary autonomic failure (13 males and 5 females) of mean age 62±10 years and range 42-79 years were studied. The total number of patients included 10 with pure autonomic failure (PAF; mean age 66±8, 7 males and 3 females) and 8 with multiple system atrophy (MSA; mean age 57±10, 6 males and 2 females).

All patients had detailed investigations, which included physiological and biochemical autonomic testing in addition to neurological and other relevant investigations. The

patients had not been withdrawn from their pharmacological treatment, which mostly included antihypotensive agents such as fludrocortisone and ephedrine.

In conjunction with the patients 10 healthy age match controls (5 males and 5 females) of mean age 62±7 years were studied, which included relatives of patients previously investigated and research staff; none was on any form of drug therapy. Furthermore none of them were smokers or had any health related problem.

The studies were performed with the understanding and consent of each subject and were approved by the local ethics committee of National hospital of Neurology and Neurosurgery.

7.2.1 Measurements

A continuous wave near-infrared spectrometer, with a sampling rate of 6Hz (NIRO 300, Hamamatsu Photonics KK) was used to measure absolute cerebral tissue oxygenation index (TOI) over the frontal cortex using the spatially resolved reflectance spectroscopy technique, together with changes in $\Delta[HbO_2]$, $\Delta[HHb]$ and total haemoglobin ($\Delta[HbT]= \Delta[HbO_2]+\Delta[HHb]$) by utilizing the modified Beer-Lambert law.

The probe was placed on the forehead (taking care to avoid the midline sinuses) and was shielded from ambient light by using an elastic bandage and a black cloth; the studies took place in a darkened room. An optode spacing of 5cm was used and optical filters were also used where necessary to optimise signal to noise ratio. The differential pathlength factor (DPF) was calculated for each subject using the age dependence Equation 7-1 [16] :

$$DPF_{780} = 5.13 + 0.07A_y^{0.81} \qquad \textbf{7-1}$$

where DPF_{780} is the DPF at 780nm and A_y is the age of the subject in years.

A Portapres® system (TNO Institute of Applied Physics, Biomedical Instrumentation) was used to continuously and non-invasively measure blood pressure (MBP) from the finger (for description of Portapres® see Chapter 5, Section 5.2.1).

Systolic blood pressure (SBP) and diastolic blood pressure (DBP) from the brachial artery was recorded at 2 minutes interval with an automatic sphygmomanometer; together with the peripheral SaO_2. MBP was later calculated by using the Equation 7-2 below:

$$MBP = \frac{1}{3} \cdot SBP + \frac{2}{3} \cdot DBP \qquad 7\text{-}2$$

Finally patient symptomatology was also recorded.

7.2.2 Protocol

Each subject was strapped onto an electrical moving tilt table and underwent three postural changes. After an initial 10 minutes resting period in the supine position, the subject was tilted upright to an angle of 60° for another 10 minutes and then returned to the supine position for an additional 10 minutes. At the end of the 10 minutes following the return to the supine position, two valsalva maneuvers were also performed.

Head up tilt was interrupted if severe symptoms of orthostatic intolerance occurred, whereupon the patient was immediately returned to the supine position. The tilting movement was performed via an electrical motor and took approximately 10 seconds for both the up and down movements. Figures 7.2 and 7.3 show typical data from a patient and a healthy volunteer respectively.

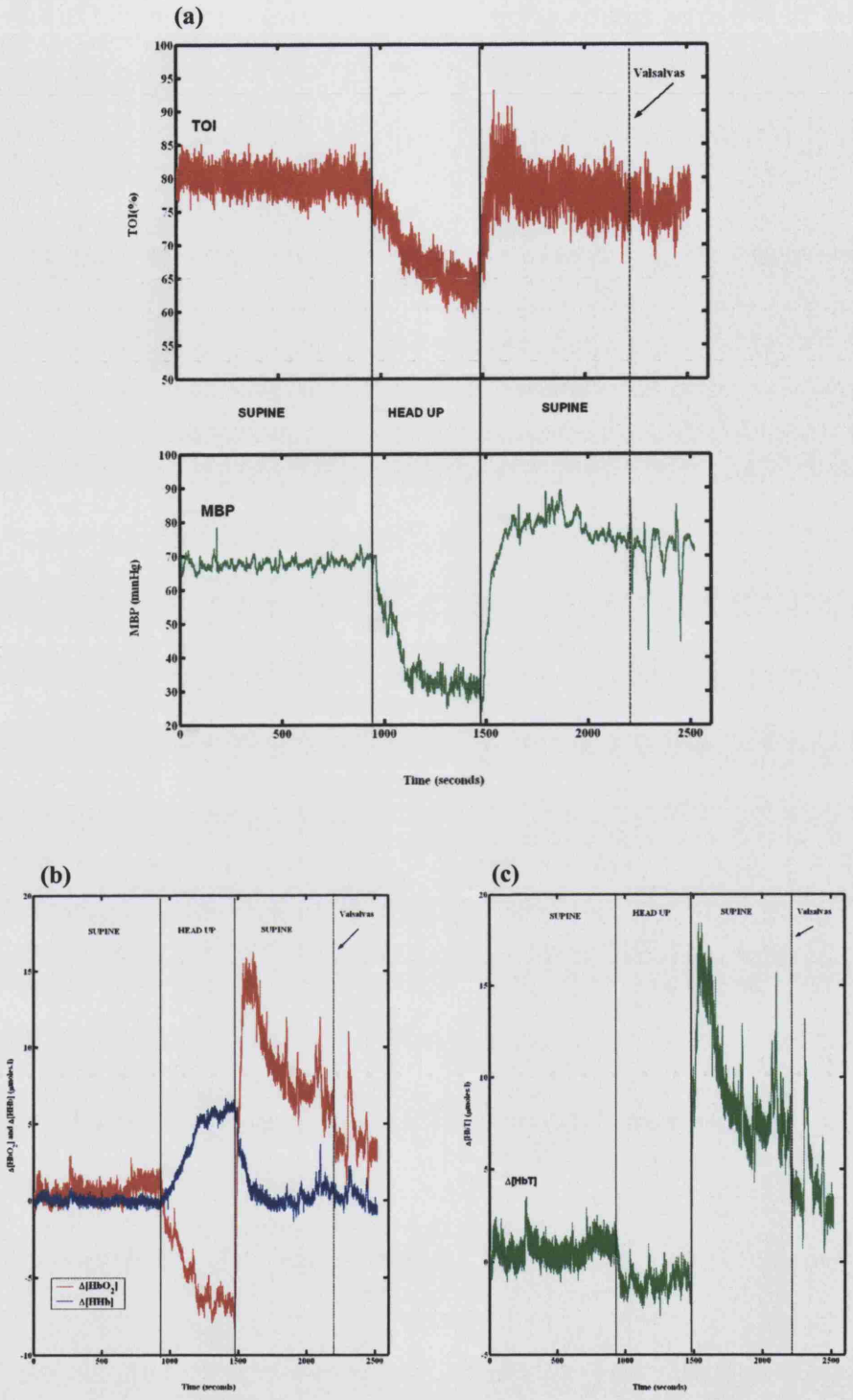

Figure 7.2: Recorded signals for one PAF patient during the whole study **(a)** cerebral TOI and MBP; **(b)** Changes in $\Delta[HbO_2]$ and $\Delta[HHb]$; **(c)** changes in $\Delta[HbT]$.

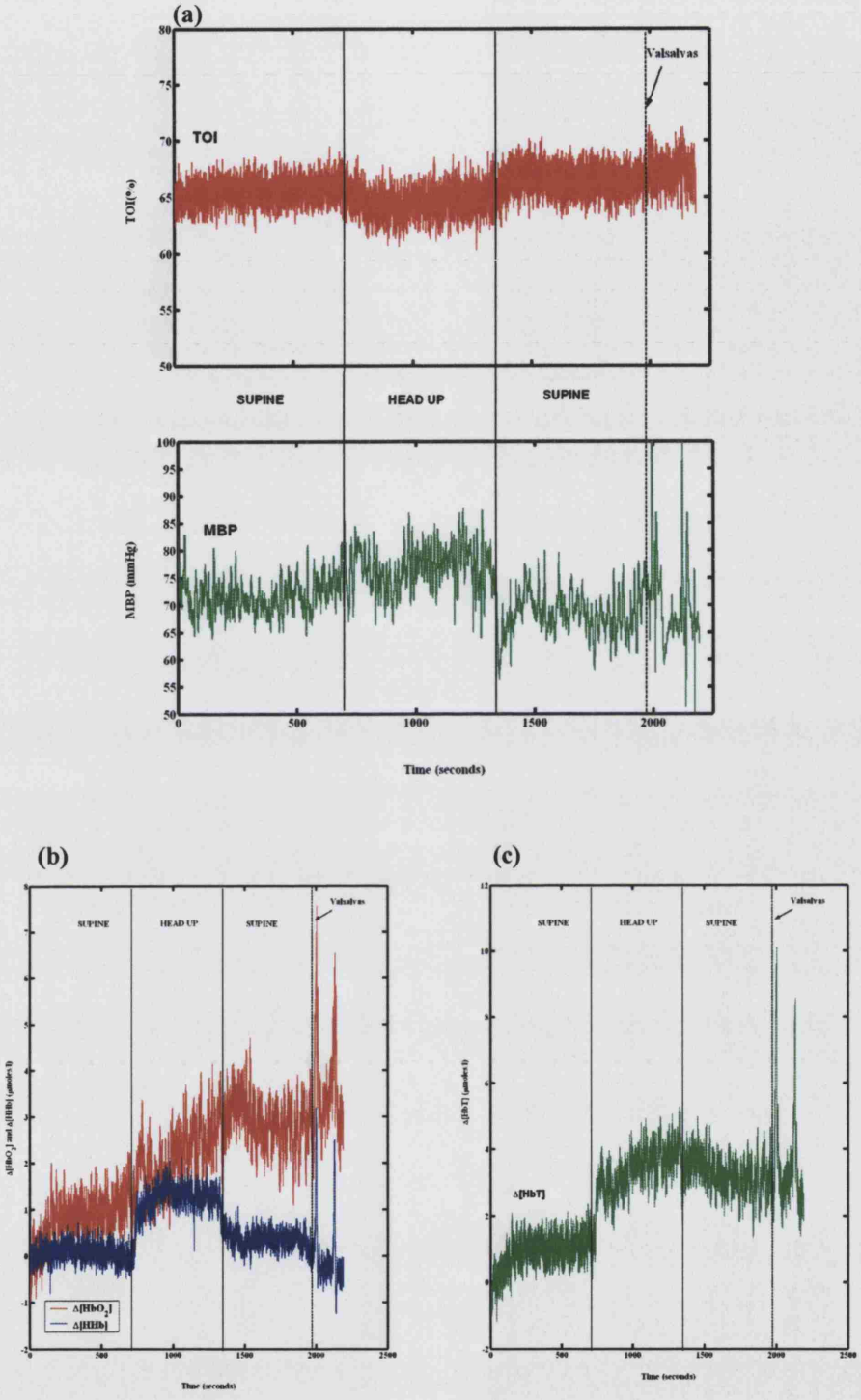

Figure 7.3: Recorded signals for one healthy volunteer during the whole study **(a)** cerebral TOI and MBP; **(b)** Changes in $\Delta[HbO_2]$ and $\Delta[HHb]$; **(c)** changes in $\Delta[HbT]$.

7.2.3 Analysis

Blood pressure analysis was done on the data from both the sphygmomanometer and the Portapres®. The last 2 minutes measurement of systolic and diastolic blood pressure recorded by the sphygnomanometer, before the end of each posture, was used to calculate MBP.

MBP was also recorded from the analogue output of the Portapres® continuously at 100Hz, which was later down resampled to 6Hz. An average value of MBP was calculated using the data from the last 2 minutes before the end of each posture (720 data points).

Mean values for TOI , THI , $\Delta[HbO_2]$, Δ[HHb] and Δ[HbT] were calculated for each subject from the last 2 minutes before the end of each posture. Data was tested for normality using the Shapiro-Wilk's test and are expressed as means with standard deviations for PAF, MSA patients and Controls.

7.3 Results

Table 7.1 show the mean and SD results for systemic blood pressure as measured by the Portapres® and the sphygmomanometer for all the three groups.

Table 7.1: Blood pressure summary results.

	Postures MBP (mmHg)		
PAF Patients	Supine	Tilt Up	Supine
sphygmomanometer	112±14	70±23	118±14
Portapres	95±15	48±19	104±16
MSA Patients			
sphygmomanometer	116±22	65±19	116±22
Portapres	104±24	58±22	110±23
Controls			
Sphygnomanometer	94±9	101±14	93±9
Portapres	75±7	88±12	76±9

A paired t-test showed a significant difference in MBP between supine and tilt up ($p<0.01$), for both the PAF and MSA patients indicating a significant decrease in MBP. At tilt reversal, MBP returned to the basal values. For the healthy volunteers MBP increased during tilt up and a paired t-test showed a significant difference in MBP as measured by the sphygmomanometer ($p=0.04$) and as measured by the Portapres® ($p<0.01$). At tilt reversal the MBP again returned to the basal values. Figure 7.4 shows the individual results for the Portapres® data.

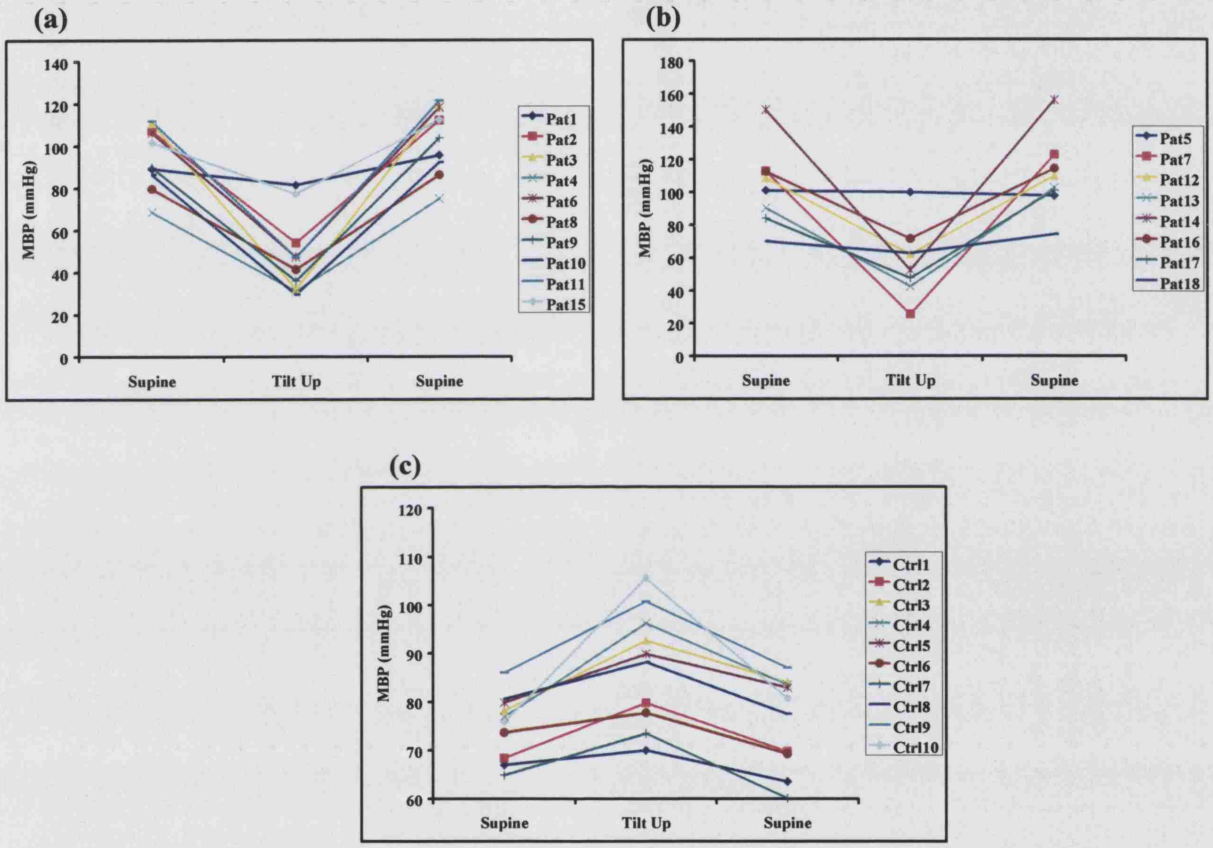

Figure 7.4: MBP recorded by Portapres with changes in postures for every **(a)** PAF patient; **(b)** MSA patient; **(c)** Control.

Table 7.2 show the mean and SD results of the haemoglobin concentration changes as measured by NIRS for all the three groups during changes in posture.

Table 7.2: Haemoglobin concentration changes summary results.

	Postures Changes in Haemoglobin Concentration (μmoles/l)		
PAF Patients	Supine	Tilt Up	Supine
$\Delta[HbO_2]$	0.25±1.53	-6.62±2.29	2.24±2.54
Δ[HHb]	-0.22±0.96	4.1±2.92	0.10±1.55
Δ[HbT]	0.03±1.92	-2.57±2.95	2.35±3.29
MSA Patients			
$\Delta[HbO_2]$	1.17±1.42	-6.51±5.35	3.68±2.78
Δ[HHb]	0.03±0.78	3.99±2.57	-0.09±0.71
Δ[HbT]	1.20±2.00	-2.51±3.26	3.59±2.88
Controls			
$\Delta[HbO_2]$	0.82±1.06	0.12±1.74	1.96±1.48
Δ[HHb]	0.02±0.57	1.08±1.19	0.10±0.63
Δ[HbT]	0.84±1.21	1.20±1.81	2.06±1.34

Figures 7.5, 7.6 and 7.7 shows the individual results for the haemoglobin changes for the PAF, MSA and Control groups respectively.

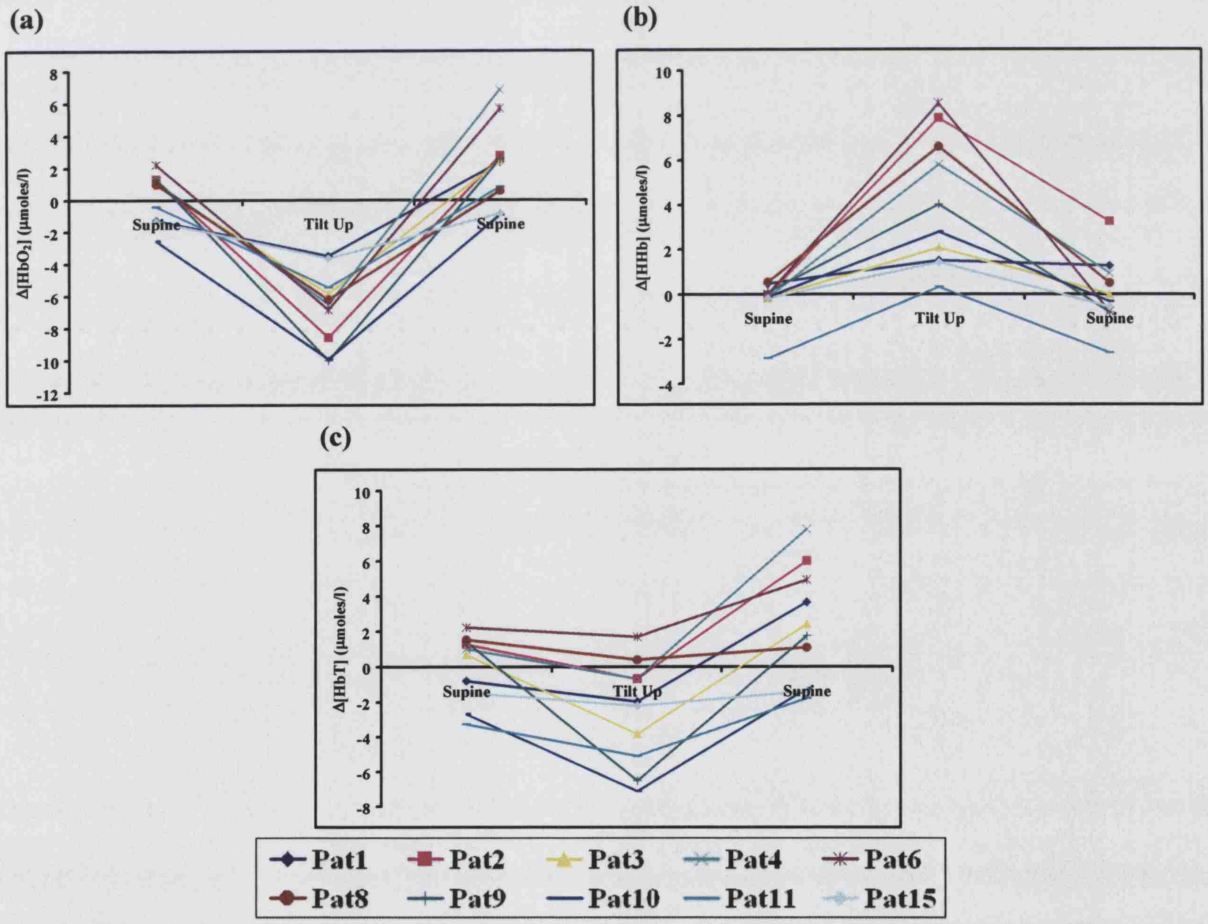

Figure 7.5: Haemoglobin changes during changes in posture for the PAF patients **(a)** $\Delta[HbO_2]$; **(b)** Δ[HHb]; **(c)** Δ[HbT].

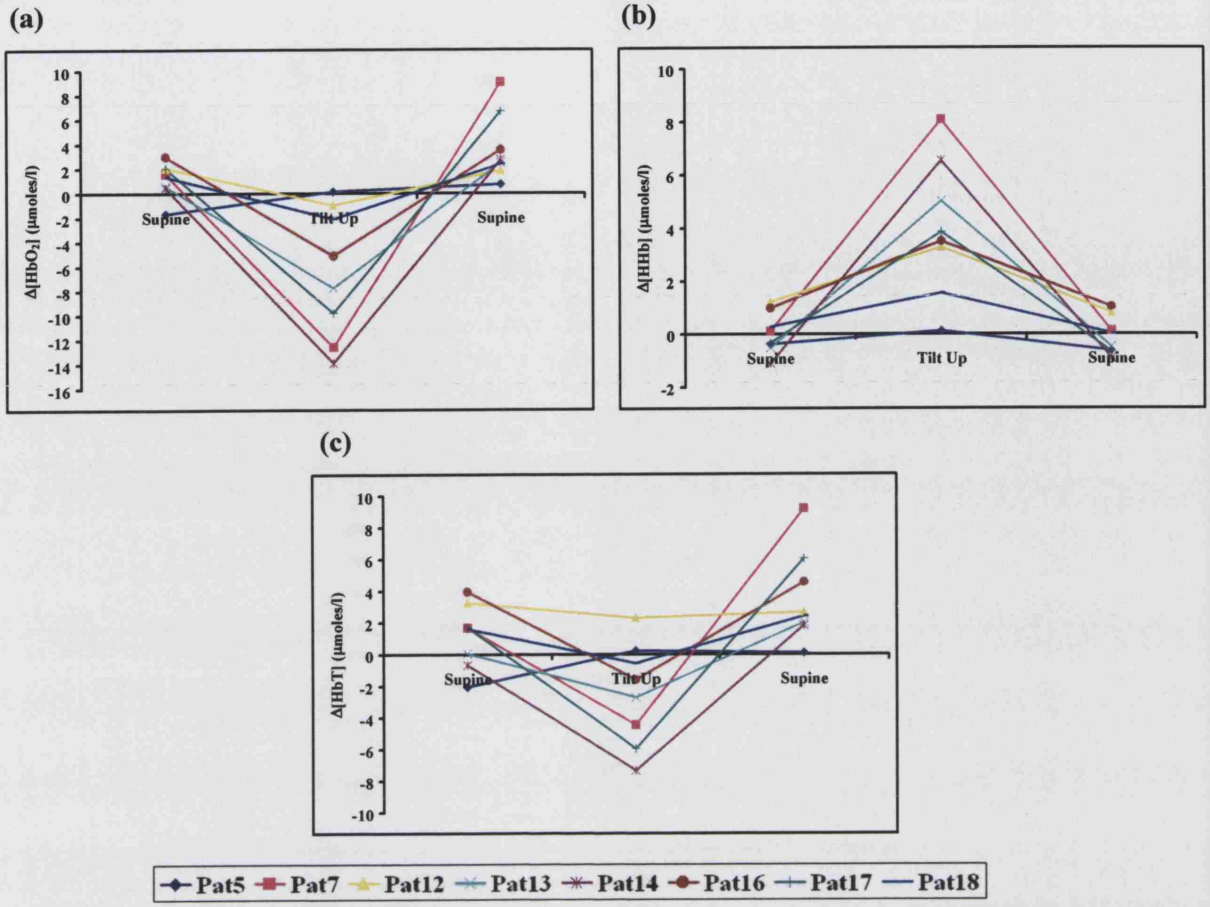

Figure 7.6: Haemoglobin changes during changes in posture for the MSA patients **(a)** $\Delta[HbO_2]$; **(b)** $\Delta[HHb]$; **(c)** $\Delta[HbT]$.

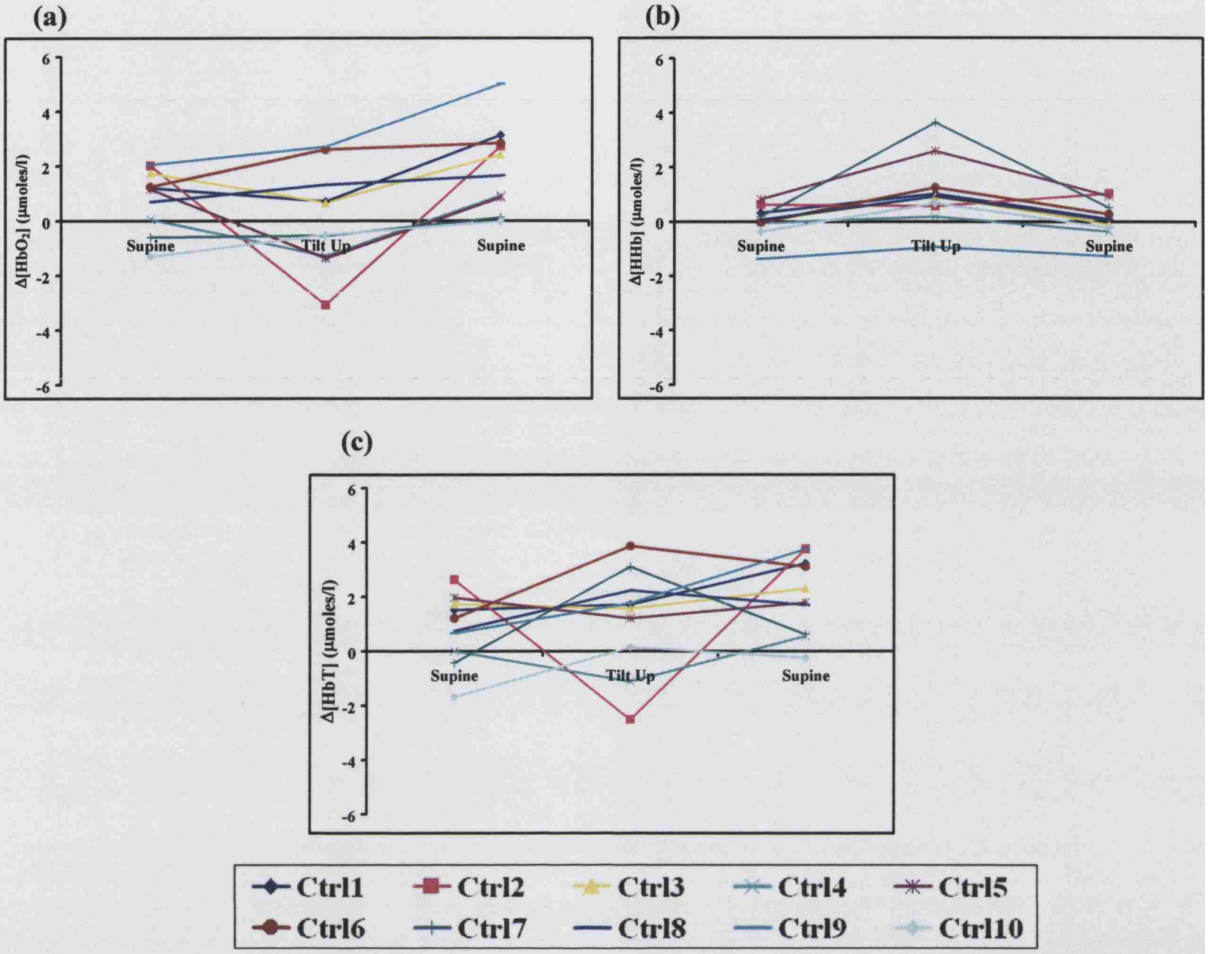

Figure 7.7: Haemoglobin changes during changes in posture for the healthy controls **(a)** $\Delta[HbO_2]$; **(b)** $\Delta[HHb]$; **(c)** $\Delta[HbT]$.

Paired t-test showed a significant difference in $\Delta[HbO_2]$, $\Delta[HHb]$, and $\Delta[HbT]$ between supine and tilt up for the PAF patients ($p<0.01$) and the MSA patients ($p=0.02$). This indicates a reduction in cerebral blood volume and oxygenation. At tilt reversal $\Delta[HbO_2]$, $\Delta[HHb]$, and $\Delta[HbT]$ returned to the basal values.

Healthy controls demonstrated no significant difference in $\Delta[HbO_2]$ and $\Delta[HbT]$ between supine and tilt up (paired t-test, $p>0.05$). A significant difference was found in $\Delta[HbO_2]$ between tilt up and back to the supine posture (paired t-test, $p<0.01$) and in $\Delta[HHb]$ from supine to head up tilt (paired t-test, $p<0.01$) indicating a significant increase.

The group means and SD of cerebral TOI for both the patient groups and the healthy controls between the different postures are shown in Table 7.3. Individual mean values are shown in Figure 7.8.

Table 7.3: Cerebral tissue oxygenation summary results.

	Mean TOI (%) ±SD with Changes in Postures		
	Supine	Tilt Up	Supine
PAF	72±7	63±8	70±6
MSA	73±6	65±8	72±7
Controls	69±4	67±4	70±5

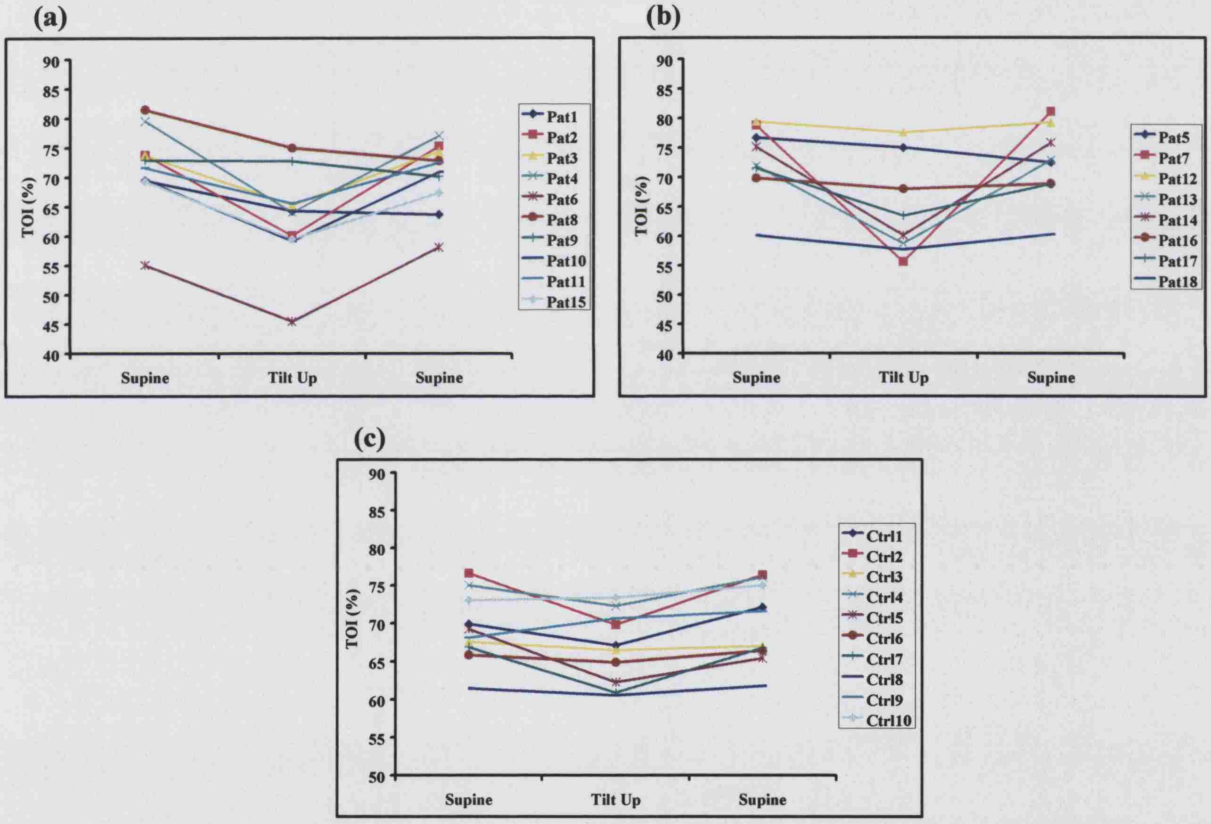

Figure 7.8: Mean values of TOI for each posture **(a)** PAF patients; **(b)** MSA patients; **(c)** Healthy controls.

Paired t-tests showed a significant difference in TOI for the PAF and the MSA patients between supine and tilt up ($p<0.01$, $p=0.02$ respectively), indicating a significant decrease in TOI when patients were tilted up to the upright posture. At tilt reversal TOI returned to the basal values. Both patients groups demonstrated a large decrease in TOI

when they were tilted up; these results agree with the severe orthostatic hypotension that those patients exhibited.

A significant difference in TOI between supine and tilt up (paired t-test, p=0.03) was also seen in the healthy controls, indicating a significant decrease in TOI when the volunteers were tilted up to the upright posture. At tilt reversal TOI returned to the basal values. The change in TOI for the healthy controls between supine and tilt up was not as large as in the patients groups

7.3.1 Symptomatology

Part of the protocol of the study was to ask the patients every two minutes for any symptoms, this was very important during the tilt as we were looking for indications of brain hypoperfusion. Previous studies [14,15] have shown that there is a distinguishable difference especially between the PAF and MSA patients regarding their symptoms. They concluded that PAF patients are more prone to syncope than those with MSA and also that the MSA patients had a mix of severity of symptoms starting from none up to syncope, something that was not reported for the PAF group.

In this study we tried to categorise the symptoms according to their severity regarding the cerebral circulation. Therefore patients that felt pain in the legs, cuffs, arm or at the back of the neck were categorised as patients with no symptoms. Even though there were patients in this category with very low blood pressures, it was felt that a pain in the neck at the suboccipital and paracervical region could only mean ischemia at this part of the body muscle without any affect to the brain. The next category were patients with mild symptoms, patients that felt light-headed were part of this category. Next were the severe category and patients that had presyncope signs and vision blurring were part of this category. Finally there were the fainters who were those patients who did not last the 10 minutes of passive head up tilt; most of these were returned to the supine position after less than 5 minutes of tilt.

Figure 7.9 summarises the results between the different categories and changes in Δ[TOI] between supine and tilt up. The difference between the categories it is very obvious, however most interestingly the fainters did not show very large changes in

Δ[TOI] between supine and tilt up. It is our belief that the syncope feeling had less to do with the change but rather the actual rate of change, meaning that the slope of downwards change in the fainters was faster than the other patients [17]. This fast disturbance in oxygenation and probably cerebral blood volume caused the fainting.

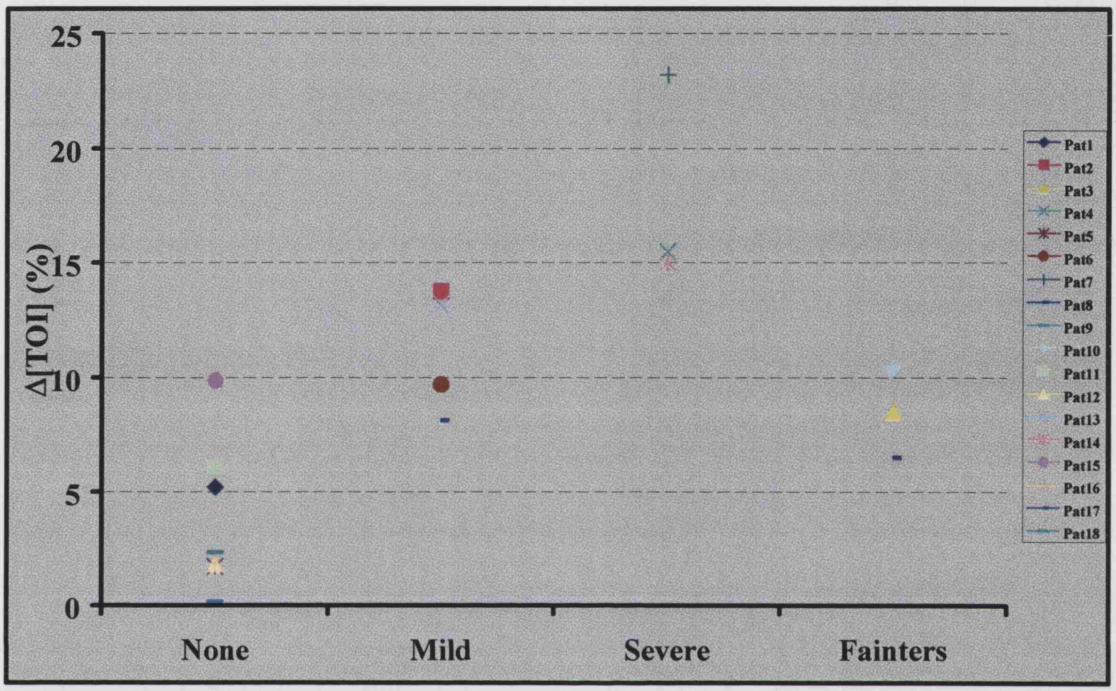

Figure 7.9: Absolute TOI changes between supine and tilt up against the different symptomatology categories.

Fainting is not a simple process [3], fainting often occurs in healthy individuals during blood loss and it demonstrates that a low blood volume is a factor underlying the mechanism of orthostatic and haemorrhagic fainting. There exists an antagonism between the controls of volume/pressure on the filling side of the heart, and of the arterial pressure. The balance between these antagonists is upset by a decrease in the central blood volume which may evoke an inhibition of the arterial pressure control. Moreover, depending on the degree of stimulation of these control mechanisms the balance may be shifted to a prevalence of the volume regulation and a fainting attack maybe occur [18].

Figure 7.10 summarises the results between the different categories of symptomatology and Δ[MBP]. There is not a clearly distinguishable difference between all the categories, however it is most likely that this has to do with the physiological patient

variability. A lot of the patients had an initial supine MBP in the range of hypertension, some of them had MBP about 107mmHg, and when tilted up MBP went down to 77mmHg, which is again inside the normal cerebral autoregulation limits even though this was a downward change of 30mmHg.

Figure 7.11 summarises the results between the different categories of symptomatology and the MBP during tilt up; again is difficult to distinguish between the different categories. However one can recognise that patients with severe symptoms and fainters demonstrated very low MBP (as low as 20mmHg).

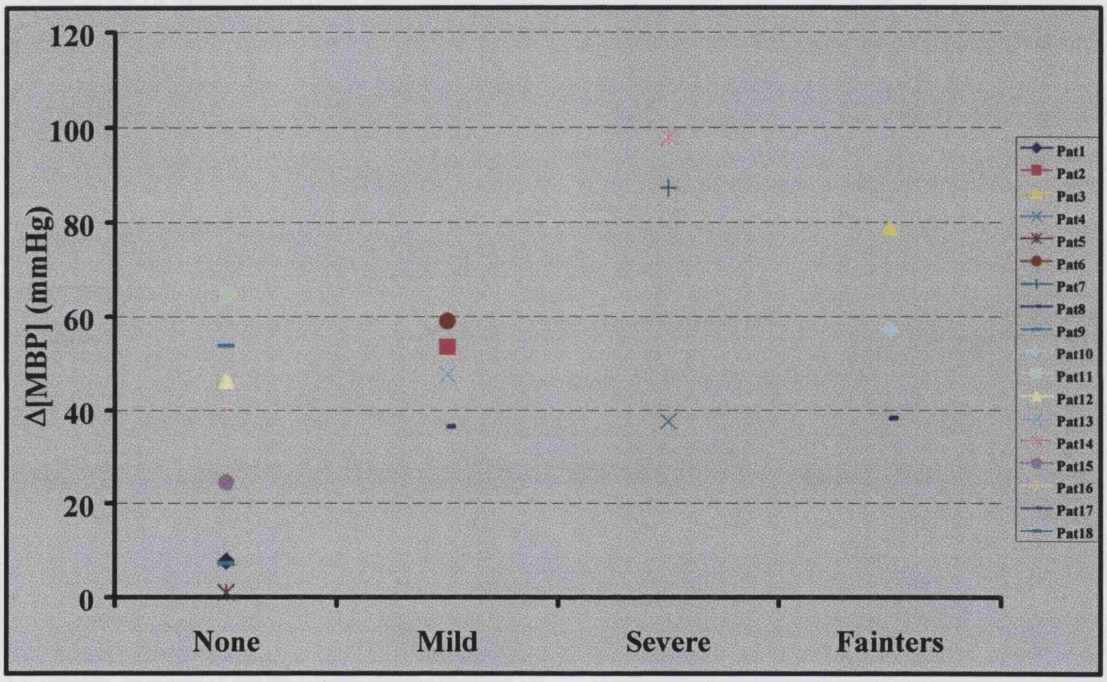

Figure 7.10: Absolute MBP changes between supine and tilt up against the different symptomatology categories.

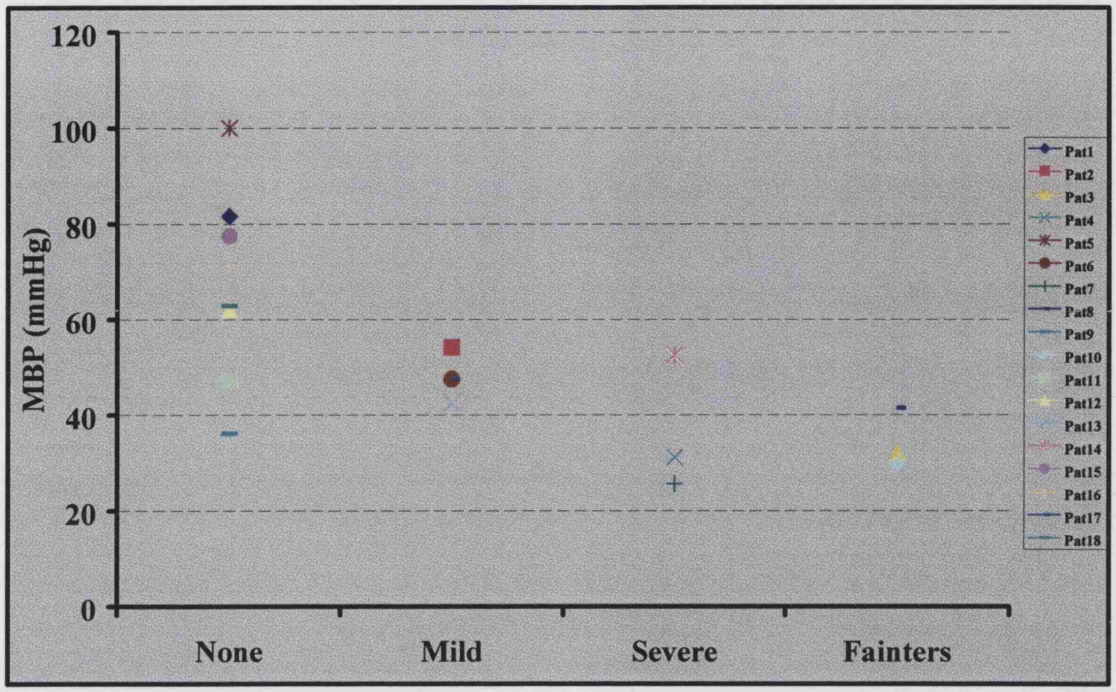

Figure 7.11: Absolute MBP values at tilt up against the different symptomatology categories.

Many of these patients have been living with this disease for number of years with the consequence that have adjusted their brain autoregulation limit to accommodate for these very large changes in blood pressure. However for some of them this process was not so successful.

7.4 Discussion

Primary autonomic failure encompasses a range of disease entities whose common feature is severe postural hypotension. Primary autonomic failure may occur because of pure autonomic failure (autonomic failure with no additional neurological symptoms), which results from peripheral damage or multiple system atrophy (autonomic failure with additional neurological symptoms), when the lesion is predominantly central [19,20].

In healthy subjects, the normal cardiovascular response to head-up tilt consists of a rise in MBP, heart rate and peripheral vascular resistance and a fall in cardiac output and stroke volume [8,13,21-27]. In the present study, the MBP changes observed in the control group are in keeping with these known responses.

In primary autonomic failure head-up tilt results in severe postural hypotension which was observed in this study. An acute reduction in cerebral perfusion is the presumed cause of symptoms in patients with postural orthostatic hypotension related to primary autonomic failure. The variability and range of the cardiovascular changes in autonomic failure means that some patients exhibit typical syncope symptoms of orthostatic hypotension whereas others may only experience non-specific symptoms such as weakness, lethargy and fatigue.

Older NIRS technologies have been used to investigate several patients groups during changes in posture in an attempt to quantify changes in cerebral oxygenation under a wide range of clinical scenarios [5,28-30]. Patient with primary autonomic failure, who exhibit large changes in blood pressure during gravitational stress, provide a unique patient population in which to study non-invasively the changes in cerebral haemodynamics and oxygenation associated with these systemic changes.

There is a statistical difference between the supine and tilt up positions for all the haemoglobin measurements for the PAF and MSA patients. $\Delta[HbO_2]$ went down during passive head up tilt, Δ[HHb] went up and Δ[HbT] went down, meaning that the NIRO 300 picked up the reduction in blood volume when both group of patients were tilted head up. However one should be cautious when interpreting the Δ[HbT] results as an indicator of changes in cerebral blood volume, because of the unknown quantity of the extracranial contamination.

In this study there was a substantial fall in cerebral TOI during orthostatic hypotension. This occurred in most patients and was temporally related to the reduction in blood pressure during head-up tilt. The average percentage drop in Δ[TOI] between supine and head up tilt for the PAF was 9% and for the MSA 8% with one MSA patient exhibiting a drop of 23%. It is possible that the fall in TOI represents an increase in oxygen extraction by the brain in an attempt to maintain oxygenation during a period of relative hypo-perfusion or a reduction in cerebral blood flow.

Table 7.4 summarises the changes seen in the cerebral NIRS signals and the blood pressure for all three groups from baseline to head-up tilt.

Table 7.4: Summary of changes between head up and baseline for all three groups.

	Δ[MBP] Mean (SD) (mmHg)	Δ[TOI] Mean (SD) (%)	Δ[HbT] Mean (SD) (μmoles/l)
PAF (n=10)	-47 (21)	-9 (4)	-2.60 (2.34)
MSA (n=8)	-46 (34)	-8 (8)	-3.71 (3.39)
Controls (n=10	12 (8)	-3 (3)	0.36 (2.43)

Changes in $\Delta[HbO_2]$ for each healthy volunteer uncover one of the most important limitations regarding NIRS, and this is skin contamination. Data from the $\Delta[HbO_2]$ show that when tilted up, for half of subjects oxy-haemoglobin went down and for the other half it went up. One can try to explain why $\Delta[HbO_2]$ changes by considering the rise in MBP present in all volunteers when tilted up. An important factor that can cause $\Delta[HbO_2]$ to increase is passive venous dilation due to an increase in venous pressure. However, the increase in MBP in a well autoregulated healthy volunteer would cause a small vasoconstriction of the arteries to keep CBF constant, therefore reducing the arterial volume and if oxygen extraction remains the same this will lead to a reduction in $\Delta[HbO_2]$. These two competing effects might produce unpredictable results.

One must also be careful when interpreting changes in the $\Delta[HbO_2]$ signal as this is a mixed arterial ($\Delta[HbO_2]_{art}$) and venous ($\Delta[HbO_2]_{ven}$) signal. Because there is three times as much cerebral venous volume as cerebral arterial volume, a unit change in venous saturation would have a comparatively larger effect in the total tissue $\Delta[HbO_2]$ signal than a unit change in arterial saturation. Bearing all the above in mind the net effect could be somewhat unpredictable and could be even more confused by contamination signals from the extracranial skin (where the autoregulatory mechanisms are largely absent).

Summarising we have a situation where $\Delta[HbO_2]$ should drop in the presence of a rise in MBP, however the experimental results do not demonstrate this. As a general rule we can believe that a true cerebral $\Delta[HbO_2]$ signal would tend to overestimate tissue

oxygenation, but due to the extracranial contamination would tend to bias towards an underestimation of tissue oxygenation.

Changes in Δ[HHb] show an increase for every volunteer when tilted up. Again for the analysis of this result one has to start by considering the rise in MBP present in all volunteers when tilted up. Furthermore one also has to think about both the changes in the Δ[HHb] signal from the cerebral cortex and the extracranial contamination. A rise in MBP causes a passive increase in venous volume in the head; it also might cause a small arterial vasoconstriction, these two effects could explain the rise in Δ[HHb]. Also the same passive effect might happen in the skin therefore producing an increase in Δ[HHb]. As a general thought the Δ[HHb] signal tends to be more robust as fewer things can affect it, and those physiological stimuli that affect it like changes in blood pressure have the same qualitative effects in both the cerebral arterial and venous compartments.

Finally changes in total haemoglobin are equally difficult to interpret because of the reasons discussed above. One would expect CBV to increase because of the increase in MBP however this effect could be underestimated because of changes in the extracerebral skin.

The modest rise in MBP during head-up tilt in the healthy volunteers was associated with a small reduction in TOI which is almost certainly physiologically insignificant. This small decrease in TOI is likely to occur because of the increase in MBP and a change in the intracranial arterial:venous volume ratio during head-up tilt. For most of the volunteers, TOI went down when tilted up, however the drop was very small and as discussed previously there is a strong belief that this is not due to change in the oxygenation status, but rather to the changes in arterial/venous volume ratio. To explain these results one again has to start by considering the effects of the rise in MBP. This rise could produce an arterial vasoconstriction and a passive venous dilation resulting in a small drop on TOI. For two volunteers TOI remained the same when they were head up and for one it went slightly up. Again those results could be explained by the natural variability of cerebral autoregulation among healthy people and especially the elderly, as a small increase in CBF could affect the final results. If the rise in MBP caused a

slight increase in CBF, this could result in an increase in venous oxygen saturation and if the oxygen extraction remained the same, the final result would be an increase in TOI.

In this study we demonstrated the effects of orthostatic hypotension on the cerebral oxygenation and haemodynamics during head up tilt. The results here indicate a severely compromised cerebral circulation in patients suffering from primary autonomic failure.

Further to the analysis presented in this thesis a more extended analysis of the rate of change is presented in reference [17] which is reproduced in Appendix C.

7.5 Simulation investigation analysis and results

Data from this group of patients provides a unique opportunity to study the effect of severe changes in blood pressure. A minor physiological challenge of 60° head up tilt produces major changes in their systemic blood pressure; furthermore according to their pathology there is no reason to believe that their metabolic autoregulatory mechanisms are impaired.

As we discussed at the beginning of this chapter MBP was monitored continuously together with the cerebral TOI. Other systemic variables monitored were finger arterial saturation (every 2 minutes) and the heart rate.

7.5.1 Simulation methodology

Simulations were done using the UCL cerebral model (version 1.0, 2004-2005). The individual measured time traces of MBP were used as input parameters to the model after being smoothed by one second non-overlapping moving averaging. The purpose of the averaging was to remove undesirable oscillations in the signals and to reduce the quantity of data to be simulated.

For the purpose of the simulations from the 18 primary autonomic failure patients there were 15 suitable for this analysis. The exclusion criteria were that in two patients a large amount of the continuous blood pressure signal was missing (due to finger hypoperfusion hence causing artifacts in the Portapres® signal) and in one case the patients response to head up tilt did not demonstrate any change.

Other parameters in the model were set to their default values; no attempt has been made to customise the model to this patient group and protocol.

Simulated output variables and simulated TOI (sTOI) as a function of time were collected and imported into MatLab for further analysis.

7.5.2 Data analysis

For each signal, seven phases were identified according to the profile of the blood pressure signal, these were baseline, start of drop, middle of drop, end of drop, middle of return, hyperaemia and return to baseline (see Figure 7.12). The start of the drop, the end of the drop and the hyperaemia phases were manually identified in the MBP signal, a program written in MatLab automatically identified the remaining phases and then calculated 30 second averages for each phase. Mean values were obtained using the trapezoidal function (*trapz*) of MatLab. Data is expressed as means with standard deviation during baseline, start of drop, middle of drop, end of drop, middle of return, hyperaemia and return to baseline.

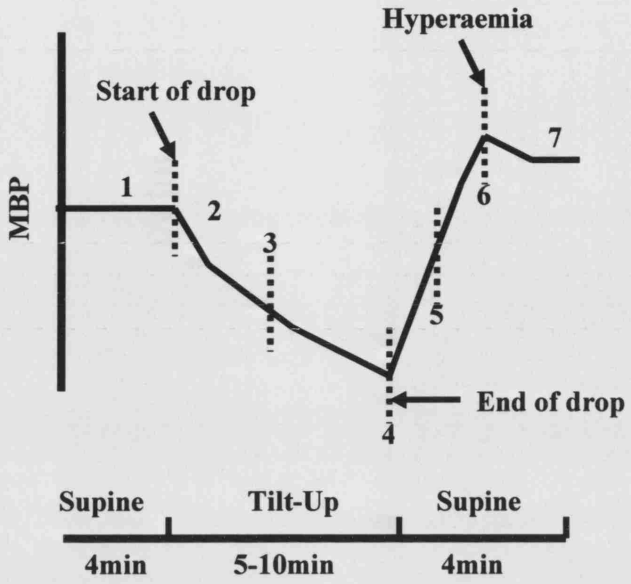

Figure 7.12: Schematic representation of the data analysis. 1: baseline, 2: start of drop, 3: middle of drop, 4: end of drop, 5: middle of return, 6: hyperaemia and 7: return to baseline.

In order to test for agreement between the model and experimental TOI measurements, the arithmetic difference between paired measurements was plotted against their average to examine the difference between paired experimental and simulated measurements [31]. If differences were normally distributed, 95% of them would lie within a range of ±2 S.D.s of the mean of arithmetical difference. This range is reported as the limits of agreement.

7.5.3 Simulation results and comparison with experimental data

In chapter 3 we presented some static autoregulation simulations with the model, during changes in blood pressure. Data collected from this group of patients was suitable to test the similarity between the cerebral simulated TOI autoregulation curve during step changes in pressure. These results are shown in Figure 7.13.

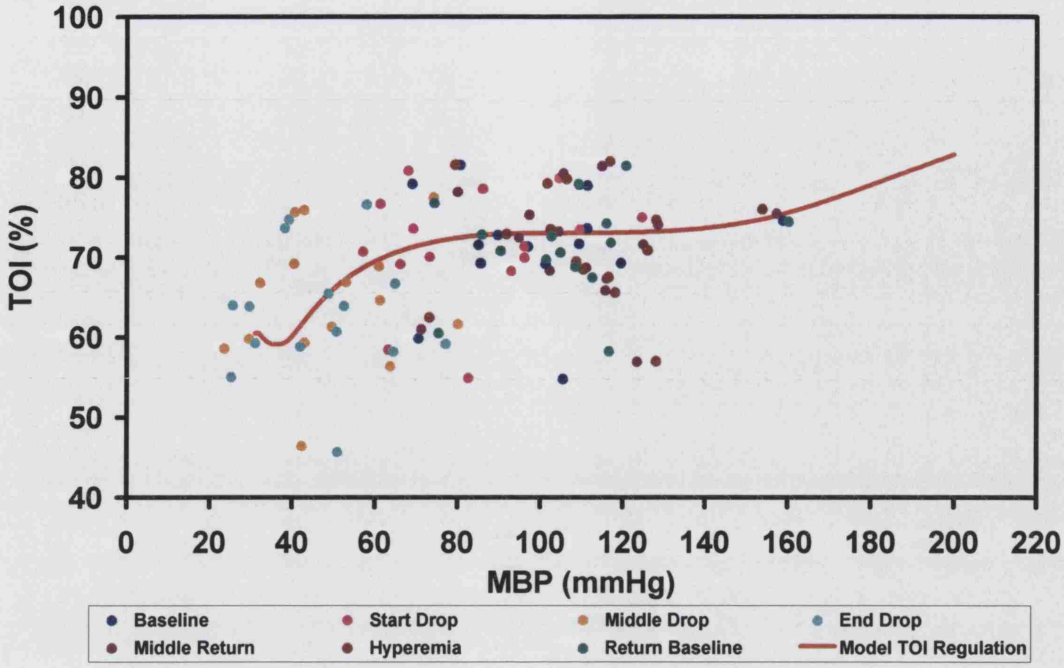

Figure 7.13: Scatter plot of patient paired measured data of cerebral TOI and MBP during all the phases, comparison with the static simulation curve from the model.

A reasonable agreement between the experimental data and the model profile of the simulated autoregulation TOI can be seen in Figure 7.13. Unfortunately the measured TOI does not present any clear trends with blood pressure and since we did not measure the arterial concentration of CO_2 is difficult to investigate this further as one might expect during the head up challenge to have changes in CO_2 and hence changes in cerebral blood flow.

In order to look for agreement and to investigate any possible relationship between the simulated and the measured cerebral TOI a plot has been done of the difference between the signals against their mean. Under these circumstances we can summarise the lack of agreement by calculating the bias estimated by the mean difference and the standard deviation of the differences. Provided differences within mean difference ± 2SD would not be clinically important we could assume that the two different signals, the simulated and experimental TOI can be used interchangeably. In Figure 7.14 we investigate the agreement between the measured and simulated TOI for both the absolute raw values and the changes from baseline.

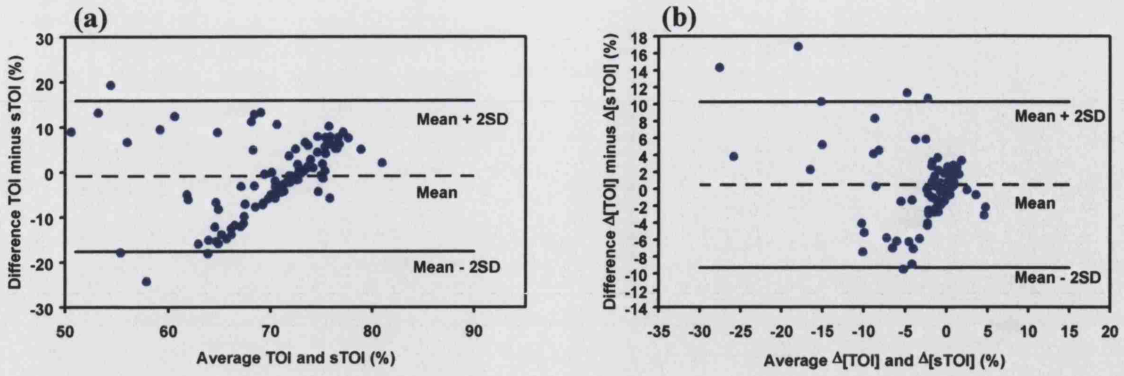

Figure 7.14: Agreement comparison between sTOI/TOI during all the phases: **(a)** absolute raw data of all subjects **(b)** the changes of all subjects.

From the Figure 7.14 it can be seen that there is no agreement between the absolute raw values of simulated and experimental TOI, the mean difference ± 2SD in this case was -0.88±17% with the data spreading from -17% to +17%, which is too high for physiological variables; however when looking the changes this was 0.47±10%, with most of the values falling in the range of ±2% demonstrating a better agreement.

The model manages again to capture the behaviour of the changes in cerebral TOI as the result of changes in blood pressure. Again, the absolute values between sTOI and TOI did not match and this has also been seen in data presented in Chapter 5 and 6. It is clear that the individual variability is the most likely source of this discrepancy and is something that needs to be investigated.

References

1. J.G. McLeod and R.R. Tuck, "Disorders of the autonomic nervous system: Part 2. Investigation and treatment," *Ann. Neurol.* **21**, 519-529 (1987).

2. C.J. Mathias and R. Bannister, "Investigation of autonomic disorders.," *Autonomic Failure: A textbook of clinical disorders of the autonomic nervous system,* Mathias C.J. and Bannister R., eds., (Oxford University Press, Oxford, 1999), 169-195.

3. P. Kligfield, "Tilt table for the investigation of syncope: there is nothing simple about fainting," *J. Am. Coll. Cardiol.* **17**, 131-132 (1991).

4. R. Sutton and D.M. Bloomfield, "Indications, methodology, and classification of results of tilt-table testing," *Am. J. Cardiol.* **84**, 10Q-19Q (1999).

5. A.T. Lovell, A.C. Marshall, C.E. Elwell, M. Smith, and J.C. Goldstone, "Changes in Cerebral Blood Volume with Changes in position in awake and anesthetized subjects," *Anesthesia Analgesia* **90**, 372-376 (2000).

6. A.S. Shamsuzzaman, Y. Sugiyama, and T. Mano, "A comparison of sympathetic vasomotor and cardiovascular responses to head-up tilt and to head-up suspension in humans," *Environ. Med.* **41**, 148-150 (1997).

7. T. Kawaguchi, O. Uyama, M. Konishi, T. Nishiyama, and T. Iida, "Orthostatic hypotension in elderly persons during passive standing: a comparison with young persons," *J. Gerontol. Biol. Sci. Med. Sci.* **56**, M273-M280 (2001).

8. M. Lye and T. Walley, "Haemodynamic responses in young and elderly, healthy subjects during ambient and warm head-up tilt," *Clin. Sci. (London)* **94**, 493-498 (1998).

9. C.J. Mathias, "Orthostatic hypotension: causes, mechanisms, and influencing factors," *Neurology* **45**, S6-11 (1995).

10. E.N. Marieb, "The cardiovascular system: blood vessels," *Human anatomy and physiology,* Marieb E.N., ed., (Benjamin/Cummings Science Publishing, California, 1998), 690-743.

11. F.M. Faraci, "Cerebral circulation during aging," *The regulation of cerebral blood flow,* Phillis J.W., ed., (CRC Press, Florida, 1993), 342-349.

12. L.A. Lipsitz, "Ageing and the autonomic nervous system," *Autonomic failure: A textbook of clinical disorders of the autonomic nervous system,* Mathias C.J. and Bannister R., eds., (Oxford University Press, Oxford, 1999), 534-544.

13. M.P. Chandler and C.J. Mathias, "Haemodynamic responses during head-up tilt and tilt reversal in two groups with chronic autonomic failure: pure autonomic failure and multiple system atrophy," *J. Neurol.* **249**, 542-548 (2002).

14. K.M. Bleasdale-Barr and C.J. Mathias, "Neck and other muscle pains in autonomic failure: their association with orthostatic hypotension," *J. R. Soc. Med.* **91**, 355-359 (1998).

15. C.J. Mathias, R. Mallipeddi, and K. Bleasdale-Barr, "Symptoms associated with orthostatic hypotension in pure autonomic failure and multiple system atrophy," *J. Neurol.* **246**, 893-898 (1999).

16. C.C. Duncan, J.H. Meek, M. Clemence, C.E. Elwell, L. Tyszczuk, M. Cope, and D.T. Delpy, "Optical pathlength measurements on adult head, calf and forearm and the head of the newborn infant using phase resolved optical spectroscopy," *Phys. Med. Biol.* **40**, 295-304 (1995).

17. I. Tachtsidis, C.E. Elwell, T.S. Leung, K. Bleasdale-Barr, K. Hunt, N. Toms, M. Smith, C.J. Mathias, and D.T. Delpy, "Rate of change in cerebral oxygenation and blood pressure in response to passive changes in posture: a comparison between pure autonomic failure patients and controls," *Adv. Exp. Med. Biol.* **In press** (2004).

18. L. Bergenwald, U. Freyschuss, and T. Sjostrand, "The mechanism of orthostatic and haemorrhage fainting," *Scand. J. Clin. Lab. Invest.* **37**, 209-216 (1977).

19. M.R. Matthews, "Autonomic ganglia and preganglionic neurones in autonomic failure," *Autonomic failure: A textbook of clinical disorders of the autonomic nervous system,* Mathias C.J. and Bannister R., eds., (Oxford University Press, Oxford, 1999), 329-339.

20. S.E. Daniel, "The neuropathology and neurochemistry of multiple system atrophy," *Autonomic failure: A textbook of clinical disorders of the autonomic nervous system,* Mathias C.J. and Bannister R., eds., (Oxford University Press, Oxford, 1999), 321-328.

21. H.A. Shenkin, W.G. Scheuerman, E.B. Spitz, and R.A. Groff, "Effect of change of position upon the cerebral circulation of man," *J. Appl. Physiol.* **2**, 317-326 (1950).

22. E. Vargas and M. Lye, "Physiological responses to postural change in young and old healthy individuals," *Exp. Gerontol.* **17**, 445-451 (1982).

23. B.D. Levine, C.A. Giller, L.D. Lane, J C. Buckey, and C.G. Blomqvist, "Cerebral versus systemic hemodynamics during graded orthostatic stress in humans," *Circulation* **90**, 298-306 (1994).

24. W. Wieling, J.J. van Lieshout, and A.D. Ten Harkel, "Dynamics of circulatory adjustments to head-up tilt and tilt-back in healthy and sympathetically denervated subjects," *Clin. Sci. (London)* **94**, 347-352 (1998).

25. D. Bloomfield, M. Maurer, and J.T. Bigger Jr., "Effects of age on outcome of tilt-table testing," *Am. J. Cardiol.* **83**, 1055-1058 (1999).

26. S. Houtman, W.N. Colier, M.T. Hopman, and B. Oeseburg, "Reproducibility of the alterations in circulation and cerebral oxygenation from supine rest to head-up tilt," *Clin. Physiol.* **19**, 169-177 (1999).

27. M.E. Petersen, T.R. Williams, C. Gordon, R. Chamberlain-Webber, and R. Sutton, "The normal response to prolonged passive head up tilt testing," *Heart* **84**, 509-514 (2000).

28. W.N.J.M. Colier, N.J.C.W. van Haaren, M.J.T. van de Ven, H.T.M. Folgering, and B. Oeseburg, "Age dependency of cerebral oxygenation assessed with near infrared spectroscopy," *Journal of Biomedical Optics* **2**, 162-170 (1997).

29. W.N.J.M. Colier, R.A. Binkhorst, M.T.E. Hopman, and B. Oeseburg, "Cerebral and circulatory haemodynamics before vasovagal syncope induced by orthostatic stress," *Clinical Physiology* **17**, 83-94 (1997).

30. M.J.T. Van de Ven, W.N.J.M. Colier, M.C. van der Sluijs, D. Walraven, B. Oeseburg, and H. Folgering, "Can cerebral blood volume be measured reproducibly with an improved near infrared spectroscopy system?," *J. Cereb. Blood Flow Metab.* **21**, 110-113 (2001).

31. J.M. Bland and D.G. Altman, "Statistical methods for assessing agreement between two methods of clinical measurement," *Lancet* **1**, 307-310 (1986).

Chapter 8

Work in Progress

In this chapter, ongoing work including studies on young healthy volunteers and the clinical applications of near-infrared spectroscopy (NIRS) are discussed. Preliminary results are presented and a brief analysis of these discussed. In Section 8.4 the work in progress regarding the UCL model is discussed, in particular the possible approaches to training the model are presented and some preliminary results shown.

8.1 Introduction

The currently on going work with near-infrared spectroscopy is concentrating on a mixture of experiments involving young healthy volunteers and clinical studies in the Intensive Care Unit (ICU).

Briefly a study is underway involving young healthy volunteers using an acetazolamide provocation test. Acetazolamide is a carbonic anhydrase inhibitor, which induces brain extra cellular acidosis and hence triggers an increase in CBF [1-3]. The advantage of acetazolamide lies in its selective targeting of the cerebral circulation with minimal systemic effects [4,5]. Near-infrared spectroscopy is used to monitor the changes in the oxygenation and haemodynamic status of the brain with additional measurements of absolute CBF using indocyanine green (ICG) as an inert intra-vascular tracer. Measurements are also made of the middle cerebral artery flow velocity using transcranial Doppler.

In parallel with the young healthy volunteer studies, a clinical investigation involving stroke patients is in progress. Briefly, this involves measurements of bilateral changes in cerebral NIRS during postural changes.

Finally the current progress with the UCL model is presented with emphasis given to the training of the model to individuals. Some preliminary results are presented.

8.2 Measurement of cerebral blood flow and cerebral tissue oxygenation in volunteers using near infrared spectroscopy and indocyanine green during acetazolamide provocation.

The measurement of cerebral blood flow (CBF) is important in the understanding of the normal and injured brain. Numerous invasive and non-invasive techniques have been developed to monitor and measure CBF, including positron emission tomography, 133 Xenon clearance, nitrous oxide wash-out and transcranial Doppler (TCD). All these techniques have limitations in the clinical setting because of

the use of radioactive tracers, poor spatial resolution, low signal to noise ratio or because they provide only an indirect measurement of CBF.

Near-infrared spectroscopy can also be used to measure CBF. The measurement of CBF with this technique involves the use of indocyanine green (ICG) as an inert intravascular tracer [6,7]. ICG is a tricarbocyanine dye that binds to albumin and therefore remains in the plasma. The dye is a very strong absorber of near infrared light and this allows changes in its concentration in the brain to be measured using NIRS with a high signal to noise ratio. CBF is calculated by application of the Fick principle, which considers the ratio of the rate of tracer accumulation in the brain to the amount of tracer delivered. The Fick principle can be expressed in integral form as shown in Equation 8-1:

$$C_t(t) = F\int^{t}(C_a(t) - C_v(t))\ dt \qquad \textbf{8-1}$$

where $C_t(t)$ is the tissue concentration, F is the blood flow, $C_a(t)$ is the arterial concentration of the dye and $C_v(t)$ is the venous concentration of the dye.

The accumulation of the ICG in the brain will depend both on arterial inflow and venous clearance. However if measurements are made within the cerebrovascular transit time, venous outflow is negligible (i.e. $C_v(t)$ can be assumed to be zero). The amount of ICG delivered to the brain can be calculated from the area under the curve of the arterial ICG concentration changes. Previously it has only been possible to measure arterial ICG concentration continuously with an invasive technique using an optical device placed intra-arterially, but recently a pulse dye densitometer (Nihon Kohden, Tokyo, Japan) has been developed that uses a nose probe to measure arterial ICG concentration accurately and non invasively [8].

Most previous NIRS studies of cerebrovascular reactivity, including our own, have relied upon manipulation of $PaCO_2$ to achieve changes in CBF. However, concern has been raised regarding the use of CO_2 to produce changes in CBF because a rise in $PaCO_2$ might cause an increase in arterial blood pressure (ABP). This may result in a contradictory influence on the overall change of CBF. An increase in ABP causes cerebral vasoconstriction, whereas an increase in $PaCO_2$ causes cerebral vasodilatation.

Furthermore, the extracranial circulation responds passively to changes in ABP and this may change the relative contribution of extracranial 'contamination' in the NIRS signal, thereby rendering the measurements unreliable.

In order to overcome these limitations one can use acetazolamide, a well established drug, which induce changes in CBF [5,9]. Acetazolamide selectively targets the cerebral circulation and has no systemic effects [2]. This drug is a carbonic anhydrase inhibitor which induces brain extra cellular acidosis, triggering an increase in CBF.

The aim of this study is to investigate the use of NIRS as an alternative means of measuring CBF during an acetazolamide provocation test.

8.2.1 Methods

Results are presented of a preliminary investigation on 4 young healthy volunteers (the local ethics committee approved the protocol for the study, and all subjects gave informed consent for participation). During the experiment volunteer 2 felt unwell therefore the study was stopped after the first ICG injection, data from this study is excluded.

8.2.2 Monitoring configuration

A continuous wave near-infrared spectrometer (NIRS), with a sampling rate of 6Hz (NIRO 300, Hamamatsu Photonics KK) was used to measure absolute cerebral tissue oxygenation index (TOI) over the frontal cortex using the spatially resolved reflectance NIRS spectroscopy technique, together with changes in oxy-haemoglobin ($\Delta[HbO_2]$) deoxy-haemoglobin (Δ[HHb]) and Δ[ICG] by utilizing the modified Beer-Lambert law.

A transcranial Doppler (TCD) system (Nicolet) was situated over the temporal window and positioned to achieve an optimal flow signal from the middle cerebral artery (MCA). The TCD probe was secured in position using a commercially available probe holder. Finally, a laser Doppler probe (Moor Instruments) was placed on the forehead to provide information about the changes in skin blood flow.

Systemic variables continuously monitored were ECG, end tidal CO_2 ($EtCO_2$) via a face mask and oxygen saturation (SaO_2) from an ear probe. Blood pressure was continuously measured non-invasively throughout the study using a Portapres® system (TNO Biomedical Instrumentation). The Nihon Kohden pulse dye densitometer probe was positioned on the nose to measure arterial ICG concentration continuously.

An indwelling cannula (22g Y-Can) was inserted into an antecubital vein and a 1ml blood sample taken for measurement of haemoglobin concentration. The ICG boluses and acetazolamide were administered via this cannula.

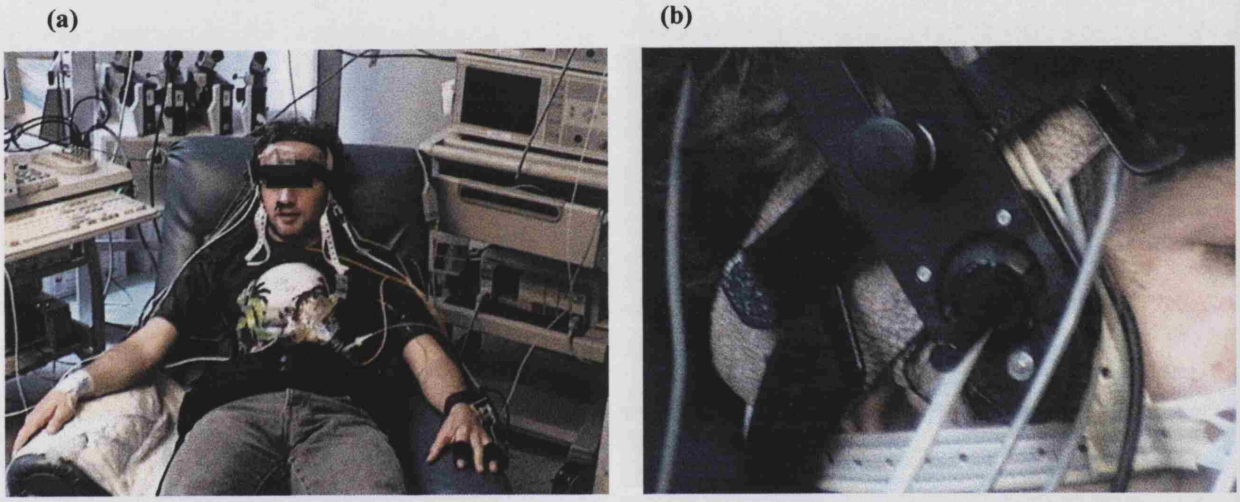

Figure 8.1: Pictures of the experimental set up. **(a)** The set up of the monitoring systems on a volunteer. **(b)** The position of the transcranial Doppler probe.

8.2.3 Protocol

The study begins with a five minute period of baseline recording. A rapid intravenous injection of ICG (0.1mg/kg) is then given and a baseline CBF calculated. After approximately 15 and 30 minutes, further ICG boluses are administered and a second and third baseline CBF calculated. ICG clearance from the bloodstream takes approximately 15 minutes and this is why this interval is required between measurements. Following the third baseline CBF measurement, acetazolamide (500mg) is then administered by slow intravenous (IV) injection and the change in blood flow velocity monitored using TCD is observed. The study continues if a 50% (or greater)

change in blood flow velocity is noted 25 minutes after the injection. If the change in blood flow velocity is < 50%, a further 500mg of acetazolamide is administered and the study continues 25 minutes after this second dose. When the rise in blood flow velocity has stabilised at its new value (assessed by stabilisation of the TCD measurements) three further doses of ICG at approximately 15 minutes intervals are given to measure absolute CBF at the new (elevated) level. The whole study lasts between 2 and 2.5 hours.

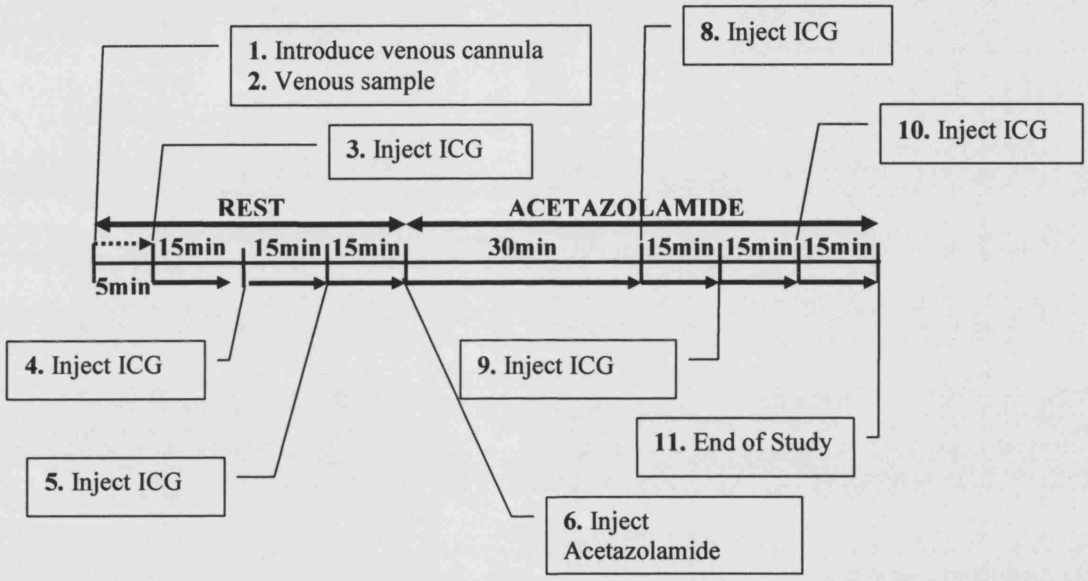

Figure 8.2: Schematic representation of the protocol.

8.2.4 Analysis

An automatic program (written in MatLab) was used to identify the bolus injection of the ICG, therefore synchronising the tissue and arterial ICG signals (Figure 8.3(a)) and then performs the flow calculation assuming a transit time of 4sec. This is done using Equation 8-1 from a linear regression between the numerically integrated arterial curve on the x-axis and the tissue curve on the y-axis (Figure 8.3(b)). The blood flow is then given by the gradient of the regression line.

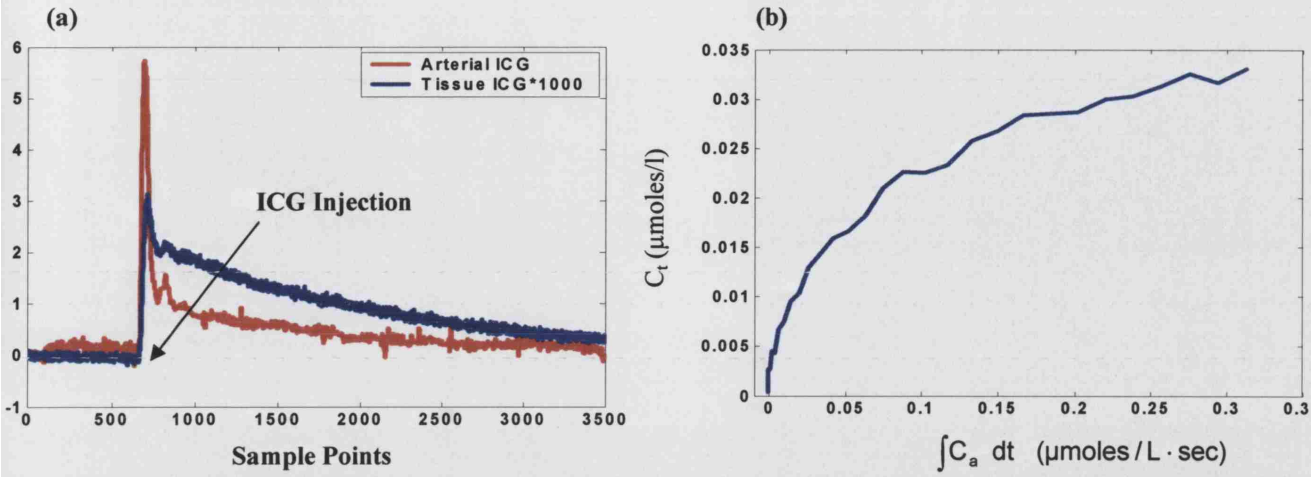

Figure 8.3: (a) Arterial and tissue ICG concentrations after synchronisation; **(b)** The integral methodology for calculation of flow.

8.2.5 Preliminary results and discussion

After injection of acetazolamide a consistent rise in the mean velocity of the middle cerebral artery, and the tissue oxygenation has been seen in all volunteers (Figure 8.4). The degree of the increase seemed to be related to the acetazolamide dosage and we are currently investigating this to determine the optimal dose for use in future studies. Table 8.1 shows the individual dosages as mg/kg administer to the volunteers.

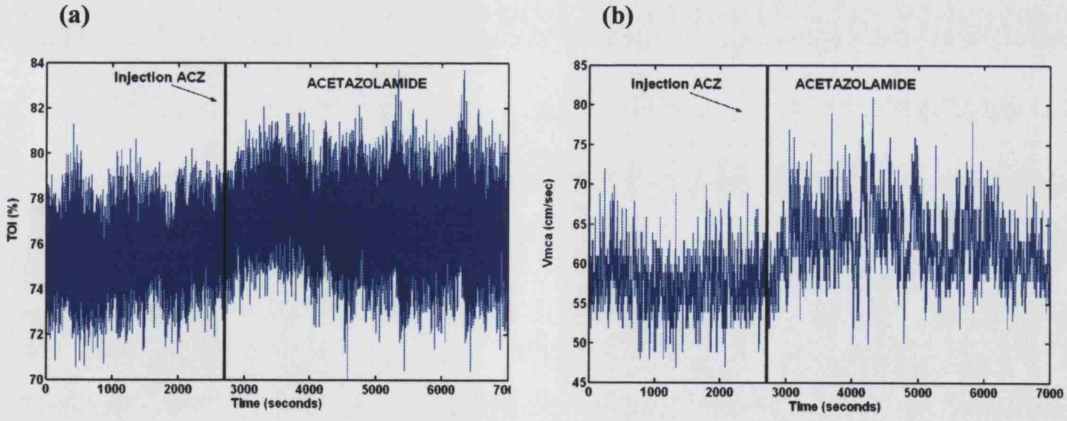

Figure 8.4: An example of the data collected from a volunteer, before and after the acetazolamide (ACZ) injection. **(a)** Cerebral TOI measurements **(b)** Mean velocity of middle cerebral artery (V_{mca}).

From the arterial and tissue ICG traces the absolute CBF values were calculated. Mean and standard deviation results at rest and after acetazolamide are shown in Table 8.1.

Table 8.1: Summary results of acetazolamide dosage and CBF for each volunteer.

	Dosage (mg/Kg)	CBF Rest (ml/100g/min) Mean(SD)	CBF ACZ (ml/100g/min) Mean(SD)
Volunteer 1	10	7.43 (1.67)	12.76 (0.91)
Volunteer 3	7.5	11.66 (4.39)	16.24 (5.97)
Volunteer 4	7.1	14.5 (0.73)	21.96 (8.01)

Figure 8.5 shows the CBF measurements for each ICG injection for all three volunteers.

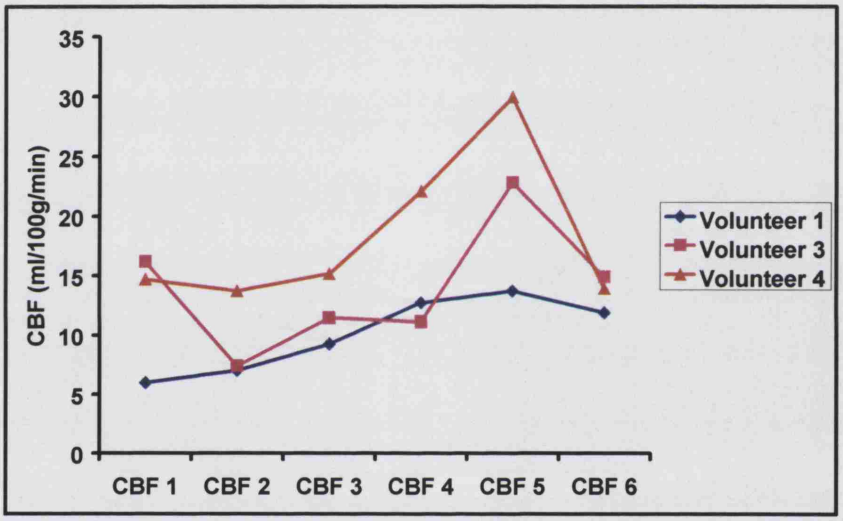

Figure 8.5: Individual CBF measurements. CBF 1 to 3 are during baseline and CBF 4 to 6 are after acetazolamide injection.

The absolute CBF results obtained using this very simple analysis method significantly underestimate the correct values and show high variability between measurements. This is mainly due to the fact that near-infrared interrogates the whole head including scalp, skull and brain resulting in an averaged blood flow, which may be lower than in the brain itself. We are currently investigating an alternative methodology to obtain CBF using the impulse residue function [10].

Furthermore due to the fact that the degree of increase in CBF is dependent on the acetazolamide dosage, the protocol has now been altered and instead of a standard dosage of 500mg we will now administer a dosage equivalent to 10mg/Kg.

Finally, data collect from this study will be used to investigate further the NIRS cerebral tissue oxygenation measurement and the experimental data will be used to test and inform the cerebral computational model. The greatest strength of this data is the selective response of the acetazolamide in the brain and the co-registration of NIRS and transcranial Doppler measurements.

8.3 Stroke studies

Stroke may be either haemorrhagic or ischemic and may lead to loss of cerebral function and numerous neurological disorders such paralysis, loss of speech or consciousness. It results from either rupture or blockage of intracranial vessels supplying a corresponding brain area.

The main aim and interest of this study is to investigate the response of the NIRS cerebral tissue oxygenation signal in patients with ischemic strokes and examine the differences between the affected and the healthy hemispheres.

8.3.1 Methods

Results are presented of a preliminary investigation on 9 patients with mean age of 61 years old (range 51 to 79 years) (the local ethics committee approved the protocol for the study, and all subjects gave informed consent for participation).

Patients were investigated within 3 weeks of admission to the stroke clinic, with some of them presenting with symptoms of hemiparesis. The infarction site was identified by computed tomography (CT) or/and magnetic reasonance imaging (MRI). Patients were well enough to sit and stand with or without assistance, and with sufficient cognition to comply safely with the protocol.

Table 8.2: Patient information summary (M: male; F: Female; L: Left; R: Right; UL: Upper Left; MCA: Middle Cerebral Artery; PCA: Posterior Cerebral Artery;).

Patient	Age	Gender	Position of Probe (Affected Side)	Symptoms	CT/MRI Scan Results
S1	77	M	L Frontal	R UL Weakness, Dysarthria	L frontal infarct (white matter)
S2	42	M	R Temporal	L Hemiparesis	R MCA infarct (internal capsule)
S3	50	F	R Parietal	L UL Paralysis	R MCA infarct fronto-temporo-parietal cortical
S4	51	M	R Frontal	L Hemiparesis	R MCA infarct (whole territory)
S5	55	M	L Frontal	R Hemiparesis, Dysphasia	L MCA infarct
S6	76	M	R Parietal	L Hemiparesis	R infarct (white matter)
S7	54	M	L Parietal	R UL weakness	L infarct (internal capsule)
S8	60	M	R Parietal	L UL weakness	R MCA infarct temporo-parietal cortical
S10	79	F	L Frontal	R Hemiparesis	L PCA infarct (thalamus and occipital lobe)

8.3.2 Monitoring configuration

A continuous wave near-infrared spectrometer (NIRS), with a sampling rate of 6Hz (NIRO 300, Hamamatsu Photonics KK) was used to measure absolute cerebral TOI using the spatially resolved reflectance NIRS spectroscopy technique, together with changes $\Delta[HbO_2]$ and $\Delta[HHb]$ by utilizing the modified Beer-Lambert law.

During the study we monitor continuously arterial saturation (SaO_2) from the ear and blood pressure non-invasively using a Portapres® system (TNO Biomedical Instrumentation).

8.3.3 Protocol

The protocol comprises 5 phases: (1) the patient is in a supine position (in bed) for 5 minutes; (2) the bed automatically rises so the patient is placed into a sitting position for another 5 minutes; these two phases are repeated (3) the patient is then positioned at the

end of the bed for 1-2 minute before (4) the patient placed into a sitting position in a chair for 5 minutes and finally (5) the patient is asked to stand, if necessary with assistance for another 5 minutes; again these two phases are repeated. Figure 8.6 shows results from one stroke study.

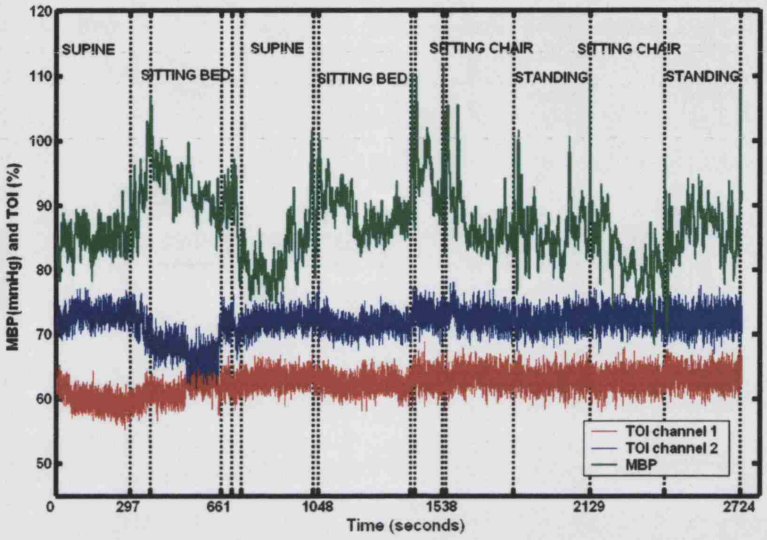

Figure 8.6: A typical study of a stroke patient. TOI channel 1 is the affected side and TOI channel 2 is the healthy side of the brain. In this particular patient there were not significant changes during standing; however there were some differences when the patient was placed into a sitting position on bed.

8.3.4 Analysis

Preliminary analysis was done between sitting on chair and standing, because during these phases most patients exhibit large changes. Mean values were calculated for one minute at the end of the rest period before the sitting up and then standing position; at the end of the standing; and finally at the end of the rest period which is the end of the study (see Figure 8.7).

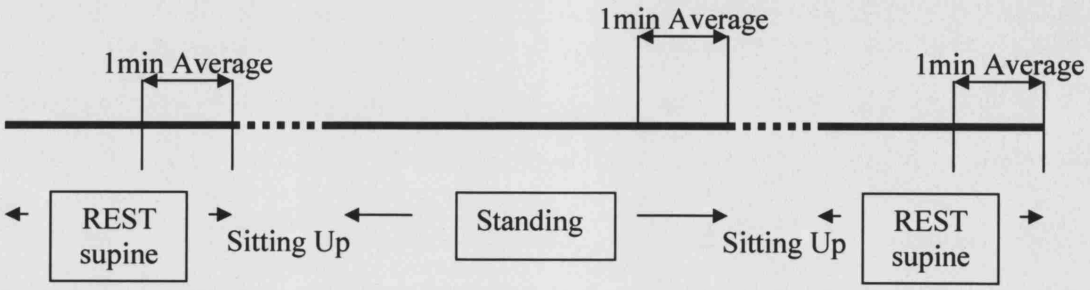

Figure 8.7: Graphical representation of the analysis.

8.3.5 Preliminary results and discussion

Initial analysis uncovered individual differences between the affected and healthy hemispheres, however the group summary data was inconclusive and failed to produced any significant evidence of differences between the healthy and the infarct side of the brain (see Figure 8.8).

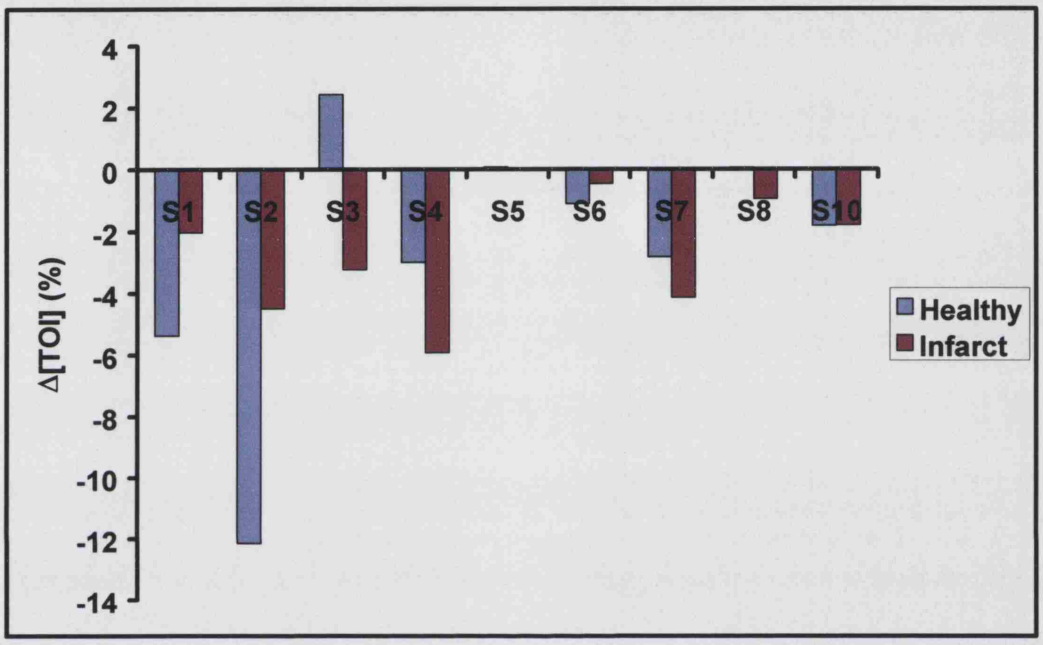

Figure 8.8: Changes in Δ[TOI] between supine and standing, comparison of the healthy versus the infarct side.

Preliminary results revealed a large intersubject variability in the data; this is probably due to the large variability in the diagnosis, symptoms and position of the infarct among the patients studied so far. There are patients with cortical infarcts but also patients with white matter infarcts.

This is a study in progress and we are currently recruiting more patients.

8.4 Current progress with the UCL cerebral computational model

Individual physiological variability is very difficult to model, this has a major effect when comparing experimentally measured and simulated data. In Chapters 5 and

7 the UCL model manages to reproduce the changes seen in the CO_2 and passive tilt experiments; however no attempt had been made to train the model to an individual. All simulations previously discussed were done with the model parameters set to their healthy adult default values.

Comparing the measured and simulated TOI signal uncovered differences in their absolute values. These can be resolved by altering certain parameters in the model so that the baselines of measured and simulated TOI are the same. However this is not a simple process as changing parameters in the model might cause a degree of instability and might also lead to unphysiological values for some parameters.

As a first attempt to train the model to an individual the baseline of the simulated TOI was adjusted so that it matched the experimentally measured TOI. The procedure used was as follows: 30 seconds of the measured baseline data was used to run the simulation, during which an automated algorithm compared the average baseline value of the experimental TOI with the average baseline value of the simulated TOI. If they did not match, the algorithm adjusted the baseline of the simulated TOI by either altering the parameter which describes the fraction of normal brain water volume that is blood *(Vol_blood_frac)*, which has a default value of 0.0475; or by altering the default values of the radii of the large and small arteries (*r_01* and *r_02* respectively), which have a default value of 0.015cm and 0.0075cm respectively (for details regarding these parameters the reader is advised to look at [11]). After this initial 30sec adjustment period these parameters were then fixed and the model was left to run with these fixed values for the remainder of the simulation. Figure 8.9 shows the changes in the simulated TOI when one changes the default values of the radii of the arteries and the volume blood fraction.

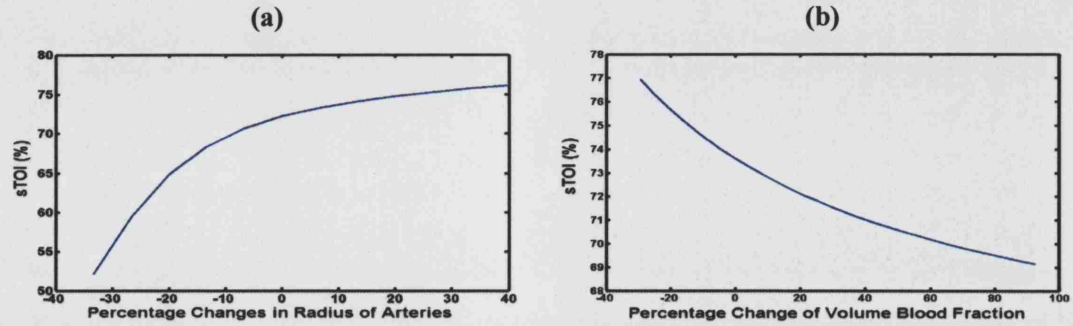

Figure 8.9: The response of the simulated TOI when change **(a)** the default values of the radius of the arteries; **(b)** the volume blood fraction.

Preliminary results with the hypercapnia data (presented in Chapter 5) and altering the resting arterial diameters parameters in the model produced positive results (see Figure 8.10).

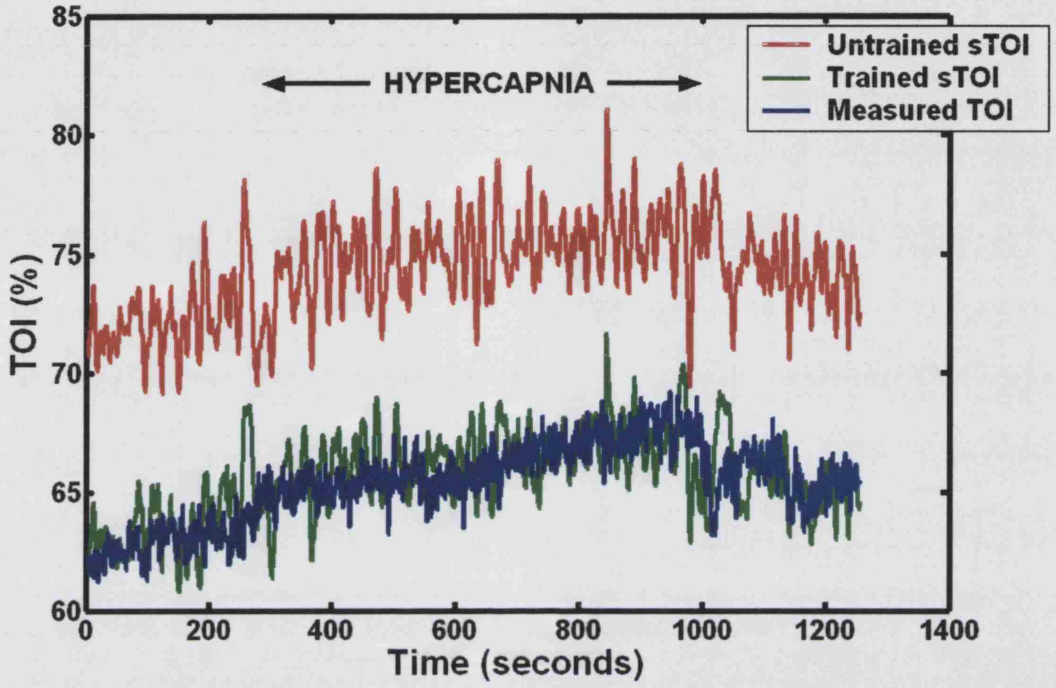

Figure 8.10: Example of CO_2 challenge for one volunteer. Comparisons between measured TOI and untrained and trained simulated TOI. By changing the resting arterial diameter values in the model it is possible to match the absolute simulated TOI value with the measured one.

In addition to the above work, a major effort is also now being put into the integration of a systemic model with the cerebral blood flow control model. Currently, systemic variables are treated as external parameters which we either use as inputs to the model or we keep unchanged during simulations. Collaborators in Oxford University are working towards a fusion of the cerebral circulation model with a model of the cardiopulmonary system (see Figure 8.11), which will include subsystems such as baroreceptor regulation and lung and tissue gas exchange. This is an extension of the previous work by Ursino and colleagues [12,13].

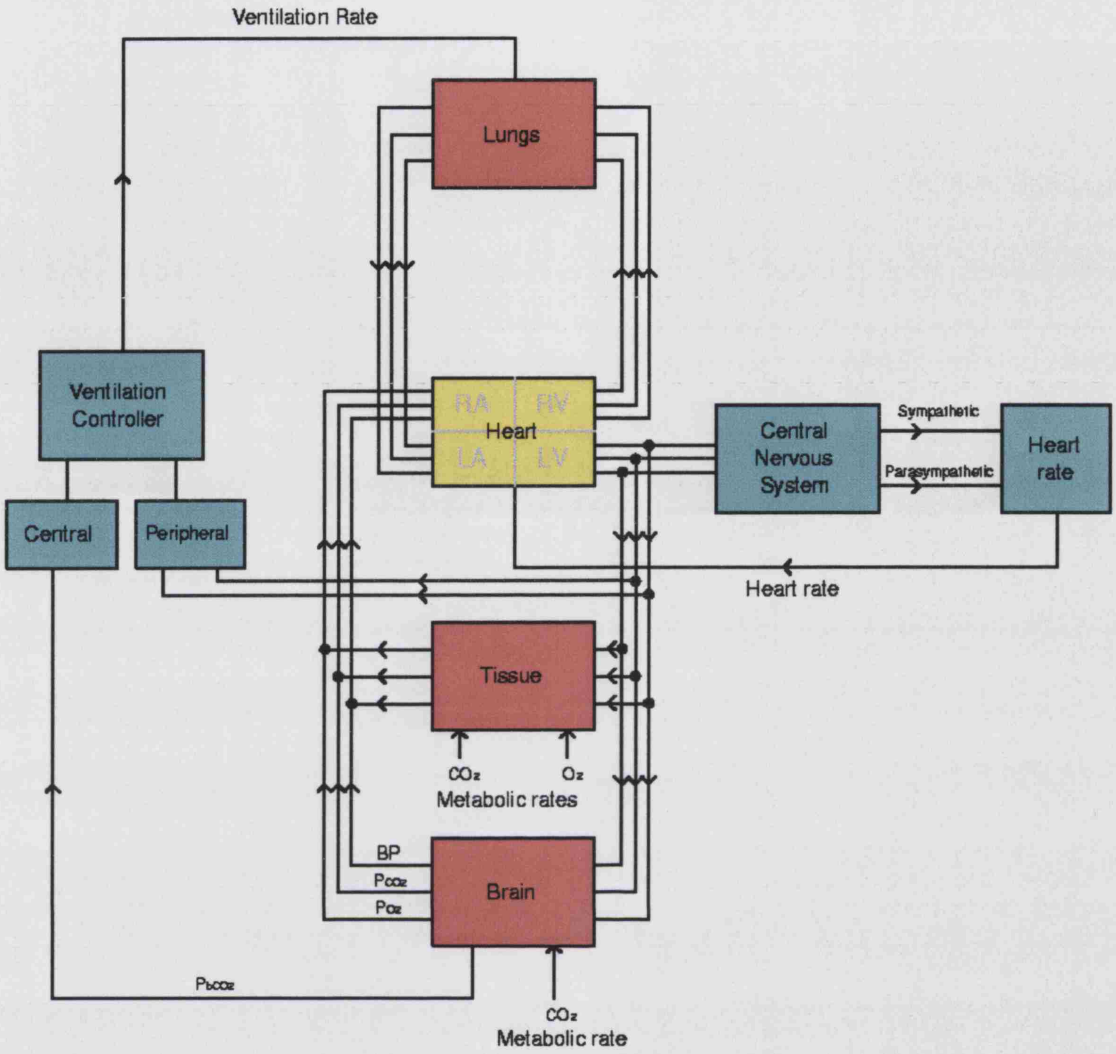

Figure 8.11: Schematic diagram of the combined systemic and cerebral physiological model (taken from [14]).

A combined systemic and cerebral model will give us greater flexibility when testing against the physiological experiment results as it will improve the exactness of the simulations by taking into account the interactions between the cardiovascular system and the physiological stimuli.

8.5 Discussion

The studies described here are ongoing work looking at the clinical application of NIRS and the significance of the cerebral tissue oxygenation signal. Furthermore data

from these studies can help in the development of the UCL cerebral model by providing more measurements for its testing and evaluation.

In addition to the previously described ongoing studies, the National Hospital of Neurology and Neurosurgery treats numerous patients every day, and the majority of these patients have head injury or stroke. Both of these groups are known to demonstrate severely impaired autoregulation. Our intent is to closely monitor and collect data from these patients during their stay in the surgical intensive treatment unit. Data from these patients can give as an insight to the cerebral autoregulation processes during acute pathology and help us to understand and model them in a much more realistic way.

References

1. D. Heuser, J. Astrup, N. A. Lassen, and B. E. Betz, "Brain carbonic acid acidosis after acetazolamide," *Acta Physiol. Scand.* **93**, 385-390 (1975).

2. A. Hauge, G. Nicolaysen, and M. Thoresen, "Acute effects of acetazolamide on cerebral blood flow in man," *Acta Physiol. Scand.* **117**, 233-239 (1983).

3. P.E. Bickler, L. Litt, D.L. Banville, and J.W. Severinghaus, "Effects of acetazolamide on cerebral acid-base balance," *J. Appl. Physiol.* **65**, 422-427 (1988).

4. H. Bruhn, A. Kleinschmidt, H. Boecker, K. D. Merboldt, W. Hanicke, and J. Frahm, "The effect of acetazolamide on regional cerebral blood oxygenation at rest and under stimulation as assessed by MRI," *J. Cereb. Blood Flow Metab.* **14**, 742-748 (1994).

5. M. Holzschuh, C. Woertgen, C. Metz, and A. Brawanski, "Comparison of changes in cerebral blood flow and cerebral oxygen saturation measured by near infrared spectroscopy (NIRS) after acetazolamide," *Acta Neurochir. (Wien.)* **139**, 58-62 (1997).

6. J. Patel, K. Marks, I. Roberts, D. Azzopardi, and A. D. Edwards, "Measurement of cerebral blood flow in newborn infants using near infrared spectroscopy with indocyanine green," *Pediatr. Res.* **43**, 34-39 (1998).

7. F. Gora, S. Shinde, C. E. Elwell, J. C. Goldstone, M. Cope, D. T. Delpy, and M. Smith, "Noninvasive measurement of cerebral blood flow in adults using near-infrared spectroscopy and indocyanine green: a pilot study," *J. Neurosurg. Anesthesiol.* **14**, 218-222 (2002).

8. M. Haruna, K. Kumon, N. Yahagi, Y. Watanabe, Y. Ishida, N. Kobayashi, and T. Aoyagi, "Blood volume measurement at the bedside using ICG pulse spectrophotometry," *Anesthesiology* **89**, 1322-1328 (1998).

9. S. Vorstrup, L. Henriksen, and O. B. Paulson, "Effect of acetazolamide on cerebral blood flow and cerebral metabolic rate for oxygen," *J. Clin. Invest.* **74**, 1634-1639 (1984).

10. D.W. Brown, P.A. Picot, J.G. Naeini, R. Springett, D. T. Delpy, and T. Y. LEE, "Quantitative Near Infrared Spectroscopy Measurement of Cerebral Hemodynamics in Newborn Piglets," *Pediatr. Res.* **51**, 564-570 (2002).

11. M. Banaji, "BRAINCIRC model and detailed documentation," *http://www. medphys. ucl. ac. uk/braincirc/* (2004).

12. M. Ursino, A. Ter Minassian, C. A. Lodi, and L. Beydon, "Cerebral hemodynamics during arterial and CO_2 pressure changes: in vivo prediction by a mathematical model," *Am. J. Physiol.* **279**, H2439-H2455 (2000).

13. E. Magosso and M. Ursino, "A mathematical model of CO2 effect on cardiovascular regulation," *Am. J. Physiol.* **281**, H2036-H2052 (2001).

14. S. Payne, "Interaction between the cardiovascular and respiratory control systems: a mathematical model," *Internal report for associated researchers* Unpublished Work (2003).

Chapter 9

Discussion

This chapter briefly summarises the work repeated in this thesis and makes suggestions for subsequent work. Section 9.2 discusses the main findings of the experimental work using near-infrared spectroscopy (NIRS) to monitor cerebral tissue oxygenation while Section 9.3 discusses the BRAINCIRC UCL computational model of cerebral physiology and metabolism and the results from the simulations that have been carried out.

9.1 Summary

This thesis has presented a thorough description of the cerebral anatomy, physiology and metabolism. The concept of cerebral autoregulation has been discussed extensively and has been presented together with examples from the literature. The concept of physiological modelling has been covered with an extensive literature review together with short descriptions of the most cited intracranial computational models. The physiological model of cerebral haemodynamics, metabolism and cerebral blood flow autoregulation developed at UCL has been described. Computational simulations of various physiological stimuli have been produced as a means to test the exactness of the model and also to provide paradigms of the control of cerebral blood flow. The theory and methodology of NIRS has been discussed with emphasis given to the near-infrared spectrometer NIRO 300 (Hamamatsu Photonics KK) and the measurement of absolute cerebral tissue oxygenation (TOI).

9.2 The NIRS cerebral tissue oxygenation index

An understanding of normal autoregulation and the effects of brain injury on autoregulatory processes is of fundamental importance in critical care. Changes in autoregulation are likely to be of prognostic significance and the choice of treatment is often directed by the state of autoregulation. The need for uncovering physiological variables as markers of the failure of cerebral autoregulation is of great importance.

Clinical experiments carried out in young healthy volunteers during hypercapnia and hypoxia helped us to identify and investigate the interaction and relationship of some of the major physiological components of the NIRS TOI signal.

The TOI association with the $EtCO_2$ was overwhelming. Both the hypercapnia and the hypoxia data indicate that there is a direct association between TOI and $EtCO_2$, suggesting maybe a relationship with flow (not measured here). Direct evidence was presented that shows that small intersubject variations in $EtCO_2$ affect the absolute value of TOI in a linear fashion, this tends to suggest that either cerebral blood flow or

the arterio:venous volume ratios which are both probably affected by the $EtCO_2$ are the ones that mainly control the absolute TOI value as hypothesised in Chapter 4.

Group analysis of the changes in arterial oxygen saturation (SaO_2) during the hypoxic swings did not show any association with the cerebral TOI, suggesting that arterial oxygenation - even though it is one of the components in TOI - might not linearly affect the cerebral TOI.

Physiological monitoring information collected from a group of patients suffering from primary autonomic failure and a group of healthy age matched controls during a passive tilt protocol has been carried out. Significant differences were found in the cerebral haemodynamics and oxygenation during posture changes. Cerebral tissue oxygenation dropped as patients started to exhibit symptoms of orthostatic hypotension. There seemed to be a threshold in blood pressure below which TOI starts to drop; this threshold also appears to be different among patients. The results tend to suggest that in the patient group, cerebral hypo-perfusion due to insufficient blood supply is the main reason for the changes seen in the TOI, however again this is not the only factor as it is probable that changes in arterial brain SaO_2, arterio:venous volume ratios, oxygen consumption and cerebral blood flow might also have a major effect.

It is our belief that even though the physiological complexity of the NIRS TOI signal renders it difficult to interpret, it might indeed provide clinicians with an additional marker of cerebral well being. A key physiological variable and one of the major effecters of the TOI signal is the cerebral blood flow (CBF). The investigations presented in this thesis tend to suggest that CBF is one of the major effecters of the TOI signal and that the two might be linked by a linear association. Currently work is being carried out to investigate this relationship.

9.3 The cerebral computational model

The UCL model is an extensive physiological based model of the cerebral circulation and metabolism, the model is currently in its 4th year of continuous development.

It has been demonstrated that it is feasible to feed real patient data into the model, and get predictions of a number of physiological quantities associated with the patient. Simulations reported in this thesis suggest that the model is able to capture qualitatively the changes seen during hypercapnia and hypotension with a tendency to overestimate the changes during hypoxia. By direct comparisons of the simulated cerebral tissue oxygenation with the experimental measured one we discovered that there is no agreement between them regarding the absolute values. It must however be pointed out that the TOI measurement is in practice quite localised and we always assume that it reflects global changes, this is probably reasonable for studies on normal subjects but is not completely true. The model however makes predictions for a true global cerebral tissue oxygenation value which is therefore likely to be different from our measurement.

Currently work is been carried out to address the training of the model and its integration with a systemic model.

Appendix A

Literature Review of Cerebral Modelling

Presented in a table format is an overview of the most relevant publications on dynamic models of blood versus flow and/or the full concept of the cerebral circulation and autoregulation for the last 20 years.

First Author (Date)	Model Description	Summary	Results and Conclusions
Hudetz A.G. et al (1987) [1]	Computational model based on geometry and topography of the rat pial arterial system. Work was based on normotensive and spontaneous hypertensive rats.	The vessels were visualised by corrosion compound and classified into branching orders by the methods of Horsfield and Strahler. The steady-state pressure distribution in the system was calculated assuming a diameter exponent flow.	The models produced a very detailed description of the rat cerebral vasculature and produced differences between normotensive and hypertensive rats.
Ursino M. (1988) [2]	A physiological model, which mimics the behaviour of the intracranial vasculature. This is a biophysical model used to simulate the production of intracranial pressure pulse waves.	This is a compartmentalised model with equations describing the intracranial arterial, venous and CSF compartments. The model parameters values were computed using physiological and anatomical data.	The model explains the cerebral hydrodynamical phenomena and reproduces some typical clinical tests.
Ursino M. (1988) [3]	The model was described previously [2].	The authors here wanted to test the model simulating the results of dynamical tests based on mock CSF injection in the subarachnoid space. They also wanted to analyse the blood flow pattern in the internal carotid artery.	Simulation results were correlated very well with experimental data.

Ursino M. & Di Giammarco P. (1991) [4]	This is a physiological model investigating the relationship between ICP, CBV and CBF. The model is based on an electrical analogous of the cerebral circulation with particular emphasis on the mechanical properties of the proximal cerebral arteries.	The model simulates the changes in cerebral vessel diameters, CBF and CBV following changes in CPP. Subsequently the model is used to analyse conditions, which lead to system instability and production of ICP plateau waves.	Simulations obtained using normal physiological parameters uncover an antagonism between ICP and autoregulatory adjustments (such as vessel diameters), which can lead to instability of the system in pathological conditions. The model provides some preliminary quantitative indications of the relationship between intracranial dynamics and oscillatory phenomena.
Ursino M. (1991) [5]	A physiological model of the cerebrovascular regulatory system in the rat. This is an extensive model of the cerebral autoregulation including feedback pathways such as the neurogenic, myogenic and chemical regulatory mechanisms.	Phenomena of the rat's vasculature included on the model are: mechanical properties, production of chemical substances by cerebral tissue, smooth muscle response and effect of neural vasomotor fibers.	Simulations were performed with neural fibers cut and artificially stimulated via external means; and with the neurogenic mechanism in a physiological closed loop condition. The model produced 60-70% of the experimental regulatory capacity.
Tiecks F.P. et al (1995) [6]	This is a 2^{nd} order linear model; a mathematical representation of the pressure velocity relationship obtained empirically from thigh cuff tests.	This is a black box model aimed at grading dynamic autoregulation for step changes in ABP, thus providing no insight information regarding the underline physiology.	The model performed well providing a reasonable representation of dynamic autoregulation; however there might be implications of using the model for clinical purposes.

Ursino M. et al (1995) [7]	This is the same hydrodynamical model from previous work [2,4]. The main biomechanical principle adopted in the model is the Monro-Kellie doctrine.	The time pattern of ICP in response to clinical tests such as saline injection in the craniospinal space was studied in acute brain damage patients. Best fitting between model simulations and clinical data was performed using the Powell minimization and the least-square criterion function.	The simulation results demonstrate that in most patients the ICP time pattern cannot be explained on the basis of a biophysical model of the CSF circulation.
Ursino M. & Lodi C.A. (1997) [8]	A model that describes the biophysical properties of the cerebral circulation based on simplifications from previous work[2,4]combined with cerebral autoregulation mechanisms which are simulated with means of a time constant and a sigmoidal static characteristic.	The model used to simulate interactions between ICP, CBV and cerebral autoregulation. Phenomena analysed were: production of plateau waves, the effects of BP drop and the cerebral haemodynamics during pressure volume index (PVI) tests.	Computer simulation results show that the model was capable of reproducing clinical phenomena concerning ICP changes. However they concluded that the model cannot be used to study ICP pulsations synchronous with cardiac beat or respiration.
Ursino M. et al (1997) [9]	The model is the same simplified biophysical and autoregulatory model from previous work [8].	In the present work the model is used to analyse the time pattern of ICP during a PVI test in 20 patients with acute brain injury.	In most cases a satisfactory correlation between model response and patient data was achieved by adjusting only four parameters: CSF outflow resistance, intracranial elastance coefficient and the gain and time constant of autoregulation.

Czosnyka M. et al (1997) [10]	This is a physiological, highly compartmentalised hydrodynamical model of the cerebral circulation.	Time dependent interactions between pressure, CBF, CBV and CSF volume were modelled using a set of non-linear differential equations.	Simulations performed and compared with recordings in patients undergoing common carotid artery compression and sustained hypoperfusion.
Gao E. et al (1998) [11]	A compartmental biophysical model was developed comprised by four departments describing the resistive arterial and arteriolar network simplified as an autoregulatory devise (ARD).	They assumed that CBF is regulated by the response of resistive arteries and arterioles to the changes in CPP. Each compartment consists of a group of identical vessels in parallel. The response of each vessel category to changes in CPP was simulated using experimental data.	The lower and the upper limits of autoregulation (LLA and ULA) were predicted as 69 and 153mmHg respectively. The slope of the CBF-pressure curve below the LLA predicted as 1.3%CBF/mmHg and above the ULA 3.3%CBF/mmHg.
Zhang R. et al (1998) [12]	This is a black box model using the technique of transfer function analysis with gain, phase and coherence function between changes in ABP and V_{MCA} estimated using the Welch method.	The impulse response function, calculated as the inverse Fourier transform of the transfer function enabled the calculation of transient changes in V_{MCA} which was compared with measurements during thigh cuff deflation.	They suggest that there is a close relationship between ABP and V_{MCA} within the frequency range of 0.07-0.3Hz the transfer function analysis also indicated that cerebral autoregulation is more effective for low rather than high frequency changes in ABP.
Ursino M. et al (1998) [13]	This is the same biophysical complex model from previous work [2,4].	They investigate the presence of any relationship between CPP, autoregulation and TCD waveform.	The main conclusion were that in conditions of altered intracranial dynamics the information contained in the TCD waveforms depends on the superimposition of many complex phenomena such as ICP, ABP, autoregulation status and intracranial compliance.

Ursino M. & Lodi C.A. (1998) [14]	This is a combined physiological model of the hydrodynamics and CO_2 reactivity of the brain. The authors here extended their previous work[8,13] by including the CO_2 activity and outputting the TCD velocity signal.	CO_2 is assumed to affect smooth muscle tension; the model response depends on the logarithm of CO_2 changes. Also autoregulation and CO_2 reactivity interact through a sigmoidal relationship.	Model simulations were performed to analyse interactions between autoregulation and CO_2 reactivity. The results were encouraging and the authors used the model in patients in a related study [15].
Lodi C.A. et al (1998) [15]	This is the same model from previous work [14].	The authors used the model to simulate the time pattern of ICP and V_{MCA} in response to maneuvers simultaneously affecting ABP and CO_2. Data from neurosurgical patients was used to investigate how well the model reproduces real measurements.	Sensitivity analysis suggested that the dynamic ICP-V_{MCA} relationship during CO_2 changes is linear in the regulatory range and the slope is affected by the intracranial elastance coefficient. Finally a satisfactory reproduction of the clinical cases was achieved with parameter values in the ranges reported in literature.
Panerai R.B. et al (1999) [16]	Here the authors used four linear models (1)zero-order model, (2)the Tiecks [6] model, (3)a fast Fourier transform model, (4) a linear Wiener-Laguerre model and a non-linear quadratic Wiener-Laguerre model.	The authors wanted to investigate the limitations of the linear assumption and compare the performance of differing modelling techniques. For this purpose they used, V_{MCA} and ABP pressure data from 47 healthy volunteers during a thigh cuff test.	It is possible to model dynamic cerebral autoregulation with linear methods; however a 2^{nd} order non-linear component contributes significantly to improve model accuracy for estimating model parameters, but it cannot automatically extended to represent the nonlinear component of velocity responses or transient changes.
Cassot F. et al (2000) [17]	This is a straightforward biophysical model of the circle of Willis within a linear framework. The autoregulation capability has not been incorporated in this model.	Assuming linearity between mean blood flow in a segment and the difference of the pressure at the ends of this segment and applying the mass conversion law leads to a set of linear equations.	Model simulations with data from patients with carotid artery diseases produced no differences between similar non-linear models. However this is only an anatomical model.

Ursino M. et al (2000)[18]	This is a simplified, mathematically less complex model based on previous work [13,14].	Main simplifications are that the model does not distinguish between large and small pial arteries and that the biomechanics of the arterial-arteriolar vasculature are reproduced by a windkessel model.	The model was validated by comparing simulation results with V_{MCA} and ICP data measured in 13 patients. The model reproduces the time patterns seen in the monitoring systems by using parameter values that lie within the ranges reported in the literature.
Golding E.M. & Golding R.M. (2001) [19]	This is a physiological model of the cerebral blood vessels that combines ion interactions with the vascular smooth muscle and the myogenic response of the vessels.	The model is formulated in terms of three parameters (1) the diameter at zero pressure, (2) the myogenic response and (3) a term associated with myogenic tone.	The model was tested on experimental data obtained from the resistance of cerebral vessels that have been isolated from rats. The simulations identify that diameter changes due to calcium ion variations is at a maximum level; blood flow affects the myogenic response; and finally qualitatively show that ATP concentration changes affected the vessel diameter.
Kirkham S.K. et al (2001) [20]	This is a mathematical model representing dynamic cerebral autoregulation as a flow dependent feedback mechanism.	Their work is based on a linear transfer function with only two parameters namely λ the rate of restoration and a time delay τ.	They have validated the model against experimental data taken from physiological tests involving rapid thigh cuff release and lower body negative pressure. The model reflected very well the general features of cerebral autoregulation.

Piechnik S.K. et al (2001) [21]	This is a detailed anatomical model of both hemispheres of the brain. The arterial part of the model contains both the myogenic and metabolic mechanisms responsible for autoregulation.	The authors wanted to study the steal [22] phenomenon where one hemisphere is reactive and the other is not. They investigated the dependence of blood flow patterns on the extent of interhemispheric arterial communication.	Their findings suggested that vasoreactive effects on ICP had major influence in both hemispheres and the interhemispheric steal effect is unlikely to happen in subjects with non-stenosed carotid arteries.
Liu Y. & Allen R. (2002) [23]	They model the cerebrovascular system using a linear ARX model based on data from a physiological model [7].	They assume that the physiological model [7] is a tuneable volunteer and they investigate the applicability of an ARX model to assess cerebral autoregulation under different conditions of ABP variation and measurement noise.	They concluded that cerebral autoregulation can be assessed from the step response of an ARX model even when the measurement conditions are noisy.
Olufsen M.S. et al (2002) [24]	They used a windkessel model with two resistors and a capacitor to reproduce beat-to-beat changes in V_{MCA} in response to ABP changes.	The resistors represent lumped systemic and peripheral resistances in the cerebral vasculature, whereas the capacitor represents lumped systemic compliance.	Even though the model is simple it is still able to capture dynamic effects arising due to posture changes.
Ursino M. & Giulioni M. (2003) [25]	This is the same model from previous work [4,14].	The authors wanted to investigate the relationship between V_{MCA} pulsatility and cerebral autoregulation.	One of their conclusions is the linear relationship between V_{MCA} and CPP over a wide range of CPP values; the authors also suggest that the slope can be used to provide quantitative information about the autoregulation status.

Yang J. et al (2003) [26]	This is an integrated physiological model mimicking the generation of active tension of the smooth muscle cell that includes electrochemical and chemomechanical subsystem models.	The submodels include: cell membrane electrophysiology, fluid compartments, Ca^{+2} uptake/release from the sarcoplasmic reticulum, cytosolic Ca^{+2} buffering, myosin phosphorylation, formation of phosphorylated myosin cross-bridges with actin, attached latch-type cross-bridges, force generation, mechanical coupling to the contracting filaments, their attachments to the protein structures.	The model mimics closely what is presently known of smooth muscle mechanics and could also predict events that are very difficult to measure.
Yang J. et al (2003) [27]	This is a physiological model of the rat cerebrovascular vessel, which simulates the myogenic response. This model also includes elements from the smooth muscle cell model [26].	This is an integrated model on several levels, it includes biophysical properties and links changes in transmural pressure to membrane voltage, intracellular Ca^{+2} and cross-bridge phosphorylation alterations.	The most important aspect of the model is that characterises the vessel as a passive elastic structure when there is no muscle activation and describes feedback mechanisms such as wall stress, chemical composition of the interstitial fluid and membrane voltage.
Liu Y. et al (2003) [28]	This is a black box model where a simple autoregressive with exogenous ARX model was used to fit the data collected from 8 volunteers in three different tests and at 2 CO_2 levels.	The authors assumed that there is a consistent relationship between autoregulation level and pCO_2 if autoregulation is in a steady state. The autoregulation grading is determined by pCO_2 and is independent of the model.	ABP and V_{MCA} data with spontaneous changes was fitted in the ARX model; there was a strong linear relationship between pCO_2 and the gradient of the step response and between pCO_2 and the phase shift.

Panerai R.B. (2003) [29]	This is a physiological hydrodynamical model that incorporates arterial wall elasticity and active wall tension, in order to investigate the critical closing pressure (CrCP).	CrCP indicates the value of ABP where CBF approaches zero.	The authors discussed the importance of CrCP and they further tested their simple linear model with the Ursino et al[4,7] models. They suggest that a much more complex anatomical model of the cerebrovascular bed could provide a better understanding of the CrCP.
Lu K. et al (2004) [30]	This is a combined systemic and cerebrovascular model.	The model is a combination of the cardiopulmonary system, which includes the whole body circulatory system, lung and peripheral tissue gas exchange and central nervous system control of arterial pressure and ventilation; together with a cerebrovascular model which includes CO_2 reactivity.	The model simulated various physiological conditions and experiments, such as thigh cuff tests and carotid artery compression with great success.

References

1. A.G. Hudetz, K.A. Conger, J.H. Halsey, M. Pal, O. Dohan, and A.G.B. Kovach, "Pressure distribution in the pial arterial system of rats based on morphometric data and mathematical models," *Journal of Cerebral Blood Flow and Metabolism* **7**, 342-355 (1987).

2. M. Ursino, "A mathematical study of human intracranial hydrodynamics. Part 1 - The cerebrospinal fluid pulse pressure," *Annals of Biomedical Engineering* **16**, 379-401 (1988).

3. M. Ursino, "A mathematical study of human intracranial hydrodynamics. Part 2 - Simulation of clinical tests," *Annals of Biomedical Engineering* **16**, 403-416 (1988).

4. M. Ursino and P. Di Giammarco, "A mathematical model of the relationship between cerebral blood volume and intracranial pressure changes: The generation of plateau waves," *Annals of Biomedical Engineering* **19**, 15-42 (1991).

5. M. Ursino, "A mathematical model of overall cerebral blood flow regulation in the rat," *IEEE Transactions on Biomedical Engineering* **38**, 795-807 (1991).

6. F.P. Tiecks, A.M. Lam, R. Aaslid, and D.W. Newell, "Comparison of Static and Dynamic Cerebral Autoregulation Measurements," *Stroke* **26**, 1014 (1995).

7. M. Ursino, M. Iezzi, and N. Stocchetti, "Intracranial pressure dynamics in patients with acute brain damage: A critical analysis with the aid of a mathematical model," *IEEE Transactions on Biomedical Engineering* **42**, 529-540 (1995).

8. M. Ursino and C.A. Lodi, "A simple mathematical model of the interaction between intracranial pressure and cerebral hemodynamics," *J. Appl. Physiol.* **82(4)**, 1256-1269 (1997).

9. M. Ursino, C.A. Lodi, S. Rossi, and N. Stocchetti, "Intracranial pressure dynamics in patients with acute brain damage," *J. Appl. Physiol.* **82(4)**, 1270-1282 (1997).

10. M. Czosnyka, S. Piechnik, H. K. Richards, P. Kirkpatric, and P. Smielewski, "Contribution of mathematical modelling to the interpretation of bedside tests of cerebrovascular autoregulation," *Journal of Neurology, Neurosurgery, and Psychiatry* **63** , 721-731 (1997).

11. E. Gao, W.L. Young, J.Pile-Spellman, E. Ornstein, and Q. Ma, "Mathematical considerations for modeling cerebral blood flow autoregulation to systemic arterial pressure," *Am. J. Physiol.* **274**, H1023-H1031 (1998).

12. R. Zhang, J.H. Zuckerman, C.A. Giller, and B.D. Levine, "Transfer function analysis of dynamic cerebral autoregulation in humans," *Am. J. Physiol.* **274**, H233-H241 (1998).

13. M.Ursino, M. Giulioni, and C.A. Lodi, "Relationships among cerebral perfusion pressure, autoregulation, and transcranial Doppler waveform: a modelling study," *J. Neurosurg.* **89**, 255-266 (1998).

14. M. Ursino and C.A. Lodi, "Interaction among autoregulation, CO_2 reactivity, and intracranial pressure: a mathematical model," *Am. J. Physiol.* **43**, H1715-H1728 (1998).

15. C.A. Lodi, A. Ter Minassian, L. Beydon, and M. Ursino, "Modeling cerebral autoregulation and CO2 reactivity in patients with severe head injury," *Am. J. Physiol.* **43**, H1729-H1741 (1998).

16. R.B. Panerai, S.L. Dawson, and J.F. Potter, "Linear and nonlinear analysis of human dynamic cerebral autoregulation," *Am. J. Physiol.* **277** , H1089-H1099 (1999).

17. F. Cassot, M. Zagzoule, and J.P. Marc-Vergnes, "Hemodynamic role of the circle of Willis in stenoses of internal carotid arteries. An analytical solution of a linear model," *J. Biomech.* **33**, 395-405 (2000).

18. M. Ursino, A. Ter Minassian, C.A. Lodi, and L. Beydon, "Cerebral hemodynamics during arterial and CO2 pressure changes: in vivo prediction by a mathematical model," *Am. J. Physiol.* **279**, H2439-H2455 (2000).

19. E.M. Golding and R.M. Golding, "Mathematical modelling of responses of cerebral blood vessels to changing intraluminal pressure," *Physiological Measurements* **22**, 727-743 (2001).

20. S.K. Kirkham, R.E. Craine, and A.A. Birch, "A new mathematical model of dynamic cerebral autoregulation based on a flow dependent feedback meachanism," *Physiological Measurements* **22**, 461-473 (2001).

21. S. K. Piechnik, M. Czosnyka, N. G. Harris, P. S. Minhas, and J. D. Pickard, "A model of the cerebral and cerebrospinal fluid circulations to examine asymmetry in cerebrovascular reactivity," *J. Cereb. Blood Flow Metab.* **21**, 182-192 (2001).

22. L. Symon, "Experimental evidence for "intracerebral steal" following CO2 inhalation," *Scand. J Clin. Lab. Invest. Suppl.* **102**, XIII (1968).

23. Y. Liu and R. Allen, "Analysis of dynamic cerebral autoregulation using an ARX model based on arterial blood pressure and middle cerebral artery velocity simulation," *Med. Biol. Eng. Comput.* **40**, 600-605 (2002).

24. M.S. Olufsen, A. Nadim, and L.A. Lipsitz, "Dynamics of cerebral blood flow regulation explained using a lumped parameter model," *Am. J. Physiol.* **282**, R611-R622 (2002).

25. M. Ursino and M. Giulioni, "Quantitative assessment of cerebral autoregulation from transcranial Doppler pulsatility: a computer simulation study," *Medical Engineering & Physics* **25**, 655-666 (2003).

26. J. Yang, J. Clark, R.M. Bryan, and C. Robertson, "The myogenic response in isolated rat cerebrovascular arteries: smooth muscle cell model," *Medical Engineering & Physics* **25**, 691-709 (2003).

27. J. Yang, J. Clark, R.M. Bryan, and C. S. Robertson, "The myogenic response in isolated rat cerebrovascular arteries: vessel model," *Medical Engineering & Physics* **25**, 711-717 (2003).

28. Y. Liu, A.A. Birch, and R. Allen, "Dynamic cerebral autoregulation assessment using an ARX model: comparative study using step response and phase shift analysis," *Medical Engineering & Physics* **25**, 647-653 (2003).

29. R.B. Panerai, "The critical closing pressure of the cerebral circulation," *Medical Engineering & Physics* **25**, 621-632 (2003).

30. K. Lu, J.W. Clark Jr., F.H. Ghorbel, C.S. Robertson, D.L. Ware, J.B. Zwischenberger, and A. Bidani, "Cerebral autoregulation and gas exchange studied using a human cardiopulmonary model," *Am. J. Physiol.* **286**, H584-H601 (2004).

Appendix B

Spatially Resolved Spectroscopy Derivation

This appendix describes the derivation of the principle of SRS from the diffusion approximation.

The integration of the diffusion equation for a continuous wave system in respect to the intensity of the reflected light *(R)* at a distance *(ρ)* away from the source is given by the equation:

$$R(\rho) = z_o \cdot \left(\frac{1}{q} + \mu_{eff}\right) \cdot \frac{\exp(-\mu_{eff} \cdot q)}{2 \cdot \pi \cdot q^2} \qquad \textbf{A-1}$$

where $z_o = 1/\mu_{st}$, $q = (\rho^2 + z_o^2)^{1/2}$ and $\mu_{eff} = 3[\mu_a(\mu_a + \mu_{st})]^{1/2}$.

For a semi-infinite slab geometry attenuation *(A)* is defined as:

$$A = -\log_{10}(R(\rho)) \qquad \textbf{A-2}$$

If we assume that $\rho >> z_o$, then $q \approx \rho$ therefore Equation A-1 becomes:

$$\begin{aligned} R(\rho) = z_o \cdot \left(\frac{1}{\rho} + \mu_{eff}\right) \cdot \frac{\exp(-\mu_{eff} \cdot \rho)}{2 \cdot \pi \cdot \rho^2} = \\ = \left(\frac{z_o}{\rho} + z_o \cdot \mu_{eff}\right) \cdot \frac{\exp(-\mu_{eff} \cdot \rho)}{2 \cdot \pi \cdot \rho^2} = \\ = z_o \cdot \mu_{eff} \cdot \frac{\exp(-\mu_{eff} \cdot \rho)}{2 \cdot \pi \cdot \rho^2} \end{aligned} \qquad \textbf{A-3}$$

where $z_o/\rho \approx 0$.

We define attenuation in natural logarithm:

$$\begin{aligned} A_e &= -\ln(R(\rho)) = \\ &= -\ln\left(z_o \cdot \mu_{eff} \cdot \frac{\exp(-\mu_{eff} \cdot \rho)}{2 \cdot \pi \cdot \rho^2}\right) = \\ &= -\left[\ln(z_o \cdot \mu_{eff}) - (\mu_{eff} \cdot \rho) - \ln(2 \cdot \pi \cdot \rho^2)\right] = \\ &= (\mu_{eff} \cdot \rho) - \ln\left(\frac{(z_o \cdot \mu_{eff})}{(2 \cdot \pi \cdot \rho^2)}\right) = \\ &= (\mu_{eff} \cdot \rho) - \ln\left(\frac{(z_o \cdot \mu_{eff})}{(2 \cdot \pi)}\right) + 2\ln\rho \end{aligned} \qquad \textbf{A-4}$$

From equations A-3 and A-4 we have:

$$\begin{aligned} A &= -\log_{10}(R(\rho)) = \\ &= \frac{1}{\ln 10} \cdot \left[(\mu_{eff} \cdot \rho) + 2\ln\rho - \ln\left(\frac{(z_o \cdot \mu_{eff})}{(2 \cdot \pi)}\right)\right] \end{aligned} \qquad \textbf{A-5}$$

By differentiating *(A)* with respect to *(ρ)* Equation A-5 becomes:

$$\begin{aligned} \frac{\partial A}{\partial \rho} &= \frac{1}{\ln 10} \cdot \left(\mu_{eff} + \frac{2}{\rho}\right) = \\ &= \frac{1}{\ln 10} \cdot \left(\sqrt{3 \cdot \mu_a \cdot \mu_{st}} + \frac{2}{\rho}\right) \end{aligned} \qquad \textbf{A-6}$$

Equation A-6 is Equation 4-21 from Chapter 4.

Appendix C

Published Papers

Pages: 248-256

Tachtsidis I., Elwell C.E., Leung T.S, Lee C.W., Smith M., Delpy D.T., "Investigation of cerebral haemodynamics by near infrared spectroscopy in young healthy volunteers reveals posture dependent spontaneous oscillations." Physiological Measurement, 25(2):437-445, (2004).

Pages: 257-261

Tachtsidis I., Elwell C.E., Lee C.W., Leung T.S, Smith M., Delpy D.T. "Spectral characteristics of spontaneous oscillations in cerebral haemodynamics are posture dependent." Advances in Experimental Medicine and Biology, 540:31-36, (2004)

Pages: 262-267

Tachtsidis I., Elwell C.E., Leung T.S., Bleasdale-Barr K., Hunt K., Toms N., Smith M., Mathias C.J., Delpy D.T. "Rate of change in cerebral oxygenation and blood pressure in response to passive changes in posture: a comparison between Pure Autonomic Failure patients and Controls." Advances in Experimental Medicine and Biology, In Press, (Submitted 2003).

Pages: 268-273

Tachtsidis I., Leung T.S., Oliver C., Henty J.R., Jones H., Smith M., Delpy D.T., Elwell C.E. "Quantification of adult cerebral blood volume using tissue oxygenation index." Advances in Experimental Medicine and Biology, In Press, (Submitted 2004).

Pages: 274-322

Banaji M., **Tachtsidis I.**, Delpy D., Baigent S. "A physiological model of cerebral blood flow control." Mathematical Biosciences, 194(2):125-173 (2005).